Stratification thermohaline dans l'Atlantique tropical sud-ouest : des processus physiques à l'écologie acoustique

Ramilla Vieira de Assunçáo

THESE DE DOCTORAT EN CO-TUTELLE DE

L'UNIVERSITÉ DE BRETAGNE OCCIDENTALE

ECOLE DOCTORALE N° 598
SCiences de la Mer et du littoral
*SP*écialité : Océanographie physique et Environnement

Avec L'UNIVERSITÉ FÉDÉRALE DE PERNAMBUCO
Programme d'études supérieures en Océanographie - Centre de Technologie et de Géosciences
Spécialité : Océanographie

Par
Ramilla VIEIRA DE ASSUNÇÃO

Thermohaline stratification in the southwestern tropical Atlantic: from physical processes to acoustic ecology

Thèse présentée et soutenue à Recife, le 29 juin 2021
Unité de recherche : Laboratoire des Sciences de l'Environnement Marin – LEMAR
Laboratório de Oceanografia Física, Estuarina e Costeira - LOFEC

Rapporteurs avant soutenance :

Matthieu LENGAIGNE, Directeur de recherche à l'IRD, France
Mariano GUTIÉRREZ TORERO, Professeur à l'Université Nationale Federico Villarreal (UNFV), Pérou

Composition du Jury :

Président Jury :	Géraldine SARTHOU	Directrice de Recherche à CNRS, France
Examinateurs :	Carmen LIMONGI	Professeure à l'Université Fédérale de Pernambuco (UFPE), Brésil
	Fabrice HERNANDEZ	Chargé de Recherche à IRD, France Professeur Invité à l'Université Fédérale de Pernambuco (UFPE), Brésil
	Matthieu LENGAIGNE	Directeur de recherche à l'IRD, France
	Mariano GUTIÉRREZ TORERO	Professeur à l'Université Nationale Federico Villarreal (UNFV), Pérou
Dir. de thèse :	Bernard BOURLÈS	Directeur de Recherche à l'IRD (UBO)
	Alex COSTA DA SILVA	Professeur à l'Université Fédérale de Pernambuco (UFPE)

Invité(s)

Anne LEBOURGES-DHAUSSY	Ingénieure de Recherche à l'IRD, France (co-directrice - UBO)
Arnaud BERTRAND	Directeur de Recherche à l'IRD, Professeur Invité à l'Université Fédérale de Pernambuco (UFPE), Brésil (co-directeur - UFPE)

ACKNOWLEDGEMENTS

The last stage of this journey has arrived, this incredible challenge, both in my professional and personal life. I acknowledge the people who accepted to enter this journey with me. Those who accepted me as a PhD student and who have guided me to achieve this co-badged (Brazil and France) PhD. Thank you very much, Arnaud Bertrand, Alex C. Silva, Anne Lebourges-Dhaussy and Bernard Bourlès. Your expertise and effort were crucial in formulating the research questions and methodology of this work.

I extend my regards to all the organizations, laboratories, institutions and financial supporters, which made this research possible. My special thanks to UFPE (Universidade Federal de Pernambuco), UBO (Université de Bretagne Occidentale), LOFEC (Laboratório de Oceanografia Física, Estuarina e Costeira), MARBEC and LEMAR (Laboratoire des Sciences de l'environnement Marin). Also, thanks to CNPq (Conselho Nacional de Desenvolvimento Científico e Tecnológico), IRD (Institut de recherche pour le développement), and CAPES-COFECUB program (88881.142689/2017-01) for the financial support. This research is also a contribution to the International Joint Laboratory TAPIOCA. I also acknowledge the French oceanographic fleet for funding the at sea survey and the officers and crew of the R/V Antea for their contribution to the success of the operations during the ABRACOS cruises.

This co-badged and multidisciplinary PhD allowed me to interact with many other researchers. My best regards to everyone who contributed to the long discussions involved in this thesis. In special, Natanael, Syumara, Leandro, Julie, Gary, Simone, Gabriela, Everton, Marcão, Lucas, Deco e Sara. Your contributions were a milestone in the completion of this thesis. I am even more grateful for offering me much more than scientific debates, such as a friendship, conversations and affection during difficult times. I also wish to show my gratitude for the helpful feedback and hard work given by co-authors on all the chapters of this thesis.

The PhD in my life was a challenge at each stage, with a set of emotions. It was not simple nor easy, but it was a dream. A dream in my life, in the lives of my sisters, Priscilla e Tíscilla, and in the lives of my parents, Edilton e Irenilda. To them is my most intense gratitude. They are my base, my strength, and where I find the most real love of God.

ABSTRACT

The dynamic of the thermohaline structure of the upper ocean drives most near surface oceanic processes. The thermohaline circulation of the southwest tropical Atlantic (SWTA), a key region for diagnosing variation of the Atlantic Meridional Overturning Circulation, has prime impact on global climate. The thermohaline variability also plays a driving role in the vertical structuring of pelagic habitats. In order to fill information gaps on the thermohaline structure in the SWTA and to bring insights into the relationships between these physical processes and the distribution of the acoustic backscattering energy (proxy of organisms biomass), this thesis was organised over three main scientific objectives, each addressed in a separate Chapter. To develop this study, we took advantage of the two multidisciplinary scientific surveys (Acoustic along the BRAzilian COaSt) performed in the STWA in austral spring (Sep. – Oct.) 2015 and fall (Apr. – May) 2017.

The first objective of this thesis was to characterise the 3D thermohaline structure of the upper layer (down to 300 m). Characterising the thermohaline structure is typically based on the application of classical statistical methods on vertical profiles. However, classical methods do not explicitly contemplate the vertical nature of the profiles. Functional Data Analysis (FDA) is an alternative to solve such drawbacks. Here, we apply an FDA approach to characterise the 3D canonical thermohaline structure of the SWTA in austral spring and fall. Our results reveal a clear spatial pattern with the presence of three areas with significantly different thermohaline characteristics. Area 1, mostly located along the continental slope, reflects the western boundary current system (WBCS), with low static stability and high frequency of occurrence of barrier layer (BL). Conversely, Area 2, located along the Fernando de Noronha chain, presents strong static stability with a well-marked thermocline. This area, under the influence of the eastern Atlantic, is characterised by a low BL frequency, which is seasonally modulated by the latitudinal oscillation of the intertropical convergence zone, controlling the regime of precipitation. In turn, Area 3 behaves as a transition zone between the areas 1 and 2 with the presence of the water core of maximum salinity in subsurface, and therefore presence of strong-moderate BL. Beyond this study, FDA approach emerges as a powerful way to describe, characterise, classify and compare ocean patterns and processes. It can be applied to in situ data but could also be used to explore ocean model output deeply and comprehensively.

Second, we examined the feasibility of extracting the thermohaline structure from echosounder data collected in the SWTA. Indeed, in some systems, acoustics allow for a robust estimation of the depth of the pycnocline or thermocline. Here to examine the feasibility of extracting the thermohaline structure (mixed-layer depth, upper and lower thermocline) from echosounder data we tested three approaches: (i) the vertical extension of the epipelagic community; (ii) the use of acoustic gradients; and (iii) a cross-wavelet approach. Results show that, even if the thermohaline structure impacts the vertical distribution of acoustic scatters, the resultant structuring do not allow for a robust estimation of the thermohaline limits indicating that other oceanographic or biological processes are acting. This unexpected result prevents for a fine-scale representation of the upper-layer turbulence from acoustic data. However, studying the proportion of acoustic biomass within each layer provides interesting insights on ecosystem structure in different thermohaline, seasonal and diel scenarios. In particular, in regions where the thermocline is highly stratified, and less mixed, some organisms seemed to avoid the region layer of highest gradient. This led us to investigate the fine-scale vertical relationships between acoustic biomass and a variety of environmental factors, which is the third objective.

Ocean dynamics initiates the structure of primary producers and these, in turn, shape the distribution of subsequent trophic levels until the whole pelagic community reflects the physicochemical structure of the ocean. Despite the importance of the bottom-up structuring in pelagic ecosystems, fine scale studies of biophysical interactions along depth are scarce and challenging. By investigating the fine-scale vertical relationships between a variety of environmental parameters (currents, stratification, oxygen concentration and fluorescence) and acoustic backscattering energy, we show that fluorescence, oxygen, current and stratification are important drivers, but that their relative importance depends on the area, the depth range and the diel cycle. In the epipelagic layer, the strongest acoustic responses were associated with depths of greatest stability (highest stratification), even in areas where the fluorescence peaks were deeper than the peak of stratifications, as in the WBCS during spring. Dissolved oxygen does not seem to be a key factor in the WBCS where the entire water column is well oxygenated while it seems to be a driver in the system where lower oxygen concentration occur in sub-surface. Finally, our results suggest that organisms seem to avoid strong currents core. However, future works are needed to better understand the role of currents on the vertical distribution of organisms.

RESUMO

A dinâmica da estrutura termohalina do oceano superior dirige grande parte dos processos oceânicos mais próximos a superfície. A circulação termohalina do Atlântico tropical sudoeste (S*outhwest Tropical Atlantic*, SWTA), uma região chave para diagnosticar a variação da Célula de Revolvimento Meridional do Atlântico, tem um impacto primordial no clima global. A variabilidade termohalina também desempenha um papel chave na estruturação vertical dos habitats pelágicos. Com o propósito de preencher lacunas de informação sobre a estrutura termohalina no SWTA e de trazer insights sobre as relações entre esses processos físicos e a distribuição da energia acústica (proxy de biomassa dos organismos), esta tese foi organizada em três objetivos científicos principais, cada um deles abordado em um capítulo separado. Para desenvolver este estudo, aproveitamos as duas campanhas científicas multidisciplinares (*Acoustic along the BRAzilian COaSt*) realizadas no STWA na primavera (set. - out.) de 2015 e outono (abr. - maio) de 2017.

O primeiro objetivo desta tese foi caracterizar a estrutura termohalina 3D da camada superior (até 300 m). A caracterização da estrutura termohalina é tipicamente baseada na aplicação de métodos estatísticos clássicos em perfis verticais. Entretanto, os métodos clássicos não contemplam explicitamente a natureza vertical dos perfis. A Análise de Dados Funcionais (*Functional Data Analysis*, FDA) é uma alternativa para resolver tais inconvenientes. Neste caso, aplicamos uma abordagem funcional para caracterizar a estrutura termohalina 3D do SWTA da primavera e outono austral. Nossos resultados revelam um padrão espacial claro com a presença de três áreas com características termohalinas significativamente diferentes. A área 1, localizada principalmente ao longo do talude continental, reflete o sistema de corrente de borda oeste (*Western Boundary current system*, WBCS), com baixa estabilidade estática e alta frequência de ocorrência de camadas de barreira (BL). Por outro lado, a Área 2, localizada ao longo da cadeia de Fernando de Noronha, apresenta forte estabilidade estática com uma termoclina bem definida. Esta área, sob a influência do Atlântico leste, é caracterizada por uma baixa frequência de BLs, que é modulada sazonalmente pela oscilação latitudinal da zona de convergência intertropical,

controlando o regime de precipitação. Por sua vez, a Área 3 comporta-se como uma zona de transição entre as áreas 1 e 2, com a presença do núcleo de água de salinidade máxima em subsuperfície e, portanto, frequência de ocorrência forte-moderada de BL. Além deste estudo, a abordagem da FDA surge como uma forma poderosa de descrever, caracterizar, classificar e comparar padrões e processos oceânicos. Ela pode ser aplicada aos dados *in situ*, mas também pode ser usada para explorar de forma profunda e abrangente as saídas de modelos oceânicos.

Como segundo objetivo, examinamos a viabilidade de extrair a estrutura termohalina dos dados de ecosonda coletados no SWTA. De fato, em alguns sistemas, a acústica permite uma estimativa robusta da profundidade da picnoclina ou termoclina. Para examinar a viabilidade de extrair a estrutura termohalina (profundidade da camada de mistura, termoclina superior e inferior) dos dados de ecosonda, testamos três abordagens: (i) a extensão vertical da comunidade epipelágica; (ii) o uso de gradientes acústicos; e (iii) uma abordagem de ondas cruzadas (*wavelets*). Os resultados mostram que, mesmo que a estrutura termohalina impacte a distribuição vertical dos dispersores acústicos, a estrutura resultante não permite uma estimativa robusta dos limites termohalinos indicando que outros processos oceanográficos ou biológicos estão agindo. Estes resultados inesperados impedem uma representação em escala fina de processos turbulentos na camada superior do oceano a partir de dados acústicos. Entretanto, o estudo da proporção de biomassa acústica dentro de cada camada termohalina fornece uma visão interessante da estrutura do ecossistema em diferentes cenários termohalinos, sazonais e diários. Em particular, em regiões onde a termoclina é altamente estratificada, e menos misturada, alguns organismos parecem evitar a camada da região de maior gradiente. Isto nos levou a investigar as relações verticais em escala fina entre a biomassa acústica e uma variedade de fatores ambientais, que é o terceiro objetivo.

A dinâmica oceânica inicia a estruturação dos produtores primários e estes, por sua vez, moldam a distribuição dos níveis tróficos subsequentes até que toda a comunidade pelágica reflita a estrutura físico-química do oceano. Apesar da importância da estruturação *bottom-up* nos ecossistemas pelágicos, os estudos em escala fina das interações biofísicas ao longo da profundidade são escassos e desafiadores. Ao investigar as relações verticais em escala fina entre uma variedade de parâmetros ambientais (correntes, estratificação, concentração de oxigênio e fluorescência) e a energia acústica refletida, mostramos que a fluorescência, o oxigênio, a corrente e a estratificação são fatores importantes, mas que sua importância relativa depende da área, da faixa de

profundidade e do ciclo diário. Na camada epipelágica, as respostas acústicas mais fortes foram associadas a profundidades de maior estabilidade (estratificação mais alta), mesmo em áreas onde os picos de fluorescência eram mais profundos que o pico das estratificações, como no WBCS durante a primavera. O oxigênio dissolvido não parece ser um fator chave no WBCS onde toda a coluna de água está bem oxigenada enquanto parece ser um condutor no sistema onde menores concentrações de oxigênio ocorrem em subsuperfície. Finalmente, nossos resultados sugerem que os organismos parecem evitar o núcleo de correntes fortes. Entretanto, são necessários trabalhos futuros para entender melhor o papel das correntes na distribuição vertical dos organismos.

RÉSUMÉ

La dynamique de la structure thermohaline de la couche supérieure océanique détermine la plupart des processus océaniques proches de la surface. La circulation thermohaline du sud-ouest de l'Atlantique tropical (S*outhwest Tropical Atlantic*, SWTA), une région clé pour diagnostiquer la variation de la circulation méridienne de retournement Atlantique, a un impact primordial sur le climat global. La variabilité thermohaline joue également un rôle déterminant dans la structuration verticale des habitats pélagiques. Afin de combler le manque d'information sur la structure thermohaline dans le SWTA et améliorer la compréhension sur les liens entre ces processus physiques et la distribution de l'énergie de rétrodiffusion acoustique (indicateur de la biomasse des organismes), cette thèse a été organisée autour de trois objectifs scientifiques principaux, chacun abordés dans un chapitre distinct. Pour développer cette étude, nous avons profité des deux campagnes scientifiques multidisciplinaires (*Acoustic along the BRAzilian COaSt*) réalisées dans le STWA au printemps (Sep. - Oct.) 2015 et à l'automne (Avr. - Mai) 2017 austral.

Le premier objectif de cette thèse était de caractériser la structure thermohaline 3D de la couche supérieure (jusqu'à 300 m). La caractérisation de la structure thermohaline est typiquement basée sur l'application de méthodes statistiques classiques sur des profils verticaux. Cependant, les méthodes classiques ne prennent pas explicitement en compte la nature verticale des profils. L'analyse fonctionnelle des données (*Functional Data Analysis*, FDA) est une alternative pour résoudre ces inconvénients. Ici, nous appliquons une approche FDA pour caractériser la structure thermohaline canonique 3D de la SWTA au printemps et à l'automne austral. Nos résultats révèlent un schéma spatial clair avec la présence de trois zones présentant des caractéristiques thermohalines significativement différentes. La zone 1, principalement située le long du talus continental, reflète le système de courant de courant de bord ouest (*Western Boundary current system*, WBCS), avec une faible stabilité statique et une fréquence élevée d'apparition de la couche barrière (*Barrier Layer*, BL). A l'inverse, la zone 2, située le long de la chaîne de Fernando de Noronha, présente une forte stabilité statique avec une thermocline bien marquée. Cette zone, sous l'influence de l'Atlantique Est, est caractérisée par une faible fréquence de BL, qui est modulée de façon saisonnière par l'oscillation latitudinale de la zone de convergence intertropicale, contrôlant

le régime des précipitations. Et enfin, la zone 3 se comporte comme une zone de transition entre la zone 1 et 2 avec la présence du noyau d'eau de salinité maximale en subsurface, et donc la présence de BL fortes-modérées. Au-delà de cette étude, l'approche FDA apparaît comme un outil efficace pour décrire, caractériser, classer et comparer les modèles et processus océaniques. Elle peut être appliquée aux données *in situ* mais pourrait également être utilisée pour explorer en profondeur et de manière exhaustive les résultats des modèles océaniques.

Deuxièmement, nous avons examiné la possibilité d'extraire la structure thermohaline à partir des données d'échosondeurs collectées dans le SWTA. En effet, dans certains systèmes, l'acoustique permet une estimation robuste de la profondeur de la pycnocline ou de la thermocline. Ici, pour examiner la faisabilité de l'extraction de la structure thermohaline (profondeur de la couche mélangée, thermocline supérieure et inférieure) à partir des données du sondeur, nous avons testé trois approches : (i) l'extension verticale de la communauté épipélagique ; (ii) l'utilisation de gradients acoustiques ; et (iii) une approche par ondelettes croisées. Les résultats montrent que, même si la structure thermohaline a un impact sur la distribution verticale des diffusions acoustiques, la structuration résultante ne permet pas une estimation robuste des limites thermohalines indiquant que d'autres processus océanographiques ou biologiques agissent. Ces résultats inattendus empêchent une représentation à échelle fine des processus turbulents dans la couche supérieure de l'océan à partir des données acoustiques. Cependant, l'étude de la proportion de la biomasse acoustique dans chaque couche thermohaline fournit un aperçu intéressant de la structure de l'écosystème sous différents scénarios thermohalins, saisonniers et diurnes. En particulier, dans les régions où la thermocline est fortement stratifiée, et moins mélangée, certains organismes semblent éviter la couche de la région où le gradient est le plus élevé. Ceci nous a conduit à étudier les relations verticales à fine échelle entre la biomasse acoustique et une variété de facteurs environnementaux, ce qui constitue le troisième objectif.

La dynamique océanique est à l'origine de la structure des producteurs primaires qui, à leur tour, façonnent la distribution des niveaux trophiques suivants jusqu'à ce que l'ensemble de la communauté pélagique reflète la structure physico-chimique de l'océan. Malgré l'importance de la structuration *bottom-up* dans les écosystèmes pélagiques, les études à fine échelle des interactions biophysiques en profondeur sont rares et difficiles. En étudiant les relations verticales à fine échelle entre une variété de paramètres environnementaux (courants, stratification, concentration en

oxygène et fluorescence) et l'énergie de rétrodiffusion acoustique, nous montrons que la fluorescence, l'oxygène, le courant et la stratification sont des facteurs importants, mais que leur importance relative dépend de la zone, de la gamme de profondeur et du cycle diurne. Dans la couche épipélagique, les réponses acoustiques les plus fortes sont associées aux profondeurs de plus grande stabilité (stratification la plus élevée), même dans les zones où les pics de fluorescence étaient plus profonds que le pic des stratifications, comme dans le WBCS au printemps. L'oxygène dissous ne semble pas être un facteur clé dans le WBCS où toute la colonne d'eau est bien oxygénée alors qu'il semble être un facteur déterminant dans le système où une concentration d'oxygène plus faible se produit dans la sous-surface. Enfin, nos résultats suggèrent que les organismes semblent éviter le cœur des courants forts. Cependant, des travaux futurs sont nécessaires pour mieux comprendre le rôle des courants sur la distribution verticale des organismes.

CONTENTS

ACKNOWLEDGEMENTS **2**
ABSTRACT **3**
RESUMO **5**
RÉSUMÉ **8**
CONTENTS **11**
CHAPTER I: GENERAL INTRODUCTION **14**
1. Preface 14
2. The Southwestern Tropical Atlantic 16
3. Ecosystem Acoustic 24
4. Motivation and objectives 30
Objective 1: Characterise the 3D thermohaline structure of the SWTA in austral spring and fall by the functional statistics approach. (Chapter II) 31
Objective 2: Test if the variation of the thermohaline structure could be extracted from acoustic data in the SWTA. (Chapter III) 31
Objective 3: Investigate how environmental factors may be driving the vertical distribution of organisms in the southwestern tropical Atlantic. (Chapter IV) 32
References 33
CHAPTER II: 3D CHARACTERISATION OF THE THERMOHALINE STRUCTURE IN THE SOUTHWESTERN TROPICAL ATLANTIC DERIVED FROM FUNCTIONAL DATA ANALYSIS OF IN SITU PROFILES **42**
Abstract 42
1. Introduction 43
2. Material and Methods 45
2.1. Data 45
2.2. Defining the thermohaline structure 47
2.3. Functional Data Analysis (FDA) 49
3. Results 54
3.1. Merging the datasets 54
3.2. Typology of thermohaline patterns 55
3.3. 3D thermohaline patterns 57
4. Discussion 67

4.1. Thermohaline structure and associated processes 68
5. Conclusion 73
Declaration of Competing Interest 73
Acknowledgments 74
References 74
Supplementary material 90
From Chapter II to Chapter III **94**
CHAPTER III: ON THE USE OF ACOUSTIC DATA TO CHARACTERISE THE THERMOHALINE STRATIFICATION IN A TROPICAL OCEAN **95**
Abstract 95
1. Introduction 96
2. Material and Methods 98
2.1. Data 98
2.2. Thermocline structure 100
2.3. Linking acoustic profiles to thermohaline properties 100
3. Results and Discussion 103
3.1. Thermohaline limits vs. cumulative sum of the acoustic echoes 103
3.2. Thermohaline limits vs. acoustic backscattering gradient 107
3.3. Wavelet approach 109
4. Conclusion 113
References 113
From Chapter III to Chapter IV **119**
CHAPTER IV: FINE-SCALE VERTICAL RELATIONSHIPS BETWEEN ENVIRONMENTAL CONDITIONS AND SOUND SCATTERING LAYERS IN THE SOUTHWESTERN TROPICAL ATLANTIC **120**
Abstract 120
1. Introduction 121
2. Methods 124
2.1. Data 124
2.2. Data analysis 127
3. Results 129
3.1. Oceanscape 129
3.2. Epipelagic echoscape 131

3.3. Cross-correlations in the epipelagic layer.....133
3.4. Mesopelagic echoscape.....135
3.5. Cross-correlation in the mesopelagic layer.....135
4. Discussion.....136
4.1. Epipelagic layer.....139
4.2. Mesopelagic layer.....141
5. Conclusion.....142
Acknowledgements.....143
References.....143
Supplementary Material.....151
CHAPTER V: GENERAL CONCLUSION.....161
Objective 1: Characterise the 3D thermohaline structure of the SWTA in austral spring and fall by the functional statistics approach. (Chapter II).....161
Objective 2: Test if the variation of the thermohaline structure could be extracted from acoustic data in the SWTA. (Chapter III).....163
Objective 3: Investigate how environmental factors may be driving the vertical distribution of organisms in the southwestern tropical Atlantic. (Chapter IV).....164
References.....166

CHAPTER I:
GENERAL INTRODUCTION

1. Preface

Oceans are the most extensive and prominent feature on Earth. Covering 71% of the Earth's surface, oceans constitute a major part of the Earth's hydrosphere, which is one component of the Earth's climate system (the other components being atmosphere, geosphere, biosphere and cryosphere). The Earth's climate system is complex and interactive, involving exchanges of energy and moisture throughout these five spheres, functioning as an interactive unit. In this way, changes in the climate system always reflect on more than one component. The ocean is the most massive component of this system playing, therefore, an important role in understanding the functioning of the Earth's climate system (Thurman, 2019).

The coupling of the ocean and atmosphere drives, primarily, part of the ocean circulation. The winds blowing across the ocean surface drive exchanges of momentum, heat, water, and gases (e.g., oxygen, carbon dioxide, and other trace gases). Globally, wind-driven currents transfer heat from warmer to colder areas of the Earth, as do the large wind belts. Ocean currents are also density-driven, which unlike wind-driven currents occurring beyond the basin scale, drawing part of the global ocean circulation, moving water masses vertically. The density-driven or thermohaline (*thermo* = *heat*; *haline* = *salt*) circulation is driven by differences in ocean temperature and salinity, which together draw the density of the ocean (Siedler et al., 2013).

The variability in temperature and salinity arises from a variety of processes including atmosphere-ocean surface buoyancy exchanges: heating/cooling at the sea surface and surface freshwater fluxes (evaporation and sea ice formation enhance salinity; precipitation, runoff and ice melting decrease salinity). Vertically, ocean structuring also involves temperature and salinity variations and is referred to as thermohaline stratification. The upper waters layer, directly influenced by the warming sun, wind, surface currents, waves and tides, is the well-mixed ocean layer with a uniform or nearly uniform water mass. Below this, when atmospheric effects are no longer felt, the slopes

(*clines*) of temperature, salinity, and density are present, being referred to as the thermocline (*therm* = *heat*), the halocline (*halo* = *salt*) and the pycnocline (*pycno* = *density*), respectively.

The thermocline and pycnocline occur well developed at low and mid latitudes, separating the surface well-mixed layer from the deeper, denser and colder waters layer that extend toward the deep-ocean floor from the lower thermocline. The thermocline and pycnocline have a high gravitational stability and thus tend to physically isolate the adjacent water, forming a barrier to vertical mixing, preventing the replenishment of nutrients to the well-sunlit surface layer (Siedler et al., 2013; Thurman, 2019). The degree to which oceanic regions develop a thermocline also affects the patterns of biological production observed at different latitudes (Longhurst and Pauly, 1987). Air-sea interactions also have important implications for global warming. In recent decades, multiple studies have confirmed that the atmosphere is experiencing unprecedented warming because of carbon dioxide and other gases emissions that absorb and trap heat in the atmosphere. This atmospheric heat is being transferred to the oceans and has the potential to cause changes to the marine ecosystem (Fahey et al., 2017; Lüthi et al., 2008; Sallée et al., 2021).

Understanding the causes and effects of the different physicochemical oceanscapes on the marine ecosystem has progressed significantly, however studies still require the collection of abiotic and biotic data on a continuing basis. One of the remote methods that has made it possible to complete these gaps is the use of underwater acoustics. Acoustic tools allows picturing the oceanic environment, from abiotic to biotic (Benoit-Bird and Lawson, 2016; Bertrand et al., 2010; Grados et al., 2016; Medwin and Clay, 1997; Trenkel et al., 2011). Associated with the changes in the ocean conditions, as the stratification, there are especially changes in the marine ecosystem that affect the acoustic responses (Benoit-Bird and Lawson, 2016; Cullen, 1982; Leach et al., 2018). Contrarily to most sampling device observing a specific vertical profile or aggregation (CTD, plankton net, trawls, etc.), acoustics is the unique sampling devices allowing quasi-continuous sampling of oceanscape (Lavery et al., 2010; Trenkel et al., 2016; Warren and Wiebe, 2008). Some of these studies have focused on the separation of physical and biological sources of scattering (e.g., Fer et al., 2010; Warren et al., 2003). Conversely, many of studies have been dedicated to understanding the relationship of biological scattering to environmental factors (e.g., Coyle and Cooney, 1993; Pérez-Santos et al., 2018), even the potential use of biological scattering to provide information of oceanographic structures (e.g., Bertrand et al., 2010; Grados et al., 2016). As such,

advances in collaborations between physical oceanography and acoustic ecology may lead to a greater understanding of how organisms respond to and influence their habitat. This interrelationship from a dynamic and oligotrophic environment such as the southwest tropical Atlantic (SWTA) is the general subject of this thesis.

Before describing the main objectives of the thesis, we provide the background on which this thesis was founded. This thesis is structured into five chapters. In Chapter 1, we provide the background and describe the objectives of the thesis; in Chapter II, we provide a 3D characterisation of the thermohaline structure in the southwestern tropical Atlantic derived from functional data analysis of *in situ* profiles; in Chapter III we test for the use of acoustic data to characterise the thermohaline stratification in a tropical ocean; in Chapter IV, we describe the relationships between physical and biogeochemical features and the sound scattering layers in the SWTA at a fine-scale respectively. Chapters II – IV are in article format. In Chapter IV, we present a general conclusion. Furthermore, we present the applicability of our findings as well as perspectives.

2. The Southwestern Tropical Atlantic

The tropical Atlantic Ocean can be considered a home of multiple coupled climate variations. These changes occur over a wide range of temporal and spatial scales involving the ocean, atmosphere and land. Impacting adjacent continental areas with for example seasonal to interannual variability of rainfall events in South America and West Africa and hurricane activity in the Atlantic (Foltz and McPhaden, 2008; Hounsou-gbo et al., 2015; Segura et al., 2020). The tropical Atlantic (Fig. 1) links the southern and northern branches of the Atlantic meridional overturning circulation (AMOC), that is one of the strongest current systems (advection). The AMOC is one of the main processes that determine the interannual variability in the distribution of heat, salt and tracers in the tropical Atlantic (Caesar et al., 2021; Matos et al., 2020; Roemmich and Wunsch, 1985; Venancio et al., 2020).

Figure 1. Diagrams of the key components that make up the Atlantic Ocean ocean-atmosphere system. Simplified illustration of the Atlantic Meridional Overturning Circulation represented by the warm currents (red) and by the cold deep currents (blue). The position of the Intertropical convergence zone (ITCZ) is plotted according to seasonality, associated with trade winds.

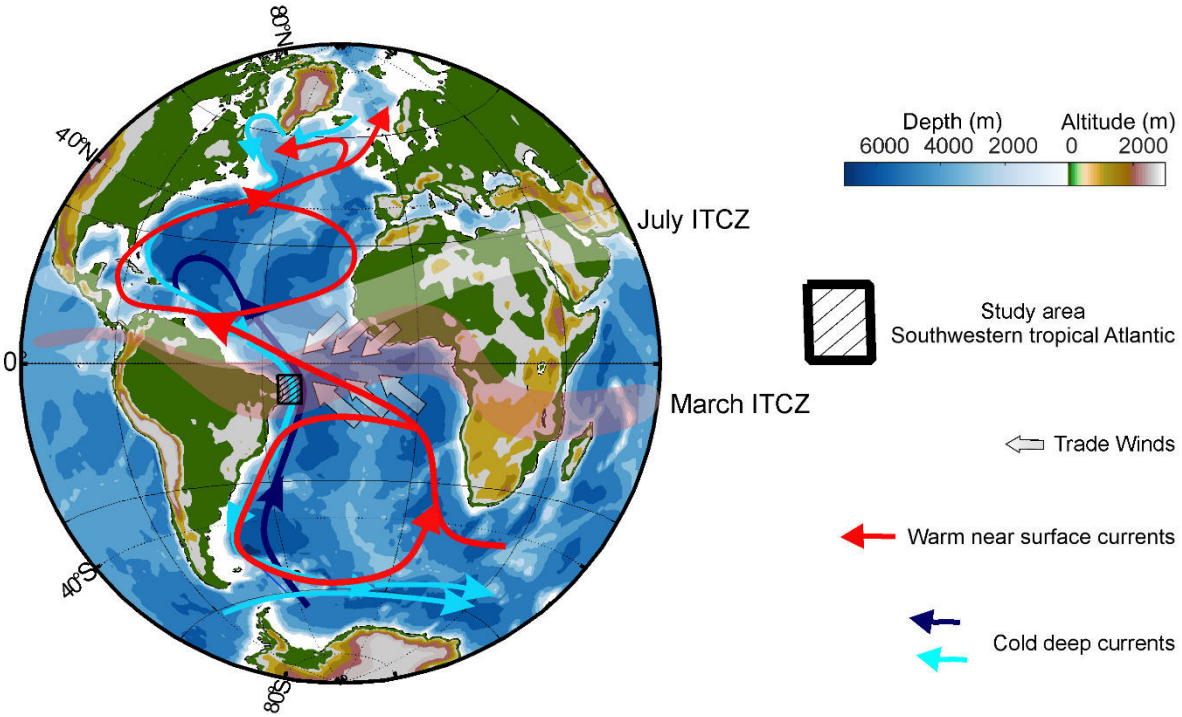

Source: Personal collection.

The AMOC is an example of a circulation driven by both thermohalines forcing, and the wind. The AMOC can be divided into two cells (Fig. 1). The “upper cell” (red and light blue arrows, Fig. 1) transports warm and saline surface waters from the tropics to the northern hemisphere as well as southward return flow of the North Atlantic Deep Water (NADW). While the cold and dense “lower cell” (dark blue arrows, Fig. 1) comprising the Antarctic bottom water mass (AABW), that supplies northwards fluid to the abyssal ocean (Buckley and Marshall, 2016; Cheng et al., 2013; Lumpkin and Speer, 2007).

The southwestern edge of the tropical Atlantic (SWTA, highlighted in Fig.1) is a key region for understanding and monitoring the North Brazil Current (NBC)/North Brazil Undercurrent (NBUC) system (warm near surface current in Fig. 1; Fig. 2) and the Deep western Boundary Current (DWBC; light blue current in Fig. 1), which play an important role of the mass transport within the AMOC. Further, the NBUC that is part of the subtropical cell, is the main connection between the

subduction regions of the subtropical South Atlantic and the eastward equatorial and off-equatorial undercurrents that supply the equatorial and eastern-boundary upwelling regimes (Bourlès et al., 2002; da Silveira et al., 1994; Hummels et al., 2015; Schott et al., 2002; Zhang et al., 2003).

At seasonal scales, the meridional migration of the Intertropical Convergence Zone (ITCZ, Fig. 1), defined as a tropical *rainbelt* (Schneider et al., 2014), drives, primarily, the variability of the wet and dry seasons in the tropical Atlantic. Its mean position varies seasonally from 9°N to 2°N over the Atlantic Ocean (Colna, 2017; Schneider et al., 2014). The rainfall on Earth is the most intense in the ITCZ, and the Northeast of Brazil is one of the most vulnerable regions to seasonal rainfall events in South America (Hounsou-gbo et al., 2015; Utida et al., 2019). During the seasonal southward migration of the ITCZ, higher precipitations in the SWTA is associated to weakest southeast trade winds, warmer sea surface, and narrow mixed layer. The seasonal positioning of the ITCZ also controls the origin (latitude range) and intensity of the main currents along the SWTA (Fig. 1), these are the equatorward NBUC and the westward South Equatorial current (SEC) (Dossa et al., 2021; Rodrigues et al., 2007; Stramma et al., 2005).

The SEC (Fig. 2) is the main source of water for the tropical Atlantic, as a westwards surface current that extends down to 100 m. The SEC is a broad current, typically occupying the latitudinal range between 4°N and 15-25°S, depending mainly on the seasonal position of the ITCZ. Globally, the SEC consists in three main branches: the northern (nSEC), central (cSEC) and southern (sSEC). The sSEC is fed by the relatively cool Benguela current, which crosses the Greenwich meridian south of 20°S. Extending between 10°S and 25°S, the sSEC flowing towards the Brazilian coast, where it bifurcates and gives rise to the equatorward NBC/NBUC system and the weaker southward Brazil current (Peterson and Stramma, 1991; Stramma, 1991). The cSEC (Fig. 2) extends from about 3°S to 9°S, limited by the presence of the South Equatorial Undercurrent (SEUC, 3°-5°S) and the South Equatorial Countercurrent (SECC, 6°-9°S) (Molinari, 1982; Peterson and Stramma, 1991; Stramma, 1991). The cSEC can be further subdivided into two other branches at about 5° and 6°S. The northern portion of the cSEC, north of 5°S, coalesces with the NBUC/NBC (da Silveira et al., 1994; Dossa et al., 2021; Silva et al., 2009).

Figure 2. Schematic map showing the horizontal distribution of the major tropical currents at about 0-500 m depth. Shown are the North Equatorial Current (NEC), the Guinea Dome (GD), the North Equatorial Undercurrent (NEUC), the South Equatorial Current (SEC) with the northern (nSEC), equatorial (eSEC), central (cSEC) and southern (sSEC) branches, the Equatorial Undercurrent (EUC), the North Brazil Undercurrent (NBUC), the Angola Gyre (AG), the South Equatorial Undercurrent (SEUC), the South Equatorial Countercurrent (SECC) and the Brazil Current (BC). Solid lines represent surface currents, and dashed lines, subsurface currents. The highlighted rectangle refers to the SWTA, the study area.

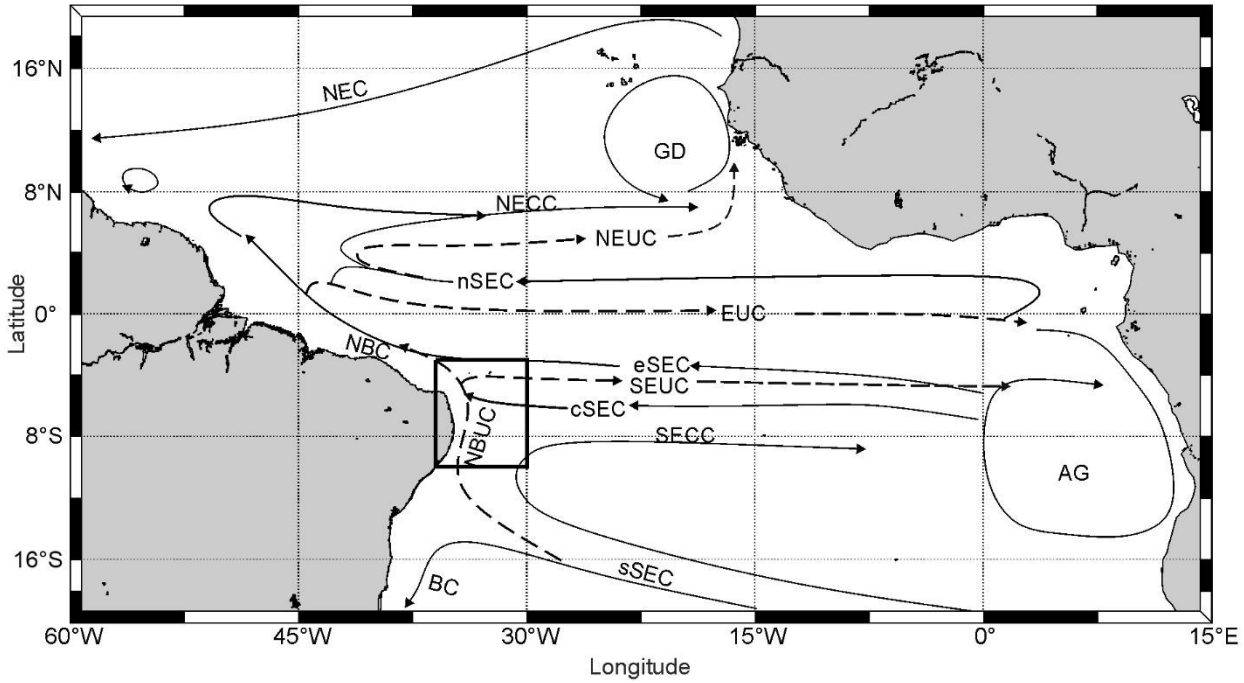

Source: Personal collection, adapted from Stramma and Schott (1999).

The SWTA is also characterized by the presence of five main water masses (Fig. 3): the Tropical Surface Water, the South Atlantic Central Water (SACW), the Subtropical Underwater (STUW), the Antarctic Intermediate Water (AAIW) and the North Atlantic Deep Water (NADW) (Stramma and England, 1999). A water mass is defined as a body of water that originates in a particular area of the ocean with a common formation history (Poole and Tomczak, 1999). These water bodies share common properties such as temperature, salinity, oxygen and other biogeochemical variables that are distinct from surrounding water. Further, the water masses have a measurable extent both vertically and horizontally. Once they leave the formation regions, the water masses tend to mix (both along and across dense surfaces), so that in certain regions there may be water masses with different properties compared to those of the formation area (Liu and Tanhua, 2019).

The surface layer of the tropical Atlantic is occupied by the warm Tropical Surface Water. Underneath lies the SACW which is still warm (5° - 20 °C) and saline (34.5 - 36), ($24.5 < \sigma\theta < 27$ kg m^{-3}; Stramma and England, 1999) compared to the underneath water mass. The SACW is subducted into the thermocline and formed in the southern hemisphere, subducted in the Subtropical Convergence (STC; Fig. 3) (Liu and Tanhua, 2019; Sprintall and Tomczak, 1993). Although the STC is well-defined and continuous across the Southern Ocean, detailed studies of temperature-salinity (T-S, Fig. 3) diagrams, reveal that the T-S properties of the SACW in the tropics are closer to those typical of the western Indian Ocean Subtropical Convergence, than those found along the STC in the Atlantic Ocean. This indicates that much of the SACW is not subducted in the Atlantic portion of the STC, but corresponds in fact the Central Indian Water (ICW) brought into the Atlantic Ocean by the eddies of the Agulhas Current (Sprintall and Tomczak, 1993) (Fig. 3b).

In the upper part of the SACW lies the STUW (Fig.3a; Stramma and England, 1999), characterized by high salinity (> 36.5) and the highest dissolved oxygen concentrations around the upper thermocline. Formed in the region of high evaporation in the subtropical gyres (Fig. 3b). The STUW first enters the SWTA region carried by the sSEC. It is then trapped over the Brazilian slope region by the NBUC/NBC system (Fig. 2). Underneath the SACW, below ~500 m depth, lies the colder and fresher AAIW (Fig. 3a). The isopicnal of $\sigma\theta = 27.1$ kg m^{-3} marks the transition between them. The AAIW in the South Atlantic originates from a surface region of the circumpolar layer, especially in the northern Drake Passage and the Falkland Current loop (Fig. 3b; Talley, 1996). The NADW ($\sigma\theta = 27.7 – 27.88$ kg m^{-3}; Fig. 3a) appears from 1200 m depth, being transported to the South Atlantic by the DWBC (light blue current in Fig. 1) from the northern hemisphere (Liu and Tanhua, 2019; Stramma and England, 1999).

Figure 3. Diagram of the potential temperature (°C) versus salinity for (a) full water column and (b) section locations map with colours indicating the latitude range. The SWTA is in the dark blue section. The main water masses are the Subtropical Underwater (STUW); the South Atlantic Central Water (SACW); the Antarctic Intermediate Water (AAIW); and the North Atlantic Deep Water (NADW). The regions of origin of the water masses are also represented, with emphasis on the regions of formation of the west and east South Atlantic Central Water (SACW). In addition, the influence of the Indian Central Water (ICW) on the east SACW (eSACW) through the Agulhas eddies can be observed. The highlighted rectangle refers to the SWTA, the study area.

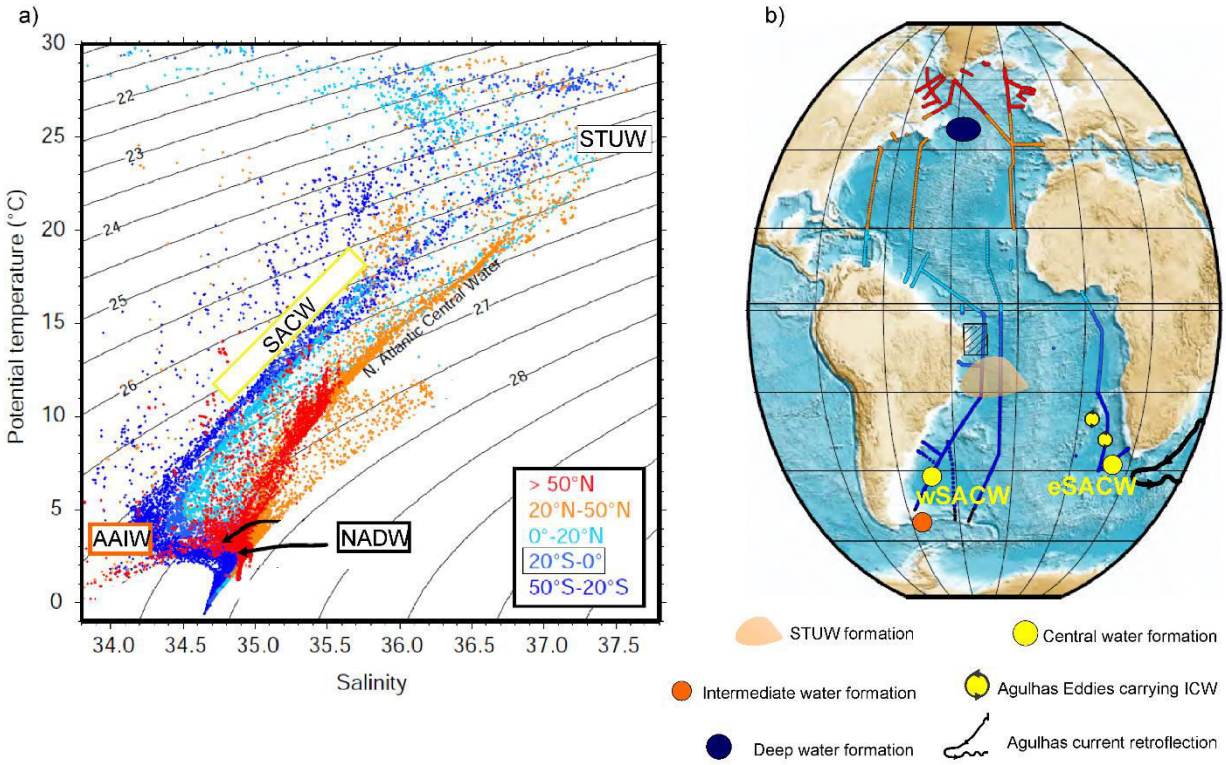

Source: Personal collection, adapted in accordance with Talley et al. (2011), Liu and Tanhua (2019a), Talley et al. (2011) and Stramma and England (1999).

The effect of all these physical processes, water masses transport, mixing and stratification is reflected in the concentration of chlorophyll in the upper SWTA. Tropical oceans are generally considered oligotrophic, due to minimal vertical flow of nutrients and subsequent low biological productivity (Longhurst and Pauly, 1987). The existence of a permanent thermocline separating the warm, well-mixed surface layer from the cooler, denser subsurface layer (Araújo et al., 2011; Foltz et al., 2019; Lumpkin and Garzoli, 2005) plays an important role in these features. The permanent thermocline tends to inhibit upward flow from deeper, nutrient-rich layers, restricting

primary production in surface waters (Siedler et al., 2013; Thurman, 2019). However, the SWTA is an interesting region to investigate different groups of organisms, from primary producers to higher levels of the food chain, due to its varied morphological and oceanographic properties, and thus important productivity gradients (e.g., Olivar et al., 2017; Sampaio de Souza et al., 2013). The western sector has been characterized as one of the most oligotrophic subtropical zones in the global ocean (Morel et al., 2010).

The presence of seamounts, island and plateaus in the SWTA (Fig. 4) impact the local productivity in this overall oligotrophic region. Oceanic islands, covering about 3% of the earth's surface, are particularly productive environments, hosting remarkable high productivity and biodiversity with many endemic species. The Fernando de Noronha chain (Fig. 4) is an E-W trending submarine volcanic sequence along the 4°S latitude and is referenced as an "oasis of desert ocean life" (Hazin, 1993; Lira et al., 2014; Serafini et al., 2010). The seamounts are distributed over an area of 490 km long and 110 km wide. The highest elevations constitute the Fernando de Noronha island and Rocas Atoll (Motoki and Freire Motoki, 2020). Their rich waters are extremely important for the breeding and feeding of tuna, sharks, turtles and marine mammals. The islands are home to the largest concentration of tropical seabirds in the western Atlantic (UNESCO World Heritage Centre).

Figure 4. 3D diagram of the SWTA (highlighted in figures 1, 2 and 3) showing the main geological features and associated warm near surface current system, the North Brazil Undercurrent (NBUC), the North Brazil Current (NBC), the South Equatorial Undercurrent (SEUC), and the central branch of the South Equatorial Current (cSEC) and the Deep western Boundary Current (DWBC).

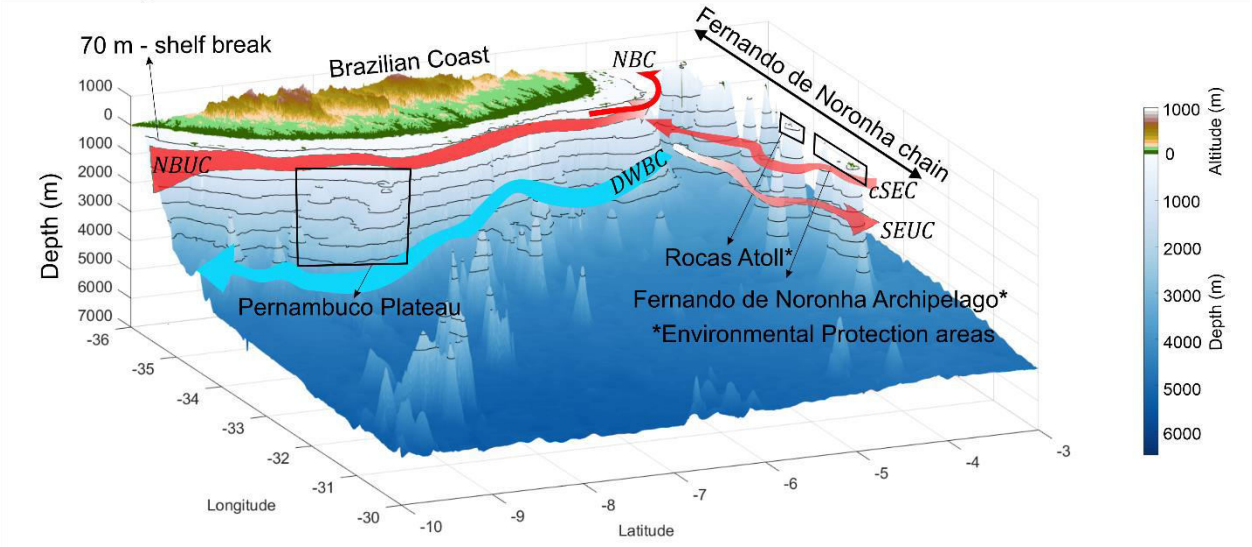

Source: Personal collection.

Eddies, turbulence and vertical displacements of isopycnals generally occur in island and seamount regions, enhancing, in addition to local productivity, mass and energy fluxes through the trophic chain (Cardoso et al., 2020; Silva et al., 2021; Tchamabi et al., 2017). This process is also called the "island mass effect" and has been known for over 60 years, classically defined by the increase in primary production around an island (Doty and Oguri, 1956; Gilmartin and Revelante, 1974).

Besides seamounts and islands, the presence of plateaus along the continental slope is a characteristic feature of the SWTA. Three plateaus are present, two small ones (Ceará Plateau and Rio Grande do Norte Plateau) and the more extensive, the Pernambuco Plateau (Fig. 4). The Pernambuco plateau is an area of magmatic basement, which extends from the base of the slope to the 2250 m isobath, forming seamounts in the southern and eastern parts (Kowsmann and Costa, 1976). The presence of marginal features such as these has also been reported to have orographic effects on local dynamics (Badal et al., 2010) and consequently on the local ecosystem (Figueiredo et al., 2020; Tosetto et al., 2021).

3. Ecosystem Acoustic

Over a wide range of wavelengths, the ocean is opaque to electromagnetic radiation but relatively transparent to sound. Underwater, the sound suffers very much less attenuation than the light. In clear ocean water, sunlight may be detectable (with instruments) down to 1000 m, but the range at which humans can see details of objects is rarely more than 50 m, and usually less. On the other hand, sound waves can be detected over vast distances and are a much better vehicle for undersea information than light (Talley et al., 2011). However, although sound (energy) can be transmitted over long distances by the periodic compression and expansion (waves), water is nevertheless an imperfect acoustic medium. Indeed, the emitted sound energy is removed (scattered, backscattered and refracted) as it encounters a suspended obstacle, be it solids, biota or entrained gas, or simply converted into heat by physical absorption (Simmonds and MacLennan, 2005; Talley et al., 2011). The ocean stratification is the main responsible physical structure for the generation of beams (convergent and/or divergent), depending on the change in the sound speed due to the depth (Pensieri and Bozzano, 2017; Talley et al., 2011). All these effects are why the sound has motivated a growing group of researchers to explore the possibilities of using sound as a tool for ocean measurement.

The Acoustic Oceanography is defined as the use of sound to study physical parameters and processes, as well as biological species and behaviours, at sea (Medwin and Clay, 1997). References to underwater acoustic can be traced back as far as mediaeval times. Urick (1983) mentions a notebook, dated 1490, in which Leonardo da Vinci observed that by listening to one end of a long tube, with the other end in the sea, ‘you will hear ships at a great distance’. However, practical applications had to await more advanced technology, notably the piezo-electric transducer which was invented by the French physicist Langevin in 1917 (Sabra, 2015). As a result of research instigated by the First World War, it was discovered that submarines could be detected by listening to the echo of a sound transmission. Since then, the benefits of underwater acoustics were proportional to the technological developments in both hardware and software components, especially for oceanographic applications (e.g., Pensieri and Bozzano, 2017).

The many successes of the underwater acoustic range from the identification, counting and monitor aquatic fauna, structures and physical processes (e.g., internal waves, ocean frontal systems, eddies, and others) in the water column and the shape of the sea floor (Medwin, 1997; Wood, 1935). In some cases, a natural sound in the sea is analysed to reveal the physical or biological characteristics of the sound source and is called *passive acoustics* approach (Medwin and Clay, 1997). Each source has unique spectral characteristics that can be used to classify its type (physical, biological, anthropogenic, atmospheric), even if the background noise levels may differ between basins (Fig. 5).

Figure 5. Relevant time and space scales of several physical and biological processes (Cronin et al., 2012; Dickey, 1993).

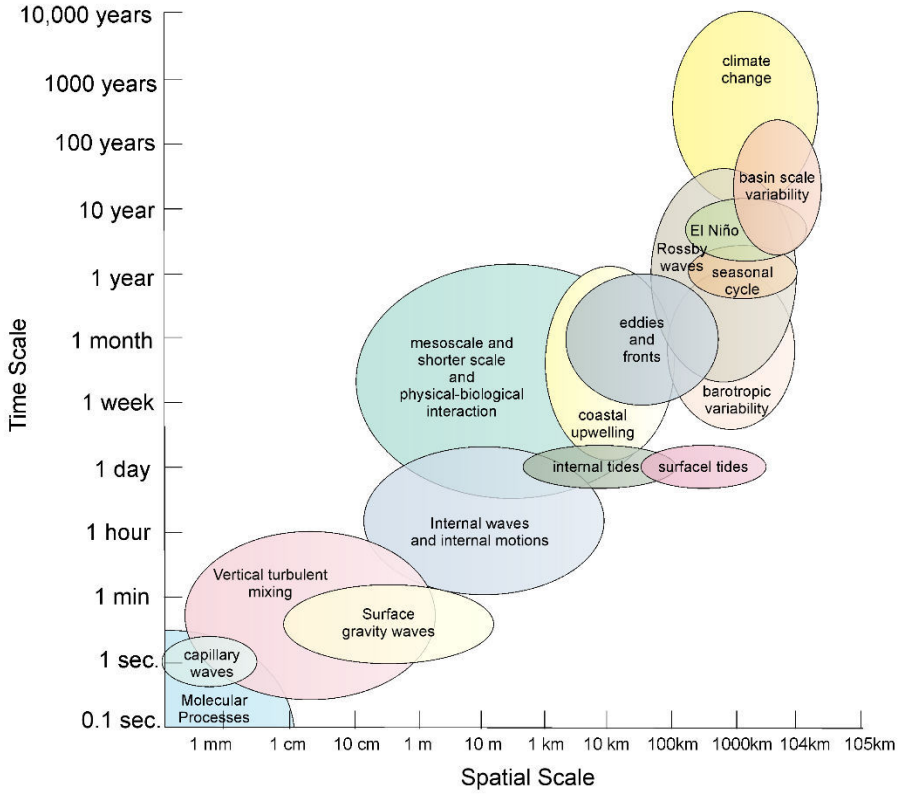

Source: Personal collection.

In other research, conversely, a specifically sound source (transducer) is used to learn about the ocean and its boundaries, through emitted and listen sound, and is referred to as *active acoustics* (Fig. 6). More commonly, this means that a sound pulse is transmitted to the water by a transducer which receive an electric energy from a transceiver and converts it into mechanical energy thanks

to its piezoelectric properties. A pulse transmission is called a "ping". The wave propagates at the sound speed in the water and in a directional manner, following the beam pattern of the transducer which depends on the wavelength and of the transducer geometry. During propagation, the wave reflects on encountered obstacles, i.e., changes of acoustic impedance (equals: density*sound celerity) that can be biological or physical. The part of the mechanical energy that goes back to the transducer (the backscattered energy) is received, converted to its turn into electrical energy and amplified by the transceiver (Medwin and Clay, 1997; Simmonds and MacLennan, 2005).

In the ocean, sound pressure levels (SPL) are recovered using the sonar equation as the difference between the transmitted power (SL) and the transmission loss (TL) through the path, including geometric dispersion and absorption (Urick, 1983). For a one way propagation, the SPL is calculated following Eq. (1):

$$SPL(dB) = SL(dB) - TL(dB) = 10\,log\left(\frac{P_0}{P_R}\right)^2 - \left[20\,log\left(\frac{R}{R_0}\right) + \propto (R - R_0)\right] \text{ Eq. 1}$$

P_0 is the pressure of the transmitted signal at a known distance R_0, P_R is the reference pressure (generally equal to $1\,\mu Pa$), and R is the distance of the listener from the source. As active instruments are able to transmit a pulse and hear its echo, this equation must be completed for the return path, considering this time the target as a source, having a capacity to return acoustic energy back towards the transducer, defined by its "Target Strength" (TS). Thus, Eq. (1) for a round trip between the transducer and the target is modified into Eq.2:

$$SPL(dB) = SL(dB) - 2TL(dB) + TS(dB) = 10\,log\left(\frac{P_0}{P_R}\right)^2 - 2\left[20\,log\left(\frac{R}{R_0}\right) + \propto (R - R_0)\right] + TS \text{ Eq.2}$$

Therefore, from the measurement of the delay time of the received tick signal and the knowledge of the local speed of sound in water column it is possible to calculate the distance of the targets, and the intensity of the return sound (Volume Scattering Strength, s_v in dB re 1 m^{-1}, Maclennan et al. (2002) reveals information about the targets (Benoit-Bird and Lawson, 2016; Medwin and Clay, 1997). After some time (for example 1 time per second), the transmitter produces another pulse and the whole process is repeated. The echoes are displayed on the echogram as a graphical representation of the insonified water (Fig. 6). An ecogram is therefore a two-dimensional picture of targets as connected echo. The early echograms were greyscale display, where detected signals appeared as dark traces on a white background (Wood, 1935). However, most echograms nowadays

use a range of colours to give a better visual contrast; in this case the strongest signals are (usually) presented in dark red, descending through various colours and hues to blue/grey for the weakest signals (Fig. 7).

Figure 6. Concept of echosounding. Along the path of the ship, the transmitted pulses generate echoes from the targets below the transducer which are displayed on an echogram. s_v is the volume scattering strength.

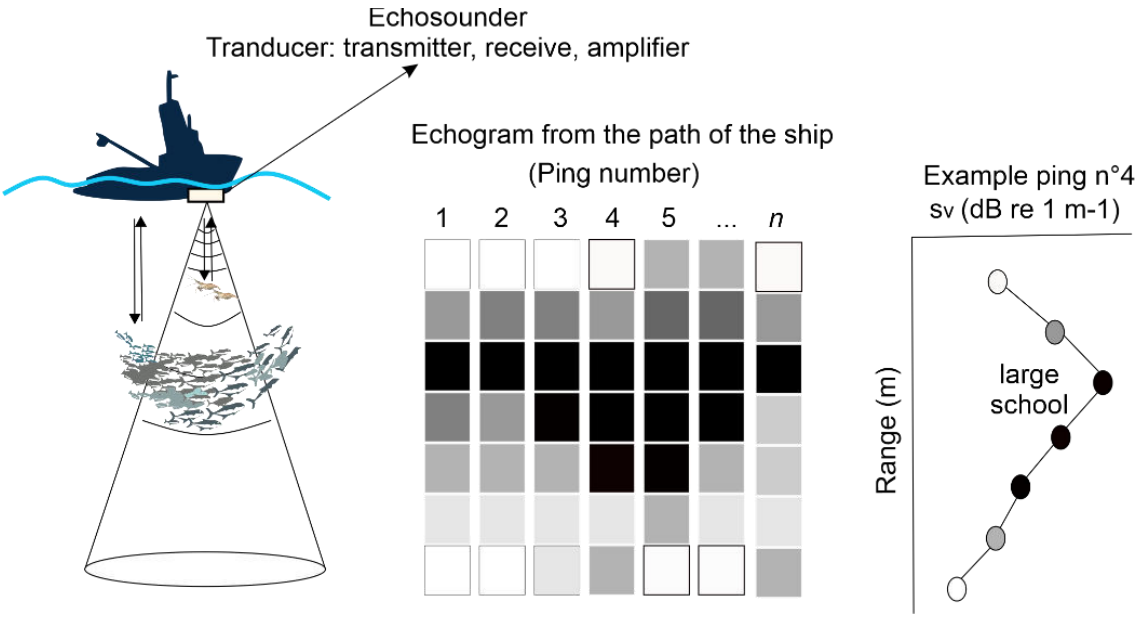

Source: Personal collection.

Figure 7. Example of fish detection around Fernando de Noronha archipelago. (a) Video screenshots showing aggregation of black triggerfish. (b) Corresponding original echograms at 200 kHz for black triggerfish.

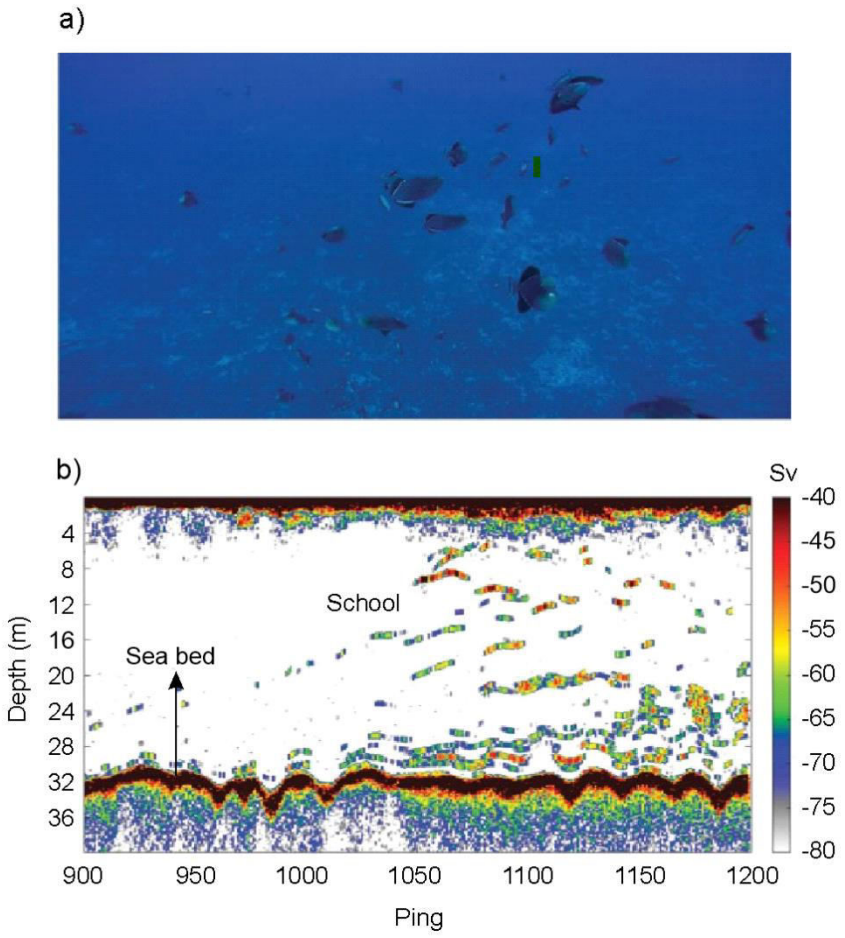

Source: Adapted from Salvetat et al (2020).

The intensity of the backscattered energy is a complex function of the size of the organism, its shape, swimming orientation and anatomical physical properties, as well as of the transmitted acoustic frequency (or its wavelength). Each organism has its frequency signature, but in order to understand the scattering produced by a wide diversity of organisms, they have been categorized within wide groups determined by their anatomy and boundary conditions: organisms including gas (gas bladder for fish, gas inclusion for siphonophores, lung for whale), fluid-like organisms where longitudinal waves only can propagates and have weak density and sound speed contrast with surrounding water, hard shelled organisms with higher contrasts and possible Lamb wave

propagation in the shell in addition to the longitudinal one (Fig. 8; Benoit-Bird and Lawson, 2016; Lavery et al., 2007; Stanton, 1994; Stanton et al., 1998). These frequency characteristics provide keys to classify the organisms and try to infer community composition from multifrequency (Ballón et al., 2011; Béhagle et al., 2017; De Robertis et al., 2010), or more recently wide band echosounders (Verma et al., 2017).

Figure 8. Frequency responses characteristic of the different types of animals . Dashed lines denote curves derived from empirical observations; solid lines indicate predictions based on physics-based scattering models validated through empirical measurements. The vertical dotted lines show typical sampling frequencies (18, 38, 70, 120, and 200 kHz). The line colours indicate animal types that are similar kinds of acoustic scatterers. Fluid-like scatterers (orange lines) shown here are responses characteristic of (1) copepod and (2) euphausiid. Shell-bearing scatterers (brown line) shown here is a response characteristic of (3) shelled pteropod. Gas-filled structures (blue lines) shown here are responses characteristic of (5) a small bubble such as might be produced by a diving seabird, (6) air-filled whale lungs, and (7) a swim-bladder-bearing fish (the curve shown here is representative of an ~23 cm herring). Large organisms that do not have gas inclusions, such as fishes without swim bladders or squid, and even parts of large animals such as whale bodies (6), behave as fluid-like scatterers (red lines), but the contribution to target strength of hard parts such as bones or cartilage can lead to complicated frequency responses, as shown here for (8) squid.

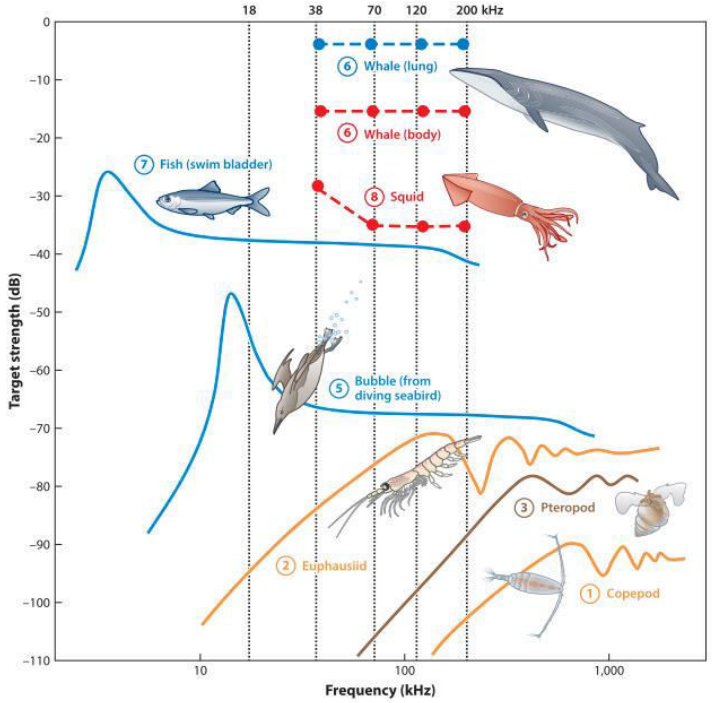

Source: (Benoit-Bird and Lawson, 2016).

4. Motivation and objectives

As briefly reviewed in the previous sections, the SWTA is characterised by the presence of a permanent thermocline (Araújo et al., 2011; Siedler et al., 2013; Thurman, 2019). A stably stratified thermocline plays an important and essential role in both the vertical flow of nutrients from deep water to the surface (e.g., Chen et al., 2018), and in the heat balance of the mixing layer in the tropical Atlantic (e.g., Jouanno et al., 2011; Nogueira Neto et al., 2018). In addition to the thermocline stratification, the depth of the mixing layer (ML) and the presence of barrier layers (BL) are other key factors governing the seasonal flux of heat content at the surface (Foltz et al., 2020; Nogueira Neto et al., 2018). Thermohaline variability also play a key role in the vertical structuring of pelagic habitats along the SWTA (e.g., Chaves et al., 2008; Sampaio de Souza et al., 2013). Nevertheless, in the SWTA data are still insufficient to access thermohaline structure information (vertical stratification/thermocline, ML depth, frequency of occurrence and thickness of BLs) at a high spatial and seasonal scale (e.g., Araújo et al., 2011; de Boyer Montégut et al., 2007; Nogueira Neto et al., 2018).

Moreover, the application of underwater acoustics tools in the SWTA, is still a little explored field. Most previous studies used passive acoustics for cetacean monitoring (e.g., Sousa-Lima et al., 2018; Wedekin et al., 2014). Whereas the use of active acoustics (scientific echosounder) is only reported for seabed classifications (Costa et al., 2013), the study of the behaviour of shallow water acoustic propagation (Chaves et al., 2011) and for observations of fish migration in a macrotidal mangrove channel (Krumme and Saint-Paul, 2003).

To further advance in these fields, we took advantage of the Acoustic along the BRAzilian COaSt (ABRACOS) surveys. These surveys were performed aboard the IRD R/V Antea (35 m long) in Sep. – Oct. 2015 and Apr. – May 2017 (Fig. 9). During these multidisciplinary surveys a variety of data were collected, including (i) Conductivity, Temperature, Depth (CTD), oxygen and fluorescence profiles; (ii) rosette sampling (e.g., nutriments, phytoplankton, particulate organic matter); (iii) ship-mounted Acoustic Doppler Current Profiler (SADCP); (iv) multifrequency echosounder (38, 70, 120 and 200 kHz); (iv) zooplankton hauls; and (v) bottom and pelagic trawls.

Figure 9. Acoustics along the Brazilian coast (ABRACOS) data were collected continuously along the two survey tracks (black lines) - ABRACOS 1 (a) and ABRACOS 2 (b) - and stations (green points). The surveys were performed on-board the French R/V Antea (c) equipped, among others, with SBE19 CTD mounted on a rosette (d), and multifrequency echosounders (38,70,120,200 kHz) operated from the scientific lab (e). RA: Rocas Atoll. FN: Fernando de Noronha archipelago.

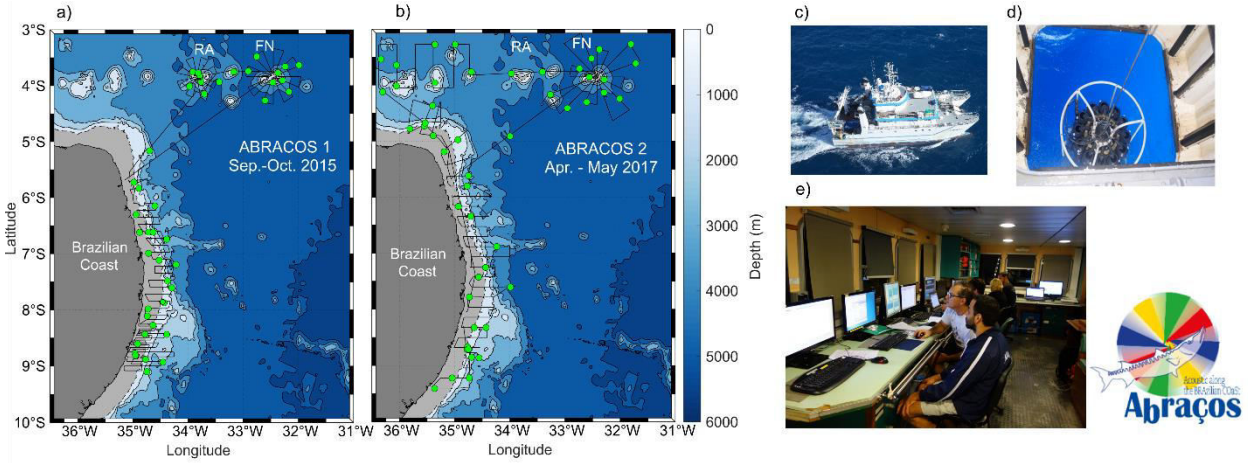

Source: Personal collection.

Based on this multidisciplinary framework this PhD thesis is organised over three main scientific objectives:

Objective 1: Characterise the 3D thermohaline structure of the SWTA in austral spring and fall by the functional statistics approach. (Chapter II)

Characterising the thermohaline structure in the upper ocean is typically based on the application of classical statistical methods on in situ vertical profiles. Such approach has important limitations since they do not explicitly contemplate the vertical nature of the profiles. Functional Data Analysis (FDA) (Pauthenet et al., 2017; Ramsay, 2006) is an alternative to address such drawbacks. Here we propose to apply an FDA framework to characterise the 3D thermohaline structure of the SWTA in spring and austral fall using CTD data from the ABRAÇOS surveys complemented by data available (CTD profiles or profiling floats data).

Objective 2: Test if the variation of the thermohaline structure could be extracted from acoustic data in the SWTA. (Chapter III)

In situ observations from CTD, XBT, Argo, and thermistors (Maze et al., 2017; Wijesekera and Boyd, 2001; Woods, 1968) provide high vertical resolution information on discrete stations. They allow for process description from large scales to mesoscales, but not on smaller scales. Within this perspective, active acoustic is a powerful tool since echosounders can capture fine-scale oceanographic structures typically attributed to biological scattering or turbulent structures (e.g., Klymak and Moum, 2003; Lavery et al., 2003; Pingree and Mardell, 1985). For instance, active acoustics has allowed the detections of abiotic properties such as the oxycline (Bertrand et al., 2010), internal waves (Grados et al., 2016; Holbrook et al., 2009; Holbrook and Fer, 2005; Orr et al., 2000), submesoscale to mesoscale eddies (Biescas et al., 2008; Grados et al., 2016; Ménesguen et al., 2012), thermocline (Ker et al., 2016; Stranne et al., 2018) and thermohaline staircases (Biescas et al., 2008; Fer et al., 2010; Ross and Lueck, 2005; Stranne et al., 2017). Following this framework, and the presence of a permanent thermocline in the SWTA, we hypothesise that it is possible to obtain information on the variation of the thermohaline structure (MLD, upper and lower limits of the thermocline) from acoustic data (proxy of the acoustic biomass). To test for this, we applied three different methods.

Objective 3: Investigate how environmental factors may be driving the vertical distribution of organisms in the southwestern tropical Atlantic. (Chapter IV)

Beyond large biogeographical constraints, the pelagic ecosystem structure can quickly respond to changes in water masses properties, hydrodynamic structures (Bertrand et al., 2014; Godø et al., 2012; Legendre, 1981; Prairie et al., 2012). More generally, physical forcing (e.g., light, stratification, oxygen, temperature, eddies) initiates the structuring of the oceanscape, and the distribution of planktonic organisms and predators tends to reflect the patchy distribution of their prey (Legendre, 1981; Margalef and Margalef, 1979). However, the description, quantification and understanding of the fine-scale relationships between biophysical and acoustic biota signal is still an exploratory science. In the SWTA it can even be considered an absent science until this moment. In this context, we propose to investigate the relationship between biophysical factors other than thermohaline structure on the vertical structuring of acoustic biomass in the SWTA. Beyond the upper ocean (10 - 300 m depth), we propose to extend the analyses to 650 m (vertical limit of acoustic sampling). In this way, we aim at filling some gaps in the understanding of the

relationships between physical oceanography and acoustic ecology in an oligotrophic environment such as the SWTA.

Finally, in Chapter V, we conclude this thesis by a general discussion.

References

Araújo, M., Limongi, C., Servain, J., Silva, M., Leite, F.S., Veleda, D., Lentini, C.A.D., 2011. Salinity-induced mixed and barrier layers in the southwestern tropical Atlantic Ocean off the northeast of Brazil. Ocean Sci. 7, 63–73. https://doi.org/10.5194/os-7-63-2011

Badal, M., Rughooputh, S., Rydberg, L., Robinson, I., Pattiaratchi, C., 2010. Eddy formation around South West Mascarene Plateau (Indian Ocean) as evidenced by satellite 'global ocean colour' data. West. Indian Ocean J. Mar. Sci. 8. https://doi.org/10.4314/wiojms.v8i2.56969

Ballón, M., Bertrand, A., Lebourges-Dhaussy, A., Gutiérrez, M., Ayón, P., Grados, D., Gerlotto, F., 2011. Is there enough zooplankton to feed forage fish populations off Peru? An acoustic (positive) answer. Prog. Oceanogr. 91, 360–381. https://doi.org/10.1016/j.pocean.2011.03.001

Béhagle, N., Cotté, C., Lebourges-Dhaussy, A., Roudaut, G., Duhamel, G., Brehmer, P., Josse, E., Cherel, Y., 2017. Acoustic distribution of discriminated micronektonic organisms from a bi-frequency processing: The case study of eastern Kerguelen oceanic waters. Prog. Oceanogr. https://doi.org/10.1016/j.pocean.2017.06.004

Benoit-Bird, K.J., Lawson, G.L., 2016. Ecological Insights from Pelagic Habitats Acquired Using Active Acoustic Techniques. Ann. Rev. Mar. Sci. 8, 463–490. https://doi.org/10.1146/annurev-marine-122414-034001

Bertrand, A., Ballón, M., Chaigneau, A., 2010. Acoustic observation of living organisms reveals the upper limit of the oxygen minimum zone. PLoS One 5. https://doi.org/10.1371/journal.pone.0010330

Bertrand, A., Grados, D., Colas, F., Bertrand, S., Capet, X., Chaigneau, A., Vargas, G., Mousseigne, A., Fablet, R., 2014. Broad impacts of fine-scale dynamics on seascape structure from zooplankton to seabirds. Nat. Commun. 5. https://doi.org/10.1038/ncomms6239

Biescas, B., Sallarès, V., Pelegrí, J.L., Machín, F., Carbonell, R., Buffett, G., Dañobeitia, J.J., Calahorrano, A., 2008. Imaging meddy finestructure using multichannel seismic reflection data. Geophys. Res. Lett. 35, L11609. https://doi.org/10.1029/2008GL033971

Bourlès, B., D'Orgeville, M., Eldin, G., Gouriou, Y., Chuchla, R., DuPenhoat, Y., Arnault, S., 2002. On the evolution of the thermocline and subthermocline eastward currents in the Equatorial Atlantic. Geophys. Res. Lett. 29, 32-1-32–4. https://doi.org/10.1029/2002GL015098

Brazilian Atlantic Islands: Fernando de Noronha and Atol das Rocas Reserves - UNESCO World Heritage Centre [WWW Document], n.d. URL https://whc.unesco.org/en/list/1000 (accessed

10.21.19).

Buckley, M.W., Marshall, J., 2016. Observations, inferences, and mechanisms of Atlantic Meridional Overturning Circulation variability: A review. Rev. Geophys. https://doi.org/10.1002/2015RG000493.Received

Caesar, L., McCarthy, G.D., Thornalley, D.J.R., Cahill, N., Rahmstorf, S., 2021. Current Atlantic Meridional Overturning Circulation weakest in last millennium. Nat. Geosci. 14, 118–120. https://doi.org/10.1038/s41561-021-00699-z

Cardoso, C., Caldeira, R.M.A., Relvas, P., Stegner, A., 2020. Islands as eddy transformation and generation hotspots: Cabo Verde case study. Prog. Oceanogr. 184, 102271. https://doi.org/10.1016/j.pocean.2020.102271

Chaves, A.H.S., Pessek, K., Guimarães, L.G., Ribeiro, C.E.P., 2011. Shallow Water Acoustic Propagation at Arraial do Cabo, Brazil, in: 12th International Congress of the Brazilian Geophysical Society & EXPOGEF, Rio de Janeiro, Brazil, 15–18 August 2011. Brazilian Geophysical Society, pp. 926–928. https://doi.org/10.1190/sbgf2011-191

Chaves, T.B.C., Mafalda Jr., P.O., Santos, C., Souza, C.S., Moura, G., Sampaio, J., Melo, G., 2008. Biomassa planctônica e hidrografia na zona econômica exclusiva do nordeste do brasil. Trop. Oceanogr. 36, 14–27.

Cheng, W., Chiang, J.C.H., Zhang, D., 2013. Atlantic meridional overturning circulation (AMOC) in CMIP5 Models: RCP and historical simulations. J. Clim. 26, 7187–7197. https://doi.org/10.1175/JCLI-D-12-00496.1

Colna, K.E., 2017. Latitudinal Position and Trends of the Intertropical Convergence Zone (ITCZ) and its Relationship with Upwelling in the Southern Caribbean Sea and Global Climate Indices. University of South Florida.

Costa, P.L., Madureira, L.A.S.P., de Pinho, M.P., 2013. Seabed acoustic classification in the Pelotas basin, Brazil. Brazilian J. Oceanogr. 61, 13–22. https://doi.org/10.1590/S1679-87592013000100002

Coyle, K.O., Cooney, R.T., 1993. Water column sound scattering and hydrography around the Pribilof Islands, Bering Sea. Cont. Shelf Res. 13, 803–827. https://doi.org/10.1016/0278-4343(93)90028-V

Cronin, M.F., Weller, R.A., Lampitt, R.S., Send, U., 2012. Ocean Reference Stations, in: Earth Observation. InTech. https://doi.org/10.5772/27423

Cullen, J.J., 1982. The deep chlorophyll maximum: comparing vertical profiles of chlorophyll a. Can. J. Fish. Aquat. Sci. 39, 791–803. https://doi.org/10.1139/f82-108

da Silveira, I.C.A., Miranda, L.B., Brown, W.S., 1994. On the origins of the North Brazil Current. J. Geophys. Res. 99, 22501. https://doi.org/10.1029/94JC01776

de Boyer Montégut, C., Mignot, J., Lazar, A., Cravatte, S., 2007. Control of salinity on the mixed layer depth in the world ocean: 1. General description. J. Geophys. Res. Ocean. 112, 1–12. https://doi.org/10.1029/2006JC003953

De Robertis, A., McKelvey, D.R., Ressler, P.H., 2010. Development and application of an empirical multifrequency method for backscatter classification. Can. J. Fish. Aquat. Sci. 67, 1459–1474. https://doi.org/10.1139/F10-075

Dossa, A.N., Silva, A.C. da, Chaigneau, A., Eldin, G., Araújo, M., Bertrand, A., 2021. Near-surface western boundary circulation off Northeast Brazil. Prog. Oceanogr. 190, 102475. https://doi.org/10.1016/j.pocean.2020.102475

Doty, M.S., Oguri, M., 1956. The Island Mass Effect. ICES J. Mar. Sci. 22, 33–37. https://doi.org/10.1093/icesjms/22.1.33

Fahey, D.., Doherty, S.J., Hibbard, K.A., Romanou, A., Taylor, P.C., 2017. Ch. 2: Physical Drivers of Climate Change. Climate Science Special Report: Fourth National Climate Assessment, Volume I. Washington, DC. https://doi.org/10.7930/J0513WCR

Fer, I., Nandi, P., Holbrook, W.S., Schmitt, R.W., Páramo, P., 2010. Seismic imaging of a thermohaline staircase in the western tropical North Atlantic. Ocean Sci. 6, 621–631. https://doi.org/10.5194/os-6-621-2010

Figueiredo, G.G.A.A. de, Schwamborn, R., Bertrand, A., Munaron, J.-M., Le Loc'h, F., 2020. Body size and stable isotope composition of zooplankton in the western tropical Atlantic. J. Mar. Syst. 212, 103449. https://doi.org/10.1016/j.jmarsys.2020.103449

Foltz, G.R., Brandt, P., Richter, I., Rodríguez-Fonseca, B., Hernandez, F., Dengler, M., Rodrigues, R.R., Schmidt, J.O., Yu, L., Lefevre, N., Da Cunha, L.C., McPhaden, M.J., Araújo, M., Karstensen, J., Hahn, J., Martín-Rey, M., Patricola, C.M., Poli, P., Zuidema, P., Hummels, R., Perez, R.C., Hatje, V., Lübbecke, J.F., Polo, I., Lumpkin, R., Bourlès, B., Asuquo, F.E., Lehodey, P., Conchon, A., Chang, P., Dandin, P., Schmid, C., Sutton, A., Giordani, H., Xue, Y., Illig, S., Losada, T., Grodsky, S.A., Gasparin, F., Lee, T., Mohino, E., Nobre, P., Wanninkhof, R., Keenlyside, N., Garcon, V., Sánchez-Gómez, E., Nnamchi, H.C., Drévillon, M., Storto, A., Remy, E., Lazar, A., Speich, S., Goes, M., Dorrington, T., Johns, W.E., Moum, J.N., Robinson, C., Perruche, C., de Souza, R.B., Gaye, A.T., López-Parages, J., Monerie, P.-A., Castellanos, P., Benson, N.U., Hounkonnou, M.N., Duhá, J.T., Laxenaire, R., Reul, N., 2019. The Tropical Atlantic Observing System. Front. Mar. Sci. 6. https://doi.org/10.3389/fmars.2019.00206

Foltz, G.R., Hummels, R., Dengler, M., Perez, R.C., Araújo, M., 2020. Vertical turbulent cooling of the mixed layer in the Atlantic ITCZ and trade wind regions. J. Geophys. Res. Ocean. 125. https://doi.org/10.1029/2019jc015529

Foltz, G.R., McPhaden, M.J., 2008. Seasonal mixed layer salinity balance of the tropical North Atlantic Ocean. J. Geophys. Res. 113, C02013. https://doi.org/10.1029/2007JC004178

Gilmartin, M., Revelante, N., 1974. The "island mass" effect on the phytoplankton and primary production of the Hawaiian Islands. J. Exp. Mar. Bio. Ecol. 16, 181–204. https://doi.org/10.1016/0022-0981(74)90019-7

Godø, O.R., Samuelsen, A., Macaulay, G.J., Patel, R., Hjøllo, S.S., Horne, J., Kaartvedt, S., Johannessen, J.A., 2012. Mesoscale Eddies Are Oases for Higher Trophic Marine Life. PLoS One 7, e30161. https://doi.org/10.1371/journal.pone.0030161

Grados, D., Bertrand, A., Colas, F., Echevin, V., Chaigneau, A., Gutiérrez, D., Vargas, G., Fablet, R., 2016. Spatial and seasonal patterns of fine-scale to mesoscale upper ocean dynamics in an Eastern Boundary Current System. Prog. Oceanogr. 142, 105–116. https://doi.org/10.1016/j.pocean.2016.02.002

Holbrook, W.S., Fer, I., 2005. Ocean internal wave spectra inferred from seismic reflection transects. Geophys. Res. Lett. 32, 2–5. https://doi.org/10.1029/2005GL023733

Holbrook, W.S., Fer, I., Schmitt, R.W., 2009. Images of internal tides near the Norwegian continental slope. Geophys. Res. Lett. 36, 1–5. https://doi.org/10.1029/2009GL038909

Hounsou-gbo, G.A., Araújo, M., Bourlès, B., Veleda, D., Servain, J., 2015. Tropical Atlantic Contributions to Strong Rainfall Variability Along the Northeast Brazilian Coast. Adv. Meteorol. 2015, 1–13. https://doi.org/10.1155/2015/902084

Hummels, R., Brandt, P., Dengler, M., Fischer, J., Araújo, M., Veleda, D., Durgadoo, J. V., 2015. Interannual to decadal changes in the western boundary circulation in the Atlantic at 11°S. Geophys. Res. Lett. 42, 7615–7622. https://doi.org/10.1002/2015GL065254

Jouanno, J., Marin, F., du Penhoat, Y., Sheinbaum, J., Molines, J.-M., 2011. Seasonal heat balance in the upper 100 m of the equatorial Atlantic Ocean. J. Geophys. Res. 116, C09003. https://doi.org/10.1029/2010JC006912

Ker, S., Le Gonidec, Y., Marié, L., 2016. Multifrequency seismic detectability of seasonal thermoclines assessed fromARGO data. J. Geophys. Res. Ocean. 3741–3756. https://doi.org/10.1002/2015JC011228.Received

Klymak, J.M., Moum, J.N., 2003. Internal solitary waves of elevation advancing on a shoaling shelf. Geophys. Res. Lett. 30, 2003GL017706. https://doi.org/10.1029/2003GL017706

Kowsmann, R.O., Costa, M.P.A., 1976. Estratigrafia sismica do plato de pernambuco. Rev. Bras. Geociencias 6, 95–101.

Krumme, U., Saint-Paul, U., 2003. Observations of fish migration in a macrotidal mangrove channel in Northern Brazil using a 200-kHz split-beam sonar. Aquat. Living Resour. 16, 175–184. https://doi.org/10.1016/S0990-7440(03)00046-9

Lavery, A.C., Chu, D., Moum, J.N., 2010. Measurements of acoustic scattering from zooplankton and oceanic microstructure using a broadband echosounder. ICES J. Mar. Sci. 67, 379–394. https://doi.org/10.1093/icesjms/fsp242

Lavery, A.C., Wiebe, P.H., Stanton, T.K., Lawson, G.L., Benfield, M.C., Copley, N., 2007. Determining dominant scatterers of sound in mixed zooplankton populations. J. Acoust. Soc. Am. 122, 3304–3326. https://doi.org/10.1121/1.2793613

Leach, T.H., Beisner, B.E., Carey, C.C., Pernica, P., Rose, K.C., Huot, Y., Brentrup, J.A., Domaizon, I., Grossart, H.P., Ibelings, B.W., Jacquet, S., Kelly, P.T., Rusak, J.A., Stockwell, J.D., Straile, D., Verburg, P., 2018. Patterns and drivers of deep chlorophyll maxima structure in 100 lakes: The relative importance of light and thermal stratification. Limnol. Oceanogr. 63, 628–646. https://doi.org/10.1002/lno.10656

Legendre, L., 1981. Hydrodynamic Control of Marine Phytoplankton Production: The Paradox of

Stability, in: Elsevier Oceanography Series. pp. 191–207. https://doi.org/10.1016/S0422-9894(08)70410-0

Lira, S.M. de A., Teixeira, I. de Á., de Lima, C.D.M., Santos, G. de S., Leitão, S.N., Schwamborn, R., 2014. Spatial and nycthemeral distribution of the zooneuston off fernando de noronha, Brazil. Brazilian J. Oceanogr. 62, 35–45. https://doi.org/10.1590/S1679-87592014058206201

Liu, M., Tanhua, T., 2019. Distribution of Water Masses in the Atlantic Ocean based on GLODAPv2. Ocean Sci. Discuss. 1–32. https://doi.org/10.5194/os-2018-140

Longhurst, A.R., Pauly, D., 1987. Ecology of Tropical Oceans, Ecology of tropical oceans. Elsevier. https://doi.org/10.1016/C2009-0-02861-X

Lumpkin, R., Garzoli, S.L., 2005. Near-surface circulation in the Tropical Atlantic Ocean. Deep Sea Res. Part I Oceanogr. Res. Pap. 52, 495–518. https://doi.org/10.1016/j.dsr.2004.09.001

Lumpkin, R., Speer, K., 2007. Global ocean meridional overturning. J. Phys. Oceanogr. 37, 2550–2562. https://doi.org/10.1175/JPO3130.1

Lüthi, D., Le Floch, M., Bereiter, B., Blunier, T., Barnola, J.-M., Siegenthaler, U., Raynaud, D., Jouzel, J., Fischer, H., Kawamura, K., Stocker, T.F., 2008. High-resolution carbon dioxide concentration record 650,000–800,000 years before present. Nature 453, 379–382. https://doi.org/10.1038/nature06949

MacLennan, D.N., Fernandes, P.G., Dalen, J., 2002. A consistent approach to definitions and symbols in fisheries acoustics. ICES J. Mar. Sci. 59, 365–369. https://doi.org/10.1006/jmsc.2001.1158

Margalef, Ramón, Margalef, Ramon, 1979. The Organization of Space. Oikos 33, 152. https://doi.org/10.2307/3543992

Matos, F.D.A.O., Pereira, J., Dengler, M., 2020. Salinity Biases and the Variability of the Atlantic Meridional Overturning Circulation in GFDL-CM3. Ocean Sci. J. 55, 505–520. https://doi.org/10.1007/s12601-020-0040-8

Maze, G., Mercier, H., Fablet, R., Tandeo, P., Lopez Radcenco, M., Lenca, P., Feucher, C., Le Goff, C., 2017. Coherent heat patterns revealed by unsupervised classification of Argo temperature profiles in the North Atlantic Ocean. Prog. Oceanogr. 151, 275–292. https://doi.org/10.1016/j.pocean.2016.12.008

Medwin, H., Clay, C.S., 1997. Fundamentals of Acoustical Oceanography, 1st ed. Academic Press.

Ménesguen, C., Hua, B.L., Carton, X., Klingelhoefer, F., Schnürle, P., Reichert, C., 2012. Arms winding around a meddy seen in seismic reflection data close to the Morocco coastline. Geophys. Res. Lett. 39, 1–6. https://doi.org/10.1029/2011GL050798

Molinari, R.L., 1982. Observations of Eastward Currents in the Tropical South Atlantic Ocean: 1978-1980. J. Geophys. Res. 87, 9707–9714.

Morel, A., Claustre, H., Gentili, B., 2010. The most oligotrophic subtropical zones of the global ocean: similarities and differences in terms of chlorophyll and yellow substance. Biogeosciences Discuss. 7, 5047–5079. https://doi.org/10.5194/bgd-7-5047-2010

Motoki, A., Freire Motoki, K., 2020. Satellite gravimetry for the Fernando de Noronha Chain, Northeast Brazil, and its bearing on the volcanic seamount structure 1–6. https://doi.org/10.22564/5simbgf2012.108

Nogueira Neto, A. V., Giordani, H., Caniaux, G., Araújo, M., 2018. Seasonal and Interannual Mixed-Layer Heat Budget Variability in the Western Tropical Atlantic From Argo Floats (2007–2012). J. Geophys. Res. Ocean. 123, 5298–5322. https://doi.org/10.1029/2017JC013436

Olivar, M.P., Hulley, P.A., Castellón, A., Emelianov, M., López, C., Tuset, V.M., Contreras, T., Molí, B., 2017. Mesopelagic fishes across the tropical and equatorial Atlantic: Biogeographical and vertical patterns. Prog. Oceanogr. 151, 116–137. https://doi.org/10.1016/j.pocean.2016.12.001

Orr, M.H., Haury, L.R., Wiebe, P.H., Briscoe, M.G., 2000. Backscatter of high-frequency (200 kHz) acoustic wavefields from ocean turbulence. J. Acoust. Soc. Am. 108, 1595–1601. https://doi.org/10.1121/1.1286883

Pensieri, S., Bozzano, R., 2017. Active and Passive Acoustic Methods for In-situ Monitoring of the Ocean Status, in: Advances in Underwater Acoustics. InTech. https://doi.org/10.5772/intechopen.68998

Pérez-Santos, I., Castro, L., Ross, L., Niklitschek, E., Mayorga, N., Cubillos, L., Gutierrez, M., Escalona, E., Castillo, M., Alegría, N., Daneri, G., 2018. Turbulence and hypoxia contribute to dense biological scattering layers in a Patagonian fjord system. Ocean Sci. 14, 1185–1206. https://doi.org/10.5194/os-14-1185-2018

Peterson, R.G., Stramma, L., 1991. Upper-level circulation in the South Atlantic Ocean. Prog. Oceanogr. 26, 1–73. https://doi.org/10.1016/0079-6611(91)90006-8

Pingree, R.D., Mardell, G.T., 1985. Solitary internal waves in the Celtic Sea. Prog. Oceanogr. 14, 431–441. https://doi.org/10.1016/0079-6611(85)90021-7

Poole, R., Tomczak, M., 1999. Optimum multiparameter analysis of the water mass structure in the Atlantic Ocean thermocline. Deep Sea Res. Part I Oceanogr. Res. Pap. 46, 1895–1921. https://doi.org/10.1016/S0967-0637(99)00025-4

Prairie, J.C., Sutherland, K.R., Nickols, K.J., Kaltenberg, A.M., 2012. Biophysical interactions in the plankton: A cross-scale review. Limnol. Oceanogr. Fluids Environ. 2, 121–145. https://doi.org/10.1215/21573689-1964713

Rodrigues, R.R., Rothstein, L.M., Wimbush, M., 2007. Seasonal Variability of the South Equatorial Current Bifurcation in the Atlantic Ocean: A Numerical Study. J. Phys. Oceanogr. 37, 16–30. https://doi.org/10.1175/JPO2983.1

Roemmich, D., Wunsch, C., 1985. Two transatlantic sections: meridional circulation and heat flux in the subtropical North Atlantic Ocean. Deep Sea Res. Part A, Oceanogr. Res. Pap. 32, 619–664. https://doi.org/10.1016/0198-0149(85)90070-6

Ross, T., Lueck, R., 2005. Estimating turbulent dissipation rates from acoustic backscatter. Deep. Res. Part I Oceanogr. Res. Pap. 52, 2353–2365. https://doi.org/10.1016/j.dsr.2005.07.002

Sabra, K.G., 2015. Paul Langevin's contributions to the development of underwater acoustics. J. Acoust. Soc. Am. 137, 2273–2273. https://doi.org/10.1121/1.4920301

Sallée, J., Pellichero, V., Akhoudas, C., Pauthenet, E., Vignes, L., Schmidtko, S., Garabato, A.N., Sutherland, P., Kuusela, M., 2021. Summertime increases in upper-ocean stratification and mixed-layer depth. Nature 591, 592–598. https://doi.org/10.1038/s41586-021-03303-x

Salvetat, J., Lebourges-Dhaussy, A., Travassos, P., Gastauer, S., Roudaut, G., Vargas, G., Bertrand, A., 2020. Insitu target strength measurement of the black triggerfish Melichthys niger and the ocean triggerfish Canthidermis sufflamen. Mar. Freshw. Res. 1–18. https://doi.org/10.1071/MF19153

Sampaio de Souza, C., Guimarães da Luz, J.A., Macedo, S., Montes, M.D.J.F., Mafalda, P., 2013. Chlorophyll a and nutrient distribution around seamounts and islands of the tropical south-western Atlantic. Mar. Freshw. Res. 64, 168. https://doi.org/10.1071/MF12075

Schneider, T., Bischoff, T., Haug, G.H., 2014. Migrations and dynamics of the intertropical convergence zone. Nature. https://doi.org/10.1038/nature13636

Schott, F.A., Brandt, P., Hamann, M., Fischer, J., Stramma, L., 2002. On the boundary flow off Brazil at 5-10°S and its connection to the interior tropical Atlantic. Geophys. Res. Lett. 29, 21-1-21–4. https://doi.org/10.1029/2002GL014786

Segura, H., Espinoza, J.C., Junquas, C., Lebel, T., Vuille, M., Garreaud, R., 2020. Recent changes in the precipitation-driving processes over the southern tropical Andes/western Amazon. Clim. Dyn. 54, 2613–2631. https://doi.org/10.1007/s00382-020-05132-6

Serafini, T.Z., França, G.B. De, Andriguetto-Filho, J.M., 2010. Ilhas oceânicas brasileiras: biodiversidade conhecida e sua relação com o histórico de uso e ocupação humana. Rev. Gestão Costeira Integr. 10, 281–301. https://doi.org/10.5894/rgci178

Siedler, G., Griffies, S., Gould, J., Church, J., 2013. Ocean Circulation and Climate. Academic Press.

Silva, A.C. da, Chaigneau, A., Dossa, A.N., Eldin, G., Araújo, M., Bertrand, A., 2021. Surface circulation and vertical structure of upper ocean variability around Fernando de Noronha archipelago and Rocas atoll during spring 2015 and fall 2017. Front. Mar. Sci. https://doi.org/10.3389/fmars.2021.598101

Silva, M., Araújo, M., Servain, J., Penven, P., Lentini, C.A.D., 2009. High-resolution regional ocean dynamics simulation in the southwestern tropical Atlantic. Ocean Model. 30, 256–269. https://doi.org/10.1016/j.ocemod.2009.07.002

Simmonds, J., MacLennan, D., 2005. Fisheries Acoustics, Fisheries Acoustics: Theory and Practice: Second Edition. Blackwell Publishing Ltd, Oxford, UK. https://doi.org/10.1002/9780470995303

Sousa-Lima, R., Engel, M.H., Sábato, V., Lima, B.R., Queiróz, T.S.M., Casagrande, T., Honda, L.K., Gonçalves, M.I.C., Baumgarten, J.E., Andriolo, A., Ribeiro, M.C., Clark, C.W., 2018. Acoustic ecology of humpback whales in Brazilian waters investigated with basic and sophisticated passive acoustic technologies over 17 years. WIO J. Mar. Sci. 23–40.

Sprintall, J., Tomczak, M., 1993. On the formation of central water and thermocline ventilation in the southern hemisphere. Deep. Res. Part I 40, 827–848. https://doi.org/10.1016/0967-0637(93)90074-D

Stanton, T., 1994. Acoustic characterization and discrimination of marine zooplankton and turbulence. ICES J. Mar. Sci. 51, 469–479. https://doi.org/10.1006/jmsc.1994.1048

Stanton, T.K., Chu, D., Wiebe, P.H., 1998. Sound scattering by several zooplankton groups. II. Scattering models. J. Acoust. Soc. Am. 103, 236–253. https://doi.org/10.1121/1.421110

Stramma, L., 1991. Geostrophic transport of the South Equatorial Current in the Atlantic. J. Mar. Res. 49, 281–294. https://doi.org/10.1357/002224091784995864

Stramma, L., England, M., 1999. On the water masses and mean circulation of the South Atlantic Ocean. J. Geophys. Res. Ocean. 104, 20863–20883. https://doi.org/10.1029/1999JC900139

Stramma, L., Rhein, M., Brandt, P., Dengler, M., Böning, C., Walter, M., 2005. Upper ocean circulation in the western tropical Atlantic in boreal fall 2000. Deep Sea Res. Part I Oceanogr. Res. Pap. 52, 221–240. https://doi.org/10.1016/j.dsr.2004.07.021

Stramma, L., Schott, F.A., 1999. The mean flow field of the tropical Atlantic Ocean. Deep Sea Res. Part II Top. Stud. Oceanogr. 46, 279–303. https://doi.org/10.1016/S0967-0645(98)00109-X

Stranne, C., Mayer, L., Jakobsson, M., Weidner, E., Jerram, K., Weber, T.C., Anderson, L.G., Nilsson, J., Björk, G., Gårdfeldt, K., 2018. Acoustic mapping of mixed layer depth. Ocean Sci. 14, 503–514. https://doi.org/10.5194/os-14-503-2018

Stranne, C., Mayer, L., Weber, T.C., Ruddick, B.R., Jakobsson, M., Jerram, K., Weidner, E., Nilsson, J., Gårdfeldt, K., 2017. Acoustic mapping of thermohaline staircases in the arctic ocean. Sci. Rep. 7, 1–9. https://doi.org/10.1038/s41598-017-15486-3

Talley, L.D., Pickard, G.L., Emery, W.J., Swift, J.H., 2011. Descriptive Physical Oceanography. An introduction, 6th ed.

Tchamabi, C.C., Araújo, M., Silva, M., Bourlès, B., 2017. A study of the Brazilian Fernando de Noronha Island and Rocas Atoll wakes in the tropical Atlantic. Ocean Model. https://doi.org/10.1016/j.ocemod.2016.12.009

Thurman, H.V., 2019. Essentials of oceanography, Thirteenth. ed. Pearson Education: Hoboken.

Tosetto, E.G., Bertrand, A., Neumann-Leitão, S., Costa da Silva, A., Nogueira Júnior, M., 2021. Spatial patterns in planktonic cnidarian distribution in the western boundary current system of the tropical South Atlantic Ocean. J. Plankton Res. 43, 270–287. https://doi.org/10.1093/plankt/fbaa066

Trenkel, V.M., Handegard, N.O., Weber, T.C., 2016. Observing the ocean interior in support of integrated management, in: ICES Journal of Marine Science. Oxford University Press, pp. 1947–1954. https://doi.org/10.1093/icesjms/fsw132

Trenkel, V.M., Ressler, P.H., Jech, M., Giannoulaki, M., Taylor, C., 2011. Underwater acoustics for ecosystem-based management: State of the science and proposals for ecosystem

indicators. Mar. Ecol. Prog. Ser. 442, 285–301. https://doi.org/10.3354/meps09425

Trevorrow, M. V., 1998. Observations of internal solitary waves near the Oregon coast with an inverted echo sounder. J. Geophys. Res. Ocean. 103, 7671–7680. https://doi.org/10.1029/98JC00101

Urick, R.J., 1983. Principles of Underwater Sound.

Utida, G., Cruz, F.W., Etourneau, J., Bouloubassi, I., Schefuß, E., Vuille, M., Novello, V.F., Prado, L.F., Sifeddine, A., Klein, V., Zular, A., Viana, J.C.C., Turcq, B., 2019. Tropical South Atlantic influence on Northeastern Brazil precipitation and ITCZ displacement during the past 2300 years. Sci. Rep. 9, 1–8. https://doi.org/10.1038/s41598-018-38003-6

Venancio, I.M., Shimizu, M.H., Santos, T.P., Lessa, D.O., Portilho-Ramos, R.C., Chiessi, C.M., Crivellari, S., Mulitza, S., Kuhnert, H., Tiedemann, R., Vahlenkamp, M., Bickert, T., Sampaio, G., Albuquerque, A.L.S., Veiga, S., Nobre, P., Nobre, C., 2020. Changes in surface hydrography at the western tropical Atlantic during the Younger Dryas. Glob. Planet. Change 184, 103047. https://doi.org/10.1016/j.gloplacha.2019.103047

Verma, A., Kloser, R.J., Duncan, A.J., 2017. Potential Use of Broadband Acoustic Methods for Micronekton Classification. Acoust. Aust. 45, 353–361. https://doi.org/10.1007/s40857-017-0105-8

Waliser, D.E., Gautier, C., 1993. A Satellite-derived Climatology of the ITCZ. J. Clim. 6, 2162–2174. https://doi.org/10.1175/1520-0442(1993)006<2162:ASDCOT>2.0.CO;2

Warren, J.D., Stanton, T.K., Wiebe, P.H., Seim, H.E., 2003. Inference of biological and physical parameters in an internal wave using multiple-frequency, acoustic-scattering data. ICES J. Mar. Sci. 60, 1033–1046. https://doi.org/10.1016/S1054-3139(03)00121-8

Warren, J.D., Wiebe, P.H., 2008. Accounting for biological and physical sources of acoustic backscatter improves estimates of zooplankton biomass, Canadian Journal of Fisheries and Aquatic Sciences. https://doi.org/10.1139/F08-047

Wedekin, L., Rossi-Santos, M., Baracho, C., Cypriano-Souza, A., Simões-Lopes, P., 2014. Cetacean records along a coastal-offshore gradient in the Vitória-Trindade Chain, western South Atlantic Ocean. Brazilian J. Biol. 74, 137–144. https://doi.org/10.1590/1519-6984.21812

Wijesekera, H., Boyd, T.J., 2001. Upper Ocean Heat And Freshwater Budgets, in: Encyclopedia of Ocean Sciences. Elsevier, pp. 3079–3083. https://doi.org/10.1006/rwos.2001.0153

Woods, J.D., 1968. Wave-induced shear instability in the summer thermocline, J. Fluid Mech.

Zhang, D., McPhaden, M.J., Johns, W.E., 2003. Observational Evidence for Flow between the Subtropical and Tropical Atlantic: The Atlantic Subtropical Cells*. J. Phys. Oceanogr. 33, 1783–1797. https://doi.org/10.1175/2408.1

CHAPTER II:
3D CHARACTERISATION OF THE THERMOHALINE STRUCTURE IN THE SOUTHWESTERN TROPICAL ATLANTIC DERIVED FROM FUNCTIONAL DATA ANALYSIS OF IN SITU PROFILES

This chapter corresponds to the article of the same title and referenced as: ***Ramilla V. ASSUNÇÃO**, Alex C. SILVA, Amédèe ROY, Bernard BOURLÈS, Carlos HENRIQUE S. SILVA, Jean-François TERNON, Moacyr ARAUJO, Arnaud BERTRAND, 3D characterisation of the thermohaline structure in the southwestern tropical Atlantic derived from functional data analysis of in situ profiles, **PROGRESS IN OCEANOGRAPHY**, **Volume 187, 2020, 102399, ISSN 0079-6611.** https://doi.org/10.1016/j.pocean.2020.102399.*

Abstract

The dynamic of the thermohaline structure of the upper ocean, which depends on ocean-atmosphere interactions, drives most near surface oceanic processes, including the control of gases and heat fluxes, and nutrient availability in the photic layer. The thermohaline structure of the southwestern tropical Atlantic (SWTA), a key region for diagnosing variation of the Atlantic Meridional Overturning Circulation, has prime impact on global climate. Characterising the thermohaline structure is typically based on the application of classical statistical methods on vertical profiles. Such approach has important limitations since classical methods do not explicitly contemplate the vertical nature of the profiles. Functional Data Analysis (FDA) is a new alternative to solve such drawbacks. Here, we apply an FDA approach to characterise the 3D canonical thermohaline structure of the SWTA in austral spring and fall. Our results reveal a clear spatial pattern with the presence of three areas with significantly different thermohaline structure. Area 1, mostly located along the continental slope, reflects the western boundary current system, with low static stability and high frequency of occurrence of barrier layer (BL). Conversely, Area 2, located along the Fernando de Noronha chain, presents strong static stability with a well-marked thermocline. This area, under the influence of the eastern Atlantic, is characterised by a low BL frequency, which is seasonally modulated by the latitudinal oscillation of the Intertropical

Convergence Zone, controlling the regime of precipitation. In turn, Area 3 behaves as a transition zone between A1 and A2 with the presence of the water core of maximum salinity in subsurface, and therefore presence of strong-moderate BL. Beyond this study, FDA approach emerges as a powerful way to describe, characterise, classify and compare ocean patterns and processes. It can be applied to *in situ* data but could also be used to explore ocean model output deeply and comprehensively.

Keywords: Thermocline, barrier layer, mixed layer, western boundary current, ocean stratification, North Brazilian Undercurrent system

1. Introduction

An important and prevalent feature of the thermohaline structure of the upper ocean (here defined as the ocean region from the surface to 300 m depth) is the mixed layer (ML) occupying the first meters of the water column, in which temperature and salinity are vertically homogenous (Brainerd and Gregg, 1995). The thickness of the ML (Mixed Layer Depth - MLD) and the underlying discontinuity layers vary at different spatiotemporal scales (Grados et al., 2016; Kara, 2003). They are indeed controlled by surface forcing (heat exchange, wind-driving turbulent mixing, evaporation – precipitation budget, river inputs), Ekman pumping, advection of upwelled waters and internal waves (Halpern, 2002; Ker et al., 2016; Liu, 1993; Sprintall and Cronin, 2010).

Dynamical interactions between the oceanic ML and the thermocline/pycnocline drive most near surface oceanic motions (Chen et al., 1994; Rippert et al., 2015). In addition to ocean–atmosphere interaction, the storage of several gases (e.g., carbon dioxide and methane) and heat content are influenced by the variations in MLD (de Boyer Montégut et al., 2004; Kraus and Businger, 1994). Changes in MLD and thermocline thickness also affect the primary productivity (Jang et al., 2011; Sverdrup, 1953) by altering nutrients availability in the photic layer (Carranza et al., 2018; Madhupratap et al., 1981). Furthermore, deformations of the thermocline/pycnocline drive the seascape biological structure from zooplankton to top predators (Bertrand et al., 2014).

In some oceanic areas, the upper limit of the halocline is shallower than that of the thermocline, generating a barrier layer (BL) (Lukas and Lindstrom, 1991; Sprintall and Tomczak, 1992). The BL exerts an important influence on ML dynamics and, in particular, the interplay between kinetic

and potential energy processes. This may affect the ocean heat budget (Pailler et al., 1999; Swenson and Hansen, 1999) through the heat fluxes with the atmosphere impacting meteorological conditions and rainfall regimes, with, for example, the generation of heavy precipitations (Balaguru et al., 2012; Hounsou-gbo et al., 2015). The BL also inhibits the transport of nutrients from deep water into the ML, which may results in nutrients depleted surface water (Williams and Grottoli, 2010).

The thermohaline circulation and associated inter-hemispheric transports of mass, heat, and salt in the southwestern tropical Atlantic (SWTA) has prime impact on global climate (Bourlès et al., 1999). The western boundary current system off Brazil is indeed a key region for diagnosing variations of the Atlantic Meridional Overturning Circulation (AMOC) by the southern wind-driven subtropical–tropical cell (STC). The STC is a shallow meridional overturning circulation transporting water subducted in the subtropics during the winter season to the tropics, where it is upwelled to the surface (Hummels et al., 2015; Zhang et al., 2003). It is an area through which oceanic signals on various timescales, from intra-seasonal to decadal scales pass (Dengler et al., 2004; Stramma and England, 1999). In this region, the intrusion of subtropical underwater (SUW) advected by the southern branch of the South Equatorial Current (sSEC) and then by North Brazilian Undercurrent (NBUC) (Bourlès et al., 1999; Rodrigues et al., 2007; Silva et al., 2009; Stramma and Schott, 1999), is pointed out as a major process contributing to seasonal BL variability (Araujo et al., 2011).

The characterization of the thermohaline structure of an ocean region, as the SWTA, is typically based on vertical profiles measurements, where data is as discrete set of observations of temperature and salinity sampled at varying depths. However, the use of classical statistical methods for comparing or clustering such datasets (e.g., Principal Component Analysis (PCA) and Analysis of variance (ANOVA)) have important limitations. Indeed, classical methods do not explicitly contemplate the vertical nature of the profiles. For example, in a PCA matrix, vertical profiles depths are ordered in columns, but PCA is invariant under permutation of columns in the data matrix. Functional Data Analysis (FDA) are a new alternative to solve this and other problems such as the use of diverse and heterogeneous datasets (Nerini et al., 2010; Pauthenet et al., 2019, 2017; Reyes et al., 2015).

FDA accounts for the functional nature of the data i.e., observed data are considered as a function rather than a vector of multiple measurements (Bayle et al., 2015; Pauthenet et al., 2017). Besides that, the extension of kriging techniques to the functional setting meets the need of interpolating complex data collected in a limited number of spatial locations and thus improve spatial inference (Menafoglio et al., 2013). If the functional nature of a functional dataset is ignored, results typically are sub-optimal as valuable information related to the functional nature of a dataset is not properly utilised (Hadjipantelis and Müller, 2018; Nerini et al., 2010).

Here, we propose to use functional statistics methods to characterise the 3D thermohaline structure of the SWTA in austral spring and fall. For that purpose, we used temperature and salinity profiles from two multidisciplinary surveys performed in northeast Brazil in spring 2015 and fall 2017. To construct a canonical picture of the spring and fall conditions we also used available profiles achieved in the SWTA in the same seasons in other years. Merging these databases was possible since the results of functional ANOVA did not reveal significant difference among datasets. From this, we provide a synoptic view of seasonal states of the thermohaline structure in the SWTA and reveal the presence of two different areas and one transition region, evidencing the variety of ocean–atmosphere processes in play in the region.

2. Material and Methods

2.1. Data

Conductivity, Temperature, Depth (CTD) hydrographic profiles were acquired using a CTD Seabird SBE911 + during the two multidisciplinary surveys Acoustic along the BRAzilian CoaSt (ABRACOS). The surveys were performed in northeast Brazil (Fig. 1, triangles) on-board the French R/V Antea in September and October 2015 (austral spring; ABRACOS1; Bertrand, 2015) and in April and May 2017 (austral fall; ABRACOS2; Bertrand, 2017).

To provide a more comprehensive view of the thermohaline structure in the SWTA in spring and fall, we also considered the use of ancillary vertical CTD profiles or profiling floats data from: (i) the World Ocean Atlas 2013 (https://www.nodc.noaa.gov/OC5/WOD13/); (ii) the REVIZEE program (Araujo et al. 2019); and (iii) the PANGEA Data Publisher for Earth & Environmental Science (https://www.pangaea. de/). These ancillary data were selected considering the months of the ABRACOS surveys and the SWTA area (3° − 10°S/30° − 36°W), whatever the year. A total of

182 and 176 hydrographic profiles were considered for the periods of spring (Sep. – Oct.) and fall (Apr. - May), respectively (Table 1, Fig. 1). To describe the upper ocean thermohaline structure, ABRACOS and ancillary profiles were considered from the surface to 300 m depth.

To investigate the atmospheric forcing, we analysed monthly average freshwater budget (evaporation minus precipitation – E-P) and near surface wind speed. For that, we used product composites of the Hamburg Ocean Atmosphere Parameters and Fluxes (HOAPS – v.4) with a regular 0.5° x 0.5° from 1988 to 2014. All variables were derived from recalibrated and intercalibrated measurements from SSM/I and SSMIS passive microwave radiometers compiled by the EUMETSAT's Satellite Application Facility on Climate Monitoring (CM SAF) (Andersson et al., 2017).

Figure 1. Study area in the southwestern tropical Atlantic (SWTA). Triangles: ABRACOS data; Circles: WOA 2013, REVIZEE and PANGEA datasets. Red symbols: spring data; Yellow symbols: fall data. The continental shelf is represented in light grey; the dashed line represents the shelf break (60 m isobath); other bathymetric contours (solid lines) are by 1000 m intervals. RA: Rocas Atol; FN: Fernando de Noronha archipelago.

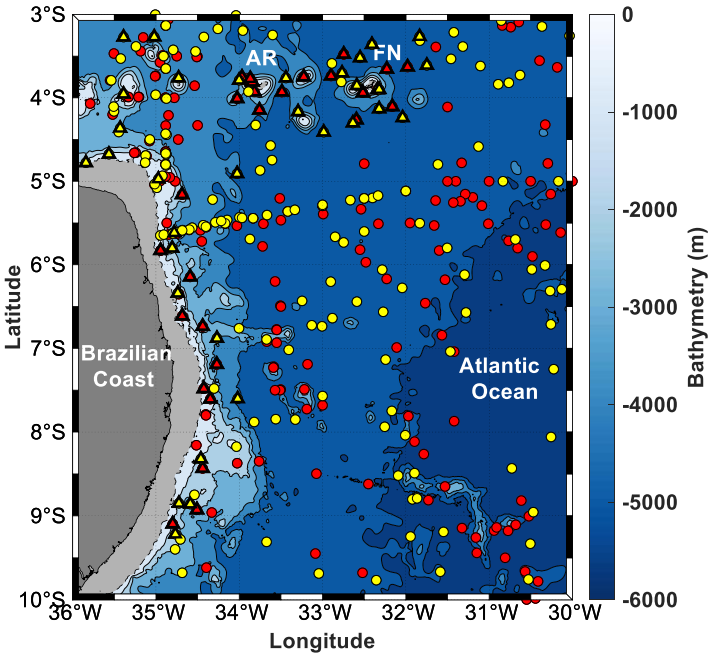

Source: Personal collection.

Table 1. Databases in use.

Data	Number of profiles	Year of data acquisition **Spring**	**Fall**	Coverage area Lat - Long
ABRACOS	62	2015	2017	3.26°S - 9.21°S 36.38°W - 31.97°W
WOA	237	1990,1992,1993,1995	1983,1984,1993 1994,1995,2003 2010,2017,2018	3.00°S - 9.99°S 31.5°W - 35.88°W
REVIZEE	39	1995,2000	1997,1999	3.39°S – 9.67°S 31.33°W - 35.01°W
PANGEA	80	2015,2016	2000,2003,2014	3.00°S – 5.63°S 31.5°W – 35.10°W

Source: Personal collection.

2.2. Defining the thermohaline structure

To describe the thermohaline structure, we defined a series of parameters or limits (Fig. 2): the MLD, the BLT, the upper and lower limits of the thermocline and the pycnocline. There is no consensus for such definitions that vary according to the thermohaline structure of the studied area (Araújo et al., 2011; de Boyer Montégut et al., 2004; Holte and Talley, 2009; Ker et al., 2016, 2015). Here we defined these limits considering the specificity of the vertical profiles in the SWTA (Fig. 2).

Figure 2. Examples of CTD profiles from ABRACOS 1 (spring) with the representation of the thermohaline structure as defined from the temperature, salinity, density and squared buoyancy frequency (N^2). MLD: mixed layer depth; UTD: upper thermocline depth; LTD/LPD: lower thermocline/pycnocline depth; BL: barrier layer (present in the right profile only).

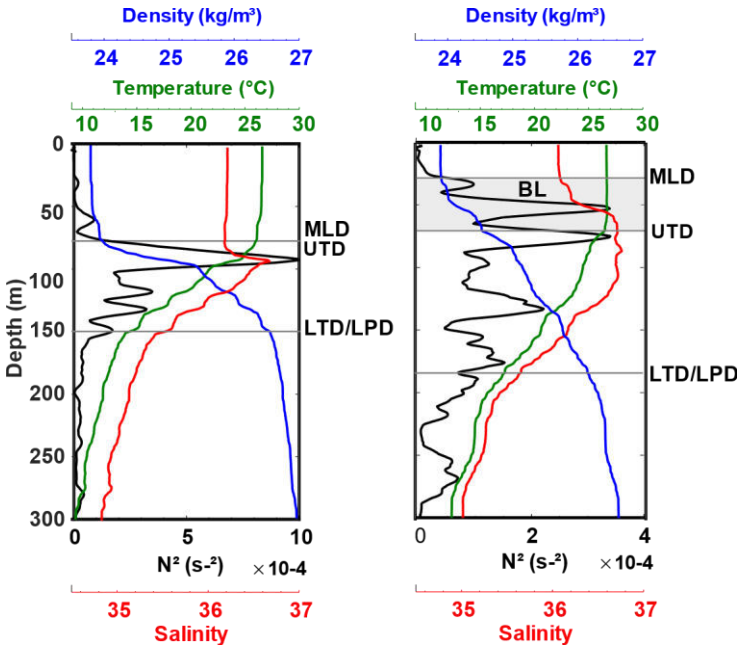

Source: Personal collection.

We determined the MLD using the criteria from Sprintall and Tomczak (1992), i.e., the depth at which density (σ) is equal to the density at the reference depth ($z_{0=}10$ m depth), plus an increment ($\frac{\partial_{\sigma_\theta}}{\partial_\theta}\Delta_\theta$), which is equivalent to temperature steps $-\Delta_\theta = 0.5\,°C$ and its equivalent in density change at constant salinity (S_{z_0}). Moreover, previous studies in the western tropical Atlantic also used the 0.5°C criterion for the isothermal layer and its equivalent in density change (Araújo et al., 2011; Silva et al., 2005; Tanguy et al., 2010), whose are found to be the most adaptable due to their robustness.

$$MLD = z\left(\sigma_{\theta_{z_0}} + \frac{\partial_{\sigma_\theta}}{\partial_\theta}\Delta_\theta\right) \qquad \text{(Eq. 1)}$$

To define the Upper Thermocline Depth (UTD), we compared three criteria: the depth of the maximum temperature gradient, the isothermal layer with 0.5°C as a threshold (Tangy et al., 2010), and (Ker et al., 2016). The two last criteria reached similar results, while the maximum gradient

method tends to overestimate the UTD. Following Ker et al. (2016) and checking by visual inspection, we used to identify the UTD.

To determine the Lower Thermocline Depth (LTD), which also coincides with the Lower Pycnocline Depth (LPD) (Fig. 2), we used the Brunt Väisälä frequency (N^2, the buoyancy frequency squared),

$$N^2 = -\frac{g}{\sigma_0}\frac{\partial \sigma_z}{\partial z} \qquad \text{(Eq. 2)}$$

where, g is the acceleration of gravity and σ_0 is a reference density at 10 m (Kim and Miller, 2007; Liu et al., 2016). Specifically, we considered the lower thermocline/pycnocline depth to be the last depth below the UTD where N^2 is of up to four orders of magnitude ($N^2 \geq 10^{-4}$). This method was chosen based on evidence that in the thermocline/pycnocline that acts as a transition layer, the shear instabilities can produce higher buoyancy frequencies compared to the stable layers above and below it. In vertical profiles (Fig. 2), N^2 is close to zero (in the order of $1x10^{-6}$) above the pycnocline; it increases continuously within the thermocline/pycnocline layer (Maes and O'Kane, 2014) reaching values greater than $1x10^{-3}$. Below the pycnocline/thermocline, decreases to reach values similar to those of the mixed layer (Johnston and Rudnick, 2009; Maes and O'Kane, 2014; Sun et al., 2013). In such an environment, the criterion $N^2 \geq 10^{-4}$) was well fitted to define the base of the thermocline.

The thermocline thickness (TT) was calculated by the difference between the upper and lower limits of the thermocline (TT = LTD/LPD - UTD). Finally, the Barrier layer thickness (BLT) was calculated as the difference between the MLD and the UTD (BLT = MLD – UTD) (Lukas and Lindstrom, 1991).

2.3.Functional Data Analysis (FDA)

FDA is a branch of statistic that provides tools for describing and modelling sets of functions (or curves) rather than vectors of discrete values (Ramsay, 2006). The guiding idea of this approach is to describe data as parameterized functions, and to use these parameters for clustering, comparing or interpolating functions. In particular, classical statistical tools can be adapted to functional data such as functional principal component analysis (fPCA) to summarize and characterize significant variation in finite dimension among a sample curves (Dabo-Niang and Ferraty, 2008; Ramsay,

2006). Functional analysis of variance (fANOVA) uses all the information of each mean functional curve to test the possible differences in the datasets, based on the shape and temporal (along the depth) variability of the curves (Cuevas et al., 2004; Ramsay, 2006).

Here, each temperature and salinity profile were treated as a separate function (curve) in FDA, and we used a variety of functional statistical methods to define and characterise the 3D thermohaline structure. A summary flowchart documenting the methodology sequence for the use of FDA is presented in Fig. 3 and described below. All analyses (i.e., fitting, clustering, and kriging) were done separately for salinity and temperature profiles.

2.3.1. Fitting B-spline function

To apply FDA (Ramsay, 2006), the first step consists in transforming the data into function (Fig. 3, step 1). To describe a vertical profile as a single entity, the existence of a smooth function giving rise to the observed data is assumed. It is expressed as:

$$y_i = x(z_i) + \epsilon_i \qquad \text{(Eq. 3)}$$

where $(z_i, y_i), i = 1, \dots, N$ are the data, z is depth and y temperature or salinity, ϵ_i is a remainder that is expected to be as small as possible. The function $x(z)$ is in the form of a linear combination of each basis function $\phi_k(z)$, k = 1, …, K such that:

$$x(z) = \sum_{k=1}^{K} c_k \phi_k(z) \qquad \text{(Eq. 4)}$$

where c_k are coefficients estimated by penalized regression using pointwise data $(z_1, y_1), \dots, (z_N, y_N)$ (Ramsay, 2006).

Spline functions to smooth data are the most common choice of approximation system for non-periodic functional data. It combines fast computation of polynomials approach with substantially greater flexibility. Therefore, a B-spline basis of degree 3 (Boor, 2001) has been used. Then, to reduce the impact of noise in the measurement when interpolating, a solution is to determine a roughness parameter λ, such that parameters of x_i will be estimated by minimizing the penalized squared difference (error):

$$PSE = \sum_{k=i}^{n} \left(y_i - x_i(z)\right)^2 + \lambda \int [D^2 x(z)]^2 \, dz \qquad \text{(Eq. 5)}$$

where D^2 is the second derivative of fit.

Figure 3. Summary flowchart documenting the methodology sequence for the Functional Data Analysis approach and definition of the themohaline structure. This framework has been followed for both temperature and salinity profiles, separately.

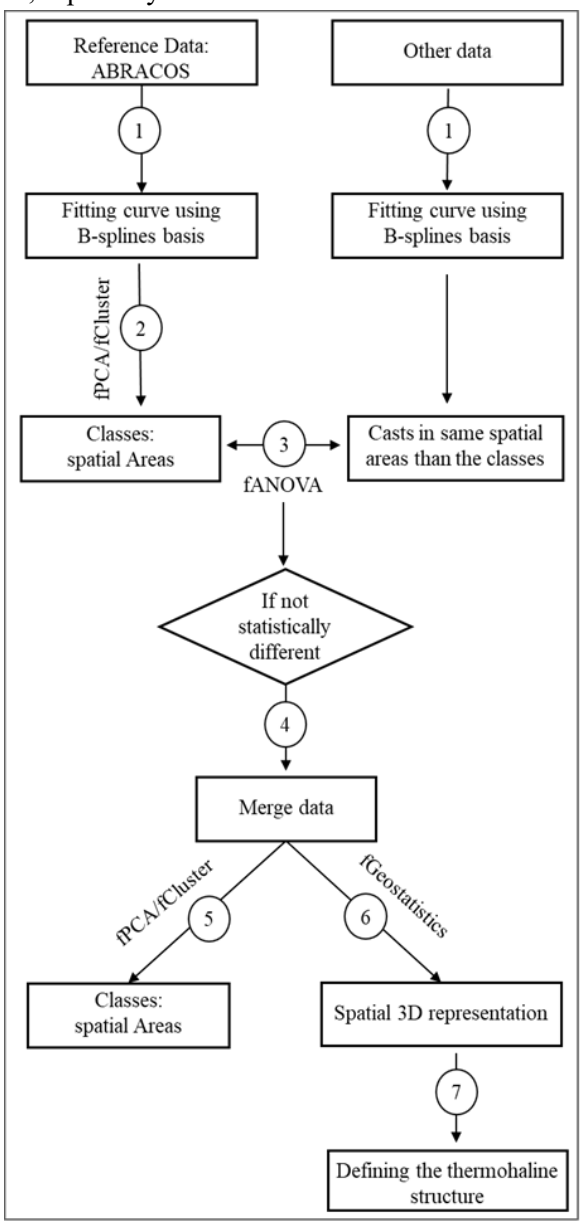

Source: Personal collection.

A good choice of the dimension of the basis K, and of the penalized parameter λ of the basis consists in finding the right balance between smoothing and interpolating the data. The higher the number of K-functions, the more complexity is preserved. We first defined an interval of potential

K, by making a sensitivity test by carrying out smoothing for temperature and salinity according to different *K*. Then, we performed a Generalized Cross-Validation (GCV) to estimate the optimal basis *K* and λ, within this interval, using the R packages "`fda`" and "`fda.usc`" (Febrero-Bande and Fuente, 2012).

2.3.1.1.Comparing ABRACOS and ancillary datasets

Once the hydrographic profiles have been described with a relevant functional basis, the next step was to compare the ABRACOS and ancillary data. Indeed, we aimed at determining if these datasets could be merged to be representative of spring and fall canonical states in the study region. This question has been addressed in two steps (Fig. 3, steps 2 and 3) using the most recent ABRACOS observations as a reference.

First (Fig. 3, step 2), we characterised the ABRACOS profiles by applying fPCA and a functional hierarchical clustering (fCluster), achieved on the coefficients of the fPCA decomposition (Febrero-Bande and Fuente, 2012). Reproducing the aim of PCA, the idea of the fPCA is to summarize multivariate dataset with principal component seen as a linear combination of the variables (the same apply for fCluster). In comparison, the method is adapted to deal with function rather than vector and the principal components corresponds to dominant modes of variation of functional data (Shang, 2014). fPCA allowed identifying the main patterns of variation of the vertical profiles while fCluster were used to statistically define homogeneous groups of profiles. These groups were then plotted spatially to determine if they correspond to specific areas.

Second (Fig. 3, step 3), once homogeneous areas were defined from ABRACOS profiles, we applied a fANOVA to compare ABRACOS and ancillary profiles present in each area. fANOVA is based on the so-called one-way analysis of variance for univariate functional data using L2-norm-based parametric bootstrap test for homoscedastic samples (Cuevas et al., 2004). This procedure considers l groups of independent random functions such that each function of the group A is assumed to be a stochastic process with mean function $\mu_k(t), A = 1 \dots l$ and tests the null hypothesis:

$$H_0: \mu_1(t) = \cdots = \mu_l(t).$$

This analysis has been performed with the use of "`fdanova`" R package (Febrero-Bande and Fuente, 2012).

2.3.1.2. Data characterisation and 3D spatial interpolation.

In case of no rejection of the null hypothesis (Fig. 3, step 4), profiles from the different datasets can be merged to build complete dataset representative of spring and fall canonical states. Then fPCA, fCluster and fANOVA can be applied on the complete merged dataset to characterise the profiles and their spatial variability (Fig. 3, step 5).

To interpolate temperature and salinity profiles in 3D (Fig. 3, step 6) we applied a functional geostatistical analysis (Giraldo et al., 2007). Geostatistics (or kriging methods) are well-known tools for model-based spatial interpolation, taking into account the spatial auto-correlation of an estimated set of variables (Matheron, 1963). The fundamental premise of kriging methods is that spatial data constitute a joint realization of spatially dependent random variables, collectively referred as a random function. Ordinary kriging refers to spatial prediction under the assumption of stationarity as specified by Cressie (1993) and Wackernagel (2003). More precisely, the random function is supposed stationary, meaning that the expectation of the random function is independent of the position. This framework has been generalized to be useful within the FDA context. Yet, because we are dealing with functions, the stumbling block remains in the estimation of a spatial covariance between curves.

The functional geostatistical analysis has been performed according to ordinary trace kriging method (Giraldo et al., 2011) in order to described the spatial autocorrelation structure of functional data. The method is implemented in "`fdagstat`" R package (https://github. com/ogru/fdagstat) and has involved the two following steps: (i) the analysis of spatial structure (i.e., through the calculation and fitting of a variogram); (ii) and the use of this structure for predicting functional data at unknown location. Spherical model has been used to fit the different variograms to temperature and salinity profiles.

To evaluate the quality of the functional geostatistical models we performed cross-validation analyses. For that, we randomly removed 2% of the sampled curves (profiles) and performed the functional Kriging predictor for the remaining 98% curves to predict the removed curves. Observed profiles, fitted with 41 and 44 B-spline basis (K) to temperature and salinity, respectively, were

compared with a Kriging- predicted curve for each site. This procedure was applied the number of times enough to cover all profiles sampled in situ. We used the Mean Square (MSD) differences i.e., the mean of the squared error between predicted and real profiles (for all depth) to evaluate the quality of the prediction. Finally (Fig. 3, step 7), we applied the criteria defining the MLD, the BLT, the upper thermocline depth, and the lower thermocline/pycnocline depth to the interpolated fields of temperature and salinity, to obtain a comprehensive vision of the thermohaline structure in the SWTA. In each area and for each season, we also calculated the BL occurrence frequency (BLF, in %) defined as the percentage of area with BLT higher than 5 m (Zeng and Wang, 2017).

3. Results

3.1. Merging the datasets

For both seasons, the fPCA and fCluster analysis of the ABRACOS thermohaline profiles revealed two significant areas (classes, the dendrograms are provided in the Supplementary Figure S1), in which profiles display similar shape (Fig. 4). The first area corresponds to the surrounding of the SWTA slope, hereafter referred to as A1. The second area hereafter referred as A2 encompasses the oceanic islands (Fernando de Noronha and Rocas Atoll) and seamounts (Fig. 4e and j).

Figure 4. Scores of the first two PCAs components temperature in spring (a) and fall (f), and salinity in spring (c) and fall (h) from ABRACOS data only. The colour corresponds to the class defined by the functional clustering preformed on the data (blue: class A1; red: class A2). Mean temperature (b, g) and salinity (d, i) profiles for each class obtained from the in spring (b, d) and fall (g, i). Spatial distribution of the classes/area for spring (e) and fall (j). The grey dashed and full lines illustrate the variation over the mean profiles.

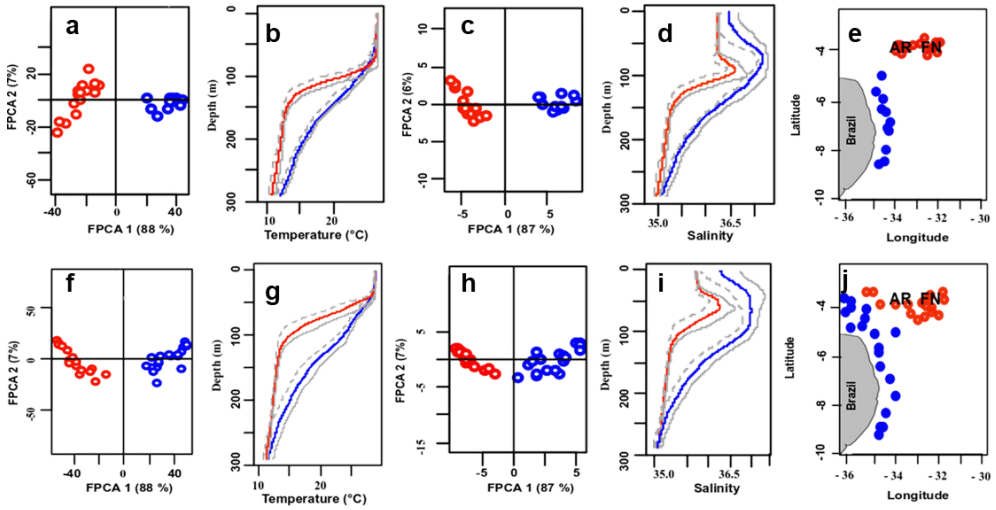

Source: Personal collection.

In each area and for each variable (temperature and salinity) and season (spring and fall), no significant differences (fANOVA, $p > 0.05$) were observed between the profiles from ABRACOS and other data (Fig. 5). fANOVA results verify that the data obtained during the ABRACOS surveys, are representative of a canonical state of spring and fall for SWTA. We thus merged all datasets in one complete dataset (from now the reference) of oceanic profiles per season (see Fig. 3, step 4). When performing the fPCA and fCluster analyses on the complete dataset, in addition to the A1 and A2, we identified a third thermohaline class, hereafter referred as A3, corresponding to the central offshore zone between A1 and A2 (Fig. 6).

Figure 5. Functional ANOVA between the mean profiles from different databases by area: spring temperature in A1 (a); spring temperature in A2 (b); fall temperature in A1 (c); fall temperature in A2 (d); spring salinity in A1 (e); spring salinity in A2 (f); fall salinity in A1 (g); and fall salinity in A2 (h). Colours refer to data sources; blue: ABRACOS, red: WOA, green: PANGEA and black: REVIZEE.

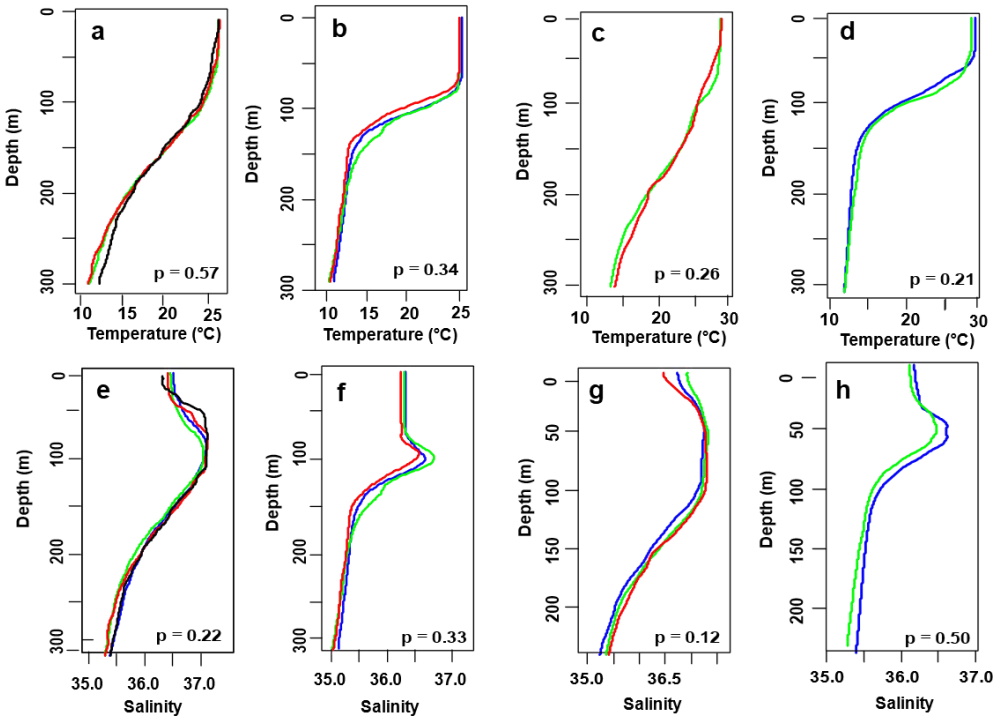

Source: Personal collection.

3.2. Typology of thermohaline patterns

The application of the fPCA and fCluster on the complete dataset allowed dividing the study area into three significantly different areas during both seasons (Fig. 6, the dendrograms are provided

in the Supplementary Figure S1). We observed the two classes of profiles already depicted using ABRACOS data only (A1 and A2 in Fig. 4) with A1 extending to the entire longitudinal extension (35°W-30°W) south of 8°S at both seasons (Fig. 6b, d, f, h). In addition to A1 and A2, we identified a third class, A3, corresponding to the central offshore zone between A1 and A2 (Fig. 6). Note that some spatial overlap between profiles characterised in different area occurs, mainly in the transition zone between A2 and A3 (Fig. 6b, d, f, h).

Figure 6. Mean vertical profiles of temperature (a, c) and salinity (f, h) of each class/area identified by functional PCA and clustering in spring (a, f) and fall (c, h). The grey solid and dashed lines illustrate the variation over the mean profiles. Spatial distribution of the classes/area for temperature (b, d) and salinity (g, i). (e) TS diagrams for each class, with spring represented by dashed lines and fall by solid lines. (j) Static stability (in terms of buoyancy frequency, N^2). In all plots, the colours blue, red and green represent the areas 1, 2 and 3, respectively.

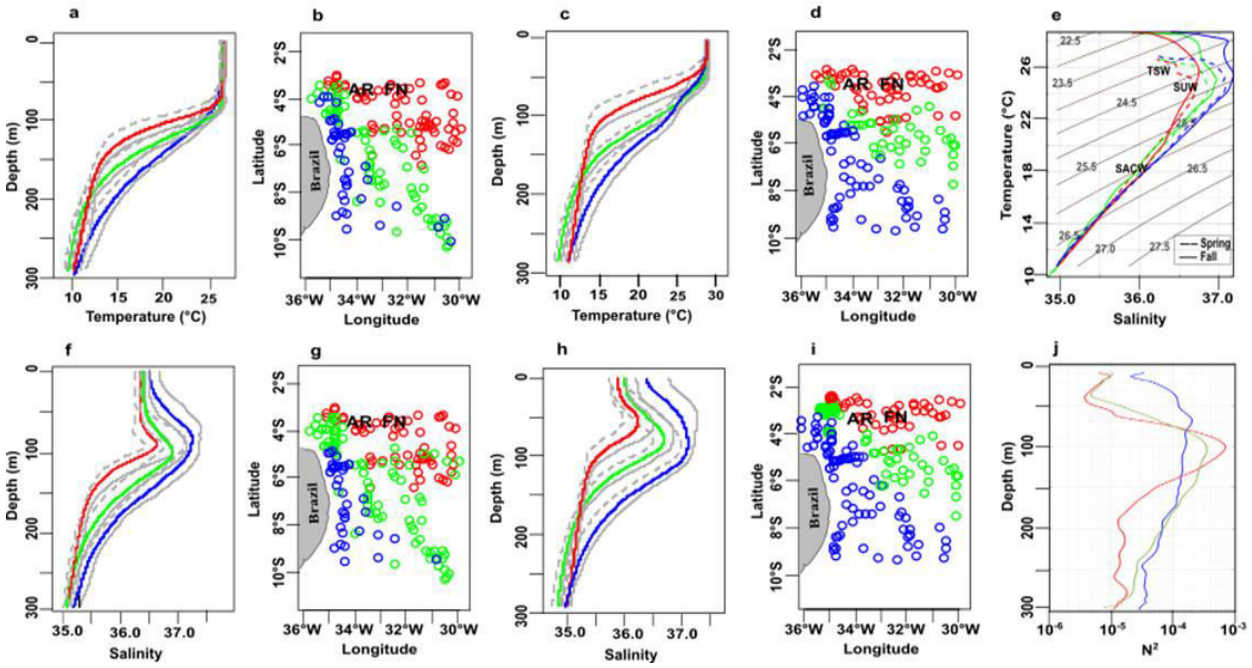

Source: Personal collection.

In A1, temperature profiles were characterised by a low stratification with a thermocline extending from 70 m to 172 m in spring (Fig. 6a) with a thermal difference of 7.7°C, and from 58 m to 166 m in fall (Fig. 6c) with a temperature difference of 9.7°C. Salinity profiles presented the saltiest waters with a peak of salinity reaching 37.1 at 98 m in spring (Fig. 6e), and 37.2 at 68 m in fall (Fig. 6g).

In A2, temperature profiles were characterized by a high stratification with a sharp thermocline extending from 86 m to 132 m in spring (Fig. 6a) with a thermal difference of 10.8°C, and from 50 m to 100 m in fall (Fig. 6c) with a thermal difference of 12.3°C. Salinity profiles presented the lowest salinity, with maximum values reaching 36.6 at 100 m in spring (Fig. 6e) and 36.4 at 72 m in fall (Fig. 6g).

In A3, temperature profiles were characterized by low stratification with a thermocline extending from 90 m to 160 m in spring (Fig. 6a) with a thermal difference of 10.7°C in, and from 64 to 158 m in fall (Fig. 6c) with a thermal difference of 9.9°C. Salinity profiles presented intermediate salinity values with a maximum of 36.7 at 108 m in spring (Fig. 6e), and 36.8 at 92 m in fall (Fig. 6g).

To identify the water-masses present in each area for each season we used TS diagram (Fig. 6e). Surface Tropical South Water are warm surface water (Stramma and England, 1999) with σ_θ above 24.5 kg.m^{-3} (Gasparin et al., 2014; Urbano et al., 2008) observed in all three areas with seasonal changes mostly driven by the temperature. Below, in the upper part of the thermocline, lies the Subtropical Underwater (SUW) (Lambert and Sturges, 1977) formed by the excess of evaporation over precipitation in the subtropics (Sup. Fig. 3) and advected westward within the subtropical gyre (Bourlès et al., 1999a). This water-mass, observed in all three areas, is characterised by its high salinity (>36.5; Stramma and England, 1999). Finally, in subsurface, in the lower part and below the thermocline, the South Atlantic Central Water ($24.5<\sigma_\theta<27$ kg.m^{-3}, Stramma and England, 1999) dominates, whatever the season or area.

3.3. 3D thermohaline patterns

From functional geostatistics, we characterised the 3D temperature and salinity fields for the canonical state of spring and fall in the SWTA. Validation procedure (Fig. 7 for spring, see Sup. Fig. S2 for fall) shows that the ordinary trace-kriging provides an acceptable estimation of temperature and salinity profiles at any locations of the sampled domain, independent of the areas (A1, A2 and A3). Examples of original profiles for randomly selected sites and their predicted equivalents are shown, for each profile the root mean square of the differences between predicted and observed values (applied along the profile) was calculated to estimate the accuracy. The boxplots of the MSD (Fig. 7) and associated global statistics show that in most cases the goodness

of fit was good with similar predicted and observed smoothed curves. However, in some extreme cases the goodness of fit was not optimal (e.g., profiles 2 and 4 in Fig. 7) but the shape was preserved.

Figure 7. Validation for Functional Ordinary Kriging of temperature (°C) (a, b, c) and salinity (d, e, f) in spring using the Mean Square Difference (MSD). Maps of the distribution of the MSD for all stations for temperature (a) and salinity (b). Examples or good (1 and 3) and worst (2 and 4) predictions for temperature (b) and salinity (e). The corresponding profiles are circled in (a) and (d). The red solid lines correspond to the observations and the blue solid line to the predictions. The boxplots of the MSD for temperature (c) and salinity (f) are presented to evaluate the global performance of the estimators.

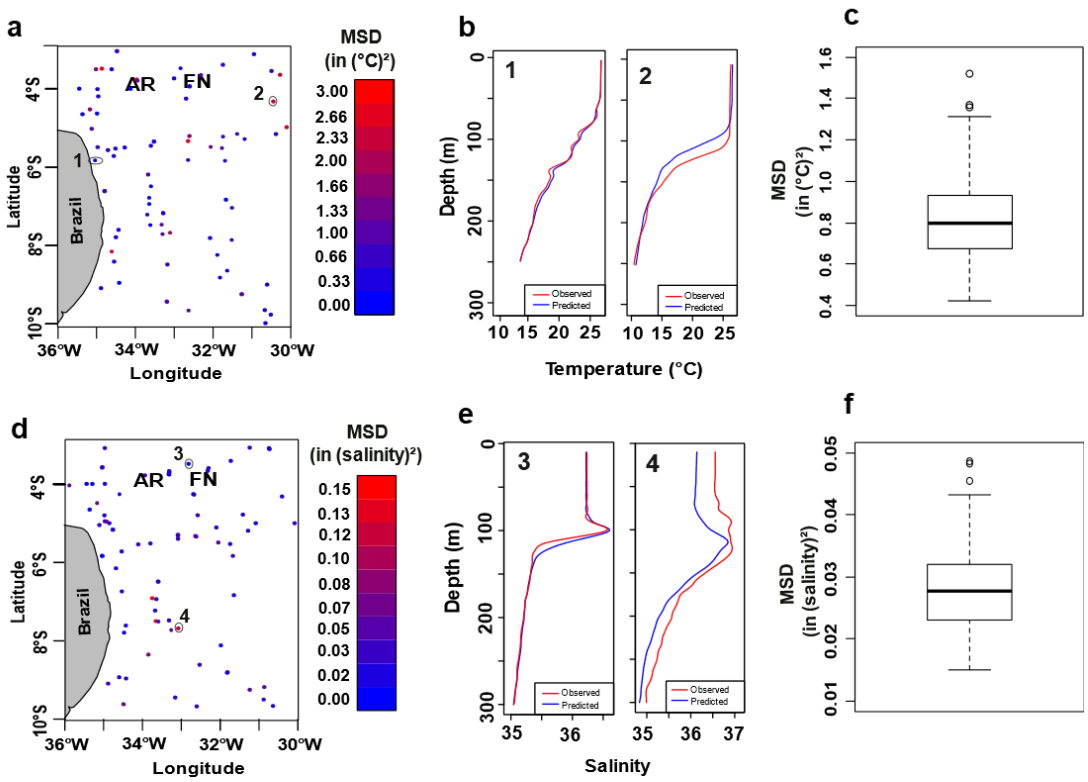

Source: Personal collection.

3.3.1. Temperature and salinity 3D field

3D temperature and salinity interpolated fields are available in supplementary material (supplementary movies SM1, 2, 3 and 4) and are presented in 2D at three depths (Figs. 8 and 9). These depths were chosen to represent the patterns in surface (10 m), within (110 m) and below (200 m) the thermocline/pycnocline. In spring, the Sea Surface Temperature (SST, temperature at

10 m depth) (Fig. 8a) was nearly homogeneous (median ~26.6°C) over the whole study area, while it was about 2°C higher in fall (Fig. 8b), ranging from 28.0°C to 29.2°C (median ~28.6°C), with highest values in the central part of A3. At 110 m, a clear temperature gradient was observed during both seasons (Fig. 8c, d) with lower temperature north of ~6°S (A2) than further south (A1 and A3). At 200 m (Fig. 8e, f), we observed strong spatial patterns with a core of warm waters over the continental slope (A1).

In spring, the surface salinity (Fig. 9a) ranged between 36.1 and 36.6, with the highest values along the continental slope (A1). In fall, the surface salinity (Fig. 9b) gradient was stronger with the highest values (up to 37.4) also near the continental slope (A1). The lowest salinities were observed offshore between 3°S – 6°S (A2, A3). At 110 m, the salinity gradient reinforced (Fig. 9c, d) with lower salinity 36.0 (35.4) in spring (fall) north of 7°S (A2, A3) than along the continental slope and in southern region (A1) where salinity reached 37.1 (37.3) in spring (fall). At 200 m, the salinity was lower than in upper layers, but the gradient was still observed (Fig. 9e, f) with higher salinity in A1 than A2 and A3, where the lowest salinity was observed.

3.3.2. Thermohaline structure

The MLD, the BLT, the upper thermocline depth and the lower thermocline/pycnocline depth were estimated from the interpolated temperature and salinity fields for each season (Fig. 10, see Table 2 for synthetic description). To verify the robustness of these estimates we also performed these calculations using the B-spline fitted original profiles for each Area. This comparison (Table 2) reveals very small differences. To better illustrate the spatial patterns, we also plotted the thermohaline structure over vertical sections along the slope, cross- shore (at 5.5°S and 8°S) and along the Fernando de Noronha chain (Figs. 11 and 12). A clear seasonal variability was observed with shallower limits for both variables in fall compared with spring (Figs. 10–12).

The MLD was shallower in A1 than in other areas with a sharp transition in the limit between A1 and A3 (Figs. 10–12). The BLT followed an opposite pattern, with thicker BL in A1 than in other areas, although low values were also observed close to the shelf break. Some hotspots of high BLT (> 40 m) were observed in A1 in spring and in A1 and A3 in fall (Fig. 10). The BLT was in average thicker and the BLF higher in fall than spring (Table 2). More specifically, the BLF was the highest in A1 with 80% and 77% in spring and fall, respectively. A3 presented intermediate BLF values

with 63% and 70% in spring and fall, respectively. The lowest BLF were observed in A2 with 14% and 33% in spring and fall, respectively. The seasonal and spatial patterns of the UTD were alike to the one of the MLD. The LTD presented a clear spatial pattern, shallow at low latitudes (A2, and in a lesser extent, A3) and deep close to the coast and in the extreme northwest of the study area (Figs. 10–12). In addition, small-scale vertical displacements of isotherms and isohalines were observed around islands and seamounts (Fig. 11c, d and 12c, d).

Figure 8. Sea temperature in spring (a, c, e) and fall (b, d, f) at 10 m (a, b), 110 m (c, d) and 200 m (e, f) in the southwestern tropical Atlantic. Grey solid lines delimit areas A1, A2 and A3 defined in section 3.2. The continental shelf limited by the isobaths of 60 m is represented by light grey. RA: Rocas Atoll; FN: Fernando de Noronha archipelago. The main currents are represented. cSEC: central branch of the South Equatorial Current. SEUC: South Equatorial Undercurrent. NBUC. North Brazilian Undercurrent; NBC: North Brazilian Current. Note that the temperature scale varies according to the depths 10 m, 110 m and 200 m.

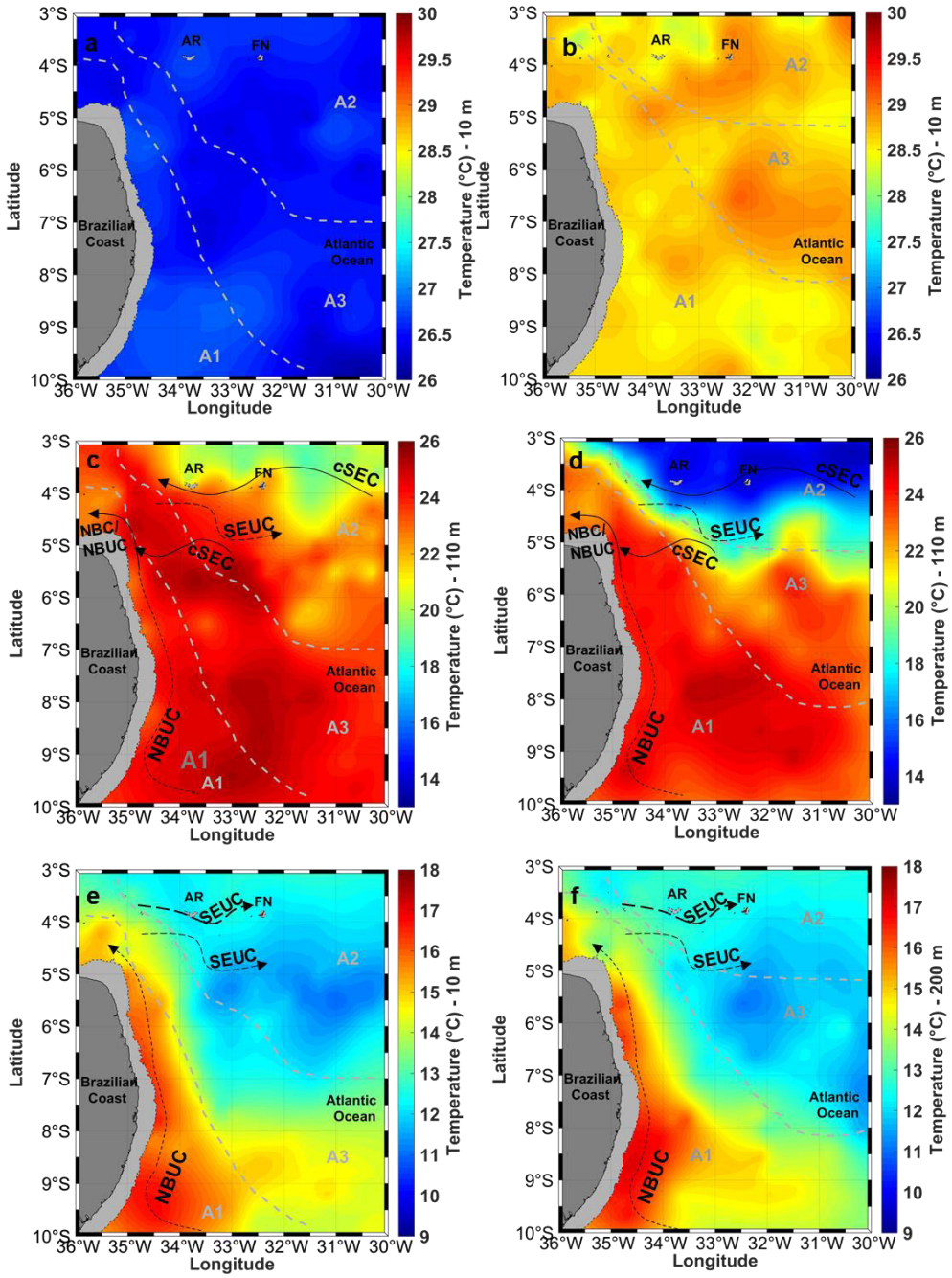

Source: Personal collection.

Figure 9. Sea salinity in spring (a, c, e) and fall (b, d, f) at 10 m (a, b), 110 m (c, d) and 200 m (e, f) in the southwestern tropical Atlantic. Grey solid lines delimit areas A1, A2 and A3 defined in section 3.2. The continental shelf limited by the isobaths of 60 m is represented by light grey. RA: Rocas Atoll; FN: Fernando de Noronha archipelago. The main currents are represented. cSEC: central branch of the South Equatorial Current. SEUC: South Equatorial Undercurrent. NBUC. North Brazilian Undercurrent; NBC: North Brazilian Current. Note that the temperature scale varies according to the depths 10 m, 110 m and 200 m.

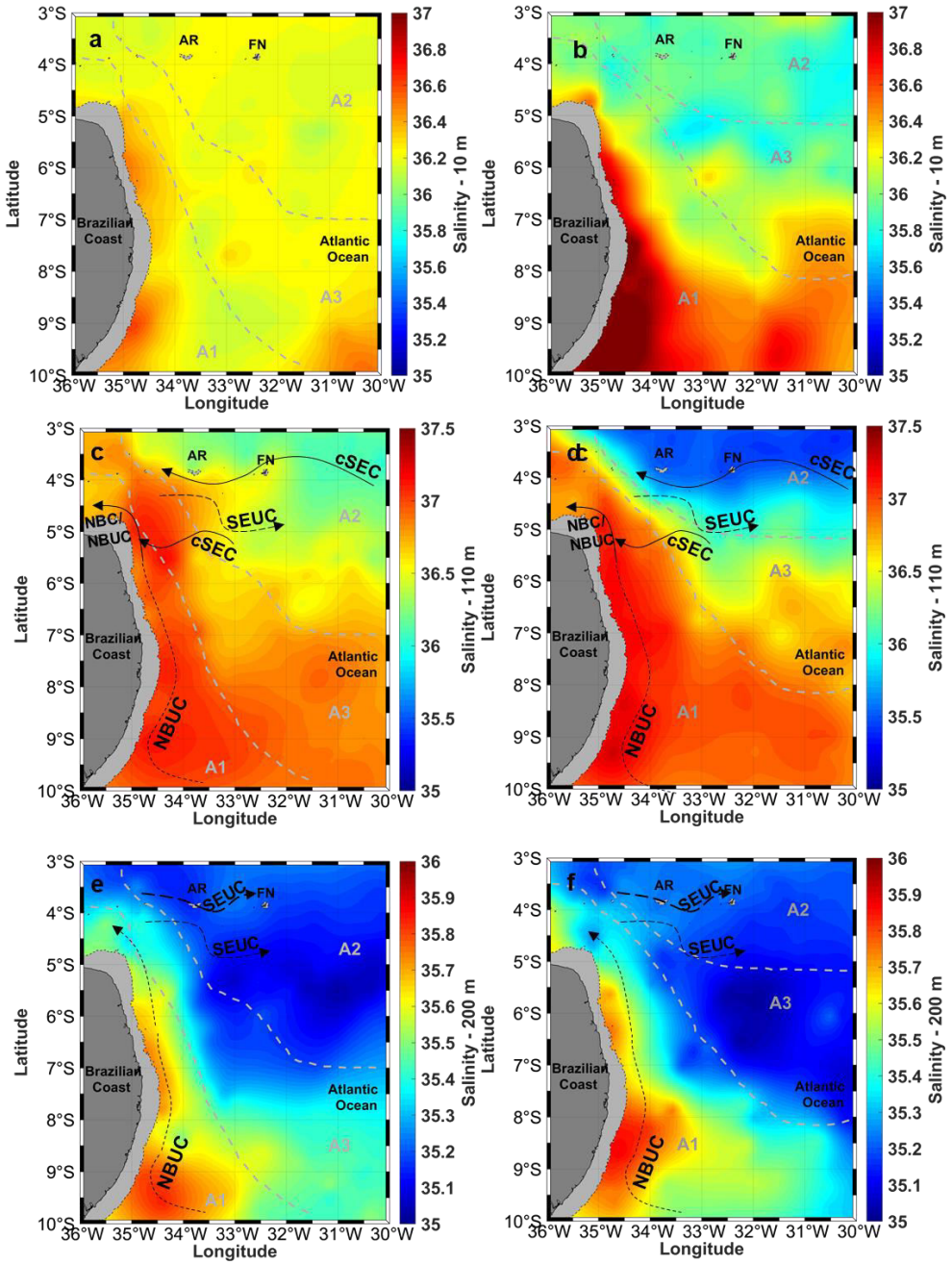

Source: Personal collection.

Figure 10. Thermohaline structure estimated from the interpolated temperature and salinity fields in spring (a, c, e, g) and fall (b, d, f, h) in the southwestern tropical Atlantic. The panels show MLD (a, b); BLT (c, d); UTD (e, f) and LTD (g, h). Grey solid lines delimit areas A1, A2 and A3 defined in section 3.2. The continental shelf limited by the isobaths of 60 m is represented in light grey. RA: Rocas Atoll; FN: Fernando de Noronha archipelago.

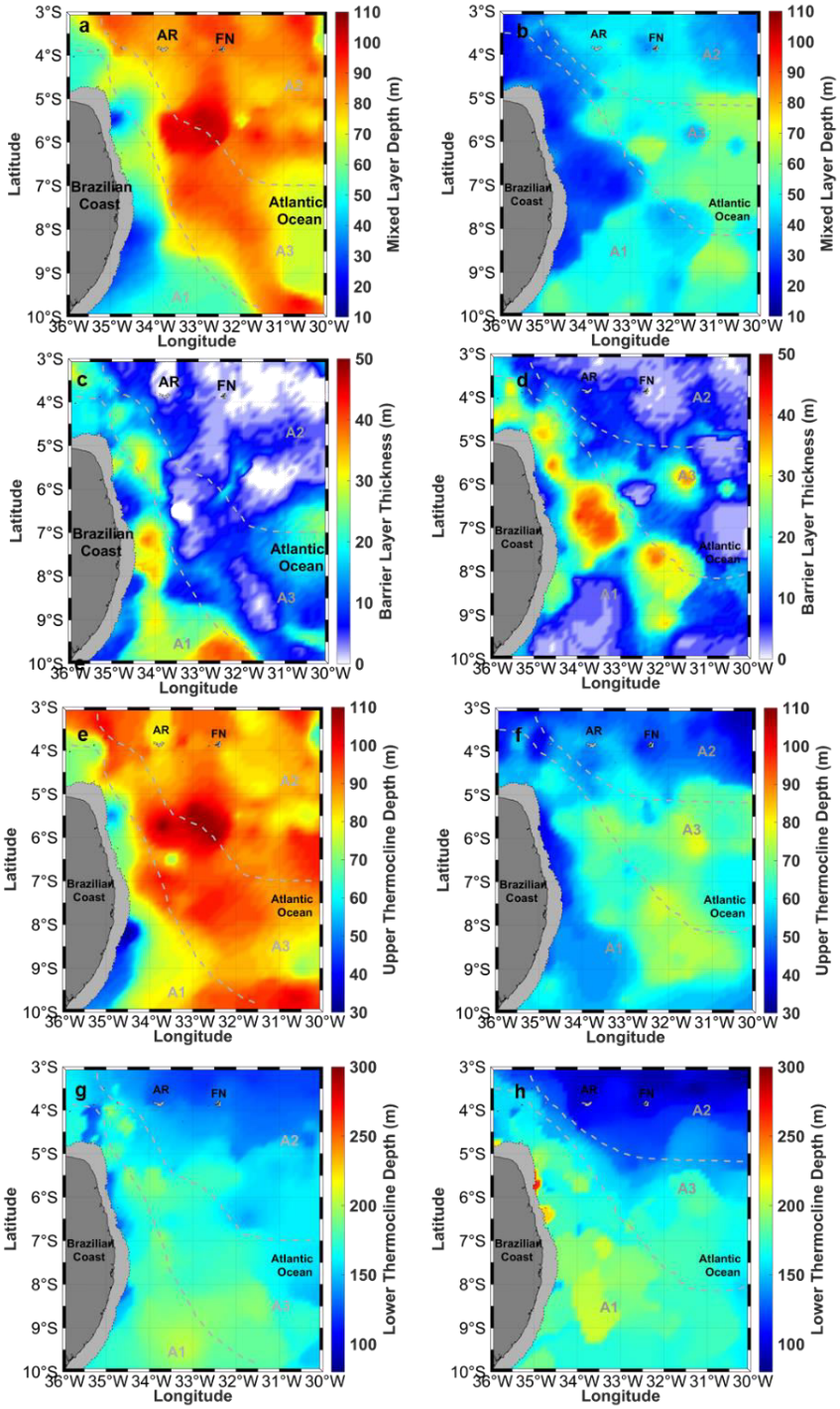

Source: Personal collection.

Table. 2. Characteristics of the thermohaline descriptors by area and by season from the smoothed original profiles and from interpolated fields (in parenthesis).

		Mixed layer depth (m)		Barrier layer thickness* (m)		Upper thermocline depth (m)		Lower thermocline depth (m)		Thermocline thickness (m)		Maximum salinity		Depth of maximum salinity (m)	
		S	F	S	F	S	F	S	F	S	F	S	F	S	F
A1	Mdn	58 (60)	36 (46)	18 (16)	20 (16)	76 (80)	60 (58)	175 (180)	168 (168)	104 (100)	110 (110)	37.2 (37.1)	37.2 (37.1)	92 (92)	80 (82)
	$\bar{m}$	53 (61)	39 (43)	19 (18)	20 (16)	73 (79)	60 (60)	187 (177)	173 (171)	104 (100)	114 (112)	37.2 (37.1)	37.2 (37.1)	92 (90)	78 (84)
	std	16 (16)	15 (11)	12 (9)	15 (11)	18 (13)	13 (9)	37 (15)	24 (11)	26 (18)	28 (14)	0.1 (0.1)	0.2 (0.1)	16 (8)	24 (20)
A2	Mdn	92 (84)	46 (44)	2 (2)	2 (4)	94 (86)	48 (48)	134 (130)	98 (102)	40 (44)	48 (52)	36.7 (36.5)	36.4 (36.4)	98 (100)	66 (66)
	$\bar{m}$	90 (85)	46 (43)	2 (2)	4 (5)	92 (87)	51 (48)	135 (130)	99 (104)	43 (44)	48 (55)	36.7 (36.5)	36.4 (36.4)	100 (99)	68 (66)
	std	7 (4)	11 (4)	3 (3)	4 (3)	9 (4)	10 (5)	12 (8)	13 (13)	12 (9)	10 (12)	0.1 (0.1)	0.2 (0.2)	7 (3)	12 (9)
A3	Mdn	85 (84)	55 (56)	7 (8)	8 (10)	94 (92)	65 (66)	178 (174)	160 (156)	88 (76)	94 (88)	37.0 (36.8)	36.8 (36.7)	107 (110)	90 (92)
	$\bar{m}$	82 (82)	52 (55)	10 (10)	12 (11)	92 (92)	64 (66)	179 (173)	157 (154)	87 (79)	93 (87)	37.0 (36.8)	36.8 (36.7)	107 (109)	89 (92)
	std	16 (10)	14 (7)	11 (6)	12 (8)	14 (6)	11 (5)	13 (9)	13 (15)	21 (8)	12 (14)	0.2 (0.1)	0.2 (0.1)	12 (6)	13 (7)

*BLT** The frequency of BLTs larger than 5 m was 80% (77%), 14% (33%) and 63% (70%) in spring (fall) for A1, A2 and A3, respectively

S = spring; F = fall; Mdn = median; $\bar{m}$ = mean; Std = standard deviation

Figure 11. Vertical sections of temperature in spring (a, c) and fall (b, d). Sections in (a, b) include two along-shore transects (9.95°S/35°W – 7.4°S/34°W and 7.4°S/34°W – 4.7°W/35°W) and two cross-shore transects (8°S/35 – 31.3°W and 5.5°S/35 – 31.3°W). Sections in (d,e) include a transect along 3.87°S from 36°W to 31° and a transect crossing Fernando de Noronha Island (FN) at 32.4°W from 3.5°S to 4.5°S. The grey areas represent the relief; RA: Rocas Atoll; FN: Fernando de Noronha archipelago. The black solid lines show the MLD. The black dashed lines show the upper and lower limits of the thermocline. The difference between the MLD and the upper limit of the thermocline illustrates the presence of the BL. The main currents are represented. cSEC: central branch of the South Equatorial Current; NBUC: North Brazilian Undercurrent; NBC: North Brazilian Current. The central panel shows the localisation of the transects depicted in the 3D plots.

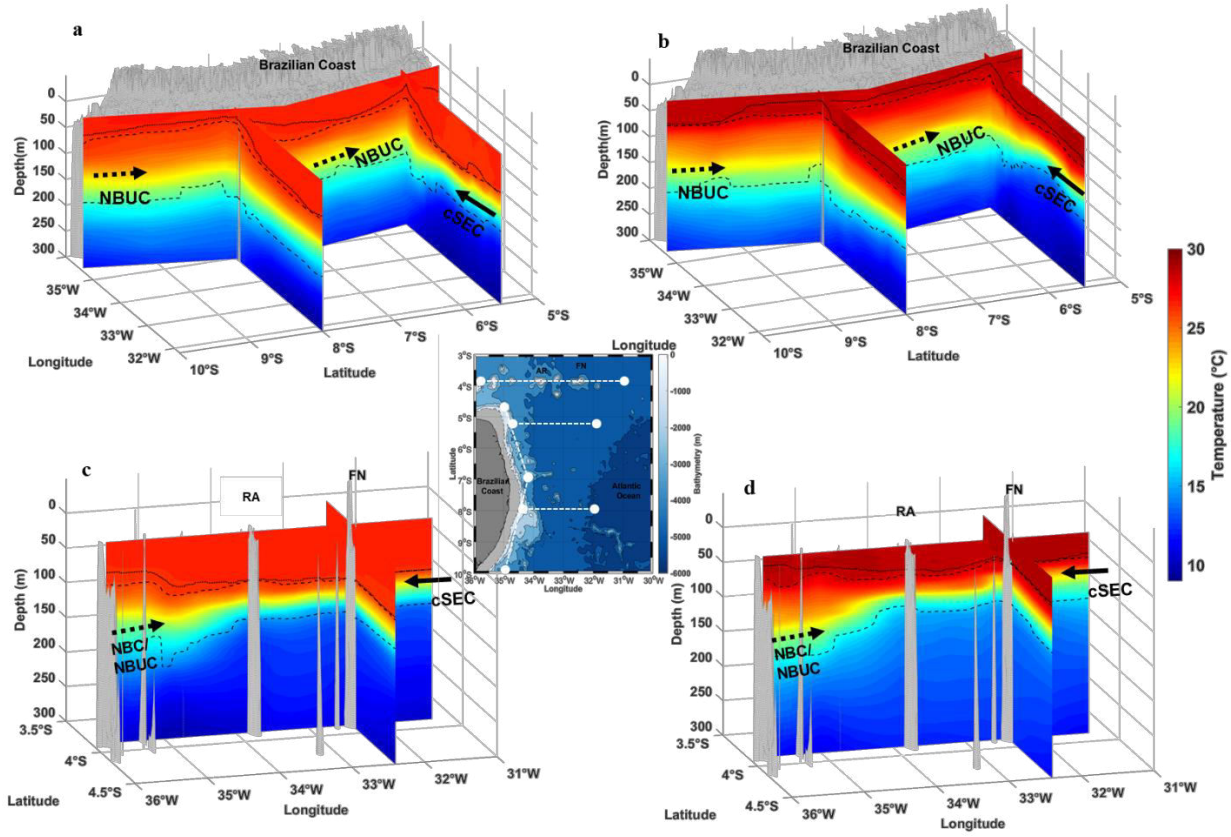

Source: Personal collection.

Figure 12. Vertical sections of salinity in spring (a, c) and fall (b, d). Sections in (a, b) include two along-shore transects (9.95°S/35°W – 7.4°S/34°W and 7.4°S/34°W – 4.7°W/35°W) and two cross-shore transects (8°S/35 – 31.3°W and 5.5°S/35 – 31.3°W). Section in (d,e) include a transect along 3.87°S from 36°W to 31° and one transect crossing Fernando de Noronha Island (FN) at 32.4°W from 3.5°S to 4.5°S. The grey areas represent the relief. RA: Rocas Atoll; FN: Fernando de Noronha archipelago. The black solid line shows the MLD. The black dashed lines show the upper and lower limits of the thermocline. The difference between the MLD and the upper limit of the thermocline illustrate the presence of the BL. The main currents are represented. cSEC: central branch of the South Equatorial Current; NBUC. North Brazilian Undercurrent; NBC: North Brazilian Current. The central panel shows the localisation of the transects depicted in the 3D plots.

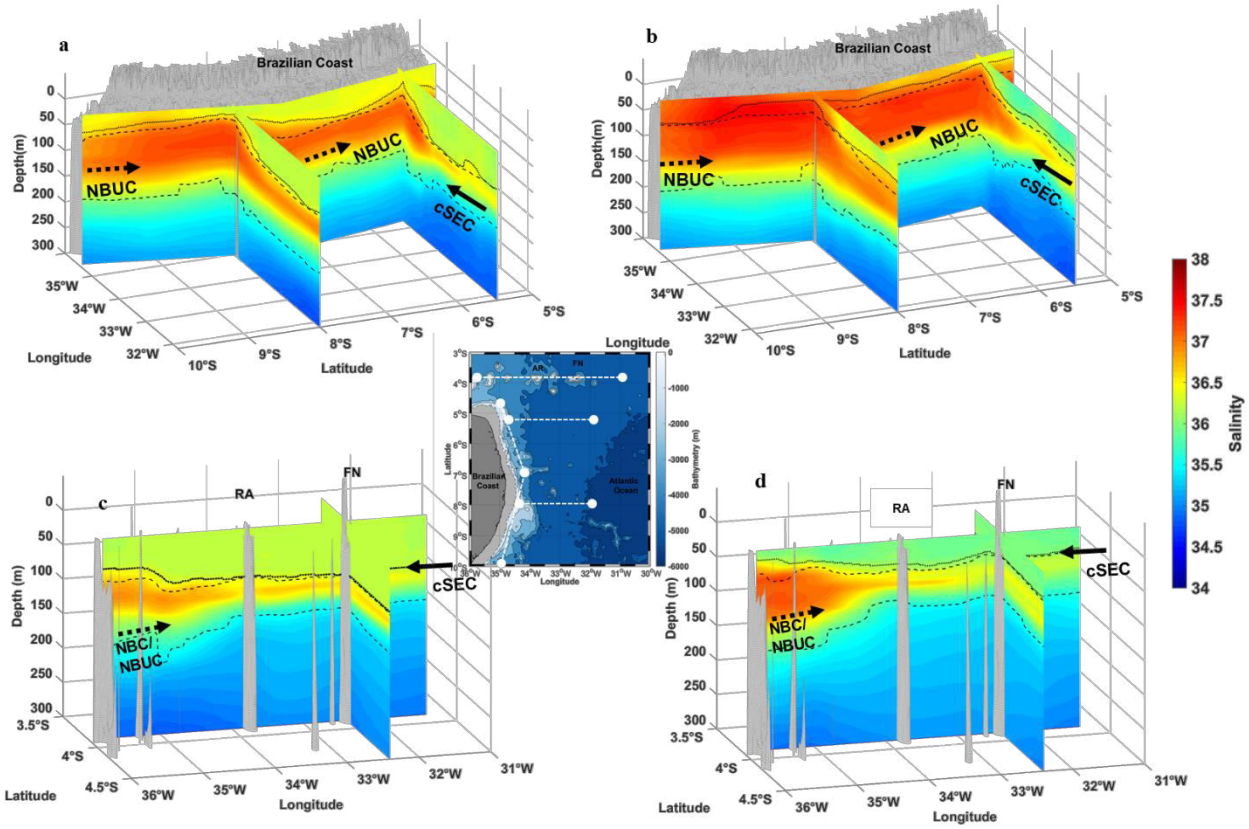

Source: Personal collection.

3.3.3. Atmospheric forcing

In spring, the E-P budget (Fig. 13a) is positive throughout the SWTA domain, with values reaching 6 mm d-1 in the offshore region, south of 8°S. In fall (Fig. 13b), a north–south gradient occurs with negative E-P budget (freshwater inflow) north of 5°S, mostly in A2 (Supplementary Figures S3). South of ~ 6°S the E-P budget was positive (up to 4 mm d^{-1}), but with lower values than in spring.

Southeast trade winds (Fig. 13c, d) are stronger in spring (7.3 to 9 m s^{-1}) than in fall (5.4 to 7 m s^{-1}). In spring, weakest winds are observed in A1, south of 8°S; while in fall, weakest winds are observed north of ~5°S in A2, and strongest winds in the southeast region of the SWTA.

Figure 13. SWTA climatology evaporation minus precipitation budget (E-P) and wind speed at 10 m in spring (a, c) and fall (b, d) according to HOAPS data for 1988 to 2014. Grey solid lines delimit areas A1, A2 and A3 defined in section 3.2.

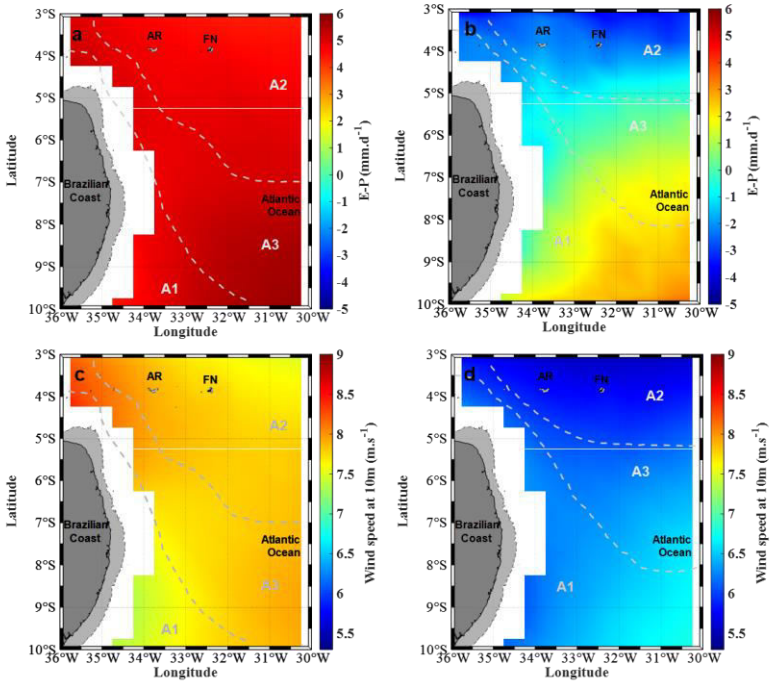

Source: Personal collection.

4. Discussion

Applying a FDA approach on CTD profiles from a variety of sources, we finely describe the canonical states of the thermohaline structure of the upper ocean of the SWTA in austral spring (Sep. – Oct.) and fall (Apr.- May). The application of an FDA approach has several advantages. First, it allows to explicitly consider the shape of the profiles (verticality) even when dealing with heterogenic data (Bayle et al., 2015; Pauthenet et al., 2017). For example, in our case most hydrographic profiles had regular sampling but some were irregular. In addition, fANOVA enable a statistical comparison of profiles (curves) that is not possible to achieve with classical methods. This allowed, for example, to objectively compare CTD profiles from different years and sources.

The application of fANOVA did not reveal significant differences in temperature and salinity profiles between the reference set of data (ABRACOS) and ancillary data sets that span over the period 1983–2017 (Fig. 5). This result was not necessarily expected since Dommenget and Latif (2000) reported decadal variability in SST in the tropical Atlantic during 1903–1994. However, our study area, was one of the least affected by such variability (Dommenget and Latif, 2000). In the same way, an increase in salinity was observed in the last decades but such trend was lower in the South Atlantic central waters (Hummels et al., 2015).

Second, FDA opens the way to robust and objective classification of thermohaline profiles (curves) that led us depicting areas statistically different and geographically separated. Third, the kriging of the profiles in a functional geostatistical framework was highly powerful to interpolate in 3D a high amount of in situ measurements and predictions considering explicitly the shape of all profiles.

Indeed, the FDA application using ordinary kriging with the assumption of stationarity led to consistent results (Fig. 7). In most cases, goodness of fit was very high with similar predictable and observed curves. Nevertheless, the presence of three areas with different thermohaline patterns led to some low adjustment (MSD - profile 4, Fig. 7) mostly in the boundaries between areas where some overlapping occurs (Fig. 6). This was expected since the boundaries between areas cannot be entirely steady. Considering the presence of 3 different areas in the SWTA demonstrating a lack of thermohaline stationarity in the SWTA domain, an alternative approach for future studies accounting for the no stationarity would be the use of Universal Kriging (Menafoglio et al., 2016, 2013), which supposes that the random field has an expectation that depends of the area. 4.1.

4.1. Thermohaline structure and associated processes

By the application of the FDA, we reveal the complex panorama of the thermohaline structure in the SWTA. The portray of the canonical thermohaline structure illustrates seasonal differences with deeper MLD and thermocline in spring (Sep. – Oct.) than in fall (Apr.-May). In addition, we reveal the existence of three spatially delimited thermohaline provinces (A1, A2 and A3) with significant structural differences (Fig. 6) corresponding to different dynamical processes (atmospheric and oceanic). In most oceanic regions and in particular in the SWTA, a precise representation of the thermohaline structure is missing. This is due to a lack of spatial or temporal coverage. This prevents describing the actual spatiotemporal variability. In consequence, large

areas encompassing a variety of conditions are often exemplified by a single TS diagram considered as representative (e.g., Tsuchiya et al., 1994). For example, Araujo et al. (2011) constructed TS diagram by latitudinal band encompassing areas that are significantly different as demonstrated in this study.

The negative surface heat flux and the lower SST (Fig. 8a) that increase the density of the surface layer (Veneziani et al., 2014). In addition, the strong winds (Fig. 13c) due northern position of the ITCZ at around 5°– 8°N; Mignot et al. (2012), the elevated density and the improved mixing cause convective overturning of water, deepening the ML to a greater depth (Lorbacher et al., 2006; Tomczak and Godfrey, 1994). In turn, the shallower MLD (Fig. 10b) and upper thermocline (Fig. 10f) in fall (Apr. – May) (Fig. 8b) are a consequence of the gained buoyancy and higher SST due to the positive heat flux trend started since late spring (Lazar, 2002; Veneziani et al., 2014). This positive buoyancy is also coupled with the relaxation of southeastern trade winds (Fig. 13b) due the southmost position, ~4°N, of the ITCZ (Supplementary Figure S4; Colna, 2017), which shallows the MLD.

4.1.1. Salinity

The seasonal rate of change of salinity (Fig. 9) is not as marked as for temperature. However, the salinity meridional gradient observed at any depth with a reduction of salinity from A1 to A2 (Fig. 9) is sharper in fall than spring. Sea surface salinity (SSS) is mainly controlled by the E-P budget (Fig. 13a, b). In fall, this gradient is driven by the higher precipitation (Supplementary Figure S3) near the equatorial band related to the move back of the ITCZ towards the equator and the evaporation-dominated subtropics (Assunção et al., 2016; Awo et al., 2018; Camara et al., 2015; Melzer and Subrahmanyam, 2017).

In subsurface (110 m and 200 m, Fig. 9c-f), maximum salinity observed in A1 corresponds to the SUW (core salinity > 36.5) advected by the NBUC (Stramma et al., 2005). Salinity vertical core was more extended in fall than spring all along A1 while evaporation is lower in fall in particular north of 8°S (Supplementary Figure S3). However, the SUW is originated by surface evaporation in the subtropical gyre region (10°-25°S) where E-P budget is always positive (Fig. 13 and Supplementary Figure S4). Salter water are then injected into the interior ocean and subsequently advected from the subtropical gyre to the SWTA region by the sSEC and the NBUC (Blanke et al.,

2002; Bourlès et al., 1999; Mémery et al., 2000). There is therefore a delay between formation and entrance of saline waters in A1. Another factor, perhaps the most important, driving the vertical expansion of the salinity core in fall (Figs. 9 and 12) is the shoaling and the greater extension of the NBUC core (Schott et al., 1998; Silva et al., 2005; Stramma et al., 1995), increasing turbulence in surface layer and saline diffusion up to the ML. Our observations are coherent with Araujo et al. (2011) and Domingues et al. (2017) but the exact processes have yet to be elucidated.

4.1.2. Barrier layer

BLs were observed in the SWTA in both spring and fall in most of the study area. However, the BLT was lower than 5 m and "porous" in most (73% in spring; 70% in fall) of the study area. In such conditions, the BL cannot effectively obstruct the heat transfer (Mignot et al., 2009). Our results complement and clarify the observations identified by de Boyer Montégut et al. (2007) who indicated that BLs are quasi-permanent in the western tropical Atlantic. However, this last study was global, with a grid of two degree, which can explain the difference with our fine-scale study at southwestern Atlantic.

The BLT was thick, reached up to 50 m, in a band roughly conforming to the shape of the coast (Fig. 10c, d). This pattern can be primarily related to a higher influence of the SUW, which is entrained into the region within the NBC/NBUC system that flows northwestward along the Brazilian continental slope (Stramma et al., 1995, 2005), in A1. In addition, sea surface salinity fronts induce the formation of BL (Sato et al., 2006; Veneziani et al., 2014). Thicker BLT (Fig. 11b) were indeed observed where salinity fronts occur (Fig. 9a, b), mainly on the fresh side of the fronts agreeing Sato et al. (2006, 2004) and Veneziani et al. (2014). Accordingly, it is in fall conditions, characterized by salty subsurface waters and striking salinity fronts, that the BLT was more preeminent, in particular in the 'frontal' central region (encompassing part of areas A1 and A3 between 6°S and 8°S) of the SWTA.

4.1.3. Diagnosing areas 1, 2 and 3

The three thermohaline domains (areas) share the same water masses (Fig. 6e), but with different density range. Tropical South Water dominates in surface, the SUW in the upper part of the thermocline and the South Atlantic Central Water below. While each water-mass encompasses a large range of temperature or salinity conditions, considering water-masses only is not enough to

portray the ocean characteristics in the study area. Our results show that more important are the actual values of temperature (Fig. 6a, c) and salinity (Fig. 6f, h) along sections between areas (also depicted by TS diagram, Fig. 6e). In the slope area (A1) where the maximum salinity values are observed (Fig. 6f, h), the thermocline is thick (Fig. 12a, c) with low static stability and thus stratification (Fig. 6j). This structure changes towards lower salinity (Fig. 6f, h), thinner thermocline (Fig. 6a, c), higher stability and stratification (Fig. 6j) when moving offshore and north with strong stratification in A2 and intermediate conditions in A3.

4.1.3.1. Area 1 (A1)

A1 corresponds to the western boundary system of the NBUC (Fig. 8) originated by the bifurcation of the sSEC at ~12°–20°S in the subsurface layer (Stramma and Schott, 1999). The NBUC flows northwards at a speed up to 1.2 m.s−1 along the continental slope with a core located within and below the thermocline (at ~ 150–450 m; Stramma et al., 2005). This system forms part of the AMOC and is a crucial link within the southern wind-driven tropical-subtropical cell (Schott et al., 2005; Zhang et al., 2003).

A1 encompasses the shallower MLD/UTD and the thickest thermocline (Table 2) associated with the lower thermic gradient and thus a weak stratification (Figs. 6, 8 and 11). As observed in other boundary systems (Preusse et al., 2010; Todd et al., 2016), the presence of strong western boundary currents (NBUC presents only in A1) reduces the static stability as illustrated by the shear instability (N2 in Fig. 6j), promoting vertical salinity diffusion from the SUW to the isothermal layer. This process favours the formation of long-lasting BL in A1. The presence of thick BLs tends to shoal the MLD (de Boyer Montégut et al., 2007). However, close to the slope, some areas do not encompass thick BL (Fig. 10c, d) but still present shallow MLD/UTD, especially in spring. The shallowest MLD in A1 is likely driven by the NBUC water influx rising the thermocline. This process is magnified in spring by the proximity of the sSEC bifurcation (at ~ 13°S) causing intense mesoscale activities (Peterson and Stramma, 1991; Schott et al., 2005; Thévenin et al., 2019). Thus, in this area, NBUC-related oceanic processes seem to overwhelm atmospheric (wind) forcing, especially in the slope area.

4.1.3.2. Area 2 (A2)

A2 encompasses most of the Fernando de Noronha chain and is characterised by high static stability due to high buoyancy frequency (Fig. 6j) at the thermocline depth. This reflects the dominance of a relatively weak (~0.34 m s^{-1}) surface current (~0–100 m), the cSEC (Fig. 11c, d), that carries water from the eastern Atlantic with lower salinity compared with the waters of the SWTA (Lumpkin and Garzoli, 2005; Peterson and Stramma, 1991). At the sub-thermocline, A2 is dominated by the eastward SEUC (Fig. 8), located between 3°S and 5°S (Goes et al., 2005) and supplied by the NBC/NBUC system (Goes et al., 2005; Stramma et al., 2005). Even under the influence of the SUW, A2 presents the lowest BLF of the study area. The increase in BLF from 14% in spring to 32% in fall can be explained by ITCZ-induced precipitations, hence negative E-P budget at low latitudes (Fig. 13b, Supplementary Figures S3 and S4; Awo et al., 2018; Da-Allada et al., 2013) decreasing the SSS (Fig. 9b).

The deeper MLD observed in spring can be associated with the negative heat flux, stronger winds (Fig. 13a; Sato et al., 2006) and low precipitation (Supplementary Figure S3a northern position of the ITCZ), leading to higher SSS and therefore higher density and convective overturning of the surface layer. In spring, the thermocline is also locally shallower downstream FN (Fig. 12d). These displacement could be originated by orographic influences on the cSEC (wake effect) as shown by Tchamabi et al. (2017). This orographic interaction reduces the thermocline depth, increasing nutrient supply and related biological production (Jales et al., 2015; Silva, 2018).

4.1.3.3. Area 3 (A3)

Overall, A3 acts as a transition zone and mixing of water bodies. Indeed, with an intermediate stratification pattern (Fig. 6j) and, therefore, moderate static stability, A3 is still influenced by the western boundary system but is not directly affected by the NBUC. The northmost part of A3 is influenced by the westward flow of the southern limb of the cSEC (3° − 5°S, Molinari, 1982). In fall, the low temperatures (Fig. 8e, f) and salinities (Fig. 9e and f) observed at 200 m along A3 could be originated by the advection of subsurface colder and less saline eastern Atlantic waters advected westwards with a ~9cms^{-1} velocity near 7°S (Bourlès et al., 1999; Molinari, 1983, 1982).

5. Conclusion

This study shows that the application of an FDA approach on hydrographic data allows for a robust and precise characterising and estimation of the ocean thermohaline 3D structure. Even if based on a stationarity assumption for the mean function in a non-stationary context, our approach brought insights on the thermohaline structure of the tropical southwestern Atlantic. By characterising the canonical seasonal states of spring and fall in the SWTA, we reveal a clear spatial pattern with the presence of three areas with significantly different thermohaline structure. Area 1, mostly located along the continental slope, reflects the western boundary current system, with low static stability and high frequency of occurrence of barrier layer (BL). Conversely, Area 2, located along the Fernando de Noronha chain, presents strong static stability with a well-marked thermocline. This area is under the influence of the eastern Atlantic. It is characterised by a low BLF, which is seasonally modulated by the latitudinal oscillation of ITCZ, controlling the regime of precipitation. In turn, A3 behaves as a transition zone between A1 and A2 with still the presence of the water core of maximum salinity in subsurface, and therefore strong/moderate presence of BL.

From our results, the spring and fall thermohaline structure of the upper ocean did not vary significantly during the last decades. However, the expected changes in AMOC circulation (Chang et al., 2008) should affect the 3D transport of heat, salt, as well as the regional distributions of water mass boundaries, and may lead to shifts in ecosystems (Foltz et al., 2019; Hummels et al., 2015). This work can thus serve as a reference for diagnosing future variations in the AMOC and subtropical–tropical cell variability.

On the basis of this and other studies (e.g., Pauthenet et al., 2019, 2017), FDA approach emerges as a powerful way to describe, characterise, classify and compare ocean patterns and processes. It can be applied to in situ data but could also be used to deeply and comprehensively explore ocean models outputs. Further, this approach is applicable to any fields where data are present in the form of curves.

Declaration of Competing Interest

The authors declare that they have no known competing financial interests or personal relationships that could have appeared to influence the work reported in this paper.

Acknowledgments

We acknowledge the French oceanographic fleet for funding the at sea survey and the officers and crew of the R/V Antea for their contribution to the success of the operations during the ABRACOS cruises. We thank the Helmholtz-Zentrum für Ozeanforschung Kiel (GEOMAR) for PANGEA data availability. The Conselho Nacional de Desenvolvimento Científico e Tecnológico (CNPq) by supported through a PhD scholarship grant for Assunção, Ramilla. M.A. thanks the support of the Brazilian Research network on Global Climate Change FINEP/Rede CLIMA (grants 01.13.0353-00). This work is a contribution to the International Joint Laboratory TAPIOCA (www.tapioca.ird.fr), CAPES/COFECUB program (88881.142689/2017-01), PADDLE project (funding by the European Union's Horizon 2020 research and innovation programme - grant agreement No. 73427).

References

Aguiar-Conraria, L., Soares, M.J., 2014. The continuous wavelet transform: moving beyond uni- and bivariate analysis. J. Econ. Surv. 28, 344–375. https://doi.org/10.1111/joes.12012

Andersson, A., Graw, K., Schröder, M., Fennig, K., Liman, J., Bakan, S., Hollmann, R., Klepp, C., 2017. Hamburg Ocean Atmosphere Parameters and Fluxes from Satellite Data - HOAPS 4.0 [WWW Document]. Satell. Appl. Facil. Clim. Monit. (CM SAF). https://doi.org/10.5676/EUM_SAF_CM/HOAPS/V002

Annasawmy, P., Ternon, J.-F., Lebourges-Dhaussy, A., Roudaut, G., Cotel, P., Herbette, S., Ménard, F., Marsac, F., 2020. Micronekton distribution as influenced by mesoscale eddies, Madagascar shelf and shallow seamounts in the south-western Indian Ocean: an acoustic approach. Deep Sea Res. Part II Top. Stud. Oceanogr. 176, 104812. https://doi.org/10.1016/j.dsr2.2020.104812

Araújo, M., Limongi, C., Servain, J., Silva, M., Leite, F.S., Veleda, D., Lentini, C.A.D., 2011. Salinity-induced mixed and barrier layers in the southwestern tropical Atlantic Ocean off the northeast of Brazil. Ocean Sci. 7, 63–73. https://doi.org/10.5194/os-7-63-2011

Assunção, R. V., Silva, A.C. da, Martins, J., Flores Montes, M., 2016. Spatial-Temporal Variability of the Thermohaline Properties in the Coastal Region of Fernando de Noronha Archipelago, Brazil. J. Coast. Res. 75, 512–516. https://doi.org/10.2112/SI75-103.1

Assunção, R. V., Silva, A.C. da, Roy, A., Bourlès, B., Silva, C.H.S., Ternon, J.-F., Araújo, M., Bertrand, A., 2020. 3D characterisation of the thermohaline structure in the southwestern tropical Atlantic derived from functional data analysis of in situ profiles. Prog. Oceanogr. 187, 102399. https://doi.org/10.1016/j.pocean.2020.102399

Awo, F.M., Alory, G., Da-Allada, C.Y., Delcroix, T., Jouanno, J., Kestenare, E., Baloïtcha, E., 2018. Sea Surface Salinity Signature of the Tropical Atlantic Interannual Climatic Modes. J. Geophys. Res. Ocean. 7420–7437. https://doi.org/10.1029/2018JC013837

Badal, M., Rughooputh, S., Rydberg, L., Robinson, I., Pattiaratchi, C., 2010. Eddy formation around South West Mascarene Plateau (Indian Ocean) as evidenced by satellite 'global ocean colour' data. West. Indian Ocean J. Mar. Sci. 8. https://doi.org/10.4314/wiojms.v8i2.56969

Balaguru, K., Chang, P., Saravanan, R., Jang, C.J., 2012. The barrier layer of the Atlantic warmpool: formation mechanism and influence on the mean climate. Tellus A Dyn. Meteorol. Oceanogr. 64, 18162. https://doi.org/10.3402/tellusa.v64i0.18162

Ballón, M., Bertrand, A., Lebourges-Dhaussy, A., Gutiérrez, M., Ayón, P., Grados, D., Gerlotto, F., 2011. Is there enough zooplankton to feed forage fish populations off Peru? An acoustic (positive) answer. Prog. Oceanogr. 91, 360–381. https://doi.org/10.1016/j.pocean.2011.03.001

Bayle, S., Monestiez, P., Guinet, C., Nerini, D., 2015. Moving toward finer scales in oceanography: Predictive linear functional model of Chlorophyll a profile from light data. Prog. Oceanogr. 134, 221–231. https://doi.org/10.1016/j.pocean.2015.02.001

Béhagle, N., Cotté, C., Lebourges-Dhaussy, A., Roudaut, G., Duhamel, G., Brehmer, P., Josse, E., Cherel, Y., 2017. Acoustic distribution of discriminated micronektonic organisms from a bi-frequency processing: The case study of eastern Kerguelen oceanic waters. Prog. Oceanogr. https://doi.org/10.1016/j.pocean.2017.06.004

Benoit-Bird, K.J., Lawson, G.L., 2016. Ecological Insights from Pelagic Habitats Acquired Using Active Acoustic Techniques. Ann. Rev. Mar. Sci. 8, 463–490. https://doi.org/10.1146/annurev-marine-122414-034001

Bertrand, A., 2017. ABRACOS 2 cruise, RV Antea. https://doi.org/10.17600/17004100

Bertrand, A., 2015. ABRACOS cruise, RV Antea. https://doi.org/10.17600/15005600

Bertrand, A., Ballón, M., Chaigneau, A., 2010. Acoustic observation of living organisms reveals the upper limit of the oxygen minimum zone. PLoS One 5. https://doi.org/10.1371/journal.pone.0010330

Bertrand, A., Grados, D., Colas, F., Bertrand, S., Capet, X., Chaigneau, A., Vargas, G., Mousseigne, A., Fablet, R., 2014. Broad impacts of fine-scale dynamics on seascape structure from zooplankton to seabirds. Nat. Commun. 5. https://doi.org/10.1038/ncomms6239

Biastoch, A., Böning, C.W., Getzlaff, J., Molines, J.-M., Madec, G., 2008. Causes of Interannual–Decadal Variability in the Meridional Overturning Circulation of the Midlatitude North Atlantic Ocean. J. Clim. 21, 6599–6615. https://doi.org/10.1175/2008JCLI2404.1

Biescas, B., Sallarès, V., Pelegrí, J.L., Machín, F., Carbonell, R., Buffett, G., Dañobeitia, J.J., Calahorrano, A., 2008. Imaging meddy finestructure using multichannel seismic reflection data. Geophys. Res. Lett. 35, L11609. https://doi.org/10.1029/2008GL033971

Blanke, B., Arhan, M., Lazar, A., Prévost, G., 2002. A Lagrangian numerical investigation of the origins and fates of the salinity maximum water in the Atlantic. J. Geophys. Res. 107, 3163. https://doi.org/10.1029/2002JC001318

Boor, C. De, 2001. A practical guide to splines. Springer Handbooks Comput. Stat. 302.

Bourlès, B., D'Orgeville, M., Eldin, G., Gouriou, Y., Chuchla, R., DuPenhoat, Y., Arnault, S., 2002. On the evolution of the thermocline and subthermocline eastward currents in the Equatorial Atlantic. Geophys. Res. Lett. 29, 32-1-32–4. https://doi.org/10.1029/2002GL015098

Bourlès, B., Gouriou, Y., Chuchla, R., 1999a. On the circulation in the upper layer of the western equatorial Atlantic. J. Geophys. Res. Ocean. 104, 21151–21170. https://doi.org/10.1029/1999JC900058

Bourlès, B., Molinari, R.L., Johns, E., Wilson, W.D., Leaman, K.D., 1999b. Upper layer currents in the western tropical North Atlantic (1989-1991). J. Geophys. Res. Ocean. 104, 1361–1375. https://doi.org/10.1029/1998JC900025

Brainerd, K.E., Gregg, M.C., 1995. Surface mixed and mixing layer depths. Deep. Res. Part I 42, 1521–1543. https://doi.org/10.1016/0967-0637(95)00068-H

Brazilian Atlantic Islands: Fernando de Noronha and Atol das Rocas Reserves - UNESCO World Heritage Centre [WWW Document], n.d. URL https://whc.unesco.org/en/list/1000 (accessed 10.21.19).

Buckley, M.W., Marshall, J., 2016. Observations, inferences, and mechanisms of Atlantic Meridional Overturning Circulation variability: A review. Rev. Geophys. https://doi.org/10.1002/2015RG000493.Received

Cade, D.E., Benoit-Bird, K.J., 2015. Depths, migration rates and environmental associations of acoustic scattering layers in the Gulf of California. Deep Sea Res. Part I Oceanogr. Res. Pap. 102, 78–89. https://doi.org/10.1016/j.dsr.2015.05.001

Cade, D.E., Benoit-Bird, K.J., 2014. An automatic and quantitative approach to the detection and tracking of acoustic scattering layers. Limnol. Oceanogr. Methods 12, 742–756. https://doi.org/10.4319/lom.2014.12.742

Caesar, L., McCarthy, G.D., Thornalley, D.J.R., Cahill, N., Rahmstorf, S., 2021. Current Atlantic Meridional Overturning Circulation weakest in last millennium. Nat. Geosci. 14, 118–120. https://doi.org/10.1038/s41561-021-00699-z

Camara, I., Kolodziejczyk, N., Mignot, J., Lazar, A., Gaye, A.T., 2015. On the seasonal variations of salinity of the tropical Atlantic mixed layer. J. Geophys. Res. Ocean. 120, 4441–4462. https://doi.org/10.1002/2015JC010865

Camara, I, Kolodziejczyk, N., Mignot, J., Lazar, A., Gaye, A.T., 2015. On the seasonal variations of salinity of the tropical Atlantic mixed layer. J. Geophys. Res. Ocean. 120, 4441–4462. https://doi.org/10.1002/2015JC010865

Cardoso, C., Caldeira, R.M.A., Relvas, P., Stegner, A., 2020. Islands as eddy transformation and generation hotspots: Cabo Verde case study. Prog. Oceanogr. 184, 102271. https://doi.org/10.1016/j.pocean.2020.102271

Carranza, M.M., Gille, S.T., Franks, P.J.S., Johnson, K.S., Pinkel, R., Girton, J.B., 2018. When Mixed Layers Are Not Mixed. Storm-Driven Mixing and Bio-optical Vertical Gradients in Mixed

Layers of the Southern Ocean. J. Geophys. Res. Ocean. 123, 7264–7289. https://doi.org/10.1029/2018JC014416

Chaves, A.H.S., Pessek, K., Guimarães, L.G., Ribeiro, C.E.P., 2011. Shallow Water Acoustic Propagation at Arraial do Cabo, Brazil, in: 12th International Congress of the Brazilian Geophysical Society & EXPOGEF, Rio de Janeiro, Brazil, 15–18 August 2011. Brazilian Geophysical Society, pp. 926–928. https://doi.org/10.1190/sbgf2011-191

Chen, D., Busalacchi, A.J., Rothstein, L.M., 1994. The roles of vertical mixing, solar radiation, and wind stress in a model simulation of the sea surface temperature seasonal cycle in the tropical Pacific Ocean. J. Geophys. Res. 99, 20345. https://doi.org/10.1029/94JC01621

Chen, G., Peng, L., Ma, C., 2018. Climatology and seasonality of upper ocean salinity: a three-dimensional view from argo floats. Clim. Dyn. 50, 2169–2182. https://doi.org/10.1007/s00382-017-3742-6

Cheng, W., Chiang, J.C.H., Zhang, D., 2013. Atlantic meridional overturning circulation (AMOC) in CMIP5 Models: RCP and historical simulations. J. Clim. 26, 7187–7197. https://doi.org/10.1175/JCLI-D-12-00496.1

Colna, K.E., 2017. Latitudinal Position and Trends of the Intertropical Convergence Zone (ITCZ) and its Relationship with Upwelling in the Southern Caribbean Sea and Global Climate Indices. University of South Florida.

Costa, P.L., Madureira, L.A.S.P., de Pinho, M.P., 2013. Seabed acoustic classification in the Pelotas basin, Brazil. Brazilian J. Oceanogr. 61, 13–22. https://doi.org/10.1590/S1679-87592013000100002

Coyle, K.O., Cooney, R.T., 1993. Water column sound scattering and hydrography around the Pribilof Islands, Bering Sea. Cont. Shelf Res. 13, 803–827. https://doi.org/10.1016/0278-4343(93)90028-V

Cressie, N.A.C., 1993. Statistics for Spatial Data, Wiley Series in Probability and Statistics. John Wiley & Sons, Inc., Hoboken, NJ, USA. https://doi.org/10.1002/9781119115151

Cronin, M.F., Weller, R.A., Lampitt, R.S., Send, U., 2012. Ocean Reference Stations, in: Earth Observation. InTech. https://doi.org/10.5772/27423

Cuevas, A., Febrero, M., Fraiman, R., 2004. An anova test for functional data. Comput. Stat. Data Anal. 47, 111–122. https://doi.org/10.1016/J.CSDA.2003.10.021

Cullen, J.J., 1982. The deep chlorophyll maximum: comparing vertical profiles of chlorophyll a. Can. J. Fish. Aquat. Sci. 39, 791–803. https://doi.org/10.1139/f82-108

Da-Allada, C.Y., Alory, G., Du Penhoat, Y., Kestenare, E., Durand, F., Hounkonnou, N.M., 2013. Seasonal mixed-layer salinity balance in the tropical Atlantic Ocean: Mean state and seasonal cycle. J. Geophys. Res. Ocean. 118, 332–345. https://doi.org/10.1029/2012JC008357

da Silveira, I.C.A., Miranda, L.B., Brown, W.S., 1994. On the origins of the North Brazil Current. J. Geophys. Res. 99, 22501. https://doi.org/10.1029/94JC01776

Dabo-Niang, S., Ferraty, F., 2008. Functional and Operatorial Statistics, Contributions to Statistics. Physica-Verlag HD, Heidelberg. https://doi.org/10.1007/978-3-7908-2062-1

Daubechies, I., 1992. Ten Lectures on Wavelets, Ten Lectures on Wavelets. Society for Industrial and Applied Mathematics. https://doi.org/10.1137/1.9781611970104

de Boyer Montégut, C., Madec, G., Fischer, A.S., Lazar, A., Iudicone, D., 2004. Mixed layer depth over the global ocean: An examination of profile data and a profile-based climatology. J. Geophys. Res. C Ocean. 109, 1–20. https://doi.org/10.1029/2004JC002378

de Boyer Montégut, C., Mignot, J., Lazar, A., Cravatte, S., 2007. Control of salinity on the mixed layer depth in the world ocean: 1. General description. J. Geophys. Res. Ocean. 112, 1–12. https://doi.org/10.1029/2006JC003953

De Robertis, A., McKelvey, D.R., Ressler, P.H., 2010. Development and application of an empirical multifrequency method for backscatter classification. Can. J. Fish. Aquat. Sci. 67, 1459–1474. https://doi.org/10.1139/F10-075

Dengler, M., Schott, F.A., Eden, C., Brandt, P., Fischer, J., Zantopp, R.J., 2004. Break-up of the Atlantic deep western boundary current into eddies at 8° S. Nature 432, 1018–1020. https://doi.org/10.1038/nature03134

Domingues, E. de C., Schettini, C.A.F., Truccolo, E.C., Oliveira Filho, J.C. de, 2017. Hydrography and currents on the Pernambuco Continental Shelf. RBRH 22, e43. https://doi.org/10.1590/2318-0331.0217170027

Doty, M.S., Oguri, M., 1956. The Island Mass Effect. ICES J. Mar. Sci. 22, 33–37. https://doi.org/10.1093/icesjms/22.1.33

Fahey, D.., Doherty, S.J., Hibbard, K.A., Romanou, A., Taylor, P.C., 2017. Ch. 2: Physical Drivers of Climate Change. Climate Science Special Report: Fourth National Climate Assessment, Volume I. Washington, DC. https://doi.org/10.7930/J0513WCR

Febrero-Bande, M., Fuente, M.O. de la, 2012. Statistical Computing in Functional Data Analysis: The R Package fda.usc. J. Stat. Softw. 51, 1–28. https://doi.org/10.18637/jss.v051.i04

Fer, I., Nandi, P., Holbrook, W.S., Schmitt, R.W., Páramo, P., 2010. Seismic imaging of a thermohaline staircase in the western tropical North Atlantic. Ocean Sci. 6, 621–631. https://doi.org/10.5194/os-6-621-2010

Folt, C.L., Burns, C.W., 1999. Biological drivers of zooplankton patchiness. Trends Ecol. Evol. 14, 300–305. https://doi.org/10.1016/S0169-5347(99)01616-X

Foltz, G.R., Brandt, P., Richter, I., Rodríguez-Fonseca, B., Hernandez, F., Dengler, M., Rodrigues, R.R., Schmidt, J.O., Yu, L., Lefevre, N., Da Cunha, L.C., McPhaden, M.J., Araújo, M., Karstensen, J., Hahn, J., Martín-Rey, M., Patricola, C.M., Poli, P., Zuidema, P., Hummels, R., Perez, R.C., Hatje, V., Lübbecke, J.F., Polo, I., Lumpkin, R., Bourlès, B., Asuquo, F.E., Lehodey, P., Conchon, A., Chang, P., Dandin, P., Schmid, C., Sutton, A., Giordani, H., Xue, Y., Illig, S., Losada, T., Grodsky, S.A., Gasparin, F., Lee, T., Mohino, E., Nobre, P., Wanninkhof, R., Keenlyside, N., Garcon, V., Sánchez-Gómez, E., Nnamchi, H.C., Drévillon, M., Storto, A., Remy, E., Lazar, A., Speich, S., Goes, M., Dorrington, T., Johns, W.E., Moum, J.N., Robinson, C., Perruche, C., de

Souza, R.B., Gaye, A.T., López-Parages, J., Monerie, P.-A., Castellanos, P., Benson, N.U., Hounkonnou, M.N., Duhá, J.T., Laxenaire, R., Reul, N., 2019. The Tropical Atlantic Observing System. Front. Mar. Sci. 6. https://doi.org/10.3389/fmars.2019.00206

Foltz, G.R., McPhaden, M.J., 2008. Seasonal mixed layer salinity balance of the tropical North Atlantic Ocean. J. Geophys. Res. 113, C02013. https://doi.org/10.1029/2007JC004178

Foote, K.G., Knudsen, H.P., Vestnes, G., 1987. Calibration of acoustic instruments for fish density estimation: A practical guide. J. Acoust. Soc. Am. 83, 831–832. https://doi.org/10.1121/1.396131

Gasparin, F., Maes, C., Sudre, J., Garcon, V., Ganachaud, A., 2014. Water mass analysis of the Coral Sea through an Optimum Multiparameter method. J. Geophys. Res. Ocean. 119, 7229–7244. https://doi.org/10.1002/2014JC010246

Gilmartin, M., Revelante, N., 1974. The "island mass" effect on the phytoplankton and primary production of the Hawaiian Islands. J. Exp. Mar. Bio. Ecol. 16, 181–204. https://doi.org/10.1016/0022-0981(74)90019-7

Giraldo, R., Delicado Useros, P.F., Mateu, J., 2007. Geostatistics for functional data: an ordinary kriging approach.

Goes, M., Molinari, R., Da Silveira, I., Wainer, I., 2005. Retroflections of the North Brazil Current during February 2002. Deep. Res. Part I Oceanogr. Res. Pap. 52, 647–667. https://doi.org/10.1016/j.dsr.2004.10.010

Grados, D., Bertrand, A., Colas, F., Echevin, V., Chaigneau, A., Gutiérrez, D., Vargas, G., Fablet, R., 2016. Spatial and seasonal patterns of fine-scale to mesoscale upper ocean dynamics in an Eastern Boundary Current System. Prog. Oceanogr. 142, 105–116. https://doi.org/10.1016/j.pocean.2016.02.002

Grinsted, A., Moore, J.C., Jevrejeva, S., 2004. Application of the cross wavelet transform and wavelet coherence to geophysical time series Nonlinear Processes in Geophysics Application of the cross wavelet transform and wavelet coherence to geophysical time series, European Geosciences Union (EGU).

Hadjipantelis, P.Z., Müller, H.-G., 2018. Functional Data Analysis for Big Data: A Case Study on California Temperature Trends, in: Springer Handbooks of Computational Statistics. pp. 457–483. https://doi.org/10.1007/978-3-319-18284-1_18

Halpern, D., 2002. Offshore Ekman transport and Ekman pumping off Peru during the 1997-1998 El Niño. Geophys. Res. Lett. 29, 19-1-19–4. https://doi.org/10.1029/2001GL014097

Holbrook, W.S., Fer, I., 2005. Ocean internal wave spectra inferred from seismic reflection transects. Geophys. Res. Lett. 32, 2–5. https://doi.org/10.1029/2005GL023733

Holbrook, W.S., Fer, I., Schmitt, R.W., 2009. Images of internal tides near the Norwegian continental slope. Geophys. Res. Lett. 36, 1–5. https://doi.org/10.1029/2009GL038909

Holte, J., Talley, L., 2009. A new algorithm for finding mixed layer depths with applications to argo data and subantarctic mode water formation. J. Atmos. Ocean. Technol. 26, 1920–1939. https://doi.org/10.1175/2009JTECHO543.1

Hounsou-gbo, G.A., Araújo, M., Bourlès, B., Veleda, D., Servain, J., 2015. Tropical Atlantic Contributions to Strong Rainfall Variability Along the Northeast Brazilian Coast. Adv. Meteorol. 2015, 1–13. https://doi.org/10.1155/2015/902084

Hummels, R., Brandt, P., Dengler, M., Fischer, J., Araújo, M., Veleda, D., Durgadoo, J. V., 2015. Interannual to decadal changes in the western boundary circulation in the Atlantic at 11°S. Geophys. Res. Lett. 42, 7615–7622. https://doi.org/10.1002/2015GL065254

Hüttl, S., Böning, C.W., 2006. Mechanisms of decadal variability in the shallow subtropical-tropical circulation of the Atlantic Ocean: A model study. J. Geophys. Res. 111, C07011. https://doi.org/10.1029/2005JC003414

Jales, M.C., Feitosa, F.A. do N., Koening, M.L., Montes, M. de J.F., Araújo, M., Silva, R.A. da, 2015. Phytoplankton biomass dynamics and environmental variables around the Rocas Atoll Biological Reserve, South Atlantic. Brazilian J. Oceanogr. 63, 443–454. https://doi.org/10.1590/S1679-87592015093906304

Jamshidi, S., 2017. Assessment of thermal stratification, stability and characteristics of deep water zone of the southern Caspian Sea. J. Ocean Eng. Sci. 2, 203–216. https://doi.org/10.1016/j.joes.2017.08.005

Jang, C.J., Park, J., Park, T., Yoo, S., 2011. Response of the ocean mixed layer depth to global warming and its impact on primary production: a case for the North Pacific Ocean. ICES J. Mar. Sci. 68, 996–1007. https://doi.org/10.1093/icesjms/fsr064

Johnston, T.M.S., Rudnick, D.L., 2009. Observations of the Transition Layer. J. Phys. Oceanogr. 39, 780–797. https://doi.org/10.1175/2008JPO3824.1

Kara, A.B., 2003. Mixed layer depth variability over the global ocean. J. Geophys. Res. 108, 3079. https://doi.org/10.1029/2000JC000736

Ker, S., Le Gonidec, Y., Marié, L., 2016. Multifrequency seismic detectability of seasonal thermoclines assessed fromARGO data. J. Geophys. Res. Ocean. 3741–3756. https://doi.org/10.1002/2015JC011228.Received

Ker, S., Le Gonidec, Y., Marié, L., Thomas, Y., Gibert, D., 2015. Multiscale seismic reflectivity of shallow thermoclines. J. Geophys. Res. Ocean. 120, 1872–1886. https://doi.org/10.1002/2014JC010478

Kim, H.-J., Miller, A.J., 2007. Did the Thermocline Deepen in the California Current after the 1976/77 Climate Regime Shift? J. Phys. Oceanogr. 37, 1733–1739. https://doi.org/10.1175/jpo3058.1

Klymak, J.M., Moum, J.N., 2003. Internal solitary waves of elevation advancing on a shoaling shelf. Geophys. Res. Lett. 30, 2003GL017706. https://doi.org/10.1029/2003GL017706

Kowsmann, R.O., Costa, M.P.A., 1976. Estratigrafia sismica do plato de pernambuco. Rev. Bras. Geociencias 6, 95–101.

Kraus, E.B. (Eric B., Businger, J.A., 1994. Atmosphere-ocean interaction. Oxford University Press.

Krumme, U., Saint-Paul, U., 2003. Observations of fish migration in a macrotidal mangrove channel in Northern Brazil using a 200-kHz split-beam sonar. Aquat. Living Resour. 16, 175–184. https://doi.org/10.1016/S0990-7440(03)00046-9

Lambert, R.B., Sturges, W., 1977. A thermohaline staircase and vertical mixing in the thermocline. Deep Sea Res. 24, 211–222. https://doi.org/10.1016/S0146-6291(77)80001-5

Lavery, A.C., Chu, D., Moum, J.N., 2010. Measurements of acoustic scattering from zooplankton and oceanic microstructure using a broadband echosounder. ICES J. Mar. Sci. 67, 379–394. https://doi.org/10.1093/icesjms/fsp242

Lavery, A.C., Wiebe, P.H., Stanton, T.K., Lawson, G.L., Benfield, M.C., Copley, N., 2007. Determining dominant scatterers of sound in mixed zooplankton populations. J. Acoust. Soc. Am. 122, 3304–3326. https://doi.org/10.1121/1.2793613

Lazar, A., 2002. Seasonality of the ventilation of the tropical Atlantic thermocline in an ocean general circulation model. J. Geophys. Res. 107, 3104. https://doi.org/10.1029/2000JC000667

Leach, T.H., Beisner, B.E., Carey, C.C., Pernica, P., Rose, K.C., Huot, Y., Brentrup, J.A., Domaizon, I., Grossart, H.P., Ibelings, B.W., Jacquet, S., Kelly, P.T., Rusak, J.A., Stockwell, J.D., Straile, D., Verburg, P., 2018. Patterns and drivers of deep chlorophyll maxima structure in 100 lakes: The relative importance of light and thermal stratification. Limnol. Oceanogr. 63, 628–646. https://doi.org/10.1002/lno.10656

Legendre, L., 1981. Hydrodynamic Control of Marine Phytoplankton Production: The Paradox of Stability, in: Elsevier Oceanography Series. pp. 191–207. https://doi.org/10.1016/S0422-9894(08)70410-0

Liu, C., Köhl, A., Liu, Z., Wang, F., Stammer, D., 2016. Deep-reaching thermocline mixing in the equatorial pacific cold tongue. Nat. Commun. 7. https://doi.org/10.1038/ncomms11576

Liu, M., Tanhua, T., 2019a. Characteristics of Water Masses in the Atlantic Ocean based on GLODAPv2 data. Ocean Sci. Discuss. 1–43. https://doi.org/10.5194/os-2018-139

Liu, M., Tanhua, T., 2019b. Distribution of Water Masses in the Atlantic Ocean based on GLODAPv2. Ocean Sci. Discuss. 1–32. https://doi.org/10.5194/os-2018-140

Liu, Z., 1993. Thermocline Forced by Varying Ekman Pumping. Part II: Annual and Decadal Ekman Pumping. J. Phys. Oceanogr. 23, 2523–2540. https://doi.org/10.1175/1520-0485(1993)023

Longhurst, A.R., Pauly, D., 1987. Ecology of Tropical Oceans, Ecology of tropical oceans. Elsevier. https://doi.org/10.1016/C2009-0-02861-X

Lorbacher, K., Dommenget, D., Niiler, P.P., Köhl, A., 2006. Ocean mixed layer depth: A subsurface proxy of ocean-atmosphere variability. J. Geophys. Res. 111, C07010. https://doi.org/10.1029/2003JC002157

Lukas, R., Lindstrom, E., 1991. The mixed layer of the western equatorial Pacific Ocean. J. Geophys. Res. 96, 3343. https://doi.org/10.1029/90JC01951

Lumpkin, R., Garzoli, S.L., 2005. Near-surface circulation in the Tropical Atlantic Ocean. Deep Sea Res. Part I Oceanogr. Res. Pap. 52, 495–518. https://doi.org/10.1016/j.dsr.2004.09.001

Lumpkin, R., Speer, K., 2007. Global ocean meridional overturning. J. Phys. Oceanogr. 37, 2550–2562. https://doi.org/10.1175/JPO3130.1

Lüthi, D., Le Floch, M., Bereiter, B., Blunier, T., Barnola, J.-M., Siegenthaler, U., Raynaud, D., Jouzel, J., Fischer, H., Kawamura, K., Stocker, T.F., 2008. High-resolution carbon dioxide concentration record 650,000–800,000 years before present. Nature 453, 379–382. https://doi.org/10.1038/nature06949

Maclennan, D.N., Fernandes, P.G., Dalen, J., 2002. A consistent approach to definitions and symbols in fisheries acoustics. ICES J. Mar. Sci. 59, 365–369. https://doi.org/10.1006/jmsc.2001.1158

Madhupratap, M., Nair, V.R., Sreekumaran Nair, S.R., Achuthankutty, C.T., 1981. Thermocline {&} zooplankton distribution. Indian J. Mar. Sci. 10, 262–265.

Maes, C., O'Kane, T.J., 2014. Seasonal variations of the upper ocean salinity stratification in the Tropics. J. Geophys. Res. Ocean. 119, 1706–1722. https://doi.org/10.1002/2013JC009366

Marchal, E., Gerlotto, F., Stequert, B., 1993. On the relationship between scattering layer, Scattering layers Equatorial dynamics Tuna fisheries thermal structure and tuna abundance in the Eastern Atlantic equatorial Couches réfléchissantes Dynamique équatoriale Pêcheries de thon current system ABSTR. Oceanol. Acta 16, 261–272.

Matheron, G., 1963. Principles of geostatistics. Econ. Geol. 58, 1246–1266. https://doi.org/10.2113/gsecongeo.58.8.1246

Matos, F.D.A.O., Pereira, J., Dengler, M., 2020. Salinity Biases and the Variability of the Atlantic Meridional Overturning Circulation in GFDL-CM3. Ocean Sci. J. 55, 505–520. https://doi.org/10.1007/s12601-020-0040-8

Maze, G., Mercier, H., Fablet, R., Tandeo, P., Lopez Radcenco, M., Lenca, P., Feucher, C., Le Goff, C., 2017. Coherent heat patterns revealed by unsupervised classification of Argo temperature profiles in the North Atlantic Ocean. Prog. Oceanogr. 151, 275–292. https://doi.org/10.1016/j.pocean.2016.12.008

Medwin, H., Clay, C.S., 1997. Fundamentals of Acoustical Oceanography, 1st ed. Academic Press.

Melzer, B.A., Subrahmanyam, B., 2017. Decadal changes in salinity in the oceanic subtropical gyres. J. Geophys. Res. Ocean. 122, 336–354. https://doi.org/10.1002/2016JC012243

Mémery, L., Arhan, M., Alvarez-Salgado, X.., Messias, M.-J., Mercier, H., Castro, C.., Rios, A.., 2000. The water masses along the western boundary of the south and equatorial Atlantic. Prog. Oceanogr. 47, 69–98. https://doi.org/10.1016/S0079-6611(00)00032-X

Menafoglio, A., Grujic, O., Caers, J., 2016. Universal Kriging of functional data: Trace-variography vs cross-variography? Application to gas forecasting in unconventional shales. Spat. Stat. 15, 39–55. https://doi.org/10.1016/j.spasta.2015.12.003

Menafoglio, A., Secchi, P., Dalla Rosa, M., 2013. A Universal Kriging predictor for spatially dependent functional data of a Hilbert Space. Electron. J. Stat. 7, 2209–2240. https://doi.org/10.1214/13-EJS843

Ménesguen, C., Hua, B.L., Carton, X., Klingelhoefer, F., Schnürle, P., Reichert, C., 2012. Arms winding around a meddy seen in seismic reflection data close to the Morocco coastline. Geophys. Res. Lett. 39, 1–6. https://doi.org/10.1029/2011GL050798

Messié, M., Petrenko, A., Doglioli, A.M., Aldebert, C., Martinez, E., Koenig, G., Bonnet, S., Moutin, T., 2020. The Delayed Island Mass Effect: How Islands can Remotely Trigger Blooms in the Oligotrophic Ocean. Geophys. Res. Lett. 47, e2019GL085282. https://doi.org/10.1029/2019GL085282

Mignot, J., de Boyer Montégut, C., Tomczak, M., 2009. On the porosity of barrier layers. Ocean Sci. 5, 379–387. https://doi.org/10.5194/os-5-379-2009

Mignot, J., Lazar, A., Lacarra, M., 2012. On the formation of barrier layers and associated vertical temperature inversions: A focus on the northwestern tropical Atlantic. J. Geophys. Res. Ocean. 117, 1–11. https://doi.org/10.1029/2011JC007435

Miller, J.R., 1976. The Salinity Effect in a Mixed Layer Ocean Model. J. Phys. Oceanogr. 6, 29–35. https://doi.org/10.1175/1520-0485(1976)006<0029:TSEIAM>2.0.CO;2

Molinari, R.L., 1983. Observations of near-surface currents and temperature in the central and western tropical Atlantic Ocean. J. Geophys. Res. 88, 4433. https://doi.org/10.1029/JC088iC07p04433

Molinari, R.L., 1982. Observations of Eastward Currents in the Tropical South Atlantic Ocean: 1978-1980. J. Geophys. Res. 87, 9707–9714.

Morel, A., Claustre, H., Gentili, B., 2010. The most oligotrophic subtropical zones of the global ocean: similarities and differences in terms of chlorophyll and yellow substance. Biogeosciences Discuss. 7, 5047–5079. https://doi.org/10.5194/bgd-7-5047-2010

Motoki, A., Freire Motoki, K., 2020. Satellite gravimetry for the Fernando de Noronha Chain, Northeast Brazil, and its bearing on the volcanic seamount structure 1–6. https://doi.org/10.22564/5simbgf2012.108

Nerini, D., Monestiez, P., Manté, C., 2010. Cokriging for spatial functional data. J. Multivar. Anal. 101, 409–418. https://doi.org/10.1016/j.jmva.2009.03.005

Olivar, M.P., Hulley, P.A., Castellón, A., Emelianov, M., López, C., Tuset, V.M., Contreras, T., Molí, B., 2017. Mesopelagic fishes across the tropical and equatorial Atlantic: Biogeographical and vertical patterns. Prog. Oceanogr. 151, 116–137. https://doi.org/10.1016/j.pocean.2016.12.001

Orr, M.H., Haury, L.R., Wiebe, P.H., Briscoe, M.G., 2000. Backscatter of high-frequency (200 kHz) acoustic wavefields from ocean turbulence. J. Acoust. Soc. Am. 108, 1595–1601. https://doi.org/10.1121/1.1286883

Pailler, K., Bourlès, B., Gouriou, Y., 1999. The barrier layer in the western tropical Atlantic ocean. Geophys. Res. Lett. 26, 2069–2072. https://doi.org/10.1029/1999GL900492

Pauthenet, E., Roquet, F., Madec, G., Nerini, D., 2017. A Linear Decomposition of the Southern Ocean Thermohaline Structure. J. Phys. Oceanogr. 47, 29–47. https://doi.org/10.1175/JPO-D-16-0083.1

Pauthenet, E., Roquet, F., Madec, G., Sallée, J.-B., Nerini, D., 2019. The Thermohaline Modes of the Global Ocean. J. Phys. Oceanogr. 49, 2535–2552. https://doi.org/10.1175/jpo-d-19-0120.1

Pensieri, S., Bozzano, R., 2017. Active and Passive Acoustic Methods for In-situ Monitoring of the Ocean Status, in: Advances in Underwater Acoustics. InTech. https://doi.org/10.5772/intechopen.68998

Pérez-Santos, I., Castro, L., Ross, L., Niklitschek, E., Mayorga, N., Cubillos, L., Gutierrez, M., Escalona, E., Castillo, M., Alegría, N., Daneri, G., 2018. Turbulence and hypoxia contribute to dense biological scattering layers in a Patagonian fjord system. Ocean Sci. 14, 1185–1206. https://doi.org/10.5194/os-14-1185-2018

Perrot, Y., Brehmer, P., Habasque, J., Roudaut, G., Behagle, N., Sarré, A., Lebourges-Dhaussy, A., 2018. Matecho: An Open-Source Tool for Processing Fisheries Acoustics Data. Acoust. Aust. 46, 241–248. https://doi.org/10.1007/s40857-018-0135-x

Peterson, R.G., Stramma, L., 1991. Upper-level circulation in the South Atlantic Ocean. Prog. Oceanogr. 26, 1–73. https://doi.org/10.1016/0079-6611(91)90006-8

Pingree, R.D., Mardell, G.T., 1985. Solitary internal waves in the Celtic Sea. Prog. Oceanogr. 14, 431–441. https://doi.org/10.1016/0079-6611(85)90021-7

Poole, R., Tomczak, M., 1999. Optimum multiparameter analysis of the water mass structure in the Atlantic Ocean thermocline. Deep Sea Res. Part I Oceanogr. Res. Pap. 46, 1895–1921. https://doi.org/10.1016/S0967-0637(99)00025-4

Prairie, J.C., Sutherland, K.R., Nickols, K.J., Kaltenberg, A.M., 2012. Biophysical interactions in the plankton: A cross-scale review. Limnol. Oceanogr. Fluids Environ. 2, 121–145. https://doi.org/10.1215/21573689-1964713

Preusse, M., Peeters, F., Lorke, A., 2010. Internal waves and the generation of turbulence in the thermocline of a large lake. Limnol. Oceanogr. 55, 2353–2365. https://doi.org/10.4319/lo.2010.55.6.2353

Radenac, M.H., Plimpton, P.E., Lebourges-Dhaussy, A., Commien, L., McPhaden, M.J., 2010. Impact of environmental forcing on the acoustic backscattering strength in the equatorial Pacific: Diurnal, lunar, intraseasonal, and interannual variability. Deep. Res. Part I Oceanogr. Res. Pap. 57, 1314–1328. https://doi.org/10.1016/j.dsr.2010.06.004

Rahter, B.A., 2010. Turbulent Dissipation in the Mid-Latitude Mixed Layer / Thermocline Transition Layer.

Ramsay, J.O., 2006. Functional Data Analysis, in: Encyclopedia of Statistical Sciences. John Wiley & Sons, Inc., Hoboken, NJ, USA, pp. 675–678. https://doi.org/10.1002/0471667196.ess3138

Reyes, A., Giraldo, R., Mateu, J., 2015. Residual kriging for functional spatial prediction of salinity curves. Commun. Stat. - Theory Methods 44, 798–809. https://doi.org/10.1080/03610926.2012.753087

Rippert, N., Baumann, K.-H., Patzold, J., 2015. Thermocline fluctuations in the western tropical Indian Ocean during the past 35 ka 30, 201–210. https://doi.org/10.1002/jqs.2767

Rodrigues, R.R., Rothstein, L.M., Wimbush, M., 2007. Seasonal Variability of the South Equatorial Current Bifurcation in the Atlantic Ocean: A Numerical Study. J. Phys. Oceanogr. 37, 16–30. https://doi.org/10.1175/JPO2983.1

Roemmich, D., Wunsch, C., 1985. Two transatlantic sections: meridional circulation and heat flux in the subtropical North Atlantic Ocean. Deep Sea Res. Part A, Oceanogr. Res. Pap. 32, 619–664. https://doi.org/10.1016/0198-0149(85)90070-6

Rosch, A., Schmidbauer, H., 2014. WaveletComp : A guided tour through the R-package 1–38.

Sabra, K.G., 2015. Paul Langevin's contributions to the development of underwater acoustics. J. Acoust. Soc. Am. 137, 2273–2273. https://doi.org/10.1121/1.4920301

Salvetat, J., Lebourges-Dhaussy, A., Travassos, P., Gastauer, S., Roudaut, G., Vargas, G., Bertrand, A., 2020. Insitu target strength measurement of the black triggerfish Melichthys niger and the ocean triggerfish Canthidermis sufflamen. Mar. Freshw. Res. 1–18. https://doi.org/10.1071/MF19153

Sampaio de Souza, C., Guimarães da Luz, J.A., Macedo, S., Montes, M.D.J.F., Mafalda, P., 2013. Chlorophyll a and nutrient distribution around seamounts and islands of the tropical south-western Atlantic. Mar. Freshw. Res. 64, 168. https://doi.org/10.1071/MF12075

Sato, K., Suga, T., Hanawa, K., 2006. Barrier layers in the subtropical gyres of the world's oceans. Geophys. Res. Lett. 33, 8–11. https://doi.org/10.1029/2005GL025631

Sato, K., Suga, T., Hanawa, K., 2004. Barrier layer in the North Pacific subtropical gyre. Geophys. Res. Lett. 31, n/a-n/a. https://doi.org/10.1029/2003GL018590

Schneider, T., Bischoff, T., Haug, G.H., 2014. Migrations and dynamics of the intertropical convergence zone. Nature. https://doi.org/10.1038/nature13636

Schott, F.A., Brandt, P., Hamann, M., Fischer, J., Stramma, L., 2002. On the boundary flow off Brazil at 5-10°S and its connection to the interior tropical Atlantic. Geophys. Res. Lett. 29, 21-1-21–4. https://doi.org/10.1029/2002GL014786

Schott, F.A., Dengler, M., Zantopp, R., Stramma, L., Fischer, J., Brandt, P., 2005. The Shallow and Deep Western Boundary Circulation of the South Atlantic at 5°–11°S. J. Phys. Oceanogr. 35, 2031–2053. https://doi.org/10.1175/JPO2813.1

Schott, F.A., Fischer, J., Stramma, L., 1998. Transports and Pathways of the Upper-Layer Circulation in the Western Tropical Atlantic. J. Phys. Oceanogr. 28, 1904–1928. https://doi.org/10.1175/1520-0485(1998)028<1904:TAPOTU>2.0.CO;2

Segura, H., Espinoza, J.C., Junquas, C., Lebel, T., Vuille, M., Garreaud, R., 2020. Recent changes in the precipitation-driving processes over the southern tropical Andes/western Amazon. Clim. Dyn. 54, 2613–2631. https://doi.org/10.1007/s00382-020-05132-6

Shang, H.L., 2014. A survey of functional principal component analysis. AStA Adv. Stat. Anal. 98, 121–142. https://doi.org/10.1007/s10182-013-0213-1

Siedler, G., Griffies, S., Gould, J., Church, J., 2013. Ocean Circulation and Climate. Academic Press.

Silva, B.J., 2018. Caracterização Do Sistema Carbonato No Arquipélago De Fernando De Noronha. Universidade Federal de Pernambuco.

Silva, A.C. da, Araújo, M., Medeiros, C., Silva, M., Bourlès, B., 2005. Seasonal changes in the mixed and barrier layers in the western Equatorial Atlantic. Brazilian J. Oceanogr. 53, 83–98. https://doi.org/10.1590/S1679-87592005000200001

Silva, A.C. da, Chaigneau, A., Dossa, A.N., Eldin, G., Araújo, M., Bertrand, A., 2021. Surface circulation and vertical structure of upper ocean variability around Fernando de Noronha archipelago and Rocas atoll during spring 2015 and fall 2017. Front. Mar. Sci. https://doi.org/10.3389/fmars.2021.598101

Silva, M., Araújo, M., Servain, J., Penven, P., Lentini, C.A.D., 2009. High-resolution regional ocean dynamics simulation in the southwestern tropical Atlantic. Ocean Model. 30, 256–269. https://doi.org/10.1016/j.ocemod.2009.07.002

Simmonds, J., MacLennan, D., 2005. Fisheries Acoustics, Fisheries Acoustics: Theory and Practice: Second Edition. Blackwell Publishing Ltd, Oxford, UK. https://doi.org/10.1002/9780470995303

Sousa-Lima, R., Engel, M.H., Sábato, V., Lima, B.R., Queiróz, T.S.M., Casagrande, T., Honda, L.K., Gonçalves, M.I.C., Baumgarten, J.E., Andriolo, A., Ribeiro, M.C., Clark, C.W., 2018. Acoustic ecology of humpback whales in Brazilian waters investigated with basic and sophisticated passive acoustic technologies over 17 years. WIO J. Mar. Sci. 23–40.

Sprintall, J., Cronin, M.F., 2010. Upper Ocean Vertical Structure. Encycl. Ocean Sci. 217–224. https://doi.org/10.1016/B978-012374473-9.00627-5

Sprintall, J., Tomczak, M., 1993. On the formation of central water and thermocline ventilation in the southern hemisphere. Deep. Res. Part I 40, 827–848. https://doi.org/10.1016/0967-0637(93)90074-D

Sprintall, J., Tomczak, M., 1992. Evidence of the barrier layer in the surface layer of the tropics. J. Geophys. Res. 97, 7305. https://doi.org/10.1029/92JC00407

Stanton, T., 1994. Acoustic characterization and discrimination of marine zooplankton and turbulence. ICES J. Mar. Sci. 51, 469–479. https://doi.org/10.1006/jmsc.1994.1048

Stanton, T.K., Chu, D., Wiebe, P.H., 1998. Sound scattering by several zooplankton groups. II. Scattering models. J. Acoust. Soc. Am. 103, 236–253. https://doi.org/10.1121/1.421110

Stramma, L., 1991. Geostrophic transport of the South Equatorial Current in the Atlantic. J. Mar. Res. 49, 281–294. https://doi.org/10.1357/002224091784995864

Stramma, L., England, M., 1999. On the water masses and mean circulation of the South Atlantic Ocean. J. Geophys. Res. Ocean. 104, 20863–20883. https://doi.org/10.1029/1999JC900139

Stramma, L., Fischer, J., Reppin, J., 1995. The North Brazil Undercurrent. Deep Sea Res. Part I Oceanogr. Res. Pap. 42, 773–795. https://doi.org/10.1016/0967-0637(95)00014-W

Stramma, L., Rhein, M., Brandt, P., Dengler, M., Böning, C., Walter, M., 2005. Upper ocean circulation in the western tropical Atlantic in boreal fall 2000. Deep Sea Res. Part I Oceanogr. Res. Pap. 52, 221–240. https://doi.org/10.1016/j.dsr.2004.07.021

Stramma, L., Schott, F., 1999. The mean flow field of the tropical Atlantic Ocean. Deep Sea Res. Part II Top. Stud. Oceanogr. 46, 279–303. https://doi.org/10.1016/S0967-0645(98)00109-X

Stranne, C., Mayer, L., Jakobsson, M., Weidner, E., Jerram, K., Weber, T.C., Anderson, L.G., Nilsson, J., Björk, G., Gårdfeldt, K., 2018. Acoustic mapping of mixed layer depth. Ocean Sci. 14, 503–514. https://doi.org/10.5194/os-14-503-2018

Stranne, C., Mayer, L., Weber, T.C., Ruddick, B.R., Jakobsson, M., Jerram, K., Weidner, E., Nilsson, J., Gårdfeldt, K., 2017. Acoustic mapping of thermohaline staircases in the arctic ocean. Sci. Rep. 7, 1–9. https://doi.org/10.1038/s41598-017-15486-3

Sun, O.M., Jayne, S.R., Polzin, K.L., Rahter, B.A., St. Laurent, L.C., 2013. Scaling Turbulent Dissipation in the Transition Layer. J. Phys. Oceanogr. 43, 2475–2489. https://doi.org/10.1175/JPO-D-13-057.1

Sverdrup, H.U., 1953. On Conditions for the Vernal Blooming of Phytoplankton. ICES J. Mar. Sci. 18, 287–295. https://doi.org/10.1093/icesjms/18.3.287

Swenson, M.S., Hansen, D. V., 1999. Tropical Pacific Ocean Mixed Layer Heat Budget: The Pacific Cold Tongue MARK. J. Phys. Oceanogr. 29, 371–398. https://doi.org/10.1007/978-3-319-15129-8_16

Talley, L.D., Pickard, G.L., Emery, W.J., Swift, J.H., 2011. Descriptive Physical Oceanography. An introduction, 6th ed.

Tanguy, Y., Arnault, S., Lattes, P., 2010. Isothermal, mixed, and barrier layers in the subtropical and tropical Atlantic Ocean during the ARAMIS experiment. Deep Sea Res. Part I Oceanogr. Res. Pap. 57, 501–517. https://doi.org/10.1016/j.dsr.2009.12.012

Tchamabi, C.C., Araújo, M., Silva, M., Bourlès, B., 2017. A study of the Brazilian Fernando de Noronha Island and Rocas Atoll wakes in the tropical Atlantic. Ocean Model. https://doi.org/10.1016/j.ocemod.2016.12.009

Thévenin, M.R., Pereira, J., Lessa, G.C., 2019. Shelf-break upwelling on a very narrow continental shelf adjacent to a western boundary current formation zone. J. Mar. Syst. 194, 52–65. https://doi.org/10.1016/j.jmarsys.2019.02.008

Thurman, H.V., 2019. Essentials of oceanography, Thirteenth. ed. Pearson Education: Hoboken.

Todd, R.E., Owens, W.B., Rudnick, D.L., 2016. Potential Vorticity Structure in the North Atlantic Western Boundary Current from Underwater Glider Observations. J. Phys. Oceanogr. 46, 327–348. https://doi.org/10.1175/JPO-D-15-0112.1

Tomczak, M., Godfrey, J.S., 1994. Regional Oceanography, 1st ed, Regional Oceanography. Elsevier. https://doi.org/10.1016/C2009-0-14825-0

Tosetto, E.G., Bertrand, A., Neumann-Leitão, S., Costa da Silva, A., Nogueira Júnior, M., 2021. Spatial patterns in planktonic cnidarian distribution in the western boundary current system of the

tropical South Atlantic Ocean. J. Plankton Res. 43, 270–287. https://doi.org/10.1093/plankt/fbaa066

Trenkel, V.M., Berger, L., Bourguignon, S., Doray, M., Fablet, R., Massé, J., Mazauric, V., Poncelet, C., Quemener, G., Scalabrin, C., Villalobos, H., 2009. Overview of recent progress in fisheries acoustics made by Ifremer with examples from the Bay of Biscay. Aquat. Living Resour. 22, 433–445. https://doi.org/10.1051/alr/2009027

Trenkel, V.M., Handegard, N.O., Weber, T.C., 2016. Observing the ocean interior in support of integrated management, in: ICES Journal of Marine Science. Oxford University Press, pp. 1947–1954. https://doi.org/10.1093/icesjms/fsw132

Trenkel, V.M., Ressler, P.H., Jech, M., Giannoulaki, M., Taylor, C., 2011. Underwater acoustics for ecosystem-based management: State of the science and proposals for ecosystem indicators. Mar. Ecol. Prog. Ser. 442, 285–301. https://doi.org/10.3354/meps09425

Trevorrow, M. V., 1998. Observations of internal solitary waves near the Oregon coast with an inverted echo sounder. J. Geophys. Res. Ocean. 103, 7671–7680. https://doi.org/10.1029/98JC00101

Tsuchiya, M., Talley, L.D., McCartney, M.S., 1994. Water-mass distributions in the western South Atlantic; A section from South Georgia Island (54S) northward across the equator. J. Mar. Res. 52, 55–81. https://doi.org/10.1357/0022240943076759

Urbano, D.F., De Almeida, R.A.F., Nobre, P., 2008. Equatorial Undercurrent and North Equatorial Countercurrent at 38°W: A new perspective from direct velocity data. J. Geophys. Res 113, 4041. https://doi.org/10.1029/2007JC004215

Urick, R.J., 1983. Principles of Underwater Sound.

Utida, G., Cruz, F.W., Etourneau, J., Bouloubassi, I., Schefuß, E., Vuille, M., Novello, V.F., Prado, L.F., Sifeddine, A., Klein, V., Zular, A., Viana, J.C.C., Turcq, B., 2019. Tropical South Atlantic influence on Northeastern Brazil precipitation and ITCZ displacement during the past 2300 years. Sci. Rep. 9, 1–8. https://doi.org/10.1038/s41598-018-38003-6

Venancio, I.M., Shimizu, M.H., Santos, T.P., Lessa, D.O., Portilho-Ramos, R.C., Chiessi, C.M., Crivellari, S., Mulitza, S., Kuhnert, H., Tiedemann, R., Vahlenkamp, M., Bickert, T., Sampaio, G., Albuquerque, A.L.S., Veiga, S., Nobre, P., Nobre, C., 2020. Changes in surface hydrography at the western tropical Atlantic during the Younger Dryas. Glob. Planet. Change 184, 103047. https://doi.org/10.1016/j.gloplacha.2019.103047

Veneziani, M., Griffa, A., Garraffo, Z., Mensa, J.A., 2014. Barrier Layers in the Tropical South Atlantic: Mean Dynamics and Submesoscale Effects*. J. Phys. Oceanogr. 44, 265–288. https://doi.org/10.1175/JPO-D-13-064.1

Verma, A., Kloser, R.J., Duncan, A.J., 2017. Potential Use of Broadband Acoustic Methods for Micronekton Classification. Acoust. Aust. 45, 353–361. https://doi.org/10.1007/s40857-017-0105-8

Wackernagel, H., 2003. Multivariate Geostatistics : an Introduction with Applications. Springer Berlin Heidelberg.

Waliser, D.E., Gautier, C., 1993. A Satellite-derived Climatology of the ITCZ. J. Clim. 6, 2162–2174. https://doi.org/10.1175/1520-0442(1993)006<2162:ASDCOT>2.0.CO;2

Warren, J.D., Stanton, T.K., Wiebe, P.H., Seim, H.E., 2003. Inference of biological and physical parameters in an internal wave using multiple-frequency, acoustic-scattering data. ICES J. Mar. Sci. 60, 1033–1046. https://doi.org/10.1016/S1054-3139(03)00121-8

Warren, J.D., Wiebe, P.H., 2008. Accounting for biological and physical sources of acoustic backscatter improves estimates of zooplankton biomass, Canadian Journal of Fisheries and Aquatic Sciences. https://doi.org/10.1139/F08-047

Wedekin, L., Rossi-Santos, M., Baracho, C., Cypriano-Souza, A., Simões-Lopes, P., 2014. Cetacean records along a coastal-offshore gradient in the Vitória-Trindade Chain, western South Atlantic Ocean. Brazilian J. Biol. 74, 137–144. https://doi.org/10.1590/1519-6984.21812

Weston, D.E., 1958. Observations on a scattering layer at the thermocline. Deep Sea Res. 5, 44–50. https://doi.org/10.1016/S0146-6291(58)80007-7

Wijesekera, H., Boyd, T.J., 2001. Upper Ocean Heat And Freshwater Budgets, in: Encyclopedia of Ocean Sciences. Elsevier, pp. 3079–3083. https://doi.org/10.1006/rwos.2001.0153

Williams, B., Grottoli, A.G., 2010. Recent shoaling of the nutricline and thermocline in the western tropical Pacific. Geophys. Res. Lett. 37, n/a-n/a. https://doi.org/10.1029/2010GL044867

Woods, J.D., 1968. Wave-induced shear instability in the summer thermocline, J. Fluid Mech.

Yao, F., Hoteit, I., 2015. Thermocline Regulated Seasonal Evolution of Surface Chlorophyll in the Gulf of Aden. PLoS One 10, e0119951. https://doi.org/10.1371/journal.pone.0119951

Zeng, L., Wang, D., 2017. Seasonal variations in the barrier layer in the South China Sea: characteristics, mechanisms and impact of warming. Clim. Dyn. 48, 1911–1930. https://doi.org/10.1007/s00382-016-3182-8

Zhang, D., McPhaden, M.J., Johns, W.E., 2003. Observational Evidence for Flow between the Subtropical and Tropical Atlantic: The Atlantic Subtropical Cells*. J. Phys. Oceanogr. 33, 1783–1797. https://doi.org/10.1175/2408.1

Supplementary material

Supplementary data to this article can be found online at
https://doi.org/10.1016/j.pocean.2020.102399

Figure S1. Dendrograms and spatial distribution of the classes/area for spring (a, c, e, g) and fall (b, d, f, h) for temperature (a - d) and salinity (e - h). Blue, red and green colours represent Areas 1, 2 and 3, respectively.

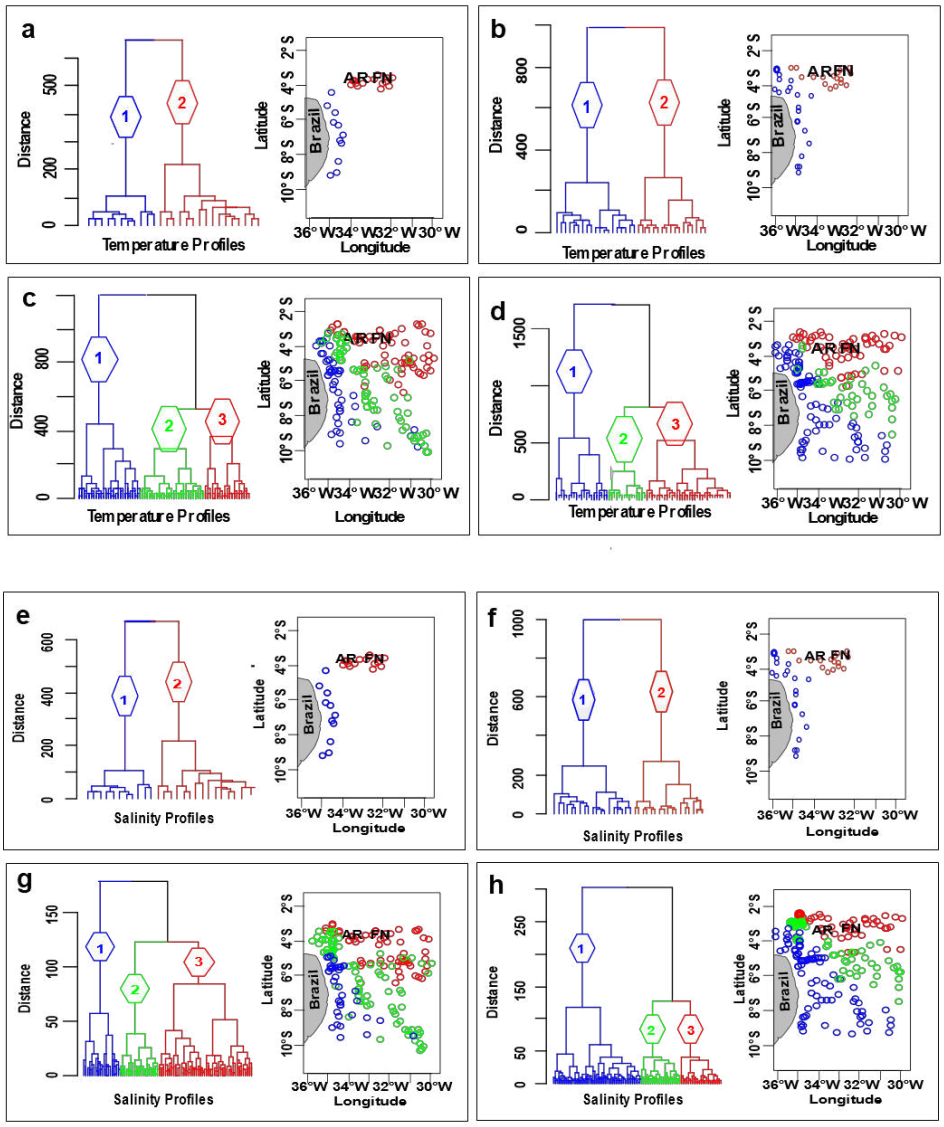

Source: Personal collection.

Figure S2. Validation for Functional Ordinary Kriging of temperature (°C) (a, b, c) and salinity (d, e, f) in fall using the Mean Square Difference (MSD). Maps of the distribution of the MSD for all stations for temperature (a) and salinity (b). Examples or good (2 and 3) and worst (1 and 4) predictions for temperature (b) and salinity (e). The corresponding profiles are circled in (a) and (d). The red solid lines correspond to the observations and the blue solid line to the predictions. The boxplots of the MSD for temperature (c) and salinity (f) are presented to evaluate the global performance of the estimators.

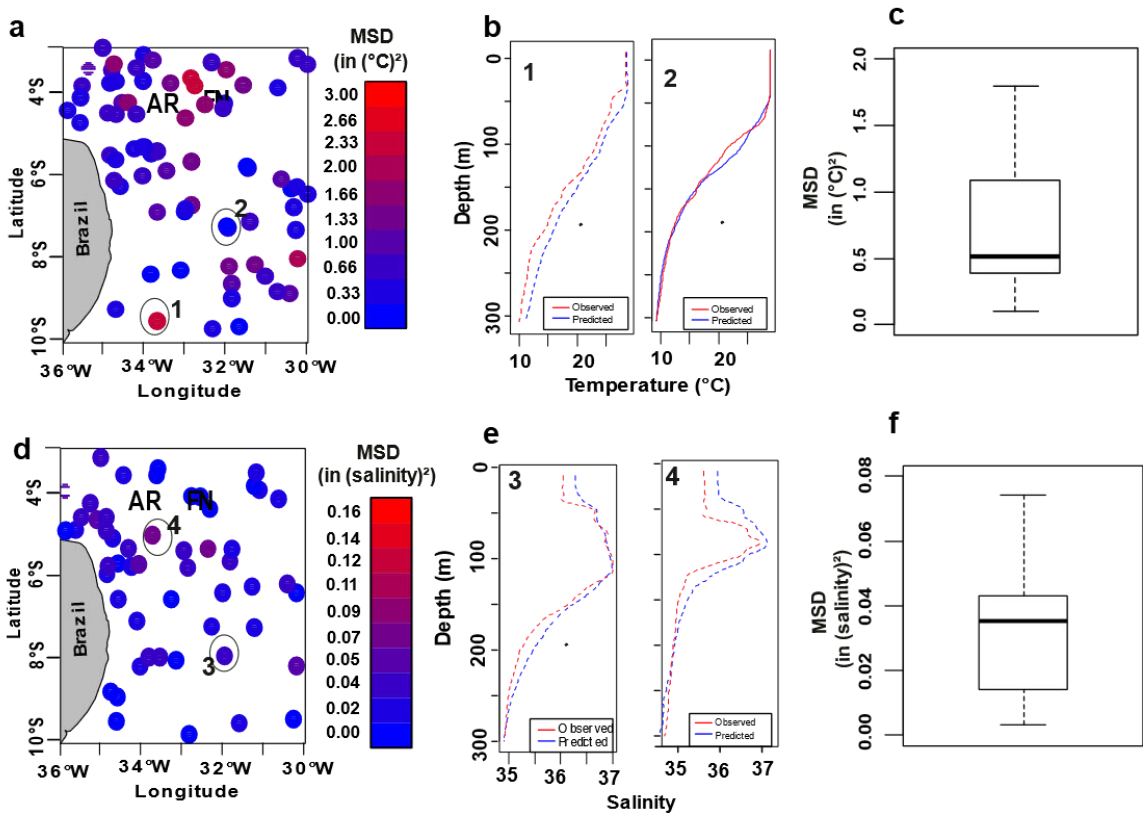

Source: Personal collection.

Figure S3. Evaporation and Precipitation in spring (a, c) and fall (b, d) according to HOAPS data for 1988 to 2014 in the southwestern tropical Atlantic. Grey solid lines delimit areas A1, A2 and A3 defined in section 3.2. The continental shelf limited by the isobaths of 60 m is represented by light grey. RA: Rocas Atoll; FN: Fernando de Noronha archipelago. Note that the scales vary between stations to highlight spatial variations.

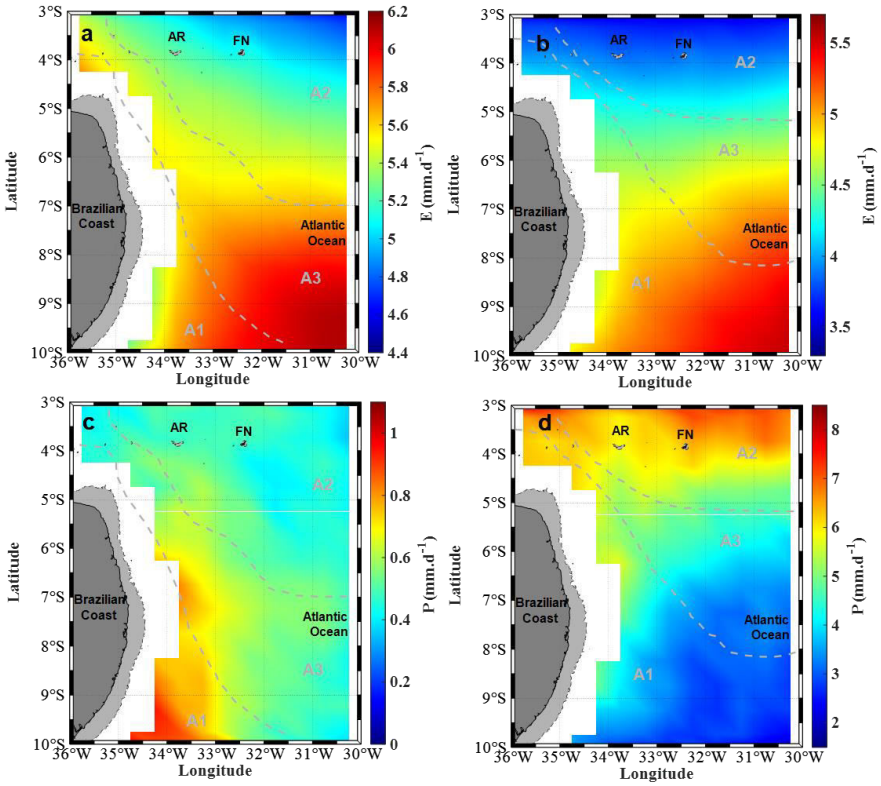

Source: Personal collection.

Figure S4. Seasonal climatology of evaporation minus precipitation budget (E-P) in the south Atlantic according to HOAPS data from 1988 to 2014. The dotted rectangle highlights the southwestern tropical Atlantic (study area). The dotted lines (E-P = 4.5 and 5.0 mm.d^{-1}) highlight the region of high evaporation.

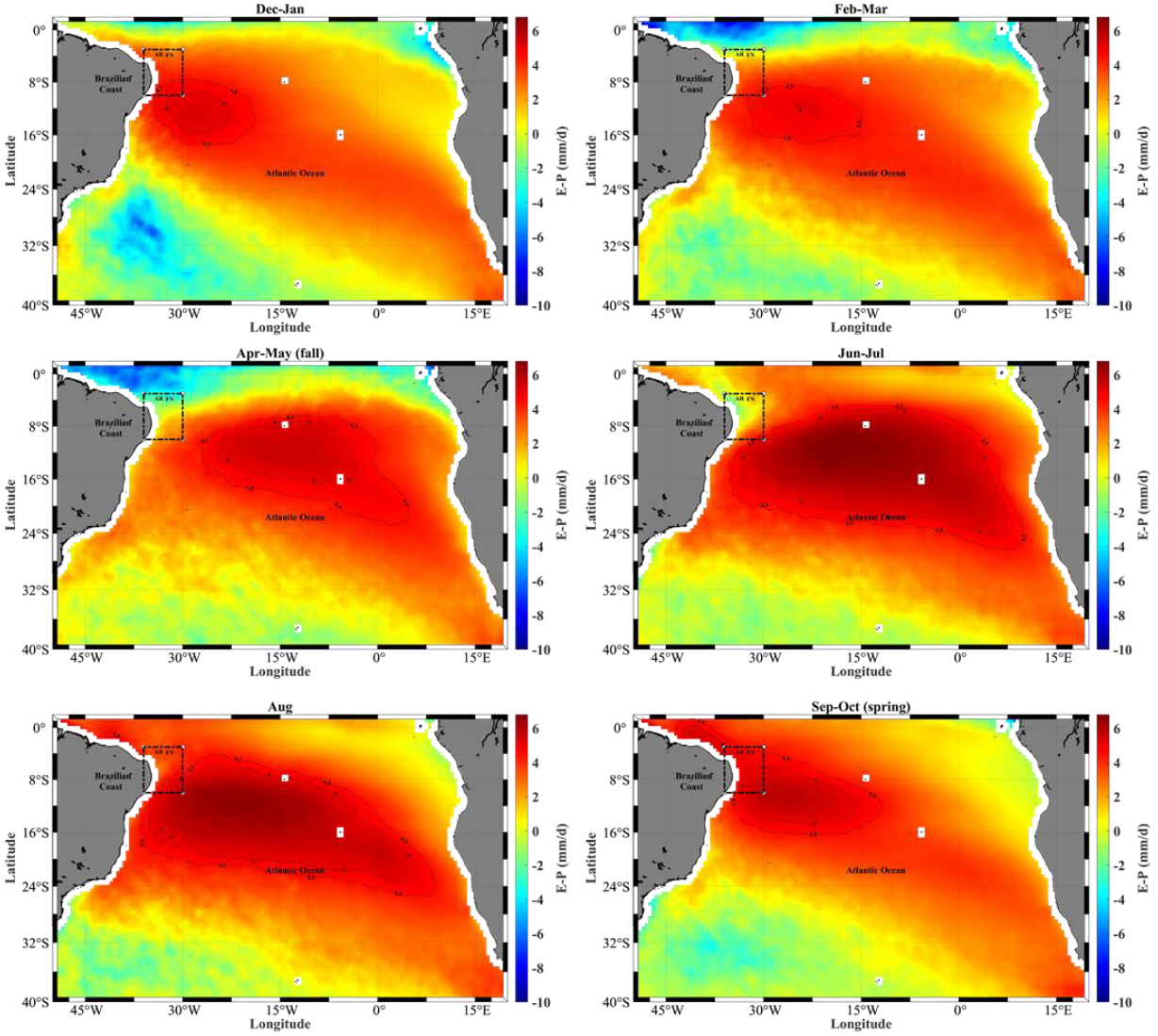

Source: Personal collection.

…

From Chapter II to Chapter III

In Chapter II, we portrayed the thermodynamic structure of the SWTA on the base of discrete CTD profiles and revealed different provinces associated to specific hydrodynamics systems. However, the use of discrete profiles prevents studying turbulent processes occurring at the internal-wave scale (100 m to 10–15 km; Munk, 1981), the submesoscale (~1–20 km, e.g., fronts and filaments; Tomas et al., 2008). Yet it has been shown that fine-scale (<10 km) turbulence plays a key role in shaping the seascape from physics to top predators (Bertrand et al., 2014). To address the fine-scale variability of the thermohaline structure, in Chapter III we investigate the possibility to detect the limits of the thermohaline layers using active acoustics. An approach that allowed for a robust and comprehensive description in other ecosystems (e.g., Grados et al., 2016).

…

CHAPTER III:
ON THE USE OF ACOUSTIC DATA TO CHARACTERISE THE THERMOHALINE STRATIFICATION IN A TROPICAL OCEAN

This chapter corresponds to the article of the same name to be submitted to *Open Research Europe*.

Ramilla V. Assunção[a,c], Anne Lebourges-Dhaussy[c], Alex C. da Silva[a], Bernard Bourlès[d], Gary Vargas[e], Arnaud Bertrand[b,a,e.]

[a]*Laboratório de Oceanografia Física Estuarina e Costeira, Depto. Oceanografia, UFPE, Recife-PE, Brazil.*
[b]*Institut de recherche pour le développement (IRD), MARBEC, Université Montpellier, CNRS, Ifremer, IRD, Sète, France.*
[c]*Institut de recherche pour le développement (IRD), LEMAR CNRS, UBO, IRD, Ifremer, Plouzané, France.*
[d]*Institut de recherche pour le développement (IRD), IMAGO, Plouzané, France.*
[e]*Universidade Federal Rural de Pernambuco, Recife-PE, Brazil.*

Abstract

The use of active acoustic to monitoring abiotic structures and processes in the ocean have been gaining ground in physical oceanography. In some systems, acoustics allow the robust estimation of the depth of the pycnocline or thermocline either directly or indirectly when the physical structures drive the one of organisms. Here we examined the feasibility of extracting the thermohaline structure (mixed-layer depth, upper and lower thermocline) from echosounder data collected in the oligotrophic Southwestern tropical Atlantic region at two seasons (spring and fall), in two different thermohaline provinces, at both day and night. For that, we tested three approaches: (i) the vertical extension of the epipelagic community; (ii) the use of acoustic gradients; and (iii) a cross-wavelet approach. Results show that, even if the thermohaline structure impacts the vertical distribution of acoustic scatters, the resultant structuring did not allow for a robust estimation of the thermohaline limits indicating that other oceanographic or biological processes are acting. This unexpected result prevents for a fine-scale representation of the upper-layer turbulence from acoustic data. However, studying the proportion of acoustic biomass within each layer provides interesting insights on ecosystem structure in different thermohaline, seasonal and diel scenarios. In particular, in regions where the thermocline is highly stratified, and less mixed, some organisms seemed to avoid the layers of highest gradient.

Keywords: acoustic scatters, thermocline, pycnocline, barrier layer, western boundary current system, equatorial current system

1. Introduction

The vertical structure of the upper ocean is primarily regulated by temperature and salinity, which together control the water column's density structure so called thermohaline structure (Sprintall and Cronin, 2010). The thermohaline structure of the upper ocean can be divided into layers associated to different features: (i) the mixed-layer (ML); (ii) the thermocline, halocline and pycnocline; and (iii) the barrier layer (BL), which is the layer between thermocline and pycnocline induced by salinity (de Boyer Montégut et al., 2007; Sprintall and Cronin, 2010). The presence or absence of these layers as well as their properties (strength and morphology) depend on ocean-atmosphere interactions and hydrodynamic processes (Araújo et al., 2011; Pailler et al., 1999). The thermohaline structure drives most near-surface oceanic processes, including the control of gases and heat fluxes and momentum between ocean-atmosphere (Mignot et al., 2009; Miller, 1976) or the nutrient availability in the photic layer (Chen et al., 2018; Rippert et al., 2015). The modulation of the pycnocline allows identifying a variety of turbulent processes along scale including internal wave (~100 m to 10–15 km; Munk, 1981), submesoscale (~1–20 km; e.g. fronts and filaments; Tomas et al., 2008) and mesoscale (~20–100 km; e.g. eddies) activity (Bertrand et al., 2014; Grados et al., 2016). These processes modulate the concentration and distribution of marine organisms, shaping the dynamics of ecosystems (Lévy et al., 2012; Bertrand et al., 2014).

Ocean thermohaline structure is classically derived from in situ measurements (e.g., Tsuchiya et al., 1994), reanalysis products (e.g., climatology; Gaillard et al., 2016) or ocean models (e.g., Venancio et al., 2020). In situ observations from CTD, XBT, Argo profiles, and thermistors (Maze et al., 2017; Wijesekera and Boyd, 2001; Woods, 1968) provide high vertical resolution information on discrete stations. They allow for process description from large scales to mesoscales, but not on smaller scales. For that, high resolution data are necessary. Within this perspective, active acoustic is a powerful tool since echosounders can capture fine-scale oceanographic structures typically attributed to biological scattering or turbulent structures (Bertrand et al., 2014; Klymak and Moum, 2003; Lavery et al., 2003; Pingree and Mardell, 1985; Stranne et al., 2018; Trevorrow, 1998). Indeed, acoustics allow covering large areas with a single signal providing continuous (along the route of the vessel and/or per sampling station) and high

resolution on a variety of biotic (Benoit-Bird and Lawson, 2016; Bertrand et al., 2014) and abiotic properties such as the oxycline (Bertrand et al., 2010), internal waves (Grados et al., 2016; Holbrook et al., 2009; Holbrook and Fer, 2005; Orr et al., 2000), submesoscale to mesoscale eddies (Biescas et al., 2008; Grados et al., 2016; Ménesguen et al., 2012), thermocline (Ker et al., 2016; Stranne et al., 2018) and thermohaline staircases (Biescas et al., 2008; Fer et al., 2010; Ross and Lueck, 2005; Stranne et al., 2017).

The accuracy of detection and monitoring of abiotic structures and processes by active acoustics depends on (i) the frequency applied; (ii) how well defined the structures of interest are (e.g. narrower thermoclines are more likely to be better detected; weaker density contrast at the base of the mixed layer decreases the chances of detection); (iii) ecosystem productivity (i.e. the amount and intensity of biological scatters); and (iv) the dominance of the biological backscatter (Ker et al., 2016; Pensieri and Bozzano, 2017; Stranne et al., 2018).

In the highly productive northern Humboldt Current system off Peru, where a shallow and intense oxygen minimum zone is present, echosounder data have been successfully used to monitor the depth of the upper oxycline, which matches the pycnocline (Bertrand et al., 2014, 2010; Grados et al., 2016). This allowed describing the variety of physical turbulent structures at scales ranging from the internal waves to the mesoscale and their further impacts on the distribution of organisms from plankton to top predators (Bertrand et al., 2014).

Thermohaline structuring as well as oxygen minimum zones play an important role in the vertical distribution of epipelagic and mesopelagic organisms (mainly zooplankton, cephalopods and small fishes). The vertical extension of the epipelagic community (VEEC) has been defined, primarily, in ocean regions where the oxygen minimum zones acted as a barrier for most marine species (Criales et al., 2008; Ayón et al., 2008a; Bertrand et al., 2010). In these regions, the depth of the VEEC (ZVEEC) has been defined as the depth where 98% of the cumulative sum (integrated downward from 10 m depth) of the acoustic echoes (s_A, nautical area scattering coefficient in $m^2.nmi^{-2}$, MacLennan et al., 2002) from epipelagic community was reached (Bertrand et al., 2010).

Here, following these authors method, but also two other approaches (acoustic gradient and cross-wavelet analysis) based on the behaviour of acoustic scattering and thermal variations along depth, we investigate whether information on the variation of the thermohaline structure could be

extracted from acoustic data in a less productive tropical system. For that, we used data acquired during two surveys in the Southwestern Tropical Atlantic (SWTA, Fig. 1). In this region, along the coast lies the western boundary current system (WBCS) formed by the North Brazil Undercurrent (NBUC) and the North Brazil Current (NBC) (Bourlès et al., 1999; Dossa et al., 2021). Further offshore, lies the South Equatorial Current System (SECS), which includes the central branch of the South Equatorial Current (cSEC) and the South Equatorial Undercurrent (SEUC) (Silva et al., 2021; Stramma and Schott, 1999). Both systems are characterized by the presence of a permanent pycnocline, varying spatially and seasonally in structure - thickness and depth of the upper and lower limits - and consequent strength (Assunção et al., 2020).

2. Material and Methods

2.1. Data

Data Data were collected during two multidisciplinary surveys “Acoustic along the BRAzilian CoaSt (ABRACOS)” performed off the coast of northeast Brazil (Fig. 1) aboard the French R/V Antea in austral spring (September - October 2015; Bertrand, 2015) and fall (April - May 2017, Bertrand, 2017).

Conductivity, temperature, depth, oxygen (CTDO) hydrographic profiles were acquired at 96 stations using a CTDO Seabird SBE911+ from the surface down to 1000 m or ten metres above the bottom depth. Conductivity, temperature, pressure, and dissolved oxygen accuracies are of 3 mS/m, 0.001°C, 0.7 dbar, and 0.09 ml l^{-1}, respectively. Here, we focus on the 52 CTD profiles deeper than 300 m (Fig. 1).

Acoustic data were acquired using four Simrad EK60 scientific echosounders operating continuously during transects and hydrological stations and connected to split-beam transducers working at 38, 70, 120 and 200 kHz. Due to its limited operational range (150 m), the 200 kHz was not used in this study. Echosounders calibrations were performed according to Foote et al. (1987) using a tungsten carbide sphere at the start of each survey. Transmit powers were 1000, 500, 200 and 90 W for the 38, 70, 120 and 200 kHz transducers, respectively. The pulse length was set to 0.512 msec for all frequencies providing a vertical resolution of the raw data of ~10 cm.

Acoustic data processing, including automatic cleaning and the removal of background, transient and impulsive noise along with the attenuated signals, was done using the Matecho software tool

(version 20191213V6; Perrot et al., 2018). Matecho is an open source IRD (*Institut de Recherche pour le Développement*) tool based on the IFREMER's Movies 3D software (Trenkel et al., 2009). To get the same vertical resolution than the CTDO, acoustic raw s_v (dB re 1 m^{-1}, MacLennan et al., 2002) data were averaged on 1m layers for each ping. A high-resolution echo-integration on 1 ping per 1m high cell was applied on Sv samples with a threshold at -100 dB, providing data at the same vertical resolution than the CTDO. Signals from less than 10 m depth were suppressed, as they were dominated by transducer back lobe reflections from the water surface, the ship hull and by surface bubbles.

At each station, the purpose is to compare the CTDO profiles with the corresponding mean acoustic profiles at the available frequencies. For that, we used 100 pings after the end of each cast of CTDO to avoid the possible noise from the descent and ascent of the CTDO and to ensure working on genuine day and night data since most CTDO were mostly performed during twilight periods.

Figure 1. Survey tracks (black lines) of ABRACOS 1 (a) and ABRACOS 2 (b) surveys. Day (yellow circle) and night (red circle) CTDO stations used in this study. The continental shelf is represented in light grey; the dashed black line represents the shelf break (70 m isobath); other bathymetric contours (solid black lines) are by 1000 m intervals. RA: Rocas Atoll; FN: Fernando de Noronha archipelago. The boundaries (solid white lines) between the Western Boundary Current System (WBCS), the South Equatorial Current System (SECS), and the transitional area are plotted according to Assunção et al. (2020). The main currents (c) of each thermohaline system are: North Brazil Undercurrent (NBUC), North Brazil Current (NBC), central branch of South Equatorial Current (cSEC) and South Equatorial Undercurrent (SEUC) (Dossa et al., 2021; Silva et al., 2021). The dotted arrows refer to the subsurface currents and the continuous arrows to the surface currents.

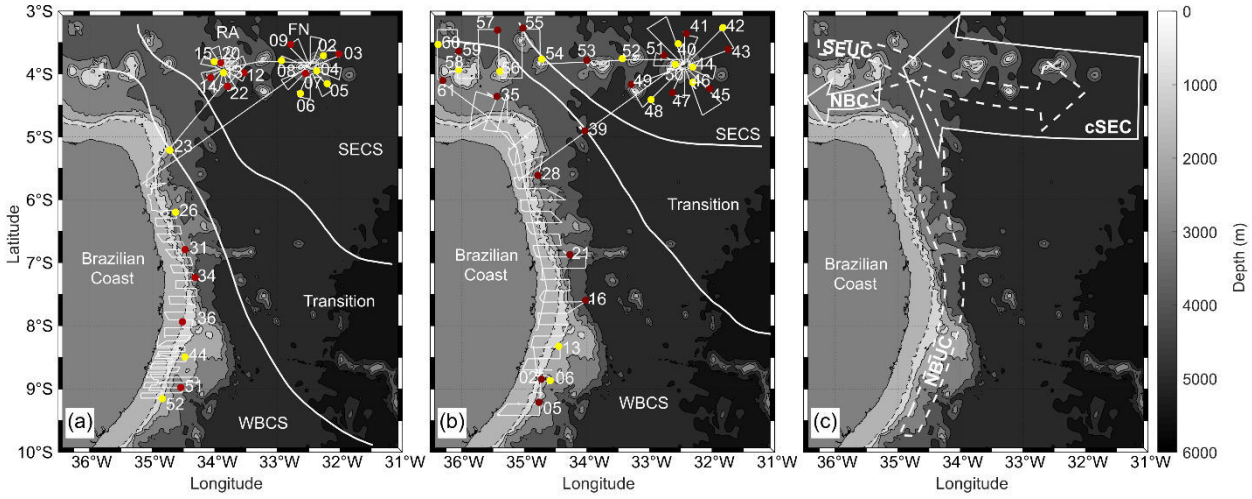

Source: Personal collection.

2.2.Thermocline structure

To describe the thermohaline structure, we have defined a series of parameters or limits (Fig. 2a): the thermocline (upper and lower limits), the mixed-layer depth (MLD), and the barrier layer thickness (BLT). There is no consensus for such definitions, depending on the most suitable adjustment from the oceanographic conditions of each region (Araújo et al., 2011; de Boyer Montégut et al., 2004; Holte and Talley, 2009; Ker et al., 2015, 2016). Here, we defined these limits using the criteria used by Assunção et al. (2020). The upper thermocline depth (UTD) is the depth at which $\partial_\theta/\partial_z = 0.1℃/m$. The lower thermocline depth (LTD) corresponds to the last depth below the UTD where the Brunt Väisälä frequency (N^2, the buoyancy frequency squared), is of up to four orders of magnitude ($N^2 \geq 10^{-4}$). To determine the stability of water column, we used the Brunt Väisälä frequency (N^2, the buoyancy frequency squared), calculated according to the equation (1),

$$N^2 = -\frac{g}{\sigma_0}\frac{\partial_{\sigma_z}}{\partial_z} \quad (1)$$

where *g* is the acceleration of gravity and *σ0* is a reference density at 10 m (Kim and Miller, 2007; Liu et al., 2016).

To define the MLD, we used the criteria from Sprintall and Tomczak (1992), i.e., the depth where the potential density (σ) has increased with respect to its value at the reference depth ($z_0 = 10\ m$) by an amount that corresponds to a drop in potential temperature by 0.5℃, according to the equation (2),

$$MLD = z\left(\partial_{z_0} + \frac{\partial_{\sigma\theta}}{\partial_\theta}\Delta_\theta\right) \quad (2)$$

Finally, the barrier layer thickness (BLT) was calculated as the difference between the MLD and the UTD (BLT = MLD – UTD) (Lukas and Lindstrom, 1991).

2.3.Linking acoustic profiles to thermohaline properties

Here, we considered separately the diel period (day; night), the hydrodynamic systems (Western Boundary Current System - WBCS; South Equatorial Current System – SECS; Fig. 1; see Assunção et al., 2020), and the seasons (spring 2015; fall 2017). To determine if the thermohaline structure could be extracted from acoustic data, we tested two criteria (Z_{VEEC} and acoustic gradient)

and a cross-wavelet analysis approach (Fig. 2b, c, d). The methods have complementary potential, but each one is based on a specific hypothesis. First (Fig. 2b), we tested the method from Bertrand et al. (2010) to determine if the LTD could be derived from a specific value (or range) of the cumulative sum (%) of the acoustic echoes (s_A, nautical area backscattering coefficient in m².nmi^{-2}) from upper ocean. The s_A (a proxy for the acoustic biomass) is defined according to the equation (3),

$$s_A = 4\pi(1852)^2 . \int_{z1}^{z2} s_v \, dz \quad (3)$$

where, s_v is the volume backscattering coefficient in m².m^{-3} (MacLennan et al., 2002).

Second (Fig. 2c), we tested if the thermocline limits could be associated to specific volume backscattering strength (Sv in dB re 1 m^{-1}) gradient (∂_{Sv}/∂_z) values (or ranges) at each acoustic frequency (38, 70 and 120 kHz). Gradient methods, as threshold ones, assume that there is a strong acoustic gradient marking the thermohaline layers interfaces. In fact, gradients are commonly used in a similar way to assess the MLD, thermocline or pycnocline depth (Assunção et al., 2020; Lukas and Lindstrom, 1991).

Finally (Fig. 2d), we applied a wavelet approach based on continuous wavelet transform (CWT), and cross-wavelet transform (XWT) to determine if the along-depth localised power variations in temperature ($x_{\partial\theta/\partial_z}$) and Sv ($y_{\partial Sv/\partial_z}$) gradients match, allowing for determining the upper and lower limits of the thermocline. Cross-wavelet analysis is indeed a powerful method for testing proposed linkages between two signals, simultaneously in frequency (or scale) and time (or location) (Grinsted et al., 2004a; Muchebve et al., 2018). The wavelet power spectrum can be interpreted as depicting the local variance of a time/space series. The XWT is computed by multiplying the CWT of one time-series by the complex conjugate of the CWT of the second time-series and depicts the local covariance between these series at each time/space and frequency. Therefore, the cross-wavelet power provides a quantification of the power similarities between two series (Aguiar-Conraria and Soares, 2014; Daubechies, 1992; Grinsted et al., 2004b; Tomás et al., 2016).

Figure 210. Example of CTD profile (a) from ABRACOS 1 from Assunção et al. (2020) with the representation of the thermohaline structure as defined from the temperature, salinity, density and squared buoyancy frequency (N^2). MLD: mixed layer depth; UTD: upper thermocline depth; LTD/LPD: lower thermocline/pycnocline depth; BL: barrier layer. Examples of the application of the three methods tested for the detection of thermocline limits through the vertical distribution of acoustic echoes are provided: (b) cumulative sum (%); (c) Sv gradients ($\nabla_{S_v} = {}^{\partial Sv}/_{\partial_z}$) respective to each layer depth (MLD, UTD and LTD); and (d) cross-wavelet transform between the gradients of temperature $\left(x_{\partial\theta/\partial_z}\right)$ and Sv $\left(y_{\partial Sv/\partial_z}\right)$.

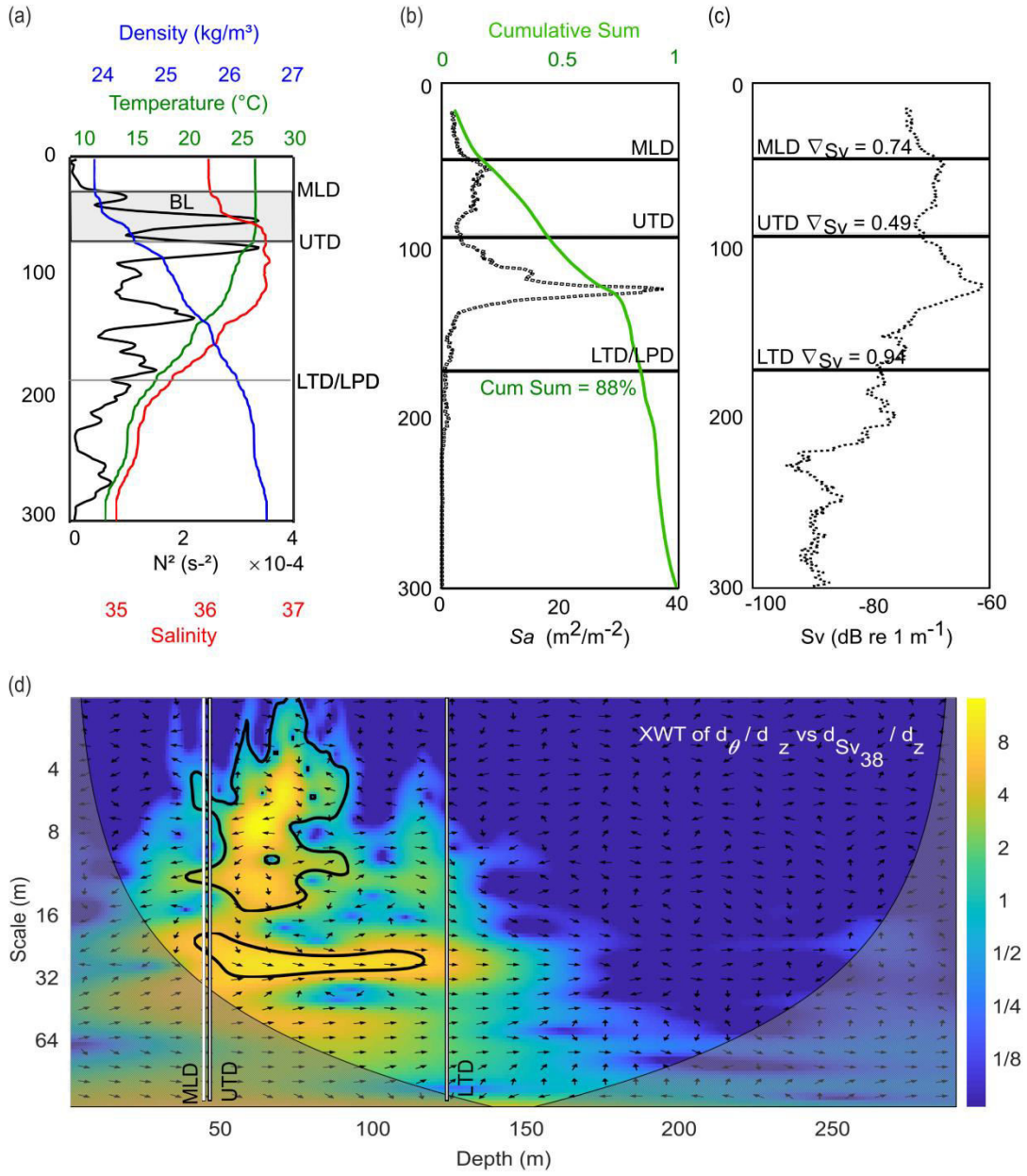

Source: Personal collection.

3. Results and Discussion

3.1. Thermohaline limits vs. cumulative sum of the acoustic echoes

The vertically cumulative sum (expressed as a percentage) of acoustic echoes (s_A, $m^2.nmi^{-2}$) at 38, 70, 120 integrated downward from the surface to a depth of 300 m, was evaluated at the three different thermohaline limits (MLD, UTD and LTD) (Fig. 3). Results show a wide variation of the cumulative sums of acoustic echoes at the three limits, whatever the frequency, for each hydrodynamics system or diel period (Figs. 3, 4 and 5). Even within a given hydrodynamic system where these limits, in particular the LTD, can be stable, the cumulative sum of acoustic echoes was highly variable from one station to another (Fig. 4, see interquartile ranges). In addition, the variance was higher in the highly stratified SECS than in the WBCS, which is less stratified (Assunção et al., 2020). This last result is rather opposite of what one might have expected. Indeed, according to previous studies (Bertrand et al., 2010), we could have expected more robust estimation in an area characterised by sharp density gradients. Therefore, this cumulative sum approach does not allow for a robust estimation of the thermohaline limits in the SWTA. However, studying the proportion of acoustic biomass within each layer provides interesting insights on ecosystem structure in different thermohaline, seasonal and diel scenarios.

Figure 3. Examples of cumulative sum (%) of the acoustic echoes (s_A, m².nmi-²) from surface to the MLD, UTD and LTD respective to the integration of acoustic echoes in the range 0 - 300 m in spring 2015 and fall 2017. MLD: mixed layer depth; UTD: upper thermocline depth; LTD: lower thermocline depth.

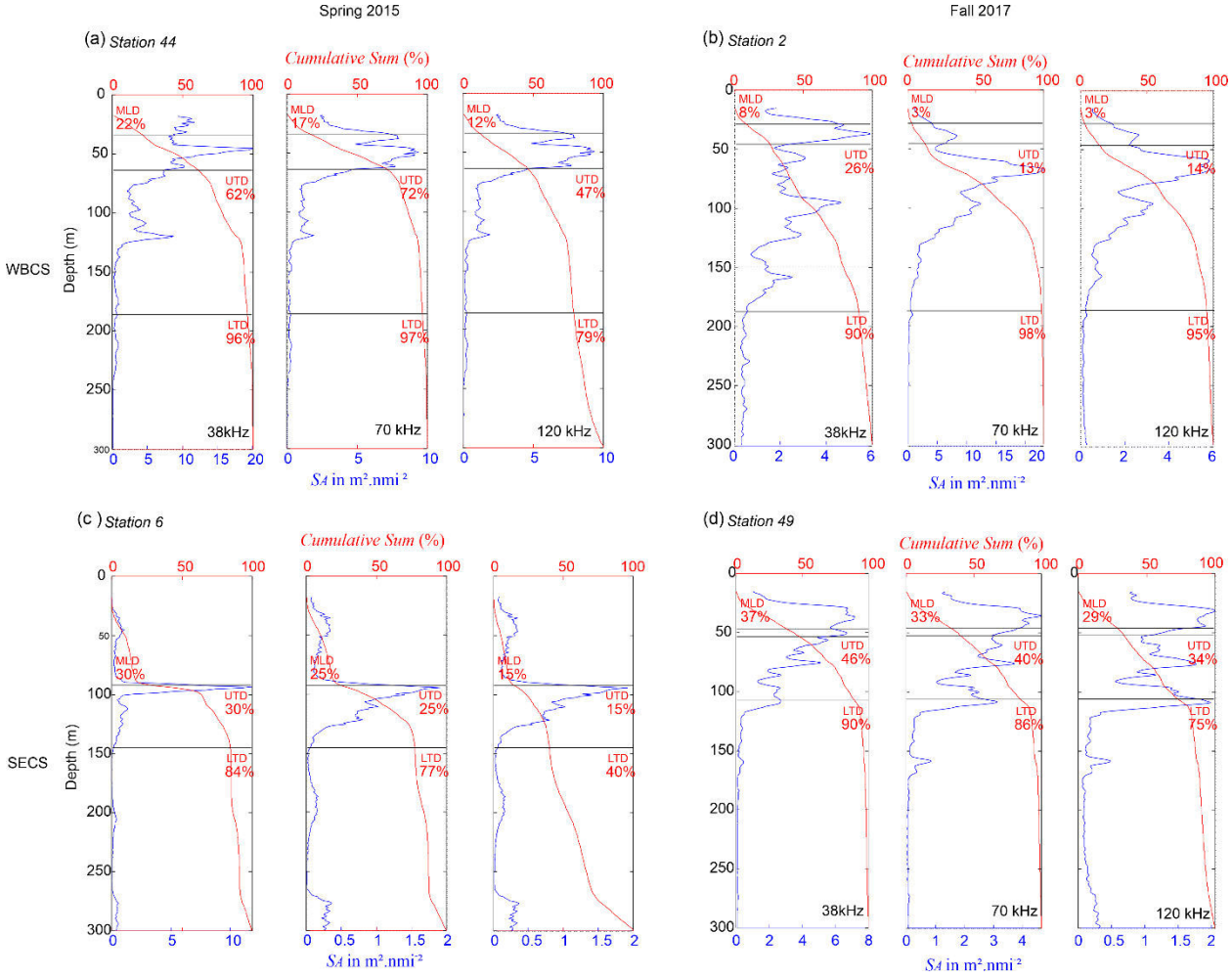

Source: Personal collection.

Figure 4. Boxplots of the cumulative sum (%) of the acoustic echoes (s_A, $m^2.nmi^{-2}$) from surface to lower thermocline depth respective to the integration of acoustic echoes in the range 0 - 300 m in (a) the WBCS in spring 2015; (b) the SECS in spring 2015; (c) the WBCS in fall 2017; (d) the SECS in fall 2017 (d). Day and night stations are represented by empty and grey boxes, respectively.

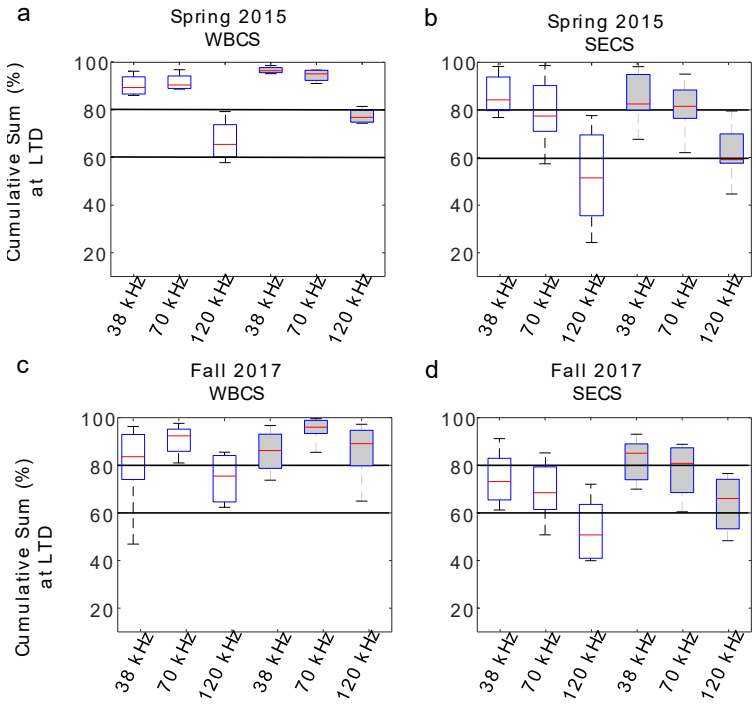

Source: Personal collection.

Except at 120 kHz during the day in the SECS at both seasons, more than 60% of the upper ocean acoustic biomass was concentrated above the LTD (Figs. 4 and 5). The cumulative sums at the LTD increased at night (Figs. 4 and 5) due to vertical diel migration of mesopelagic organisms towards the epipelagic layer (e.g., Eduardo et al., 2020). Actually, the highest the cumulative sum (in particular at night and spring), the lowest the inter-stations variability (Fig. 4, see interquartile ranges) so the highest is the possibility to estimate the LTD using the cumulative sum. Further, average s_A cumulative sums at the MLD, UTD and LTD for both diel periods, hydrodynamics systems and seasons (spring and fall), reveal that most of the acoustic biomass was concentrated within the thermocline (i.e., between UTD and LTD) in both systems in fall. In spring, however, this pattern was only observed at day in the SECS. In both systems, in spring 2015, a large proportion of organisms (up to 55% and 49% in the WBCS and SECS (only at night), respectively; less conspicuous at 120 kHz) inhabiting the water column were distributed above the thermocline, i.e., in the ML and BL ($\%_{BL} = \%_{UTD} - \%_{MLD}$). In the WBCS, this behaviour may be a strategy

of the organisms to limit the advection by the stronger NBUC (below ~100 m) at this season than in fall (Dossa et al., 2021).

Figure 5. Mean cumulative sum (%) of acoustic echoes (s_A, $m^2.nmi^{-2}$) respective to the integration of acoustic echoes in the range 0 - 300 m for each thermohaline layer limit: mixed-layer depth (MLD); upper thermocline depth (UTD) and lower thermocline depth (LTD). Results are presented according to the season (spring 2015; fall 2017), the diel period (D - day; N - night), the hydrodynamic system (WBCS; SECS) and the frequencies: 38 kHz (red), 70 kHz (green) and 120 kHz (blue).

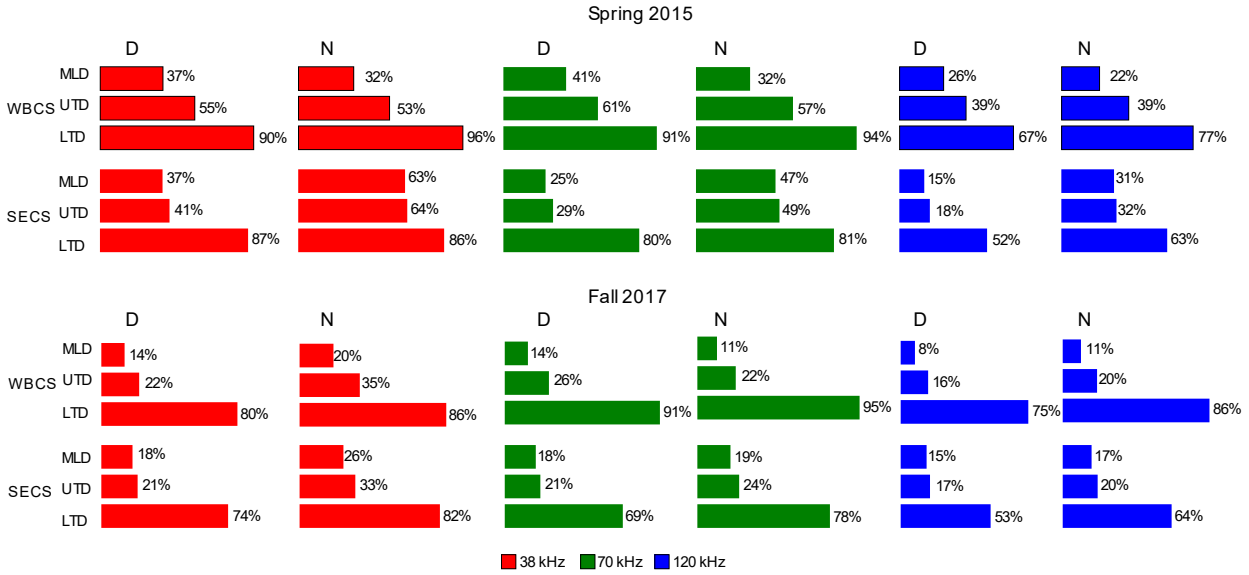

Source: Personal collection.

The acoustic biomass at the LTD were higher and with lower variability in the WBCS (Fig. 5), characterised by a smooth and thick thermocline (Assunção et al., 2020), than in the SECS, whatever the season and diel period. Interestingly, in the SECS, characterised by a sharp and narrow thermocline and shallowest LTDs, a significant part of the biomass was still below the thermocline, most visible at 120 kHz (fluid-like zooplankton proxy; Stanton et al., 1998) with up to 47% of acoustic biomass distributed below the LTD (Fig. 5). These results lead us to hypothesize that in regions where the thermocline is highly stratified, and less mixed, some organisms avoid the layer of highest gradient. These results agree with previous studies (Lee et al., 2013). This is also consistent with the fact that, in the SECS in spring, zooplankton biomass is lower than in the WBCS, but organisms are larger (Figueiredo et al., 2020). Larger zooplankton are more likely to inhabit greater depths under more stratified conditions (Hampton et al., 2014).

3.2. Thermohaline limits vs. acoustic backscattering gradient

The value of Sv gradient differed according to the thermohaline limits in the WBCS (Fig. 6a, b). However, in the SECS gradients were more alike between MLD and UTD, due to their proximity or overlap (Fig. 6c, d). Still, at all thermohaline limits (MLD, UTD and LTD), Sv gradients varied widely according to the frequency and the diel period, even within a given thermohaline system and season (Fig. 7). The largest interquartile ranges (considering the Sv gradient values of all stations) were observed for the UTD at day. Whereas the smallest interquartile ranges were more associated with the MLD and night. This seems to reflect the fact that during the day organisms present a more patchy distribution while at night they are organised over more homogeneous layers (e.g., Benoit-Bird, et al., 2003). The smallest interquartile range was observed in spring in the WBCS at night with almost no variation among stations at 70 and 120 kHz, then being the most promising condition for which a threshold may allow a robust estimation the UTD. However, according to the Sv gradient ranges observed for the other frequencies and limits, we consider that the gradient criteria is not robust enough, since for a given limit (MLD, UTD or LTD) little or no variation between stations is expected, even in this specific case. Therefore, the application of specific Sv gradient value as a criterion to detect and track the thermohaline limits is likely unreachable in the SWTA.

The vertical distribution of pelagic organisms is often very patchy and acoustic scattering can vary by several orders of magnitude over few metres (Benoit-Bird, et al., 2003). In addition, the fact that gradients cannot be robustly associated to the physical structures confirm that the acoustic scatters we observed correspond to organisms and not to sole density structures. Indeed, in some ecosystems, physical turbulence can be detected directly. For instance, in the Arctic Ocean, Stranne et al. (2018) successfully detected the MLD associated with the impedance contrasts. In such case, contrarily to ours, the number of biological scatters was low in the upper layers, facilitating the detection of genuine physically driven structures (Ker et al., 2015, 2016; Stranne et al., 2018).

Figure 11. Examples of acoustic profiles (Sv, dB re 1 m^{-1}) in spring 2015 (a, c) and fall 2017 (b, d). At each station, thermohaline structure is superimposed on the Sv profiles and their respective Sv gradients. The depth of greatest gradients is marked by a magenta asterisk. MLD: mixed layer depth; UTD: upper thermocline depth; LTD: lower thermocline depth.

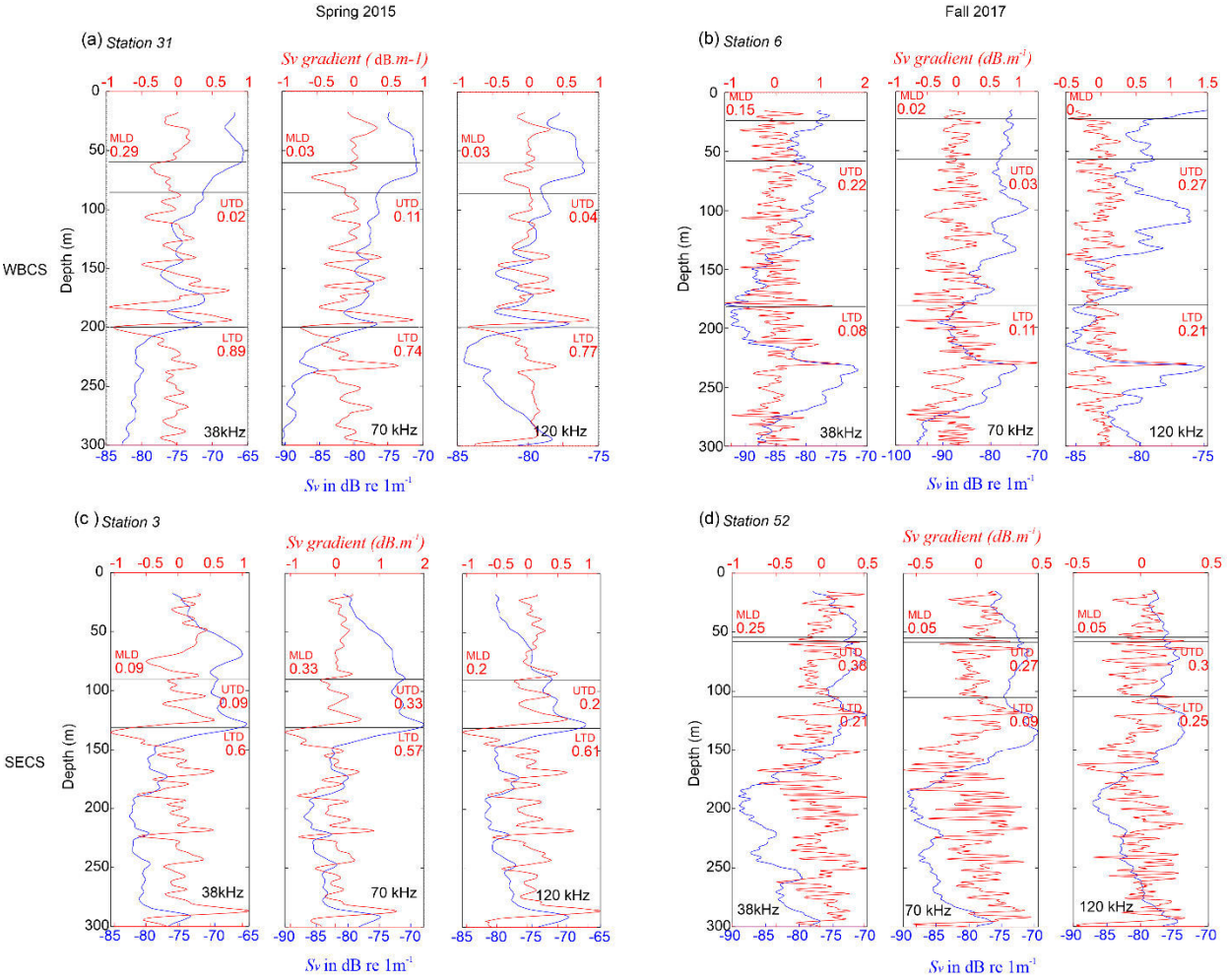

Source: Personal collection.

Figure 7. Boxplot of the acoustic gradient of Sv (in dB re 1 m^{-1}) at the thermohaline vertical limits (MLD, UTD and LTD) according to the season (spring – a, b; fall – c, d), the thermohaline system (WBCS – a, c; SECS – b, d). For each case, frequencies (38, 70 and 120 kHz) and diel period (day - empty box; night - grey box) are specified.

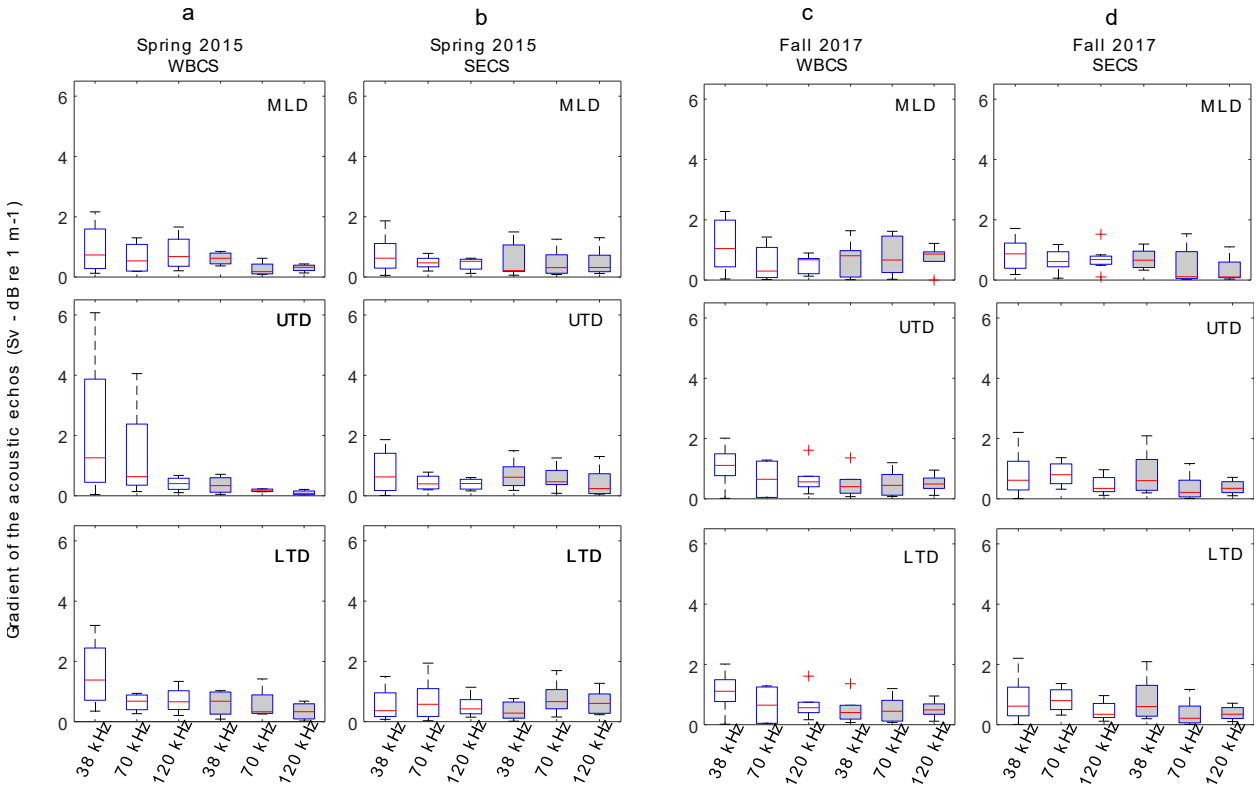

Source: Personal collection.

3.3.Wavelet approach

Here, we only present results obtained at 38kHz that, for simplicity. However, the results at 38 kHz are representative of the results observed at other frequencies (not shown).

The analysis of the continuous wavelet transforms (CWT, Figs. 8a, b and 9a, b) of the profiles of temperature gradient reveal that, as expected, the highest energy is encompassed within the thermocline. However, due to the differences in thermohaline structures, the signal energy of temperature gradient depicted more variable patterns in the WBCS, where the stratification is weak (Figs. 8a and 9a), than in the SECS (Figs. 8b and 9b). Sv gradient CWT patterns were less clear (Fig. 8c, d and 9c, d). The peaks of energy were not restricted to the thermocline and the scale varied between 4 and 32 m in the WBCS and 4 and 64 m in the SECS. We did not observe, as

expected, a well-defined pattern in the SECS (Figs.8d and 9d). Sv gradient signals varied widely not only between systems, but also between stations and seasons. Nevertheless, the interaction between temperature and Sv signals becomes clear when considering the cross-wavelet.

In both systems, cross-wavelet (XWT, Figs. 8e, f and 9e, f) reveal significant high common power mostly within the thermocline, generally in the 8 - 32 m scale. This pattern is also robust when considering the strong seasonal changes in the thermocline limits that were much shallower in fall than spring (Assunção et al., 2020). However, the common power locations neither always coincide with the thermocline limits, nor with the MLD. Moreover, the common power locations were highly variable between stations even in a given hydrodynamic system and season. Thereby, we cannot robustly draw the limits of the thermohaline layers with this method either. However, the cross-wavelet allows observing interesting relationships between the gradients of temperature and Sv. These gradients were mostly out of phase (arrow pointing left-biased). This indicate that, Sv gradients did not match the position of the ones of temperature so that organisms formed more stable patches in the zones of strong thermic gradient (more static stability). One exception was observed in the WBCS in fall 2017 where signals are mostly in phase, and thermal and Sv gradients coincided (Fig. 9a, arrow pointing right-biased).

Figure 8. Examples of time/space series of temperature (a, b) and Sv at 38 kHz (c, d) gradients and its continuous wavelet power spectrum from WBCS (a, c) and SECS (b, d) during spring 2015. Cross-wavelet transform (XWT) for $x_{\partial\theta/\partial z}$ and $y_{\partial Sv/\partial z}$ from WBCS (e) and SECS (f). Arrows represent phase difference (with in-phase pointing right, anti-phase pointing left). The black contour encompasses regions with statistically significant signal at 95% confidence level. The cone of influence (COI) where edge effects might distort the picture is shown as a lighter shade.

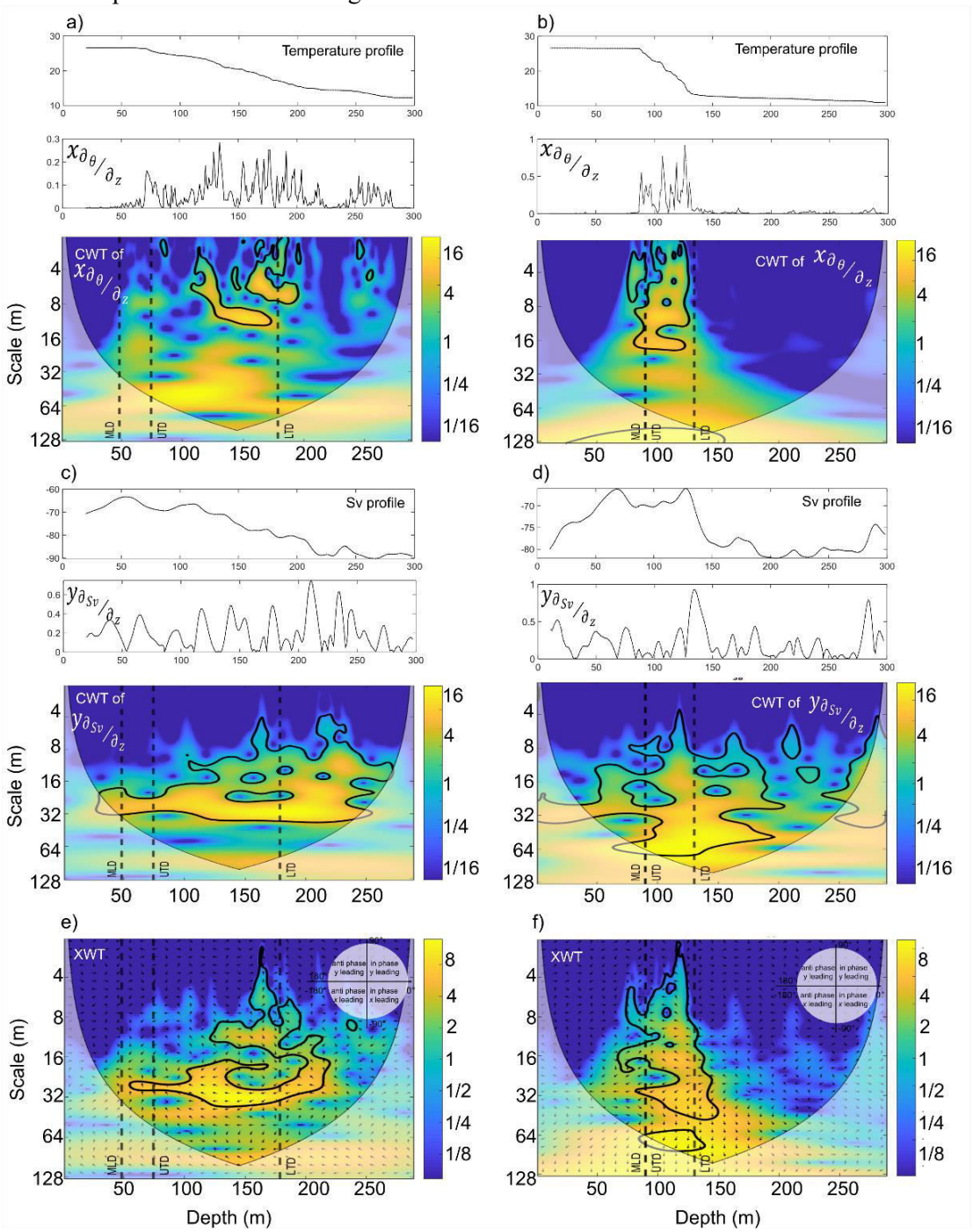

Source: Personal collection.

Figure 9. Examples of time/space series of temperature (a, b) and Sv at 38 kHz (c, d) gradients and its continuous wavelet power spectrum from WBCS (a, c) and SECS (b, d) during fall 2017. Cross-wavelet transform (XWT) for $x_{\partial\theta/\partial z}$ and $y_{\partial Sv/\partial z}$ from WBCS (e) and SECS (f). Arrows represent phase difference (with in-phase pointing right, anti-phase pointing left). The black contour encompasses regions with statistically significant signal at 95% confidence level. The cone of influence (COI) where edge effects might distort the picture is shown as a lighter shade.

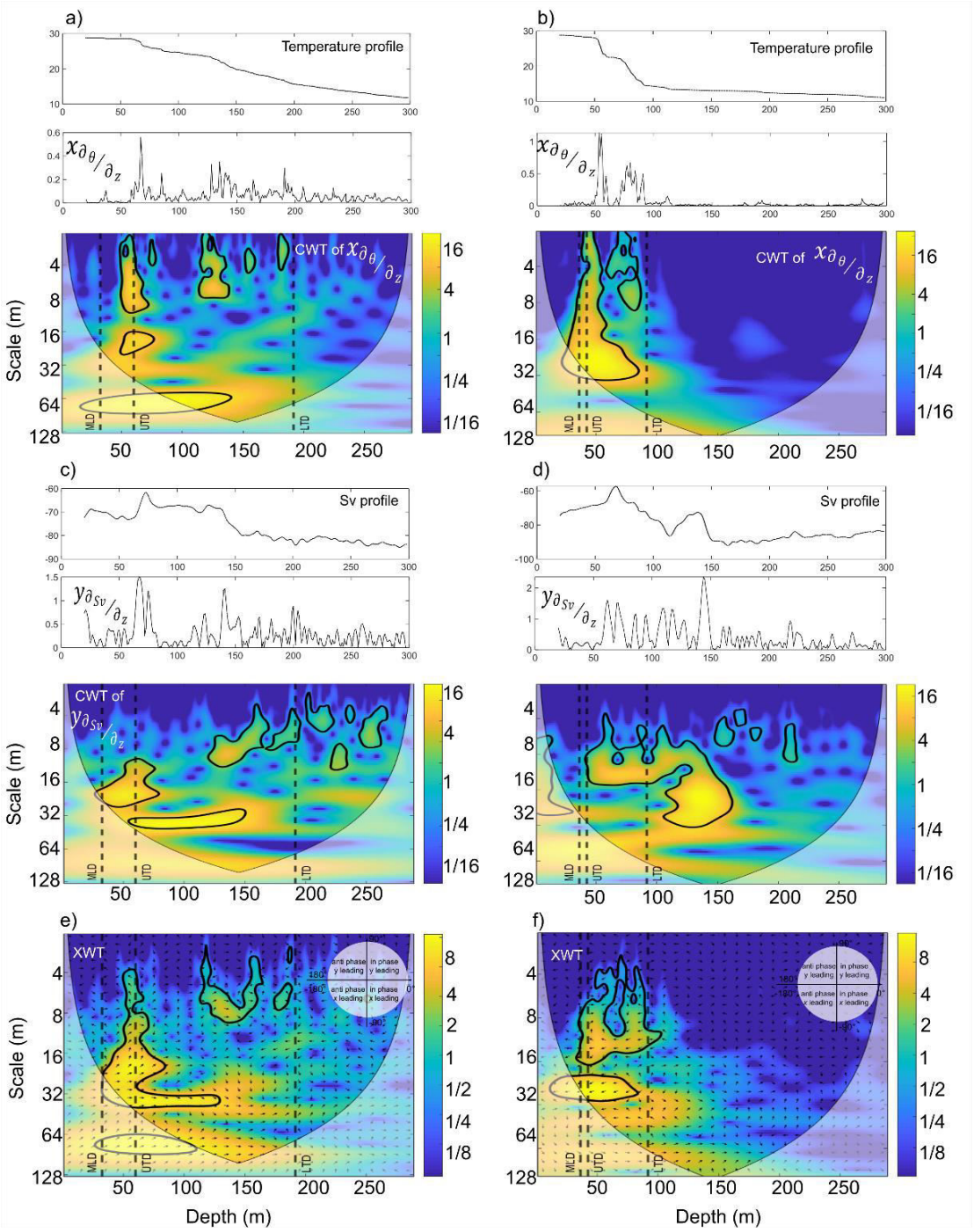

Source: Personal collection.

4. Conclusion

In summary, we aimed in this study at verifying the feasibility to draw the vertical thermohaline structure from echosounder data, based on biological scattering or turbulent structures in an oligotrophic ecosystem. None of the three tested criteria (vertical distribution of the epipelagic community, gradient of acoustic energy and signal analysis between the thermal vertical and Sv gradients) allowed for a robust estimation of the thermohaline structure.

From the analysis of the vertical integration (cumulative sum) of the acoustic echoes, we expected that the thermocline could act as a natural barrier in the vertical distribution of organisms, mainly small mesopelagic fishes and zooplankton, as observed in the northern Humboldt Current system off Peru where a strong oxygen minimum zone is present (Bertrand et al., 2010). On the contrary, even in a given hydrodynamic system (WBCS and SECS) and season (spring and fall), we could not identify specific cumulative sums or gradient of echoes fitting thermohaline limits, including at night. In addition, according to the oceanscape, highest acoustic biomasses were not systematically associated with the thermocline, indicating that other oceanographic or biological processes may be acting.

The cross-wavelet signal analysis showed promising results in the analysis of the co-variation between the thermal and Sv gradients along depth. Presently, the cross-wavelet analysis with the aim of detecting the depth of thermohaline layers can be used as preliminary analysis. However, it is not suitable for the detection of thermohaline depths with high accuracy in an oligotrophic system.

Although we could not robustly detect the thermohaline vertical structure from acoustic scatters, we revealed a variety of oceanscapes with different responses in terms of organisms vertical distribution. Additional analyses at fine vertical scales involving other environmental and biological factors need to be achieved to further understand the processes involved in the vertical structuring of the epipelagic community.

References

Aguiar-Conraria, L. and Soares, M. J.: The continuous wavelet transform: moving beyond uni- and bivariate analysis, J. Econ. Surv., 28(2), 344–375, doi:10.1111/joes.12012, 2014.

Araújo, M., Limongi, C., Servain, J., Silva, M., Leite, F. S., Veleda, D. and Lentini, C. A. D.: Salinity-induced mixed and barrier layers in the southwestern tropical Atlantic Ocean off the northeast of Brazil, Ocean Sci., 7(1), 63–73, doi:10.5194/os-7-63-2011, 2011.

Assunção, R. V., Silva, A. C. da, Roy, A., Bourlès, B., Silva, C. H. S., Ternon, J.-F., Araújo, M. and Bertrand, A.: 3D characterisation of the thermohaline structure in the southwestern tropical Atlantic derived from functional data analysis of in situ profiles, Prog. Oceanogr., 187(December 2019), 102399, doi:10.1016/j.pocean.2020.102399, 2020.

Benoit-Bird, K. J. and Lawson, G. L.: Ecological Insights from Pelagic Habitats Acquired Using Active Acoustic Techniques, Ann. Rev. Mar. Sci., 8(1), 463–490, doi:10.1146/annurev-marine-122414-034001, 2016.

Bertrand, A.: ABRACOS cruise, RV Antea, doi:10.17600/15005600, 2015.

Bertrand, A.: ABRACOS 2 cruise, RV Antea, doi:10.17600/17004100, 2017.

Bertrand, A., Ballón, M. and Chaigneau, A.: Acoustic observation of living organisms reveals the upper limit of the oxygen minimum zone, PLoS One, 5(4), doi:10.1371/journal.pone.0010330, 2010.

Bertrand, A., Grados, D., Colas, F., Bertrand, S., Capet, X., Chaigneau, A., Vargas, G., Mousseigne, A. and Fablet, R.: Broad impacts of fine-scale dynamics on seascape structure from zooplankton to seabirds, Nat. Commun., 5(May), doi:10.1038/ncomms6239, 2014.

Biescas, B., Sallarès, V., Pelegrí, J. L., Machín, F., Carbonell, R., Buffett, G., Dañobeitia, J. J. and Calahorrano, A.: Imaging meddy finestructure using multichannel seismic reflection data, Geophys. Res. Lett., 35(11), L11609, doi:10.1029/2008GL033971, 2008.

Bourlès, B., Molinari, R. L., Johns, E., Wilson, W. D. and Leaman, K. D.: Upper layer currents in the western tropical North Atlantic (1989-1991), J. Geophys. Res. Ocean., 104(C1), 1361–1375, doi:10.1029/1998JC900025, 1999.

de Boyer Montégut, C., Madec, G., Fischer, A. S., Lazar, A. and Iudicone, D.: Mixed layer depth over the global ocean: An examination of profile data and a profile-based climatology, J. Geophys. Res. C Ocean., 109(12), 1–20, doi:10.1029/2004JC002378, 2004.

de Boyer Montégut, C., Mignot, J., Lazar, A. and Cravatte, S.: Control of salinity on the mixed layer depth in the world ocean: 1. General description, J. Geophys. Res. Ocean., 112(6), 1–12, doi:10.1029/2006JC003953, 2007.

Chen, G., Peng, L. and Ma, C.: Climatology and seasonality of upper ocean salinity: a three-dimensional view from argo floats, Clim. Dyn., 50(5–6), 2169–2182, doi:10.1007/s00382-017-3742-6, 2018.

Daubechies, I.: Ten Lectures on Wavelets, Society for Industrial and Applied Mathematics., 1992.

Dossa, A. N., Silva, A. C. da, Chaigneau, A., Eldin, G., Araújo, M. and Bertrand, A.: Near-surface western boundary circulation off Northeast Brazil, Prog. Oceanogr., 190, 102475, doi:10.1016/j.pocean.2020.102475, 2021.

Fer, I., Nandi, P., Holbrook, W. S., Schmitt, R. W. and Páramo, P.: Seismic imaging of a thermohaline staircase in the western tropical North Atlantic, Ocean Sci., 6(3), 621–631, doi:10.5194/os-6-621-2010, 2010.

Figueiredo, G. G. A. A. de, Schwamborn, R., Bertrand, A., Munaron, J.-M. and Le Loc'h, F.: Body size and stable isotope composition of zooplankton in the western tropical Atlantic, J. Mar. Syst., 212, 103449, doi:10.1016/j.jmarsys.2020.103449, 2020.

Foote, K. G., Knudsen, H. P. and Vestnes, G.: Calibration of acoustic instruments for fish density estimation: A practical guide, J. Acoust. Soc. Am., 83(2), 831–832, doi:10.1121/1.396131, 1987.

Gaillard, F., Reynaud, T., Thierry, V., Kolodziejczyk, N. and von Schuckmann, K.: In Situ–Based Reanalysis of the Global Ocean Temperature and Salinity with ISAS: Variability of the Heat Content and Steric Height, J. Clim., 29(4), 1305–1323, doi:10.1175/JCLI-D-15-0028.1, 2016.

Grados, D., Bertrand, A., Colas, F., Echevin, V., Chaigneau, A., Gutiérrez, D., Vargas, G. and Fablet, R.: Spatial and seasonal patterns of fine-scale to mesoscale upper ocean dynamics in an Eastern Boundary Current System, Prog. Oceanogr., 142, 105–116, doi:10.1016/j.pocean.2016.02.002, 2016.

Grinsted, A., Moore, J. C. and Jevrejeva, S.: Application of the cross wavelet transform and wavelet coherence to geophysical time series, Nonlinear Process. Geophys., 11(5/6), 561–566, doi:10.5194/npg-11-561-2004, 2004a.

Holbrook, W. S. and Fer, I.: Ocean internal wave spectra inferred from seismic reflection transects, Geophys. Res. Lett., 32(15), 2–5, doi:10.1029/2005GL023733, 2005.

Holbrook, W. S., Fer, I. and Schmitt, R. W.: Images of internal tides near the Norwegian continental slope, Geophys. Res. Lett., 36(24), 1–5, doi:10.1029/2009GL038909, 2009.

Holte, J. and Talley, L.: A new algorithm for finding mixed layer depths with applications to argo data and subantarctic mode water formation, J. Atmos. Ocean. Technol., 26(9), 1920–1939, doi:10.1175/2009JTECHO543.1, 2009.

Hounsou-Gbo, G. A., Servain, J., Araújo, M., Martins, E. S., Bourlès, B. and Caniaux, G.: Oceanic Indices for Forecasting Seasonal Rainfall over the Northern Part of Brazilian Northeast, Am. J. Clim. Chang., 05(02), 261–274, doi:10.4236/ajcc.2016.52022, 2016.

Ker, S., Le Gonidec, Y., Marié, L., Thomas, Y. and Gibert, D.: Multiscale seismic reflectivity of shallow thermoclines, J. Geophys. Res. Ocean., 120(3), 1872–1886, doi:10.1002/2014JC010478, 2015.

Ker, S., Le Gonidec, Y. and Marié, L.: Multifrequency seismic detectability of seasonal thermoclines assessed fromARGO data, J. Geophys. Res. Ocean., 3741–3756, doi:10.1002/2015JC011228.Received, 2016.

Kim, H.-J. and Miller, A. J.: Did the Thermocline Deepen in the California Current after the 1976/77 Climate Regime Shift, J. Phys. Oceanogr., 37(6), 1733–1739, doi:10.1175/jpo3058.1, 2007.

Klymak, J. M. and Moum, J. N.: Internal solitary waves of elevation advancing on a shoaling shelf, Geophys. Res. Lett., 30(20), 2003GL017706, doi:10.1029/2003GL017706, 2003.

Lavery, A. C., Chu, D. and Moum, J. N.: Measurements of acoustic scattering from zooplankton and oceanic microstructure using a broadband echosounder, ICES J. Mar. Sci., 67(2), 379–394, doi:10.1093/icesjms/fsp242, 2010.

Lee, H., Cho, S., Kim, W. and Kang, D.: The diel vertical migration of the sound-scattering layer in the Yellow Sea Bottom Cold Water of the southeastern Yellow sea: focus on its relationship with a temperature structure, Acta Oceanol. Sin., 32(9), 44–49, doi:10.1007/s13131-013-0351-z, 2013.

Liu, C., Köhl, A., Liu, Z., Wang, F. and Stammer, D.: Deep-reaching thermocline mixing in the equatorial pacific cold tongue, Nat. Commun., 7(May 2015), doi:10.1038/ncomms11576, 2016.

Lukas, R. and Lindstrom, E.: The mixed layer of the western equatorial Pacific Ocean, J. Geophys. Res., 96(S01), 3343, doi:10.1029/90JC01951, 1991.

Maclennan, D. N., Fernandes, P. G. and Dalen, J.: A consistent approach to definitions and symbols in fisheries acoustics, ICES J. Mar. Sci., 59(2), 365–369, doi:10.1006/jmsc.2001.1158, 2002.

Maze, G., Mercier, H., Fablet, R., Tandeo, P., Lopez Radcenco, M., Lenca, P., Feucher, C. and Le Goff, C.: Coherent heat patterns revealed by unsupervised classification of Argo temperature profiles in the North Atlantic Ocean, Prog. Oceanogr., 151, 275–292, doi:10.1016/j.pocean.2016.12.008, 2017.

Ménesguen, C., Hua, B. L., Carton, X., Klingelhoefer, F., Schnürle, P. and Reichert, C.: Arms winding around a meddy seen in seismic reflection data close to the Morocco coastline, Geophys. Res. Lett., 39(5), 1–6, doi:10.1029/2011GL050798, 2012.

Mignot, J., de Boyer Montégut, C. and Tomczak, M.: On the porosity of barrier layers, Ocean Sci., 5(3), 379–387, doi:10.5194/os-5-379-2009, 2009.

Miller, J. R.: The Salinity Effect in a Mixed Layer Ocean Model, J. Phys. Oceanogr., 6(1), 29–35, doi:10.1175/1520-0485(1976)006<0029:TSEIAM>2.0.CO;2, 1976.

Muchebve, E., Nakamura, Y. and Kamiya, H.: Use of Wavelet Techniques in the Study of Seawater Flux Dynamics in Coastal Lakes, in Wavelet Theory and Its Applications, InTech., 2018.

Orr, M. H., Haury, L. R., Wiebe, P. H. and Briscoe, M. G.: Backscatter of high-frequency (200 kHz) acoustic wavefields from ocean turbulence, J. Acoust. Soc. Am., 108(4), 1595–1601, doi:10.1121/1.1286883, 2000.

Pensieri, S. and Bozzano, R.: Active and Passive Acoustic Methods for In-situ Monitoring of the Ocean Status, in Advances in Underwater Acoustics, InTech., 2017.

Perrot, Y., Brehmer, P., Habasque, J., Roudaut, G., Behagle, N., Sarré, A. and Lebourges-Dhaussy, A.: Matecho: An Open-Source Tool for Processing Fisheries Acoustics Data, Acoust. Aust., 46(2), 241–248, doi:10.1007/s40857-018-0135-x, 2018.

Peterson, R. G. and Stramma, L.: Upper-level circulation in the South Atlantic Ocean, Prog. Oceanogr., 26(1), 1–73, doi:10.1016/0079-6611(91)90006-8, 1991.

Pingree, R. D. and Mardell, G. T.: Solitary internal waves in the Celtic Sea, Prog. Oceanogr., 14(C), 431–441, doi:10.1016/0079-6611(85)90021-7, 1985.

Rippert, N., Baumann, K.-H. and Patzold, J.: Thermocline fluctuations in the western tropical Indian Ocean during the past 35 ka, , 30, 201–210, doi:10.1002/jqs.2767, 2015.

Ross, T. and Lueck, R.: Estimating turbulent dissipation rates from acoustic backscatter, Deep. Res. Part I Oceanogr. Res. Pap., 52(12), 2353–2365, doi:10.1016/j.dsr.2005.07.002, 2005.

Silva, A. C. da, Chaigneau, A., Dossa, A. N., Eldin, G., Araújo, M. and Bertrand, A.: Surface circulation and vertical structure of upper ocean variability around Fernando de Noronha archipelago and Rocas atoll during spring 2015 and fall 2017, Front. Mar. Sci., doi:10.3389/fmars.2021.598101, 2021.

Sprintall, J. and Cronin, M. F.: Upper Ocean Vertical Structure, Encycl. Ocean Sci., 217–224, doi:10.1016/B978-012374473-9.00627-5, 2010.

Sprintall, J. and Tomczak, M.: Evidence of the barrier layer in the surface layer of the tropics, J. Geophys. Res., 97(C5), 7305, doi:10.1029/92JC00407, 1992.

Stanton, T. K., Chu, D. and Wiebe, P. H.: Sound scattering by several zooplankton groups. II. Scattering models, J. Acoust. Soc. Am., 103(1), 236–253, doi:10.1121/1.421110, 1998.

Stramma, L. and Schott, F.: The mean flow field of the tropical Atlantic Ocean, Deep Sea Res. Part II Top. Stud. Oceanogr., 46(1–2), 279–303, doi:10.1016/S0967-0645(98)00109-X, 1999.

Stranne, C., Mayer, L., Weber, T. C., Ruddick, B. R., Jakobsson, M., Jerram, K., Weidner, E., Nilsson, J. and Gårdfeldt, K.: Acoustic mapping of thermohaline staircases in the arctic ocean, Sci. Rep., 7(1), 1–9, doi:10.1038/s41598-017-15486-3, 2017.

Stranne, C., Mayer, L., Jakobsson, M., Weidner, E., Jerram, K., Weber, T. C., Anderson, L. G., Nilsson, J., Björk, G. and Gårdfeldt, K.: Acoustic mapping of mixed layer depth, Ocean Sci., 14(3), 503–514, doi:10.5194/os-14-503-2018, 2018.

Tomás, R., Li, Z., Lopez-Sanchez, J. M., Liu, P. and Singleton, A.: Using wavelet tools to analyse seasonal variations from InSAR time-series data: a case study of the Huangtupo landslide, Landslides, 13(3), 437–450, doi:10.1007/s10346-015-0589-y, 2016.

Trenkel, V. M., Berger, L., Bourguignon, S., Doray, M., Fablet, R., Massé, J., Mazauric, V., Poncelet, C., Quemener, G., Scalabrin, C. and Villalobos, H.: Overview of recent progress in fisheries acoustics made by Ifremer with examples from the Bay of Biscay, Aquat. Living Resour., 22(4), 433–445, doi:10.1051/alr/2009027, 2009.

Trevorrow, M. V.: Observations of internal solitary waves near the Oregon coast with an inverted echo sounder, J. Geophys. Res. Ocean., 103(C4), 7671–7680, doi:10.1029/98JC00101, 1998.

Tsuchiya, M., Talley, L. D. and McCartney, M. S.: Water-mass distributions in the western South Atlantic; A section from South Georgia Island (54S) northward across the equator, J. Mar. Res., 52(1), 55–81, doi:10.1357/0022240943076759, 1994.

Venancio, I. M., Shimizu, M. H., Santos, T. P., Lessa, D. O., Portilho-Ramos, R. C., Chiessi, C. M., Crivellari, S., Mulitza, S., Kuhnert, H., Tiedemann, R., Vahlenkamp, M., Bickert, T., Sampaio, G., Albuquerque, A. L. S., Veiga, S., Nobre, P. and Nobre, C.: Changes in surface hydrography at the western tropical Atlantic during the Younger Dryas, Glob. Planet. Change, 184, 103047, doi:10.1016/j.gloplacha.2019.103047, 2020.

Wijesekera, H. and Boyd, T. J.: Upper Ocean Heat and Freshwater Budgets, in Encyclopedia of Ocean Sciences, pp. 3079–3083, Elsevier., 2001.

Woods, J. D.: Wave-induced shear instability in the summer thermocline. [online] Available from: http://virtualecology.org.uk/docs/research/Woods1968.pdf (Accessed 7 June 2019), 1968.

…

From Chapter III to Chapter IV

In Chapter III, we revealed the acoustic complexity in the two main hydrodynamic systems of the SWTA. Although most organisms in the upper ocean (0 – 300 m) are associated with the thermocline and shallower layers, we cannot robustly estimate the thermohaline limits (MLD, UTD and LTD) from the vertical distribution of acoustic scatters in the SWTA. Therefore, we cannot improve the detection of fine-scale horizontal processes. The results we obtained when attempting to estimate thermocline boundaries from acoustics revealed that complex biophysical interactions are in play at vertical scales. In Chapter IV, therefore, we investigate further the fine-scale vertical relationships between acoustic biomass and a variety of environmental factors.

…

CHAPTER IV:
FINE-SCALE VERTICAL RELATIONSHIPS BETWEEN ENVIRONMENTAL CONDITIONS AND SOUND SCATTERING LAYERS IN THE SOUTHWESTERN TROPICAL ATLANTIC

This chapter corresponds to the article of the same name to be submitted to *Open Research Europe*.

Ramilla V. Assunção[a,c], Anne Lebourges-Dhaussy[c], Alex C. da Silva[a], Gildas Roudaut[c], Alejandro Ariza[b], Leandro N. Eduardo[b,e], Syumara Queiroz[a], Arnaud Bertrand[b,a,e]

[a]*Laboratório de Oceanografia Física Estuarina e Costeira, Depto. Oceanografia, UFPE, Recife-PE, Brazil.*
[b]*Institut de recherche pour le développement (IRD), MARBEC, Université Montpellier, CNRS, Ifremer, IRD, Sète, France.*
[c]*IRD, UMR 6539 LEMAR IFREMER/IRD/CNRS/UBO, Technopole Brest Iroise, 29280 Plouzané, France*
[d]*Institut de recherche pour le développement (IRD), Délégation Régionale Ouest, IMAGO, Plouzané, France*
[e]*Universidade Federal Rural de Pernambuco, Recife-PE, Brazil*

Abstract

Ocean dynamics initiates the structure of primary producers and these, in turn, shape the distribution of subsequent trophic levels until the whole pelagic community reflects the physicochemical structure of the ocean. Despite the importance of the bottom-up structuring in pelagic ecosystems, fine scale studies of biophysical interactions along depth are scarce and challenging. To fill some gaps in the understanding of such relationships we use data collected in the Southwestern Tropical Atlantic (SWTA) in spring 2015 and fall 2017, periods representative of canonical spring and fall conditions in terms of thermohaline structure and currents dynamics. We show that fluorescence, oxygen, current and stratification are important drivers, but that their relative importance depends on the area, the depth range and the diel cycle. In the epipelagic layer, the strongest acoustic responses were associated with depths of greatest stability (highest stratification), even in areas where the fluorescence peaks were deeper than the peak of stratifications, as the WBCS during spring 2015. Dissolved oxygen seems to be a driver in areas where lower oxygen concentration occurs in sub-surface. Finally, our results suggest that organisms seem to avoid strong currents core. However, future works are needed to better understand the role of currents on the vertical distribution of organisms.

Keywords: sound scattering layers, physical-biological coupling, western boundary current, Fernando de Noronha chain

1. Introduction

Acoustic echosounders are widely used to detect a variety of environmental and biological components in pelagic ecosystems, from oceanic microstructure to mesoscale eddies, and from zooplankton to top predators (Benoit-Bird and Lawson, 2016; Bertrand et al., 2014; Simmonds and MacLennan, 2005, Lavery et al., 2009). Sound scattering layers (SSLs) are vertically discrete water column aggregations of organisms commonly detected during acoustic surveys (Cade and Benoit-Bird, 2014; Proud et al., 2015). Most of the signal within SSLs come from strong targets such as swimbladder fish, siphonophores and other gas-bearing organisms, and to a lesser extent, from fluid-like organisms such as crustaceans, squid are diverse gelatinous life forms (Benoit-Bird and Lawson, 2016; Proud et al., 2019).

SSLs vary over a broad range of spatial and temporal scales in response to biological and environmental forcing (Aksnes et al., 2017; Boswell et al., 2020; Folt and Burns, 1999). Beyond large biogeographical constraints, the pelagic ecosystem structure and associated SSLs can quickly respond to physicochemical changes in the water column (Bertrand et al., 2014; Godø et al., 2012; Legendre, 1981; Prairie et al., 2012). In fact, ocean forcing initiates the structure of primary producers and these, in turn, shape the distribution of subsequent trophic levels until the whole pelagic community reflects the physicochemical structure of the ocean (Legendre, 1981; Margalef and Margalef, 1979). In agreement with this bottom-up structuring, the thermohaline features (e.g., mixed layer depth-MLD, thermocline thickness, presence of barrier layer) drive the availability of new nutrients in the photic zone, controlling primary productivity and thus the vertical and horizontal distribution organisms (Benoit-Bird and McManus, 2014; Bertrand et al., 2014; Cade and Benoit-Bird, 2015; Williams and Grottoli, 2010; Yao and Hoteit, 2015).

Diel vertical migration (DVM) has long been recognised as a key factor driving changes in SSLs structure along the diel cycle (Bandara et al., 2021; Klevjer et al., 2016; Lee et al., 2013; Liu and Sun, 2010). The upward or downward movements of mixed species communities in the water column represent, in general, the trade-off between the functions of food gathering and predator avoidance (Radenac et al., 2010). DVMs are also influenced by environmental (light penetration,

temperature, stratification, oxygen concentration) and/or biological (endogenous cycle, food availability, predator avoidance, species composition) factors (Benoit-Bird and Lawson, 2016; Fennell and Rose, 2015; Folt and Burns, 1999; Lezama-Ochoa et al., 2015).

Despite the importance of the bottom-up structuring in the structure and function of pelagic ecosystems, fine scale studies of biophysical interactions along depth are scarce and challenging. Nets usually do not provide the vertical resolution required to understand fine-scale processes (e.g., Lavery et al., 2007), and acoustic studies has been so far mostly restricted to single-frequency interactions with one, two or three environmental variables (e.g., Boswell et al., 2020; Sameoto, 1976). The description, quantification, and understanding of the fine-scale relationships between physical-chemical forcing and the distribution of the acoustic biota signal is therefore still an exploratory science. Comprehensive fine-scale multivariate environmental analyses with multifrequency acoustics might help understanding group-specific biophysical interactions and structure at the scale of meters. Here, we aim at filling some gaps in the understanding of such relationships.

For that we use data collected in the Southwestern Tropical Atlantic (SWTA) in spring 2015 and fall 2017 (Fig. 1), periods representative of canonical spring and fall conditions in terms of thermohaline structure and currents dynamics (Assunção et al., 2020; Dossa et al., 2021). This oligotrophic region encompasses high biodiversity (Eduardo et al., 2020a, 2020b; Figueiredo et al., 2020; Horota and Wildner, 2011; Tosetto et al., 2021) and is a key area for diagnosing variations of the Atlantic Meridional Overturning Circulation (Cheng et al., 2013; Venancio et al., 2020). Spatially, the area along the continental slope corresponds to a western boundary current system (WBCS) constituted by the North Brazil Undercurrent (NBUC) and the North Brazil current (NBC). This WBCS is characterised by a thick thermocline and high frequency of occurrence of barrier layer (BL) (Assunção et al., 2020; Dossa et al., 2021). Conversely, the area located along the Fernando de Noronha chain corresponds to the south equatorial current system (SECS) formed by the central branch of South Equatorial current (cSEC) and the south equatorial undercurrent (SEUC). The SECS presents a narrow but well-marked thermocline and low BL frequency (Assunção et al., 2020; Silva et al., 2021). This zoning, which also displays significant seasonal variations, implies the formation of habitats with distinct thermal, saline, hydrodynamic conditions,

hosting, in some cases, assemblages of different species (Assunção et al., 2020; Dossa et al., 2021; Tosetto et al., 2021).

In this context, we investigate fine-scale vertical relationships between a variety of environmental parameters (currents, stratification, oxygen concentration and fluorescence) and acoustic backscattering. By doing so we revisit a series of relationships that are often considered in the literature but that are not always precisely evaluated.

First, deep chlorophyll maximum (DCM) that are near ubiquitous in stratified surface waters form and are maintained because phytoplankton must balance opposing gradients of sunlight and nutrient availability, which classically increase with depth under stratified conditions (Abbott et al., 1984; Cullen, 1982, 2015; Mignot et al., 2014). By regulating nutrients mixing from deep waters into the euphotic zone, the structure of the thermohaline stratification is an essential driver of the depth of the DCM (Leach et al., 2018). An increase in static stability allows the development of a phytoplankton population that is not much eroded by turbulent mixing processes. Non-motile phytoplankton may also settle at depths of neutral density along a vertical thermohaline gradient (Alldredge et al., 2002; Durham and Stocker, 2012; Leach et al., 2018). For these reasons, DCMs are classically associated with the thermocline/pycnocline, but precise evaluations are scarce and sometimes contradictory. For example, in a deep (>60 m) thermocline scenario in the tropical Atlantic, the DCM is expected to be shallower than the depth of maximal vertical stability (Agustí and Duarte, 1999; Herbland and Voituriez, 1979). However, in the Azores, Fasham et al. (1985) showed that the DCM was almost invariably located below the stability maximum associated with the seasonal pycnocline. We therefore aim at revisiting these statements in the light of our results.

In a second step, we examine the relationships between the epipelagic SSLs and both the stratification and the DCM. Indeed, SSLs have been associated with these features by various authors (e.g., Benoit-Bird et al., 2010; Berge et al., 2014; Diogoul et al., 2020; Holliday et al., 2010; Jiang et al., 2007; Lezama-Ochoa et al., 2015) but precise relationships are generally lacking or contradictory. Finally, we consider all environmental parameters to determine the main factors driving the vertical distribution of the acoustic scatters in each thermohaline area, season and diel period.

2. Methods

2.1.Data

Data were collected during two multidisciplinary surveys "Acoustic along the BRAzilian CoaSt (ABRACOS)" performed off the coast of northeast Brazil (Fig. 1) aboard the French R/V Antea in September - October 2015 (austral spring; ABRACOS 1; Bertrand, 2015) and April - May 2017 (austral fall; ABRACOS2; Bertrand, 2017). The survey track consisted of rectangular transects along the northeast shelf and adjacent oceanic area and radial transects around oceanic islands and seamounts (Fig. 1). Hydrological measurements were performed at 96 stations, including 52 stations (22 in spring; 32 in fall) achieved in areas with bottom depth higher than 300 m that are used in this study (Fig. 1).

Conductivity, temperature, depth, oxygen (CTDO), and fluorescence hydrographic profiles were acquired using a CTDO Seabird SBE911+ from the surface down to 1000 m or ten meters above the bottom. Conductivity, temperature, pressure, and dissolved oxygen accuracies are of 3 mS/m, 0.001°C, 0.7 dbar, and 0.09 ml.l^{-1}, respectively. The fluorescence sensor measures chlorophyll concentration in the range 0–125 mg m^{-3} with a sensitivity of 0.02 mg m^{-3}.

The zonal and meridional components of the currents were measured using an 'Ocean Surveyor' ship-mounted acoustic Doppler current profiler (SADCP) operating continuously at 75 kHz with a depth range of 15 - 700 m. For more information on ADCP data processing see Dossa et al. (2021). To obtain mean current velocity profiles for each station, we calculated the average currents (zonal and meridional components, and the resulting current) values over a circle of 0.02° around each CTD profile. The vertical current shear (S^2) was calculated according to $S^2 = (\partial_z u)^2 + (\partial_z v)^2$, where u and v are the zonal and meridional components, respectively (Johnston and Rudnick, 2009). To determine the stability of water column, we used the Brunt Väisälä frequency (N^2, the buoyancy frequency squared), calculated according to $N^2 = -\frac{g}{\sigma_0}\frac{\partial \sigma_z}{\partial_z}$, where g is the acceleration of gravity and σ_0 is a reference density at 10 m (Kim and Miller, 2007; Liu et al., 2016).

Acoustic data were acquired using four Simrad EK60 scientific echosounders operating continuously during transects and hydrological stations and connected to split-beam transducers working at 38, 70, 120 and 200 kHz, with operational range from the surface to 700, 500, 250 and

150 m, respectively. Due to its limited operational range, the 200 kHz was not used in this study. Echosounder calibration was performed according to Foote et al. (1987) using a tungsten carbide sphere.

Figure 1. Survey tracks (black lines) of ABRACOS 1 (a) and ABRACOS 2 (b) surveys. Day (yellow circle) and night (red circle) CTDO stations used in this study. The continental shelf is represented in light grey; the dashed black line represents the shelf break (70 m isobath); other bathymetric contours (solid black lines) are by 1000 m intervals. RA: Rocas Atoll; FN: Fernando de Noronha archipelago. The boundaries (solid white lines) between the western boundary current system (WBCS), the south equatorial current system (SECS), and the transitional area are plotted according to Assunção et al. (2020). The main currents (c) of each thermohaline system are: North Brazil Undercurrent (NBUC), North Brazil current (NBC), central branch of South Equatorial current (cSEC) and south equatorial undercurrent (SEUC) (Dossa et al., 2021; Silva et al., 2021). The dotted arrows refer to the subsurface currents and the continuous arrows to the surface currents.

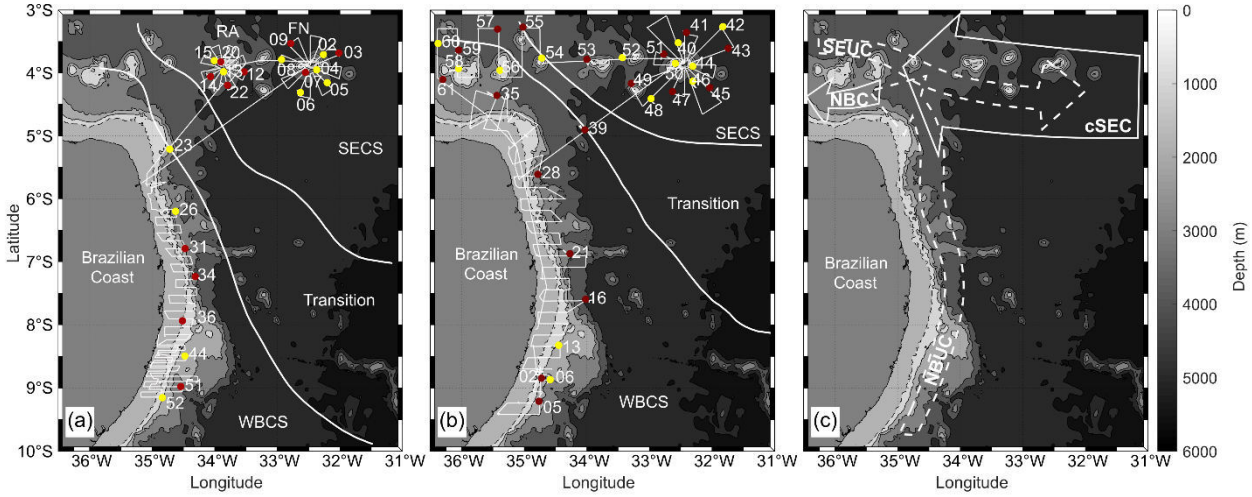

Source: Personal collection.

Acoustic data processing, including automatic extraction of different types of noise, as transient noise, attenuated signal, impulsive noise (Ryan et al., 2015) and background noise (De Robertis and Higginbottom, 2007), was achieved using the Matecho software tool (version 20191213V6; Perrot et al., 2018). The Matecho is an open source IRD tool based on the Ifremer's Movies 3D software (Trenkel et al., 2009). The bottom line correction and the removal of multiple echoes in the water column were performed manually. To get the same vertical resolution than the CTDO, acoustic raw Sv (dB re 1 m^{-1}, MacLennan et al., 2002) data were averaged on 1m layers for each ping. A high-resolution echo-integration on 1 ping per 1m high cell was applied on Sv samples with a threshold at -100 dB, providing data at the same vertical resolution than the CTDO. Near-surface noise was avoided by excluding the signal from the transducer to a fixed distance of 10 m.

In this study, we used the mean volume backscattering strength (MVBS, in dB re m^{-1}) of the 100 pings after the end of each cast of CTDO to avoid the possible noise from the descent and ascent of the CTDO and to ensure working on genuine day and night data since most CTDO were mostly performed during twilight periods.

For the visualization of the relative acoustic data at each station, a Red Green Blue (RGB) composite image was generated and superimposed to the vertical profiles of the different physico-chemical parameters (Fig. 2). To construct a RGB image, we rescaled the Sv from each frequency (38, 70, and 120 kHz) on a linear scale, which has 255 intervals from the minimal value (-100 dB) to the maximal one (-50 dB). This visualisation technique is increasingly used (Annasawmy et al., 2020; Ariza et al., under review), as it allows quick visualization of the relative contribution of each frequency through the dominance of colour: red (38 kHz); green (70 kHz); blue (120 kHz). The colour thus indicates the dominant frequency, while the brightness is an approximation of the average backscatter intensity of the three frequencies combined. For example, swimbladder-bearing fish that are expected to have high acoustic response and a flat frequency distribution would form white bright patches in RGB echograms.

Figure 2. Example of RGB plot of 100 pings long echogram for station 06 of ABRAÇOS 2 (WBCS, day, position in Figure 1b) and corresponding vertical environmental profiles from CTDO and ADCP data (solid white lines), as well as the mean Sv over the 100 pings (MVBS) at 38 (red solid line), 70 (green solid line) and 120 (blue solid line) kHz.

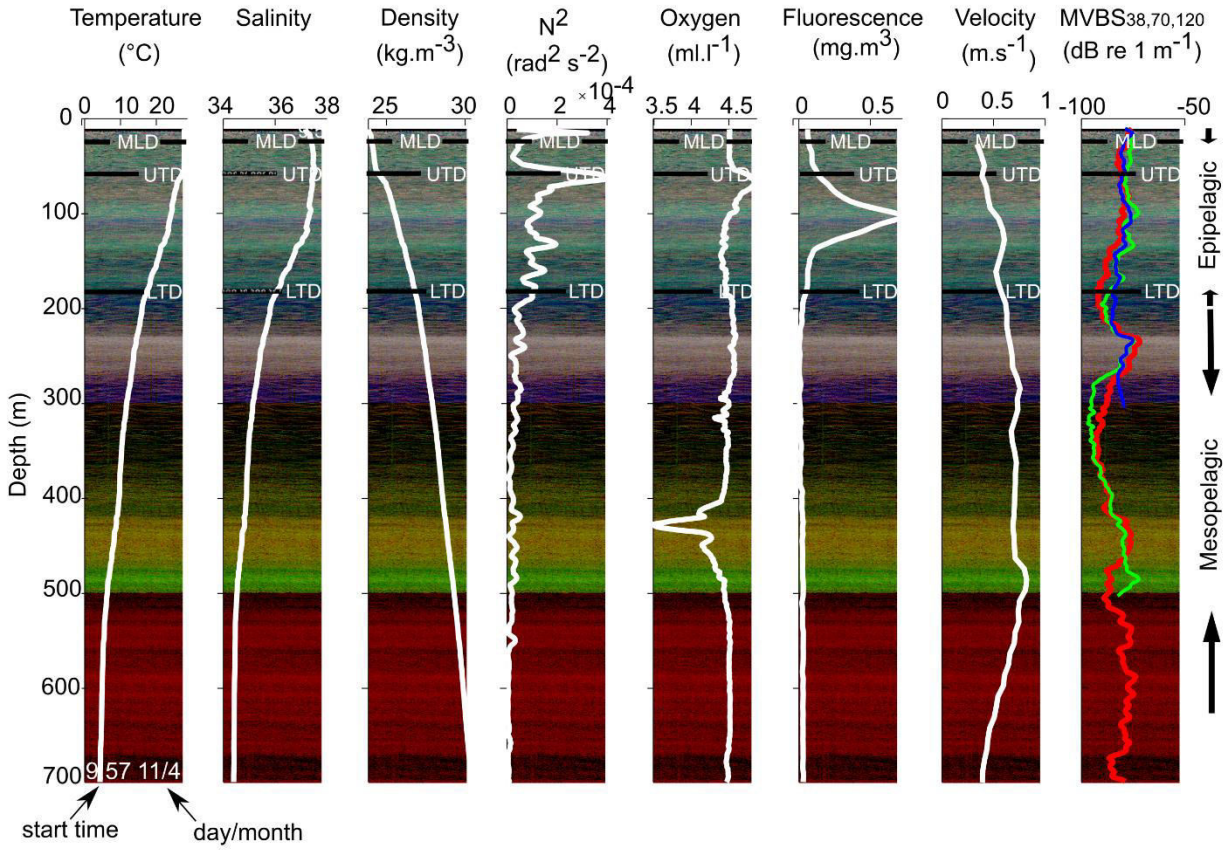

Source: Personal collection.

2.2.Data analysis

2.2.1 Oceanscape

First, we aim at describing the 'oceanscape' i.e., the vertical features of the environmental factors (currents, current shear, stratification, oxygen concentration and fluorescence) for each hydrodynamic system (WBCS and SECS) according to the season (spring and fall). In a given hydrodynamic system, to statistically test for seasonal differences in the vertical profiles of each environmental parameter, we used a functional data analysis approach (Ramsay, 2006). This branch of statistics works on functions instead of discretized vectors to analyse the distribution and variability of data over the physical dimension in which it is measured, depth in our case. Discrete

data profiles were transformed into curve using a B-spline basis of degree 3 as smoothing (Boor, 2001). B-splines are the most common system approach choices for non-periodic functional data. The number of basis functions (K) and the penalized parameter of the basis, which imply the degree of smoothing of the curve, was selected by the Generalized Cross-Validation (`GCV`) analysis performed using the R packages "`fda`", respecting the balance between smoothing and the desired scale of variability (Febrero-Bande and Fuente, 2012). Therefore, before performing `GCV`, we defined a range of potential K by performing a smoothing test for each variable individually according to different K. All environmental factors showed good smoothing within the range of 41- 42 basis (K). While the acoustic profiles fitted best with 44 basis. The higher the number of K-functions, the more complexity is preserved. Once this was done, we used, specifically the functional analysis of variance (fANOVA), which uses all the information of each mean functional curve to test for differences based on the shape and spatial (along with depth) variability of the curves (Assunção et al., 2020; Cuevas et al., 2004; Ramsay, 2006).

2.2.2. Echoscape

To describe the vertical structure of the acoustic backscattering signal we divided the data in two zones: (i) the epipelagic zone, here defined from 20 to 200 m; and (ii) the mesopelagic zone from 200 to 650 m. This choice division was made considering the thermohaline structure in the region with most thermohaline gradients restricted to the first 200 m (Assunção et al., 2020) and the scrutinising of the most recurrent SSLs in RGB echograms (Fig. 2).

To compare the shape of the acoustic profiles at each frequency for each hydrodynamic system and layer according to the season and the diel cycle we applied the same fANOVA approach as for the environmental profiles.

2.2.3. Cross-correlations

To study the potential relationships between the profiles of fluorescence and the stratification as well as between the acoustic profiles and each environmental factor (stratification, fluorescence, dissolved oxygen, and currents) along depth, we used the cross-correlations function (`CCF`, Brockwell and Davis, 1991). The `CCF` is helpful for identifying lags (h in metres) of the x (environmental factor) variable that might be useful predictors of y (MVBS in dB re 1 m^{-1}). In R, the `CCF` is defined as the set of sample correlations between x_{d+h} and y_d for h = 0, ±1, ±2, ±3, and

so on. For instance, a negative value for *h* is a correlation between the *x* variable at a depth before *d* and the *y* variable at depth *d*. The cross-correlation analyses were done for the epipelagic and mesopelagic zones, separately.

In addition, considering the different factors we explore (system, zone, season and diel period), addressing each frequency separately led to too many tests increasing the risk of stochastic results. We therefore decided to focus on the strongest acoustic response at each depth. For that purpose, we constructed a profile of maximum acoustic response (MVBSmax, in dB re m^{-1}) whatever the frequency. This MVBSmax was derived from the three frequency profiles (38, 70, and 120 kHz), in which for each depth we assumed the highest value among the analysed frequencies (supplementary material, Fig. S1).

Finally, for a comprehensive description of the structure of the acoustic profiles, we defined the SSLs as the depth range where MVBSmax exceeded the overall median value calculated in each layer, in a given hydrodynamic system, season and diel period (Table 1; Fig. 6).

Table 1 – Median MVBSmax values (in dB re m^{-1}) adopted as the threshold to define the SSLs in each season, and for each zone (EP – epipelagic; MP – mesopelagic). These thresholds correspond to the averages of the values of the stations sampled according to each condition (season, diel period, and system).

		Western boundary current system - WBCS		South equatorial current system - SECS	
		Day	Night	Day	Night
Spring 2015	EP	-82	-77	-81	-78
	MP	-87	-88	-82	-82
Fall 2017	EP	-82	-76	-80	-79
	MP	-86	-86	-83	-83

Source: Personal collection.

3. Results

3.1. Oceanscape

In the WBCS, 3 out of 5 parameters presented significant seasonal differences (Fig. 4). The undercurrent, NBUC, was significantly more intense in spring than fall, in particular between 140 - 320 m (Fig. 4a). Current shear (S^2, Fig. 4b) was also significantly more intense in spring, especially in the range 40 - 140 m (thermocline/pycnocline) and 320 - 450 m (no shearing observed

in fall). Even if the overall difference was not significant (p=0.07), the stratification (N^2, Fig. 4c) was lower in spring than in fall. The entire water column in the WBCS region was well oxygenated whatever the season (mean values between 3.8 and 5 $ml.l^{-1}$), with, however, a layer with moderate deoxygenation (~3.2 $ml.l^{-1}$) at 300 - 500 m in fall (Fig. 4d). Finally, the deep chlorophyll maximum (DCM, Fig. 4e) was shallower (~90 vs. 100 m) and slightly stronger in spring than in fall.

In the South Equatorial Current system (SECS, see Fig. 1), which encompasses the oceanic islands and seamounts, all parameters varied significantly according to the season (Fig. 4). Westward surface current (cSEC, up to 100 m) was stronger in fall, while the eastward subsurface current (SEUC) was much more intense in spring (Fig. 4f). Current shear (S^2, Fig. 4g) between the surface and subsurface opposing currents was stronger and deeper in spring (~90 - 120 m) than in fall (~40 - 60 m). The thermocline/pycnocline (maximum stratification (N^2) layer, Fig. 4h) was also deeper (~90 vs. 50 m) in spring than in fall. Unlike the WBCS, the SECS presented a deoxygenated layer below the thermocline/pycnocline with lower values in fall (2.4 $ml.l^{-1}$) than spring (2.8 $ml.l^{-1}$) (Fig. 4i). Finally, the DCM (Fig. 4j) was deeper (~100 vs. 50 m) and stronger in spring than in fall.

Figure 3. Mean profiles of the resulting currents (a, f), shear (b, g), stratification (c, h), dissolved oxygen concentration (d, i), and fluorescence with the deep chlorophyll maximum – DCM (e, j) in spring 2015 (black) and fall 2017 (pink) in the western boundary current system (WBCS, a-e) and the south equatorial current system (SECS, f-j). The range of ADCP data (current and shear) was limited to 500 m deep. Shaded areas show the standard deviation of the profiles.

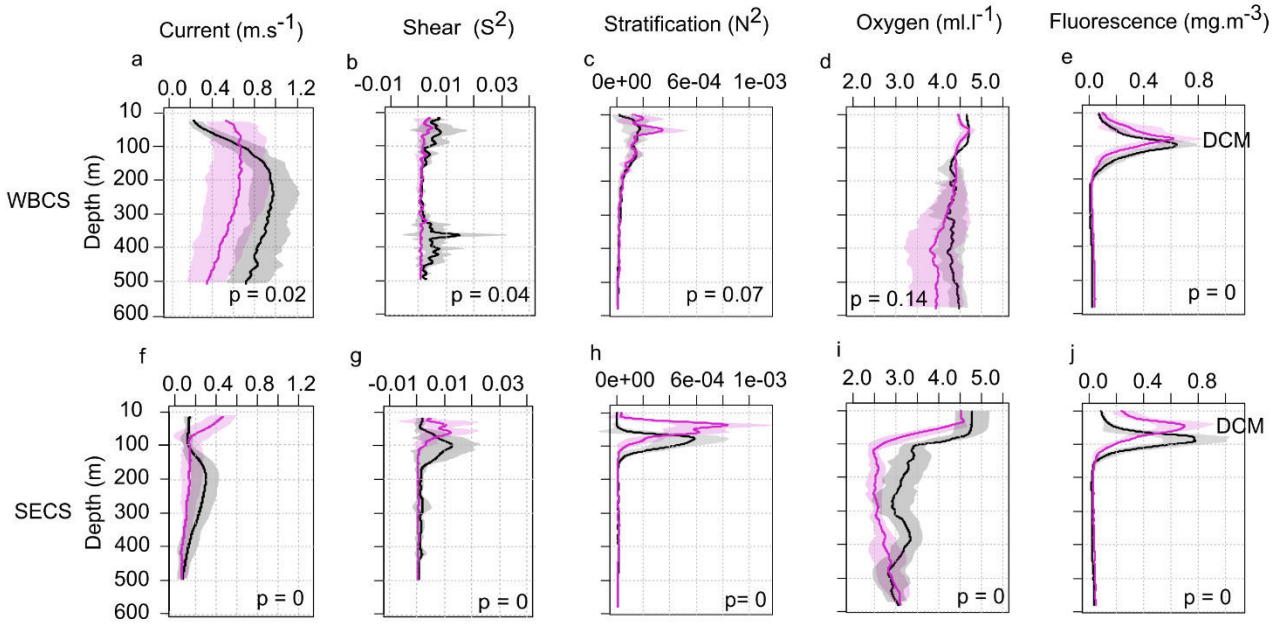

Source: Personal collection.

3.2. Epipelagic echoscape

In the epipelagic zone, the SSLs were omnipresent throughout the SWTA, varying in intensity (proxy of biomass) and vertically according to the diel period, season (spring and fall), and the hydrodynamic system (WBCS and SECS). The MVBS was stronger at night than day, whatever the system, the season, and the frequency (Fig. 5; Supplementary material Fig. S1). In the WBCS, the MVBS decreased with depth whatever the diel period, season, and frequency but at 70 and 120 kHz at night in fall, when it presented a maximum at ~70 m. In the SECS, the pattern was different since the MVBS always peaked in sub-surface (at ~70 - 120 m) but at 70 and 120 kHz at day in fall, when it decreased with depth (Fig. 5).

The profiles of maximum acoustic response (MVBSmax) allow better observing how the dominant frequency-response varies according to the depth (Fig. 6). In spring, the dominant frequency in the epipelagic zone was 38 kHz whatever the diel period and system. The only exception was in the SECS at day with the MVBS120 dominating below 150 m deep. In fall, the feature was different with an overall dominance of MVBS70 in the WBCS at both diel periods. In the SECS MVBS38 dominated at night while at day we observed an alternation between MVBS38 and MVBS70 in the first 160 m, then the dominance of MVBS120.

Figure 4. Functional ANOVA between the mean acoustic profiles (MVBS dB re m^{-1}, continuous line) with the shaded areas indicating standard deviation by frequency (38, 70 and 120 kHz), diel period (day; night), hydrodynamical system (WBCS; SECS), and season: spring 2015 (black lines) and fall 2017 (coloured lines).

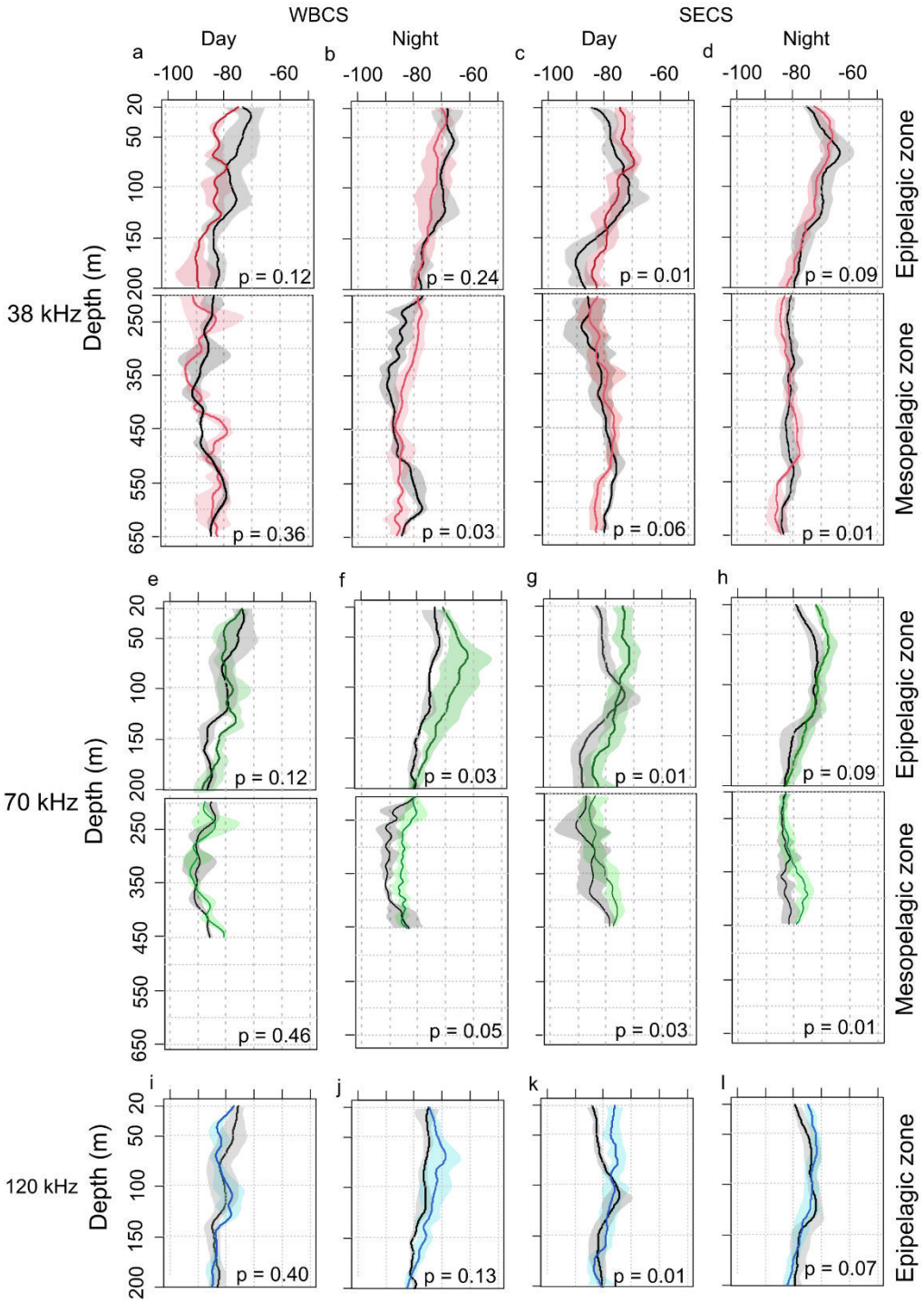

Source: Personal collection.

Figure 5. Mean MVBSmax (dB re m^{-1}) acoustic profiles in spring 2015 (continuous lines) and fall 2017 (dashed lines) for each diel period (day; night) and hydrodynamical system (WBSC; SECS). The respective profiles are composed of the frequency (38 kHz in red, 70 kHz in green and 120 kHz in blue) providing the highest backscatter at each depth. The compositions are divided between the epipelagic zone (above 200 m) and the mesopelagic zone where only 38 and 70 kHz are available. The vertical lines (solid line- spring; dotted line - fall) are the MVBSmax value adopted as thresholds to define the sound scattering layers (SSL; see Table 1). Main SSLs are highlighted in light grey.

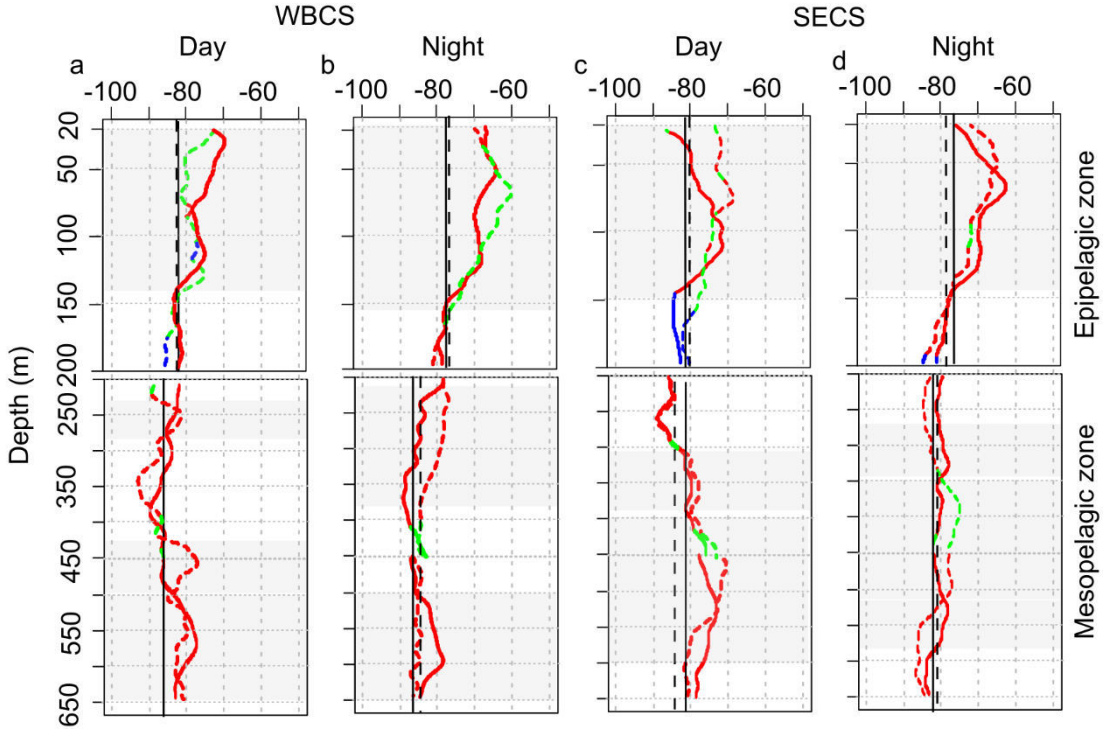

Source: Personal collection.

3.3. Cross-correlations in the epipelagic layer

In all cases, fluorescence was positively correlated with stratification. The strength of the correlation was higher in the SECS (above 0.9) than in the WBCS (~0.4 to 0.7). In the SECS, the DCM matched (lag ~0) the maximum stratification (Fig. 7d). In the WBCS, however, the DCM was ~30 to 40 m below the maximum stratification (supplementary material Fig. S3), except in spring at day when the relationship was weaker (Fig. 7a).

As for the DCM, in all cases the MVBSmax was positively correlated to the maximum stratification but to a greater extent in the SECS (Fig. 7b and f). In the WBCS (Fig. 7b), the peaks of MVBSmax matched the depth of maximum stratification except in spring at day when it was ~20 m below. In

the SECS (supplementary material Fig. S4) in fall, both peaks matched at day but the peak of MVBSmax was above the maximum stratification at night.

Epipelagic SSLs were generally positively correlated with high oxygen concentrations (Fig. 7d and h), except in fall 2017 at day, when the correlation was close to null. In the WBCS (Fig. 7d), no lag was observed between the SSLs and the maximum oxygen concentration but in spring at day when SSLs were shallower (~18 m) than maximum oxygen concentrations. In the SECS (Fig. 7h), on the other hand, SSLs were deeper than oxygen maxima, with mean lags ranging between 5 and 20 m.

Figure 6. Boxplots of the epipelagic cross-correlations (Cross-Cor.), the lag of maximum correlation, between the (a, e) stratification (N^2) and fluorescence (mg. m^{-3}), and also between the MVBSmax profiles and the (b, f) stratification, (c, g) fluorescence (mg. m^3) and (d, h) oxygen ($ml.l^{-1}$). All analyses are presented separately for each hydrodynamic system (WBCS; SECS), in relation to seasons (spring: black; fall: pink) and diel period (day: white; night: grey).

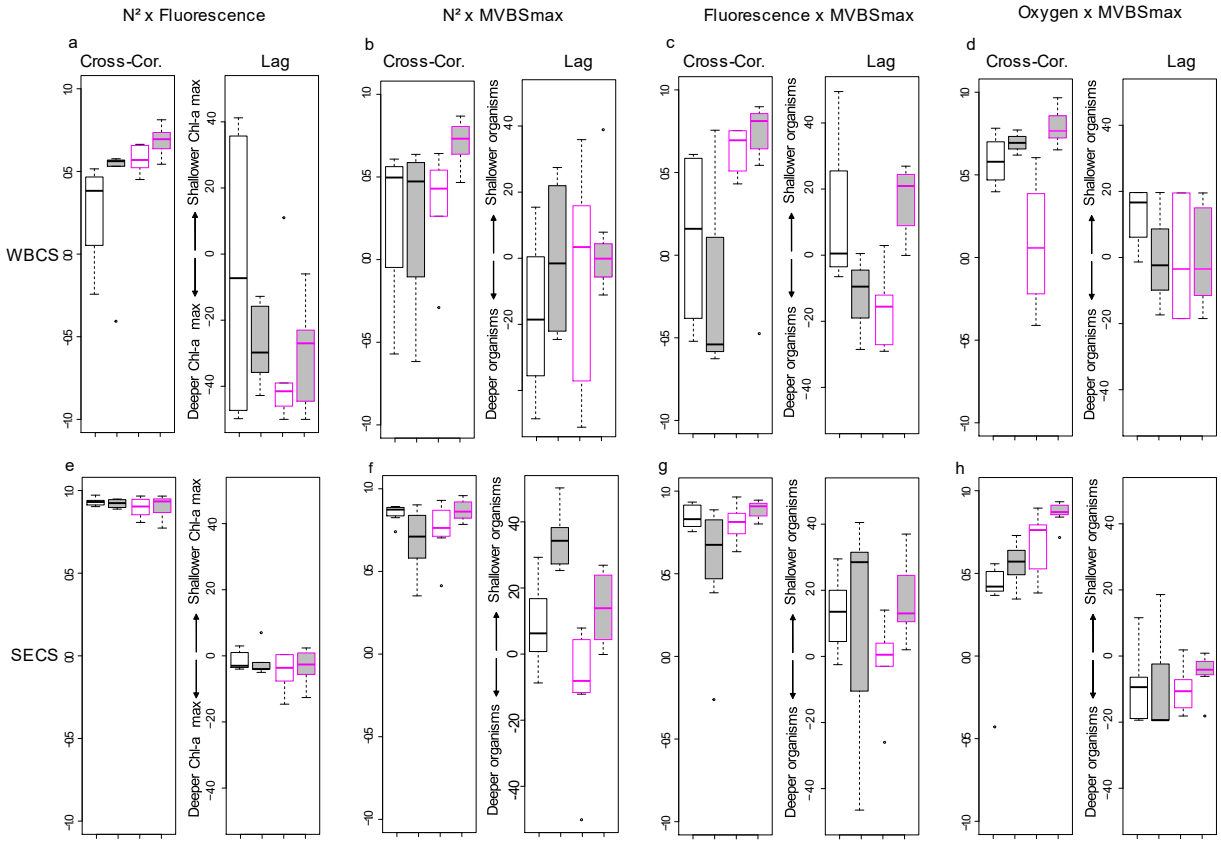

Source: Personal collection.

3.4. Mesopelagic echoscape

The mesopelagic zone was characterized by the presence of SSLs in most stations (45 out of 54) (Fig. 5). SSLs number, thickness, vertical position, and intensity varied according to the hydrodynamic system, the season, and the diel period. In the WBCS, at day, MVBS profiles at 38 and 70 kHz did not vary significantly according to the season (Fig. 5a, e). The main feature was the presence of SSL at ~250 m and below 450 m. At night (Fig. 5b, f), the seasonal difference was significant with higher intensity and more preeminent SSL in the range 200 - 350 m in fall. In spring, however, as during the day, a conspicuous SSL was present in the range 500 - 650 m depth. In the SECS (Fig. 5c, d, g, h), the vertical MVBS at 38 and 70 kHz varied significantly according to the season except at 38 kHz at day ($p=0.06$). At day, the main pattern was the presence of an SSL in the range 400 - 500 m. At night, no strong patterns were observed at 38 kHz while a pronounced SSL was observed at 70 kHz in fall in the range 350 - 450 m.

3.5. Cross-correlation in the mesopelagic layer

In the mesopelagic zone, the cross-correlation between MVBSmax and oxygen concentration varied according to the season, the system, and the diel period (Fig. 8a, d). In the WBCS, where less impact of oxygen concentration is expected, a weak positive correlation with no lag was observed in spring. In the fall, the patterns were less clear with a lower correlation associated with a high variability. In the SECS, clear negative correlation was observed (mean upward lag ranging from ~0 to 20 m), except in spring at night.

The cross-correlation between MVBSmax and resulting currents varied according to the season, the system and the diel period (Fig. 8b, e). In the WBCS, no correlation was observed except at night in fall when a strong positive correlation with no lag was observed. In the SECS positive and negative correlation with no lag were observed in spring and fall, respectively.

Finally, the cross-correlation between MVBSmax and the stratification also varied according to the season, the system and the diel period (Fig. 8c, f). In the WBCS, a positive correlation with lag close to 0 was observed in all cases except in fall at day when it was negative. In the SECS, a positive correlation was observed in all cases except in spring 2015 at day when no correlation was observed. The lag was close to 0 except in fall at day when it was negative (~20 m).

Figure 7. Boxplots of the mesopelagic cross-correlations (Cross-Cor.), and the lag of maximum correlation between the MVBSmax profiles and the (a, d) oxygen (ml.l-1), (b, e) current (m.s-1), and (c, f) stratification (N^2). All analyses are presented separately for each hydrodynamical system (WBCS; SECS), in relation to seasons (spring - black; fall - pink) and diel period (day - white; night - grey).

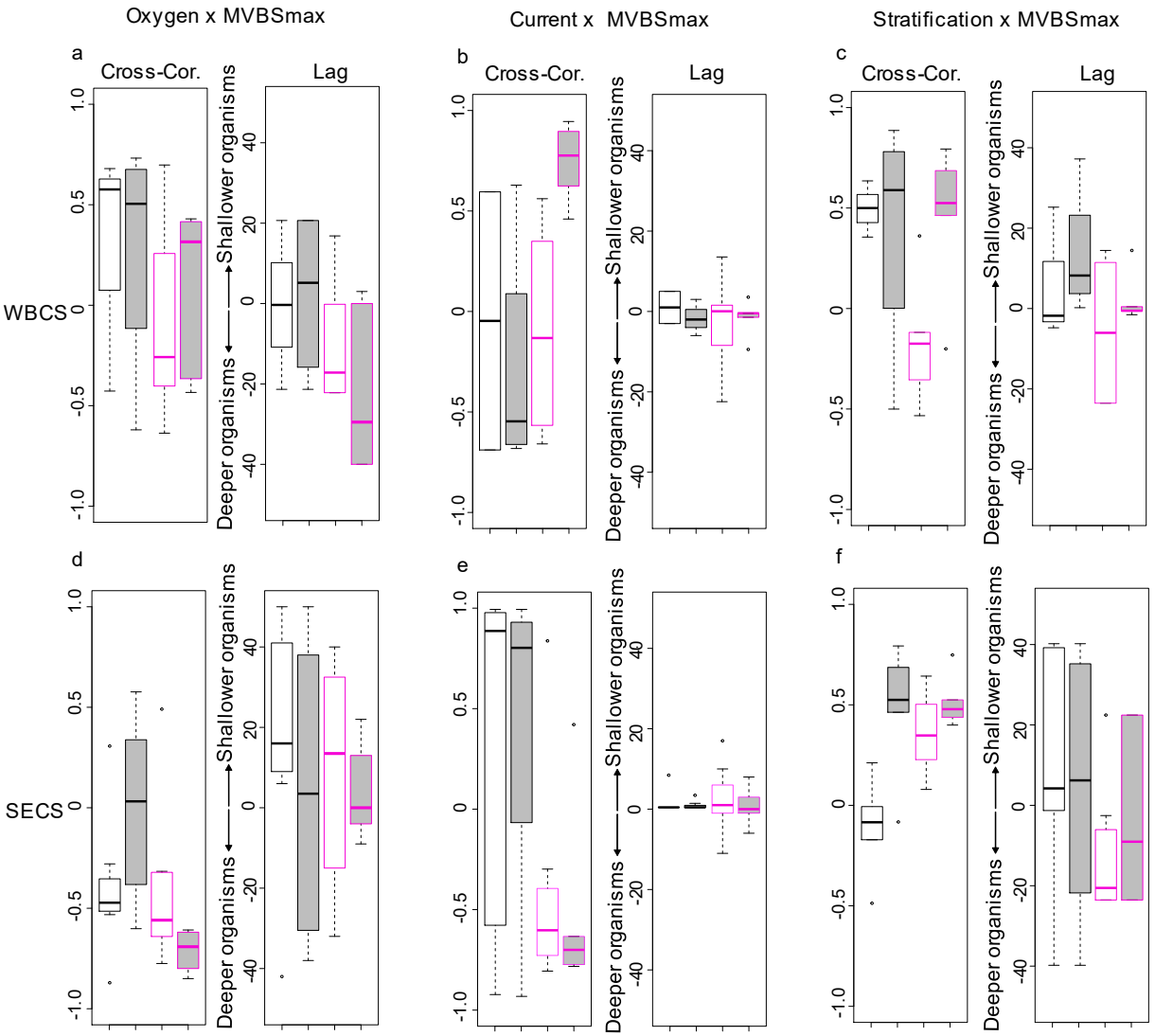

Source: Personal collection.

4. Discussion

In this work, we used multi-frequency acoustic, CTDO and ADCP data to describe the fine-scale vertical relationships between environmental factors and the vertical distribution of the acoustic backscattering energy in two seasons and two hydrodynamic systems of the SWTA according to the diel cycle. To synthesise the results, we build conceptual models relating the more robust

relationships between the characteristics of SSLs and the potential environmental drivers (Fig. 9). We propose four scenarios for both the WBCS (Fig. 8a - d) and the SECS (Fig. 8e - h), referring to seasons (spring and fall) and diel periods (day and night). The models are based on the results obtained from this work, complemented by information from the biotic database of the ABRACOS surveys (Supplementary material Table S1 and S2).

Epipelagic SSLs were omnipresent at both diel periods and seasons. Besides the expected increase in acoustic backscatter at night due to the DVM, the patterns of SSLs vertical distribution varied according to each oceanscape (Fig. 8). Here, even if the upper and mesopelagic zones are connected through the DVM (e.g., Bianchi and Mislan, 2016; Legendre, 1981; Radenac et al., 2010; Receveur et al., 2020), we discuss the main results considering the epipelagic and mesopelagic zones separately.

Figure 8. Schematic representation of the main environmental factors impacting the vertical distribution of the sound scattering layers (SSLs) in spring 2015 and fall 2017 in the western boundary current system (WBCS) and the south equatorial current system (SECS) according to the diel periods. The mean MVBSmax acoustic profiles (in dB re m^{-1}) composed by the frequency (38 kHz in red, 70 kHz in green and 120 kHz in blue) presenting the highest backscatter at each depth are presented in each panel. In these profiles, the depth sections with thick lines correspond to identified SSLs. The epipelagic zone (above 200 m) and the mesopelagic zone where only 38 and 70 kHz are available are considered separately.

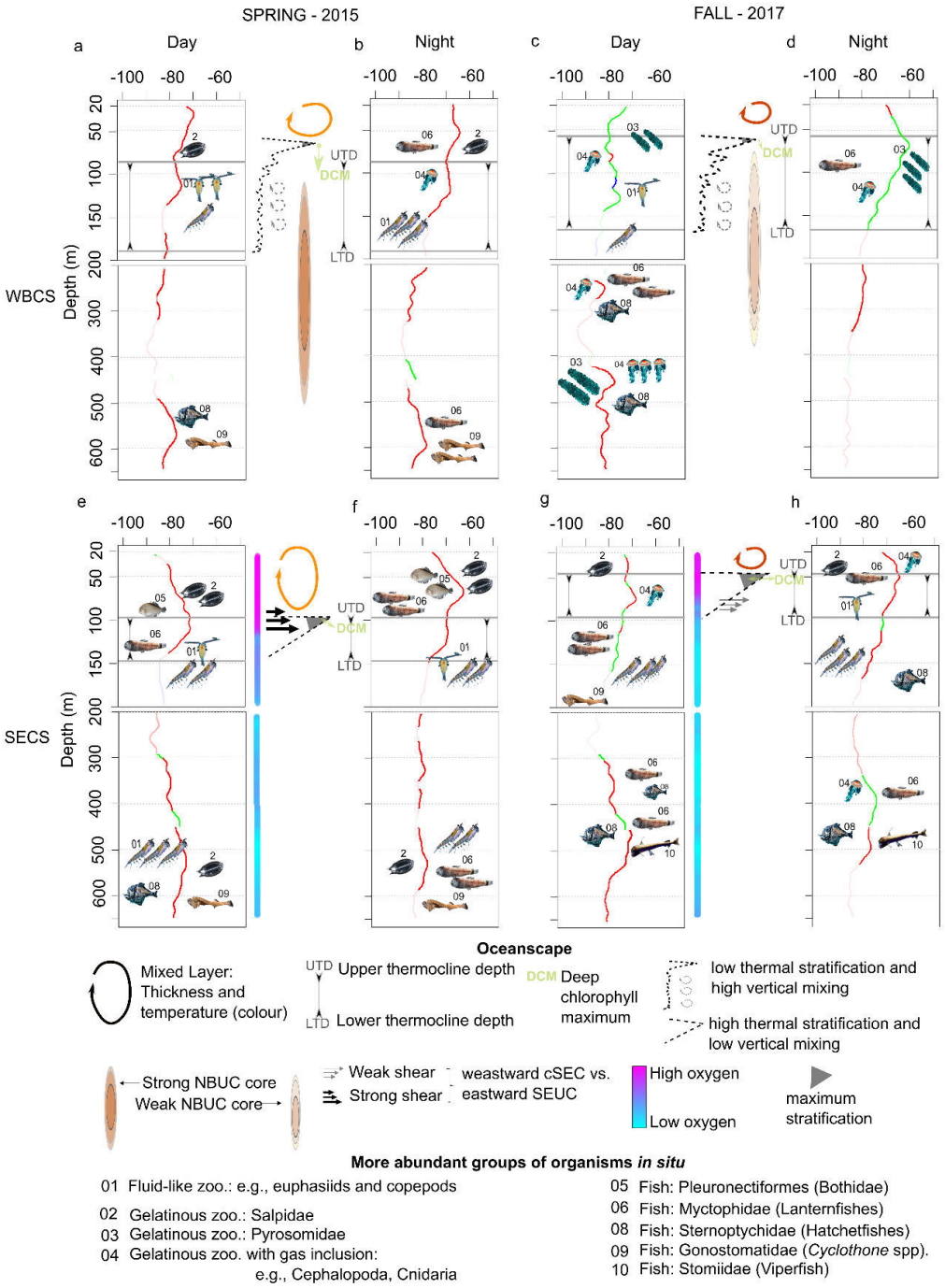

Source: Personal collection.

4.1. Epipelagic layer

According to the bottom-up structuring framework, physics drive the primary productivity, which in turn drive the distribution of organisms both horizontally and vertically (e.g., Benoit-Bird and Au, 2003; Bertrand et al., 2014). To better understand such relationships, the first step consists in evaluating the relationships between the thermohaline stratification (N^2) and the primary productivity (fluorescence).

In all cases, DCM were positively correlated with the stratification (Fig. 7). However, the form of the relationships was modulated by the thermohaline structure among hydrodynamic system. In the SECS where strong, thin, and stable thermocline occur, the correlation was remarkably high, and the DCM perfectly matched (no lag) the peak of maximum stratification. Interestingly, this relationship was not affected by the strong seasonal modulation of the thermohaline structure with a thermocline ~40 m deeper in spring than in fall (Figs. 4 and 8e - h). On the contrary, in the WBCS where the stratification is feebler, and associated with a less pronounced and thicker thermocline, the correlation between the DCM and the peak of maximum stratification was weak (Fig. 7b; Fig. 9a, b). In addition, in this case, the DCM was ~10 to 40 m deeper than the layer of maximum stratification. In this system, the maximum stratification was generally not associated with the thermocline (supplementary material Fig. S3). Instead, it was associated with the base of the mixed layer where a barrier layer occurs (Assunção et al., 2020). Therefore, the DCM was more associated with the thermocline (Fig. 8a,d), which lies deeper than the pycnocline, in coherence with the nutricline (Farias et al., submitted). Thus, whatever the season or the diel period, the vertical lag between the depth of maximum stratification and the DCM was more related to the spatial modulations of the barrier layer thickness (see Assunção et al., 2020), than to other parameters.

In a second step, we examine the relationships between the epipelagic SSLs (MVBSmax) and both the stratification and the DCM.

In the SECS, where the correlation between the peak of stratification and the DCM was extremely high and not lagged, it was not possible to fully discriminate the impact between these two parameters (Fig. 7f, g). In both cases, we observed a strong correlation with no strong seasonal difference but a clear diel effect in the lag (Figs. 7f, g and 8e - h). During the day, the lag between stratification and MVBSmax was ~0 while at night the peak of MVBSmax was ~10 to 40 m above

the one of stratification. According to Benoit-Bird et al. (2010), DCM were as likely to be found above the zooplankton layer as below, indicating that the factors driving those relationships likely vary amongst systems and species. However, Benoit-Bird and McManus (2014) observed that acoustic fine layers of zooplankton were always ~1 m deeper than the DCM. They attributed this negative offset to specific physical forcing or to a foraging tactic with predators attacking from beneath. At both diel periods and seasons, the MVBSmax was overall dominated by the 38 kHz (Fig. 8e - h), likely hiding fluid-like layers. If looking at the 120 kHz peaks (Fig. 5), likely more representative crustacean zooplankton, peaks occurred below the one of thermocline (Fig. 8e - h). In spring (Fig. 8e, f), a conspicuous layer of salps dominated the mixed layer (supplementary material Tables 1, 2). Salps, have higher per-individual filtration rates of all the marine zooplankton filter feeders, being able to feed on pico- and nanophytoplankton (Dadon-Pilosof et al., 2019; Harbison, 1992; Sutherland et al., 2014) that are less dependent on nutrients and can flourish above the DCM. In addition, many gelatinous are susceptible to degradation of colonies (mainly the small) when exposed to regions of high vertical shear stress, as observed in the SECS spring 2015, tending to avoid regions like these, which may further explain their position within the mixed layer (Graham et al., 2001). In the SECS, the reduction of the acoustic energy with depth also matches the profiles of dissolved oxygen (Fig. 5; Fig. 8e - h), organisms may indeed avoid the subsurface layer where dissolved oxygen can be close to 2 $ml.l^{-1}$, a value that is known to restrict the distribution of many organisms (e.g., Vaquer-Sunyer and Duarte, 2008). Interestingly the positive correlation with dissolved oxygen was higher at night than at day. This could be related to the 'oxygen debt' some migrant organisms need to pay (see Alegre et al., 2014) as discussed later.

In the WBCS, epipelagic SSLs were more correlated to the stratification than the fluorescence in spring (Fig. 7b, c). The SSL was below the peak of stratification during the day and at a similar depth at night (Fig. 8a, b). On the contrary, in the fall, the correlation was stronger with the DCM with a negative lag at day and a positive lag at night (Fig. 8c, d). In both cases, the trend in lag matched the diel vertical migration of organisms. In fall 2017 (Fig. 9c, d), pyrosomes (*Pyrosoma atlanticum*; supplementary material Tables 1, 2) were highly abundant in the WBCS. They peaked at 70 kHz that was the dominant frequency in the surface layer in fall. Pyrosomes diel migrate and mostly forage on phytoplankton (Décima et al., 2019; Perissinotto et al., 2007), which may explain the stronger association with fluorescence than stratification in fall. Another factor in this region is the presence of the NBUC with a core with a high current velocity (>0.6 $m.s^{-1}$) below ~100 m

(Dossa et al., 2021). Organisms may avoid this layer to limit horizontal advection (Fig. 8a-d). On the contrary, the oxygen concentration is likely not a driving factor in the region since the entire water column is well oxygenated.

4.2. Mesopelagic layer

As in most oceanic regions, several (until three during the day) SSLs were observed in the mesopelagic zone of the SWTA. This acoustic set-up depends both on the hydrodynamical and biological features of a given ocean region (Andreeva et al., 2000; Lampert, 1989; Peña et al., 2014). Here, we examine the overall relationships between the mesopelagic SSLs (MVBSmax) and the oxygen concentration, stratification, and current. Unfortunately, we do not rely on robust estimation of light profiles to examine this correlation.

We observed both migrant and non-migrant SSLs. These last one was mostly observed in the range ~500-650 m (Fig. 8). Invertebrates such as euphausiids, salps, pyrosomes and siphonophores, that are abundant in the area (supplementary material Tables 1, 2) are known to perform DVM (e.g., Brierley, 2014; Godø et al., 2009; Neitzel et al., 2021). Three mesopelagic fish families dominated in the area: Gonostomatidae, Myctophidae, Sternoptychidae (Eduardo et al., 2020b, 2020a, under review; Olivar et al., 2017). These animals exhibit a variety of diel patterns ranging from species performing large vertical migrations (e.g., most of hatchetfishes and lanternfishes; Eduardo et al., 2020a, under review) to non-migrant species that remains full-time in mesopelagic zones, in particular at ~500-650 m (e.g., *Cyclotone spp*; Eduardo et al., under review; Olivar et al., 2017). Additionally, various fish species (e.g., lanternfishes) performing DVM present an asynchronous pattern of migration, where the entire population does not respond synchronously to diel variation and only the hungry portion of the population migrates in a given day (Eduardo et al., 2020a; 2020b).

In the SECS (Fig. 8e-h), subsurface waters were overall less oxygenated ($2 > O2 < 3.8$ ml.l^{-1}), including specific layers presenting the lower concentration, due to the influence of eastern waters brought by cSEC (Sprintall and Tomczak, 1993). Except in spring 2015 at night, SSLs were negatively correlated to dissolved oxygen concentration. Further, our results shows that the correlation was stronger in fall 2017 when the water column was less oxygenated. Some fish species have indeed been observed in oxygen minimum at day (e.g., *Argyropelecus affinis* and *A.*

sladani) or all along the diel cycle (e.g., *Argyropelecus hemigymmus*) (Eduardo et al., 2020a, 2020b). Organisms may concentrate in search for cold and less oxygenated waters as a predator refuge and/or saving energy strategy (Bertrand et al., 2006; Dunlap, 1968; Sutton, 2013). In addition, organism's respiration may locally deplete the oxygen concentration creating a local minimum (Bianchi et al., 2013). These results agree with several previous studies (e.g., Bianchi et al., 2013; Cade and Benoit-Bird, 2015; Dunlap, 1968; Klevjer et al., 2016) showing that deep SSLs are generally collocated in layers of low oxygen concentrations. However, at night, normoxic condition are needed by migrant organisms in surface to supply the oxygen demand that was not achieved in less oxygenated water at greater depth (Alegre et al., 2014; Seibel, 2011).

In the WBCS, the water column is well oxygenated due to the influence of the central water from the southwestern subtropical South Atlantic, that is carried to the region by the NBUC (Stramma et al., 2003, 2005). Therefore, oxygen concentration is likely not a driving factor in the WBCS. Except at day, in fall when there is a noticeable drop in peak oxygen ~ 400 -500 m. Some gelatinous zooplankton (e.g., cnidaria and Pyrossomidae, supplementary material Table 1) and fish species have indeed been observed this layer at day (e.g., *Argyropelecus aculeatus*, Eduardo et al., 2020a). However, in this system, the presence of the strong NBUC may impact organism distribution. The NBUC core was thicker and stronger in spring 2015 than in fall 2017 (Dossa et al., 2021). The vertical distribution of SSLs in the WBCS (Fig. 5) suggests that in spring, when the NBUC is most intense, most organisms seem to avoid the core of the NBUC and distribute deeper (below 500 m) than in fall (300-400 m) when the NBUC is weaker (Fig. 8a-d). SSLs were then associated with layers of strong stratification (more in fall at day), indicating that this factor is likely a key driver not only in the thermocline layer but also below. A similar impact of stratification was observed in the SECS. In this system, an interesting pattern was observed concerning the current with a positive correlation in spring when the undercurrent, SEUC, was stronger and the opposite in fall. This pattern is particularly related to SSLs around 300 m over the influence of the core of the undercurrent SEUC, which were also correlated to low oxygen concentrations. However, these SSLs showed slightly higher densities in the fall than in the spring.

5. Conclusion

By investigating the fine-scale relationships between the vertical biophysical factors on the vertical structuring of acoustic biomass in the SWTA we show that fluorescence, oxygen, current and

stratification are important drivers, but that their relative importance depends on the area, the depth range and the diel cycle. In the epipelagic layer, the strongest acoustic responses were associated with depths of greatest stability (highest stratification), even in the WBCS during spring, where the fluorescence peaks were deeper than the peak of stratifications. In fact, the degree of correlation with the depth of higher stratification and the deep chlorophyll maximum depends not only on the local hydrodynamics (currents and presence of barrier layers) but also on the dominant organisms. Dissolved oxygen does not seem to be a key factor in the WBCS where the entire water column is well oxygenated while it seems to be a driver in the SECS where lower oxygen concentration occurs in sub-surface. Finally, our results suggest that organisms seem to avoid the currents core, especially the strong NBUC. However, future works are needed to better understand the role of currents on the vertical distribution of organisms.

Acknowledgements

We acknowledge the French oceanographic fleet for funding the at-sea survey and the officers and crew of the R/V Antea for their contribution to the success of the operations during the ABRACOS cruises. The *Conselho Nacional de Desenvolvimento Científico e Tecnológico* (CNPq) by supported through a PhD scholarship grant for Assunção, Ramilla V. This work is a contribution to the International Joint Laboratory TAPIOCA (www.tapioca.ird.fr), CAPES/COFECUB program (88881.142689/2017-01), PADDLE project (funding by the European Union's Horizon 2020 research and innovation programme - grant agreement No. 73427).

References

Abbott, M. R., Denman, K. L., Powell, T. M., Richerson, P. J., Richards, R. C. and Goldman, C. R.: Mixing and the dynamics of the deep chlorophyll maximum in Lake Tahoe1, Limnol. Oceanogr., 29(4), 862–878, doi:10.4319/lo.1984.29.4.0862, 1984.

Agustí, S. and Duarte, C. M.: Phytoplankton chlorophyll a distribution and water column stability in the central Atlantic Ocean, Oceanol. Acta, 22(2), 193–203, doi:10.1016/S0399-1784(99)80045-0, 1999.

Aksnes, D. L., Røstad, A., Kaartvedt, S., Martinez, U., Duarte, C. M. and Irigoien, X.: Light penetration structures the deep acoustic scattering layers in the global ocean, Sci. Adv., 3(5), e1602468, doi:10.1126/sciadv.1602468, 2017.

Alegre, A., Ménard, F., Tafur, R., Espinoza, P., Argüelles, J., Maehara, V., Flores, O., Simier, M. and Bertrand, A.: Comprehensive Model of Jumbo Squid Dosidicus gigas Trophic Ecology in the

Northern Humboldt Current System, edited by A. C. Tsikliras, PLoS One, 9(1), e85919, doi:10.1371/journal.pone.0085919, 2014.

Algar, A. C., Kharouba, H. M., Young, E. R. and Kerr, J. T.: Predicting the future of species diversity: macroecological theory, climate change, and direct tests of alternative forecasting methods, Ecography (Cop.)., 32(1), 22–33, doi:10.1111/j.1600-0587.2009.05832.x, 2009.

Alldredge, A., Cowles, T., MacIntyre S, S., Rines, J., Donaghay, P., Greenlaw, C., Holliday, D., Dekshenieks, M., Sullivan, J. and Zaneveld, J.: Occurrence and mechanisms of formation of a dramatic thin layer of marine snow in a shallow Pacific fjord, Mar. Ecol. Prog. Ser., 233(May), 1–12, doi:10.3354/meps233001, 2002.

Andreeva, I. B., Galybin, N. N. and Tarasov, N. N.: Vertical structure of the acoustic characteristics of deep scattering layers in the ocean, Akust. Zhurnal, 46(5), 581–587, 2000.

Annasawmy, P., Ternon, J.-F., Lebourges-Dhaussy, A., Roudaut, G., Cotel, P., Herbette, S., Ménard, F. and Marsac, F.: Micronekton distribution as influenced by mesoscale eddies, Madagascar shelf and shallow seamounts in the south-western Indian Ocean: an acoustic approach, Deep Sea Res. Part II Top. Stud. Oceanogr., 176, 104812, doi:10.1016/j.dsr2.2020.104812, 2020.

Assunção, R. V., Silva, A. C. da, Roy, A., Bourlès, B., Silva, C. H. S., Ternon, J.-F., Araújo, M. and Bertrand, A.: 3D characterisation of the thermohaline structure in the southwestern tropical Atlantic derived from functional data analysis of in situ profiles, Prog. Oceanogr., 187(December 2019), 102399, doi:10.1016/j.pocean.2020.102399, 2020.

Bandara, K., Varpe, Ø., Wijewardene, L., Tverberg, V. and Eiane, K.: Two hundred years of zooplankton vertical migration research, Biol. Rev., brv.12715, doi:10.1111/brv.12715, 2021.

Benoit-Bird, K. J. and Lawson, G. L.: Ecological Insights from Pelagic Habitats Acquired Using Active Acoustic Techniques, Ann. Rev. Mar. Sci., 8(1), 463–490, doi:10.1146/annurev-marine-122414-034001, 2016.

Benoit-Bird, K. J. and McManus, M. A.: A critical time window for organismal interactions in a pelagic ecosystem, PLoS One, 9(5), doi:10.1371/journal.pone.0097763, 2014.

Benoit-Bird, K. J., Moline, M. A., Waluk, C. M. and Robbins, I. C.: Integrated measurements of acoustical and optical thin layers I: Vertical scales of association, Cont. Shelf Res., 30(1), 17–28, doi:10.1016/j.csr.2009.08.001, 2010.

Berge, Jø., Cottier, F., Varpe, Ø., Renaud, P. E., Falk-Petersen, S., Kwasniewski, S., Griffiths, C., Søreide, J. E., Johnsen, G., Aubert, A., Bjærke, O., Hovinen, J., Jung-Madsen, S., Tveit, M. and Majaneva, S.: Arctic complexity: a case study on diel vertical migration of zooplankton, J. Plankton Res., 36(5), 1279–1297, doi:10.1093/plankt/fbu059, 2014.

Bertrand, A.: ABRACOS cruise, RV Antea, , doi:10.17600/15005600, 2015.

Bertrand, A.: ABRACOS 2 cruise, RV Antea, , doi:10.17600/17004100, 2017.

Bertrand, A., Barbieri, M., Gerlotto, F., Leiva, F. and Córdova, J.: Determinism and plasticity of fish schooling behaviour as exemplified by the South Pacific jack mackerel Trachurus murphyi, Mar. Ecol. Prog. Ser., 311, 145–156, doi:10.3354/meps311145, 2006.

Bertrand, A., Grados, D., Colas, F., Bertrand, S., Capet, X., Chaigneau, A., Vargas, G., Mousseigne, A. and Fablet, R.: Broad impacts of fine-scale dynamics on seascape structure from zooplankton to seabirds, Nat. Commun., 5(May), doi:10.1038/ncomms6239, 2014.

Bianchi, D. and Mislan, K. A. S.: Global patterns of diel vertical migration times and velocities from acoustic data, Limnol. Oceanogr., 61(1), 353–364, doi:10.1002/lno.10219, 2016.

Bianchi, D., Galbraith, E. D., Carozza, D. A., Mislan, K. A. S. and Stock, C. A.: Intensification of open-ocean oxygen depletion by vertically migrating animals, Nat. Geosci., 6(7), 545–548, doi:10.1038/ngeo1837, 2013.

Boor, C. De: A practical guide to splines, Springer Handbooks Comput. Stat., 302, 2001.

Le Borgne, R., Allain, V., Griffiths, S. P., Matear, R. J., Mckinnon, A. D., Richardson, A. J. and Young, J. W.: Vulnerability of open ocean food webs in the tropical Pacific to climate change, in Ecological Geography of the Sea., pp. 189–250., 2011.

Boswell, K. M., D'Elia, M., Johnston, M. W., Mohan, J. A., Warren, J. D., Wells, R. J. D. and Sutton, T. T.: Oceanographic Structure and Light Levels Drive Patterns of Sound Scattering Layers in a Low-Latitude Oceanic System, Front. Mar. Sci., 7, 51, doi:10.3389/fmars.2020.00051, 2020.

Brierley, A. S.: Diel vertical migration, Curr. Biol., 24(22), R1074–R1076, doi:10.1016/j.cub.2014.08.054, 2014.

Brockwell, P. J. and Davis, R. A.: Time Series: Theory and Methods, 2nd ed., Springer New York, New York, NY., 1991.

Cade, D. E. and Benoit-Bird, K. J.: Depths, migration rates and environmental associations of acoustic scattering layers in the Gulf of California, Deep Sea Res. Part I Oceanogr. Res. Pap., 102, 78–89, doi:10.1016/j.dsr.2015.05.001, 2015.

Cheng, W., Chiang, J. C. H. and Zhang, D.: Atlantic meridional overturning circulation (AMOC) in CMIP5 Models: RCP and historical simulations, J. Clim., 26(18), 7187–7197, doi:10.1175/JCLI-D-12-00496.1, 2013.

Cuevas, A., Febrero, M. and Fraiman, R.: An anova test for functional data, Comput. Stat. Data Anal., 47(1), 111–122, doi:10.1016/J.CSDA.2003.10.021, 2004.

Cullen, J. J.: The deep chlorophyll maximum: comparing vertical profiles of chlorophyll a., Can. J. Fish. Aquat. Sci., 39(5), 791–803, doi:10.1139/f82-108, 1982.

Cullen, J. J.: Subsurface Chlorophyll Maximum Layers: Enduring Enigma or Mystery Solved?, Ann. Rev. Mar. Sci., 7(1), 207–239, doi:10.1146/annurev-marine-010213-135111, 2015.

Dadon-Pilosof, A., Lombard, F., Genin, A., Sutherland, K. R. and Yahel, G.: Prey taxonomy rather than size determines salp diets, Limnol. Oceanogr., 64(5), 1996–2010, doi:10.1002/lno.11165, 2019.

Décima, M., Stukel, M. R., López-López, L. and Landry, M. R.: The unique ecological role of pyrosomes in the Eastern Tropical Pacific, Limnol. Oceanogr., 64(2), 728–743, doi:10.1002/lno.11071, 2019.

Diogoul, N., Brehmer, P., Perrot, Y., Tiedemann, M., Thiam, A., El Ayoubi, S., Mouget, A., Migayrou, C., Sadio, O. and Sarré, A.: Fine-scale vertical structure of sound-scattering layers over an east border upwelling system and its relationship to pelagic habitat characteristics, Ocean Sci., 16(1), 65–81, doi:10.5194/os-16-65-2020, 2020.

Dossa, A. N., Silva, A. C. da, Chaigneau, A., Eldin, G., Araújo, M. and Bertrand, A.: Near-surface western boundary circulation off Northeast Brazil, Prog. Oceanogr., 190, 102475, doi:10.1016/j.pocean.2020.102475, 2021.

Dunlap, C. R.: An ecological reconnaissance of the deep scattering layers in the eastern tropical Pacific, United States Naval Postgraduate school., 1968.

Durham, W. M. and Stocker, R.: Thin Phytoplankton Layers: Characteristics, Mechanisms, and Consequences, Ann. Rev. Mar. Sci., 4(1), 177–207, doi:10.1146/annurev-marine-120710-100957, 2012.

Eduardo, L. N., Bertrand, A., Mincarone, M. M., Santos, L. V., Frédou, T., Assunção, R. V., Silva, A. C. da, Ménard, F., Schwamborn, R., Le Loc'h, F. and Lucena-Frédou, F.: Hatchetfishes (Stomiiformes: Sternoptychidae) biodiversity, trophic ecology, vertical niche partitioning and functional roles in the western Tropical Atlantic, Prog. Oceanogr., 187, 102389, doi:10.1016/j.pocean.2020.102389, 2020a.

Eduardo, L. N., Lucena-Frédou, F., Mincarone, M. M., Soares, A., Le Loc'h, F., Frédou, T., Ménard, F. and Bertrand, A.: Trophic ecology, habitat, and migratory behaviour of the viperfish Chauliodus sloani reveal a key mesopelagic player, Sci. Rep., 10(1), 20996, doi:10.1038/s41598-020-77222-8, 2020b.

Fasham, M. J. R., Platt, T., Irwin, B. and Jones, K.: Factors affecting the spatial pattern of the deep chlorophyll maximum in the region of the Azores front, Prog. Oceanogr., 14(C), 129–165, doi:10.1016/0079-6611(85)90009-6, 1985.

Febrero-Bande, M. and Fuente, M. O. de la: Statistical Computing in Functional Data Analysis: The R Package fda.usc, J. Stat. Softw., 51(4), 1–28, doi:10.18637/jss.v051.i04, 2012.

Fennell, S. and Rose, G.: Oceanographic influences on Deep Scattering Layers across the North Atlantic, Deep Sea Res. Part I Oceanogr. Res. Pap., 105, 132–141, doi:10.1016/j.dsr.2015.09.002, 2015.

Figueiredo, G. G. A. A. de, Schwamborn, R., Bertrand, A., Munaron, J.-M. and Le Loc'h, F.: Body size and stable isotope composition of zooplankton in the western tropical Atlantic, J. Mar. Syst., 212, 103449, doi:10.1016/j.jmarsys.2020.103449, 2020.

Folt, C. L. and Burns, C. W.: Biological drivers of zooplankton patchiness, Trends Ecol. Evol., 14(8), 300–305, doi:10.1016/S0169-5347(99)01616-X, 1999.

Foltz, G. R., Brandt, P., Richter, I., Rodríguez-Fonseca, B., Hernandez, F., Dengler, M., Rodrigues, R. R., Schmidt, J. O., Yu, L., Lefevre, N., Da Cunha, L. C., McPhaden, M. J., Araújo, M., Karstensen, J., Hahn, J., Martín-Rey, M., Patricola, C. M., Poli, P., Zuidema, P., Hummels, R., Perez, R. C., Hatje, V., Lübbecke, J. F., Polo, I., Lumpkin, R., Bourlès, B., Asuquo, F. E., Lehodey, P., Conchon, A., Chang, P., Dandin, P., Schmid, C., Sutton, A., Giordani, H., Xue, Y., Illig, S., Losada, T., Grodsky, S. A., Gasparin, F., Lee, T., Mohino, E., Nobre, P., Wanninkhof, R.,

Keenlyside, N., Garcon, V., Sánchez-Gómez, E., Nnamchi, H. C., Drévillon, M., Storto, A., Remy, E., Lazar, A., Speich, S., Goes, M., Dorrington, T., Johns, W. E., Moum, J. N., Robinson, C., Perruche, C., de Souza, R. B., Gaye, A. T., López-Parages, J., Monerie, P.-A., Castellanos, P., Benson, N. U., Hounkonnou, M. N., Duhá, J. T., Laxenaire, R. and Reul, N.: The Tropical Atlantic Observing System, Front. Mar. Sci., 6(May), doi:10.3389/fmars.2019.00206, 2019.

Foote, K. G., Knudsen, H. P. and Vestnes, G.: Calibration of acoustic instruments for fish density estimation: A practical guide, J. Acoust. Soc. Am., 83(2), 831–832, doi:10.1121/1.396131, 1987.

Godø, O. R., Patel, R. and Pedersen, G.: Diel migration and swimbladder resonance of small fish: Some implications for analyses of multifrequency echo data, ICES J. Mar. Sci., 66(6), 1143–1148, doi:10.1093/icesjms/fsp098, 2009.

Godø, O. R., Samuelsen, A., Macaulay, G. J., Patel, R., Hjøllo, S. S., Horne, J., Kaartvedt, S. and Johannessen, J. A.: Mesoscale Eddies Are Oases for Higher Trophic Marine Life, edited by Y. Ropert-Coudert, PLoS One, 7(1), e30161, doi:10.1371/journal.pone.0030161, 2012.

Graham, W. M., Pagès, F. and Hamner, W. M.: A physical context for gelatinous zooplankton aggregations: A review, in Hydrobiologia, vol. 451, pp. 199–212, Springer., 2001.

Herbland, A. and Voituriez, B.: Hydrological structure analysis for estimating the primary production in the tropical Atlantic Ocean, J. Mar. Res., 37(1), 87–101, 1979.

Holliday, D. V., Greenlaw, C. F. and Donaghay, P. L.: Acoustic scattering in the coastal ocean at Monterey Bay, CA, USA: Fine-scale vertical structures, Cont. Shelf Res., 30(1), 81–103, doi:10.1016/j.csr.2009.08.019, 2010.

Horota, R. K. and Wildner, W.: Caracterização geoquímica do arquipélago de Fernando de Noronha, 927–930, 2011.

Jiang, S., Dickey, T. D., Steinberg, D. K. and Madin, L. P.: Temporal variability of zooplankton biomass from ADCP backscatter time series data at the Bermuda Testbed Mooring site, Deep. Res. Part I Oceanogr. Res. Pap., 54(4), 608–636, doi:10.1016/j.dsr.2006.12.011, 2007.

Johnston, T. M. S. and Rudnick, D. L.: Observations of the Transition Layer, J. Phys. Oceanogr., 39(3), 780–797, doi:10.1175/2008JPO3824.1, 2009.

Keeling, R. F. and Gruber, N.: Ocean Deoxygenation in a Warming World, Annu. Rev. Mar. Sci, 2, 199–229, doi:10.1146/annurev.marine.010908.163855, 2010.

Kim, H.-J. and Miller, A. J.: Did the Thermocline Deepen in the California Current after the 1976/77 Climate Regime Shift?, J. Phys. Oceanogr., 37(6), 1733–1739, doi:10.1175/jpo3058.1, 2007.

Klevjer, T. A., Irigoien, X., Røstad, A., Fraile-Nuez, E., Benítez-Barrios, V. M. and Kaartvedt., S.: Large scale patterns in vertical distribution and behaviour of mesopelagic scattering layers, Sci. Rep., 6(1), 19873, doi:10.1038/srep19873, 2016.

Lampert, W.: The Adaptive Significance of Diel Vertical Migration of Zooplankton, Funct. Ecol., 3(1), 21, doi:10.2307/2389671, 1989.

Lavery, A. C., Wiebe, P. H., Stanton, T. K., Lawson, G. L., Benfield, M. C. and Copley, N.: Determining dominant scatterers of sound in mixed zooplankton populations, J. Acoust. Soc. Am., 122(6), 3304–3326, doi:10.1121/1.2793613, 2007.

Leach, T. H., Beisner, B. E., Carey, C. C., Pernica, P., Rose, K. C., Huot, Y., Brentrup, J. A., Domaizon, I., Grossart, H. P., Ibelings, B. W., Jacquet, S., Kelly, P. T., Rusak, J. A., Stockwell, J. D., Straile, D. and Verburg, P.: Patterns and drivers of deep chlorophyll maxima structure in 100 lakes: The relative importance of light and thermal stratification, Limnol. Oceanogr., 63(2), 628–646, doi:10.1002/lno.10656, 2018.

Lee, H., Cho, S., Kim, W. and Kang, D.: The diel vertical migration of the sound-scattering layer in the Yellow Sea Bottom Cold Water of the southeastern Yellow sea: focus on its relationship with a temperature structure, Acta Oceanol. Sin., 32(9), 44–49, doi:10.1007/s13131-013-0351-z, 2013.

Legendre, L.: Hydrodynamic Control of Marine Phytoplankton Production: The Paradox of Stability, in Elsevier Oceanography Series, vol. 32, pp. 191–207., 1981.

Lezama-Ochoa, A., Grados, D., Lebourges-Dhaussy, A., Irigoien, X., Chaigneau, A. and Bertrand, A.: Biological characteristics of the hydrological landscapes in the Bay of Biscay in spring 2009, Fish. Oceanogr., 24(1), 26–41, doi:10.1111/fog.12090, 2015.

Li, G., Cheng, L., Zhu, J., Trenberth, K. E., Mann, M. E. and Abraham, J. P.: Increasing ocean stratification over the past half-century, Nat. Clim. Chang., 10(12), 1116–1123, doi:10.1038/s41558-020-00918-2, 2020.

Liu, C., Köhl, A., Liu, Z., Wang, F. and Stammer, D.: Deep-reaching thermocline mixing in the equatorial pacific cold tongue, Nat. Commun., 7(May 2015), doi:10.1038/ncomms11576, 2016.

Liu, H. L. and Sun, S.: Diel vertical distribution and migration of a euphausiid Euphausia pacifica in the Southern Yellow Sea, Deep. Res. Part II Top. Stud. Oceanogr., 57(7–8), 594–605, doi:10.1016/j.dsr2.2009.10.009, 2010.

Maclennan, D. N., Fernandes, P. G. and Dalen, J.: A consistent approach to definitions and symbols in fisheries acoustics, ICES J. Mar. Sci., 59(2), 365–369, doi:10.1006/jmsc.2001.1158, 2002.

Margalef, R. and Margalef, R.: The Organization of Space, Oikos, 33(2), 152, doi:10.2307/3543992, 1979.

Mignot, A., Claustre, H., Uitz, J., Poteau, A., D'Ortenzio, F. and Xing, X.: Understanding the seasonal dynamics of phytoplankton biomass and the deep chlorophyll maximum in oligotrophic environments: A Bio-Argo float investigation, Global Biogeochem. Cycles, 28(8), 856–876, doi:10.1002/2013GB004781, 2014.

Mojica, K. D. A., van de Poll, W. H., Kehoe, M., Huisman, J., Timmermans, K. R., Buma, A. G. J., van der Woerd, H. J., Hahn-Woernle, L., Dijkstra, H. A. and Brussaard, C. P. D.: Phytoplankton community structure in relation to vertical stratification along a north-south gradient in the Northeast Atlantic Ocean, Limnol. Oceanogr., 60(5), 1498–1521, doi:10.1002/lno.10113, 2015.

Neitzel, P., Hosia, A., Piatkowski, U. and Hoving, H.-J.: Pelagic deep-sea fauna observed on video transects in the southern Norwegian Sea, Polar Biol., 44(5), 887–898, doi:10.1007/s00300-021-02840-5, 2021.

Netburn, A. N. and Anthony Koslow, J.: Dissolved oxygen as a constraint on daytime deep scattering layer depth in the southern California current ecosystem, Deep Sea Res. Part I Oceanogr. Res. Pap., 104, 149–158, doi:10.1016/j.dsr.2015.06.006, 2015.

Olivar, M. P., Hulley, P. A., Castellón, A., Emelianov, M., López, C., Tuset, V. M., Contreras, T. and Molí, B.: Mesopelagic fishes across the tropical and equatorial Atlantic: Biogeographical and vertical patterns, Prog. Oceanogr., 151, 116–137, doi:10.1016/j.pocean.2016.12.001, 2017.

Oschlies, A., Brandt, P., Stramma, L. and Schmidtko, S.: Drivers and mechanisms of ocean deoxygenation, Nat. Geosci., 11(7), 467–473, doi:10.1038/s41561-018-0152-2, 2018.

Peña, M., Olivar, M. P., Balbín, R., López-Jurado, J. L., Iglesias, M. and Miquel, J.: Acoustic detection of mesopelagic fishes in scattering layers of the Balearic Sea (western Mediterranean), edited by J. M. Jech, Can. J. Fish. Aquat. Sci., 71(8), 1186–1197, doi:10.1139/cjfas-2013-0331, 2014.

Perissinotto, R., Mayzaud, P., Nichols, P. and Labat, J.: Grazing by Pyrosoma atlanticum (Tunicata, Thaliacea) in the south Indian Ocean, Mar. Ecol. Prog. Ser., 330, 1–11, doi:10.3354/meps330001, 2007.

Perrot, Y., Brehmer, P., Habasque, J., Roudaut, G., Behagle, N., Sarré, A. and Lebourges-Dhaussy, A.: Matecho: An Open-Source Tool for Processing Fisheries Acoustics Data, Acoust. Aust., 46(2), 241–248, doi:10.1007/s40857-018-0135-x, 2018.

Prairie, J. C., Sutherland, K. R., Nickols, K. J. and Kaltenberg, A. M.: Biophysical interactions in the plankton: A cross-scale review, Limnol. Oceanogr. Fluids Environ., 2(1), 121–145, doi:10.1215/21573689-1964713, 2012.

Radenac, M. H., Plimpton, P. E., Lebourges-Dhaussy, A., Commien, L. and McPhaden, M. J.: Impact of environmental forcing on the acoustic backscattering strength in the equatorial Pacific: Diurnal, lunar, intraseasonal, and interannual variability, Deep. Res. Part I Oceanogr. Res. Pap., 57(10), 1314–1328, doi:10.1016/j.dsr.2010.06.004, 2010.

Ramsay, J. O.: Functional Data Analysis, in Encyclopedia of Statistical Sciences, vol. 2, pp. 675–678, John Wiley & Sons, Inc., Hoboken, NJ, USA., 2006.

Receveur, A., Menkes, C., Allain, V., Lebourges-Dhaussy, A., Nerini, D., Mangeas, M. and Ménard, F.: Seasonal and spatial variability in the vertical distribution of pelagic forage fauna in the Southwest Pacific, Deep Sea Res. Part II Top. Stud. Oceanogr., 175, 104655, doi:10.1016/j.dsr2.2019.104655, 2020.

De Robertis, A. and Higginbottom, I.: A post-processing technique to estimate the signal-to-noise ratio and remove echosounder background noise, ICES J. Mar. Sci., 64(6), 1282–1291, doi:10.1093/icesjms/fsm112, 2007.

Ryan, T. E., Downie, R. A., Kloser, R. J. and Keith, G.: Reducing bias due to noise and attenuation in open-ocean echo integration data, ICES J. Mar. Sci., 72(8), 2482–2493, doi:10.1093/icesjms/fsv121, 2015.

Sallée, J., Pellichero, V., Akhoudas, C., Pauthenet, E., Vignes, L., Schmidtko, S., Garabato, A. N., Sutherland, P. and Kuusela, M.: Summertime increases in upper-ocean stratification and mixed-layer depth, Nature, 591(7851), 592–598, doi:10.1038/s41586-021-03303-x, 2021.

Sameoto, D. D.: Distribution of Sound Scattering Layers Caused by Euphausiids and Their Relationship to Chlorophyll a Concentrations in the Gulf of St. Lawrence Estuary, J. Fish. Res. Board Canada, 33(4), 681–687, doi:10.1139/f76-084, 1976.

Seibel, B. A.: Critical oxygen levels and metabolic suppression in oceanic oxygen minimum zones, J. Exp. Biol., 214(2), 326–336, doi:10.1242/jeb.049171, 2011.

Silva, A. C. da, Chaigneau, A., Dossa, A. N., Eldin, G., Araújo, M. and Bertrand, A.: Surface circulation and vertical structure of upper ocean variability around Fernando de Noronha archipelago and Rocas atoll during spring 2015 and fall 2017, Front. Mar. Sci., doi:10.3389/fmars.2021.598101, 2021.

Simmonds, J. and MacLennan, D.: Fisheries Acoustics, edited by J. Simmonds and D. MacLennan, Blackwell Publishing Ltd, Oxford, UK., 2005.

Sutherland, G., Reverdin, G., Marié, L. and Ward, B.: Mixed and mixing layer depths in the ocean surface boundary layer under conditions of diurnal stratification, Geophys. Res. Lett., 41(23), 8469–8476, doi:10.1002/2014GL061939, 2014.

Sutton, T. T.: Vertical ecology of the pelagic ocean: classical patterns and new perspectives, J. Fish Biol., 83(6), 1508–1527, doi:10.1111/jfb.12263, 2013.

Tosetto, E. G., Bertrand, A., Neumann-Leitão, S., Costa da Silva, A. and Nogueira Júnior, M.: Spatial patterns in planktonic cnidarian distribution in the western boundary current system of the tropical South Atlantic Ocean, edited by X. Irigoien, J. Plankton Res., 43(2), 270–287, doi:10.1093/plankt/fbaa066, 2021.

Trenkel, V. M., Berger, L., Bourguignon, S., Doray, M., Fablet, R., Massé, J., Mazauric, V., Poncelet, C., Quemener, G., Scalabrin, C. and Villalobos, H.: Overview of recent progress in fisheries acoustics made by Ifremer with examples from the Bay of Biscay, Aquat. Living Resour., 22(4), 433–445, doi:10.1051/alr/2009027, 2009.

Vaquer-Sunyer, R. and Duarte, C. M.: Thresholds of hypoxia for marine biodiversity, Proc. Natl. Acad. Sci. U. S. A., 105(40), 15452–15457, doi:10.1073/pnas.0803833105, 2008.

Venancio, I. M., Shimizu, M. H., Santos, T. P., Lessa, D. O., Portilho-Ramos, R. C., Chiessi, C. M., Crivellari, S., Mulitza, S., Kuhnert, H., Tiedemann, R., Vahlenkamp, M., Bickert, T., Sampaio, G., Albuquerque, A. L. S., Veiga, S., Nobre, P. and Nobre, C.: Changes in surface hydrography at the western tropical Atlantic during the Younger Dryas, Glob. Planet. Change, 184, 103047, doi:10.1016/j.gloplacha.2019.103047, 2020.

Williams, B. and Grottoli, A. G.: Recent shoaling of the nutricline and thermocline in the western tropical Pacific, Geophys. Res. Lett., 37(22), n/a-n/a, doi:10.1029/2010GL044867, 2010.

Yao, F. and Hoteit, I.: Thermocline Regulated Seasonal Evolution of Surface Chlorophyll in the Gulf of Aden, edited by F. G. Schmitt, PLoS One, 10(3), e0119951, doi:10.1371/journal.pone.0119951, 2015.

Supplementary Material

Figure S1. Example of three MVBS acoustic profiles at 38, 70, and 120 kHz and MVBSmax resultant profile.

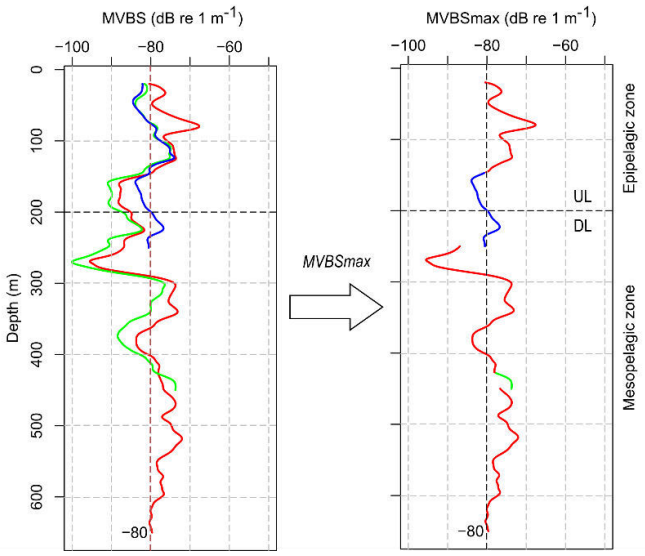

Source: Personal collection.

Figure S2. Mean MVBSmax acoustic profiles in spring 2015 and fall 2017 for each diel period (day – dark colours; night – shaded colours) and system. The respective profiles are composed of the frequency (38 kHz in red, 70 kHz in green and 120 kHz in blue) providing the highest backscatter at each depth. The compositions are divided between the epipelagic zone (above 200 m) and the mesopelagic zone where only 38 and 70 kHz are available.

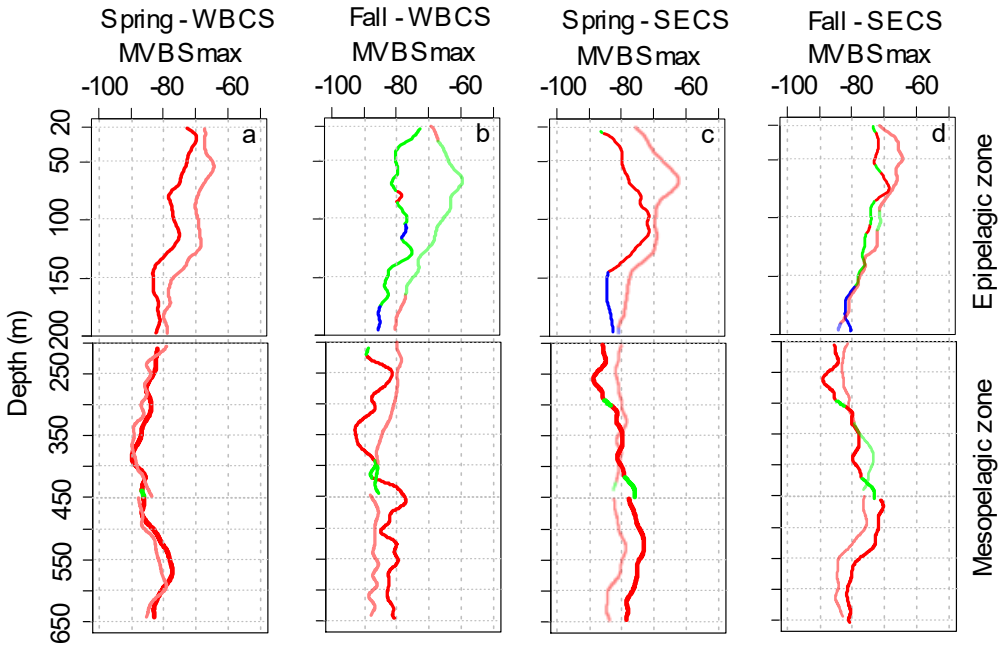

Source: Personal collection.

Figure S3. Example of a CTD profile from WBCS spring 2015 (ABRACOS I) with the representation of the thermohaline structure defined from temperature (θ), salinity, density (σ) and buoyancy frequency (N^2). With additional fluorescence profile, where the vertical lag between maximum stratification and deep chlorophyll maximum (DCM) can be clearly observed. MLD: mixed layer depth; UTD: upper thermocline depth; LTD/LPD: lower thermocline/pycnocline depth; BL: barrier layer.

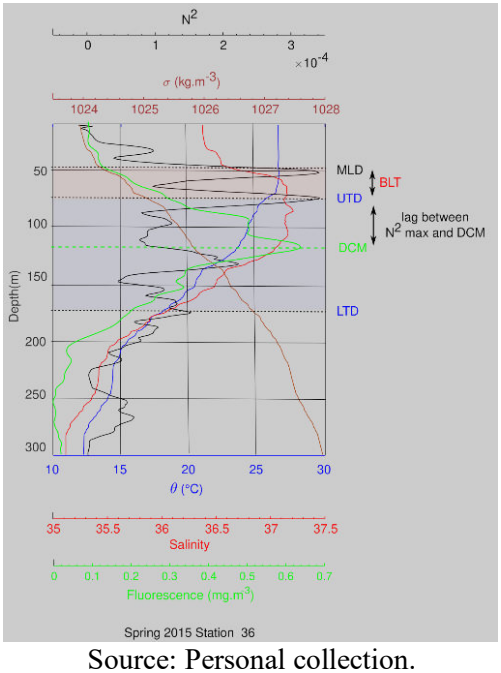

Source: Personal collection.

Figure S4. Examples of MVBS (dB re $1m^{-1}$) profiles at 38, 70 and 120 kHz from fall 2017 (ABRACOS 2) in the epipelagic zone of the SECS. In addition, stratification (N^2) and fluorescence profiles for the same stations. In highlight are superimposed the vertical lags between the stratification and the MVBSmax. MLD: mixed layer depth; UTD: upper thermocline depth; LTD/LPD: lower thermocline/pycnocline depth.

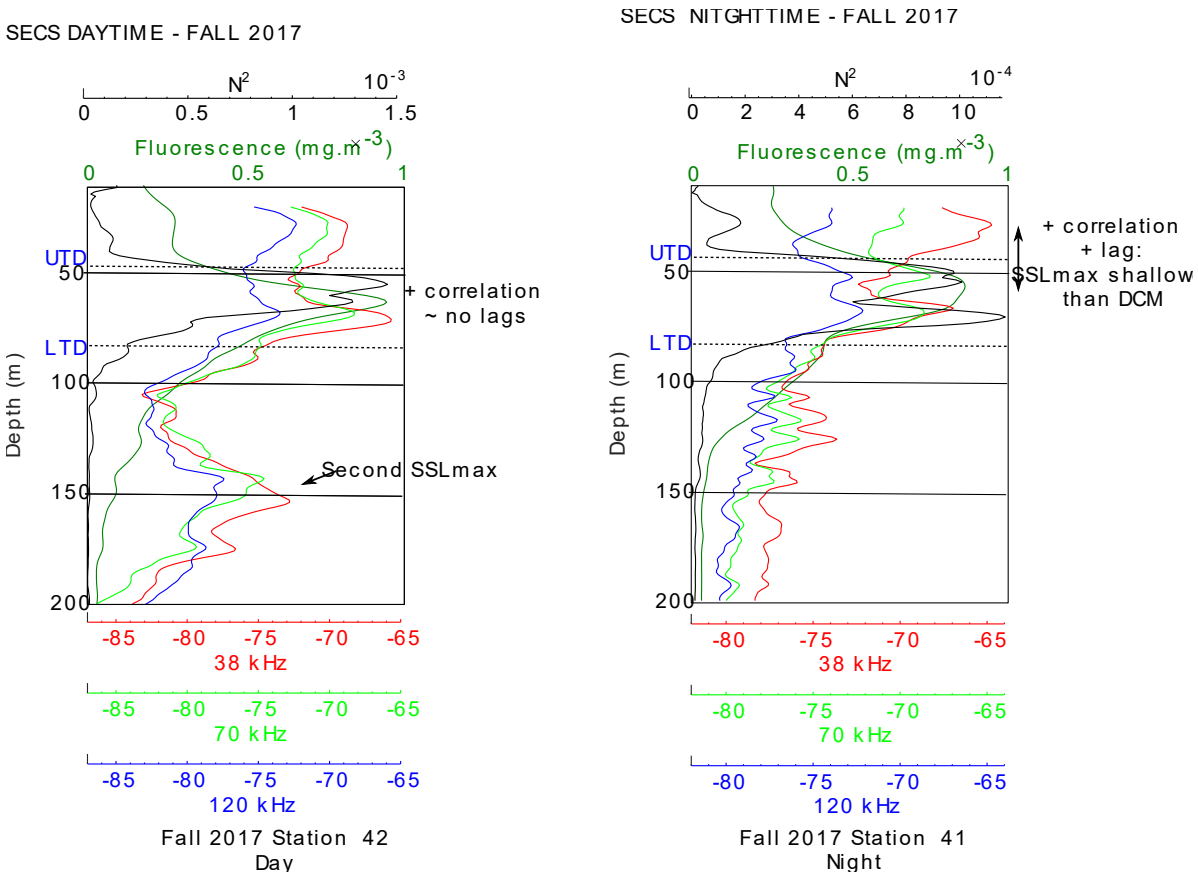

Source: Personal collection.

Table S1. Species collected from daytime stations, survey (S: ABRACOS 1; F: ABRACOS 2), number of specimens (N°), site (Western Boundary Current System – WBCS; South Equatorial Current System - SECS), depth range. This catalogue has been constructed, in summary, based on the ABRACOS project database. Please, for further information, see the references mentioned. Some papers are still in preparation or under revision and are not cited here.

REFERENCES	FILO	CLASS	ORDER	FAMILIES	N°	AREA	SEASON
			< 200 m				
	Mollusca	Cephalopoda			36	WBCS - **SECS**	S - **F**
Figueiredo, et al., 2020 doi: 10.1016/j.jmarsys.2020.103449	**Arthropoda (Crustacea)**	Malacostraca					
			Euphausiacea		192	WBCS - **SECS**	S
			Decapoda		22	**WBCS** - SECS	S
			Amphipoda		5	WBCS	S
Tosetto, et al., 2021 doi: 10.1093/plankt/fbaa066	**Cnidaria (BV)**				255.5	WBCS - **SECS**	S - **F**
	Chordata (Tunicata)	Thaliacea (bv)					
			Salpida	Salpidae	15	SECS	S
			Pyrosomida	Pyrosomatidae	279	WBCS	F
			Doliolida		26	SECS	F
	Chordata	Actinopterygii	Pleuronectiformes	Bothidae	180	SECS	S
			Myctophiformes	Myctophidae	548	WBCS - **SECS**	S - **F**
Eduardo, et al., 2020 doi: 10.1016/j.poceran.2020.102389			Stomiiformes	Sternoptychidae (Hatchetfishes)		**WBCS** - SECS	**S** - F

				Gonostomatidae	36	SECS	S - **F**
Eduardo, et al., 2020 doi: 10.1038/s41598-020-77222-8				Stomiidae			
Eduardo, et al., 2019 doi: 10.15560/15.6.965			Perciformes		37	SECS	S - **F**
Micarone, et al., 2019 doi: 10.1080/17451000.2019.1636281							
Micarone, et al., 2021 doi: 10.1080/17451000.2021.1891806			Teleostei		24	SECS	F
			200 - 300 m				
	Chordata	Actinopterygii	Myctophiformes Stomiiformes	Myctophidae	54	WBCS	F
Eduardo, et al., 2020 doi: 10.1016/j.pocean.2020.102389				Sternoptychidae (Hatchetfishes)	14	WBCS	F
Micarone, et al., 2021 doi: 10.1080/17451000.2021.1891806			Teleostei		27	WBCS	F
	Ctenophora (BV)				60	WBCS	F
	Jellyfish (BV)				143	WBCS	F
			300 - 400 m				

	Chordata	Actinopterygii	Myctophiformes	Myctophidae	56	SECS	F
Eduardo, et al., 2020 doi: 10.1016/j.poce an.2020.102389			Stomiiformes	Sternoptychidae (Hatchetfishes)	101	SECS	F
				Gonostomatidae	45	SECS	F
					5	SECS	F
					17	SECS	F
	Cndaria (colonies)			Siphonophera	5	SECS	F
			400 - 500 m				
	Cndaria (BV)				404	WBCS	F
	Ctenophora (BV)				23	WBCS	F
	Jellyfish (BV)				20	WBCS	F
	Chordata (Tunicata)	Thaliacea	Pyrosomida (BV)	Pyrossomidae	217	WBCS	F
	Arthropoda (Crustacea)	Malacostraca	Euphausiacea		7	WBCS	F
			Decapoda		32	WBCS	F
	Chordata	Actinopterygii	Stomiiformes	Gonostomatidae	39	WBCS	F
Eduardo, et al., 2020 doi: 10.1016/j.poce an.2020.102389				Sternoptychidae (Hatchetfishes)	5	WBCS	F
			500 - 600 m				

	Arthropoda (Crustacea)	Malacostraca	Euphausiacea		515	SECS	S
			Decapoda		21	WBCS	S
			Amphipoda		89	SECS	S
			Stomatopoda (Latreille, 1817)		54	SECS	S
	Cnidaria (BV)				85.5	WBCS - **SECS**	S
	Chordata (Tunicata)	Thaliacea	Pyrosomida	Pyrossomidae	5	WBCS	S
			Doliolida		10	SECS	S
			Salpida	Salpidae	50	SECS	S
	Chordata	Actinopterygii	Myctophiformes	Myctophidae	49	WBCS - **SECS**	S
Eduardo, et al., 2020 doi: 10.1016/j.poce an.2020.102389			Stomiiformes	Sternoptychidae (Hatchetfishes)	24	**WBCS** - SECS	S
				Gonostomatidae	54	**WBCS**	S
Eduardo, et al., 2019 doi: 10.15560/15.6. 965							
Micarone, et al., 2019 doi: 10.1080/174510 00.2019.163628 1			Perciformes	Decapterus (Carangidae)	22	WBCS	S

Table S2. Species collected from night stations, survey (S: ABRACOS 1; F: ABRACOS 2), number of specimens (N°), site (Western Boundary Current System – WBCS; South Equatorial Current System - SECS), depth range. This catalogue has been constructed, in summary, based on the ABRACOS project database. Please, for further information, see the references mentioned. Some papers are still in preparation or under revision and are not cited here.

REFERENCES	FILO	CLASS	ORDER	FAMILIES	N°	AREA	SEASON
			< 200 m				
	Mollusca	Cephalopoda	Oegopsida		113	**WBCS** - SECS	S - **F**
			Octopoda				
Figueiredo, et al., 2020 doi: 10.1016/j.jmarsys.2020.103449	**Arthropoda (Crustacea)**	Malacostraca					
			Euphausiacea		1004	**WBCS** - SECS	S
			Decapoda		83	SECS	S
			Stomatopoda		354	**WBCS** - SECS	S
Tosetto, et al., 2021 doi: 10.1093/plankt/fbaa066	**Cnidaria (BV)**				1333	WBCS	S-**F**
	Chordata (Tunicata)	Thaliacea (bv)	Salpida	Salpidae	287	WBCS - **SECS**	S-**F**
			Pyrosomida	Pyrosomatidae	1469	WBCS	S-**F**
			Doliolida		25		F
	Chordata	Actinopterygii	Pleuronectiformes	Bothidae	169	WBCS - **SECS**	S
			Myctophiformes	Myctophidae	82	WBCS - **SECS**	S

Eduardo, et al., 2020 doi: 10.1016/j.pocean.2020.102389			Stomiiformes	Sternoptychidae (Hatchetfishes)	43	WBCS - **SECS**	F
				Gonostomatidae			
Eduardo, et al., 2019 doi: 10.15560/15.6.965 Micarone, et al., 2019 doi: 10.1080/17451000.2019.1636281			Perciformes		89	**WBCS** - SECS	S - **F**
			Teleostei		82	WBCS	S - **F**
			Aulopiformes		358	WBCS - SECS	S-F
			Tetraodontiformes	Molidae	20	WBCS	S
			200 - 300 m				
			300 - 400 m				
			400 - 500 m				
	Mollusca	Cephalopoda	Oegopsida		14	SECS	F
	Chordata	Actinopterygii	Stomiiformes	Gonostomatidae	30	SECS	F
Eduardo, et al., 2020 doi: 10.1016/j.pocean.2020.102389				Sternoptychidae (Hatchetfishes)	55	SECS	F
			Beryciformes		15	SECS	F
			500 - 600 m				

	Arthropoda (Crustacea)	Malacostraca	Euphausiacea		337	SECS	S
			Decapoda		120	SECS	S
			Stomatopoda (Latreille, 1817)		6	SECS	S
	Cnidaria (BV)						
	Chordata	Actinopterygii	Myctophiformes	Myctophidae	220	SECS	**S** - F
Eduardo, et al., 2020 doi: 10.1016/j.pocean.2020.102389			Stomiiformes	Sternoptychidae (Hatchetfishes)	65	SECS	S - **F**
				Gonostomatidae	141	**WBCS** - SECS	**S** - F
					8	SECS	F
			Pleuronectiformes	Bothidae	211	SECS	S
			Labriformes		37	SECS	S
			Stephanoberyciformes	Melamphaidae	31	SECS	S

CHAPTER V:
GENERAL CONCLUSION

The thermohaline circulation of the southwest tropical Atlantic (SWTA) and associated inter-hemispheric transports of heat and salt has a prime impact on global climate (Bourlès et al., 1999b; Hounsou-gbo et al., 2015; Neto and Silva, 2013). This oligotrophic region is a key area for diagnosing variations of the Atlantic Meridional Overturning Circulation (Cheng et al., 2013; Venancio et al., 2020). Further, the thermohaline variability in the SWTA plays a driving role in the vertical structuring of pelagic habitats (e.g., Chaves et al., 2008; Sampaio de Souza et al., 2013). In order to fill information gaps on the thermohaline structure in the SWTA and to bring insights into the relationships of these physical processes with the distributions of acoustic backscattering energy (proxy for the distribution and biomass of organisms), this thesis was organised over three main scientific objectives addressed in chapters II, III and IV. For that, we took advantage of the two scientific surveys of the ABRACOS project performed in austral spring (Sep. – Oct.) 2015 and fall (Apr. – May) 2017, where for the first time in the SWTA, multifrequency acoustic data were acquired together with abiotic data (e.g., CTDO profiles and ADCP measurements). Here we propose to discuss the implications of the results of this thesis by placing them in a more general perspective.

Objective 1: Characterise the 3D thermohaline structure of the SWTA in austral spring and fall by the functional statistics approach. (Chapter II)

By applying a Functional Data Analysis (FDA) approach on CTD profiles from a variety of databases, we described the canonical states of the thermohaline structure of the upper ocean of the SWTA in austral spring and fall. By doing so, we have demonstrated that the application of an FDA approach on hydrographic data allows for a robust and precise characterisation and estimation of the ocean thermohaline 3D structure. The use of the FDA, which makes possible to explicitly take into account the vertical component of the studied processes, should therefore be encouraged in physical oceanography where the fields of application are wide. Using such approach, we pictured for the first time in the SWTA, three different and geographically separated

areas corresponding to different dynamical atmospheric and oceanic processes. Area 1 along the continental slope corresponds to a western boundary current system (WBCS) constituted by the north Brazil undercurrent and the north Brazil current. This WBCS is characterised by a thick thermocline and high frequency of occurrence of barrier layer (BL). Conversely, the area 2 located along the Fernando de Noronha chain corresponds to the south equatorial current system (SECS) formed by the central branch of south equatorial current and the south equatorial undercurrent. The SECS presents a narrow but well-marked thermocline and low BL frequency. The third Area between A1 and A2, behaves as a transition zone with still the presence of the water core of maximum salinity in subsurface, and therefore moderate to strong presence of BL (Assunção et al., 2020). The characteristics of these areas vary seasonally with deeper MLD and thermocline in spring 2015 than in fall 2017. Periods that we and Dossa et al. (2021) found to be representative of canonical spring and fall conditions in the area.

The upper circulation of the two main areas we defined here, the WBCS and the SECS, have recently been further detailed by Dossa et al. (2021) and Silva et al. (2021), respectively, corroborating our findings. Furthermore, the areas we defined have been used to test for spatial patterns in a variety of ecological studies. These works use our areas as references and reveal large-scale bottom-up control and structure from primary productivity to fish. Several works using this framework are still in preparation, but we can already provide some elements on the basis the work already published or under review.

First, the phytoplankton communities varied significantly according to the area and season (Farias et al., under review). In general, phytoplankton biomass is higher in SECS than in WBCS. Also, the seasonal cycle we describe has a strong influence with higher primary productivity in the fall when the thermocline and thus the nutricline are shallower. These seasonal differences are more conspicuous in the SECS.

Second, on line with the phytoplankton, the zooplankton varied in terms of community, abundance and body size (by isotopic composition) according to the area and season (Figueiredo et al., 2020; Tosetto et al., 2021). Figueiredo et al. (2020) depicted that the zooplankton was significantly smaller but more abundant in the WBCS than the SECS. Grazing effect on phytoplankton is therefore likely higher in the WBCS. Tosetto et al. (2021) also reported that planktonic cnidarian communities varied significantly among areas. Figueiredo et al. (2020) and Tosetto et al. (2021)

used data from ABRACOS 1 (spring 2015) only. However, unpublished results from the group showed that the zooplankton biomass was significantly higher in fall than spring, in accordance with the increased primary productivity.

The impact of the thermohaline structure is less evident on mesopelagic fish. Indeed, these fish, for instance lanternfish, distribute over large or even inter-oceanic provinces and have shown to be ubiquitous with respect to environmental conditions, leading to a weak horizontal segregation of the assemblage (Eduardo et al. under review).

However, when using multifrequency acoustic data, the mesopelagic communities as a whole varied significantly in terms of vertical structure and biomass according to the area and season (Ariza et al., under review). In addition, in line with primary and secondary productivity, the acoustic biomass was higher in fall than spring.

The work by Assunção et al. (2020) thus provided a heuristic basis for further investigating spatiotemporal patterns in a variety of ecological components, revealing a clear bottom-up control and structure. In addition, this work provides comprehensive information on the thermohaline structure (ML, BL and thermocline) in the SWTA. This is important information to estimate for instance, the mixed-layer heat budget variability in the western tropical Atlantic. Indeed, Nogueira Neto et al. (2018) reported that the largest errors in the heat storage calculations occurred in box 4 (the SWTA) probably due to the lack of information in the region.

Objective 2: Test if the variation of the thermohaline structure could be extracted from acoustic data in the SWTA. (Chapter III)

In chapter III, we examined the feasibility of extracting the thermohaline structure (mixed-layer depth, upper and lower thermocline) from echosounder data collected in the SWTA. Indeed, in some areas such as the Peruvian upwelling system, active acoustics has been proved a powerful tool to estimate the depth of the limit of different thermohaline structures in particular the pycnocline. This continuous estimation further allowed the description of a variety of turbulent structures at scales ranging from the internal-wave to the mesoscale (e.g., Grados et al., 2016; Stranne et al., 2017). The detections of thermohaline limits are typically attributed to biological dispersion or turbulent structures. However, in our case, none of the three tested criteria - (i) the vertical extension of the epipelagic community; (ii) the use of acoustic gradients; and (iii) a cross-

wavelet between the thermal vertical and acoustic gradients - allowed for a robust estimation of the thermohaline structure. In the same line, Campanella et al. (WGFAST, 2021) employed a different approach (identification of the scattering layers located at the depth of the pycnocline and application of machine learning methods) to detect the depth of the upper thermocline using echosounder data (at 200 kHz) in the Western English Channel and Celtic Sea. Even if they could represent the main global patterns, the error of estimation of the thermocline upper limit was too high for a robust estimation.

However, our study revealed that in certain scenarios such as in the WBCS in spring 2015, a large part of the acoustic biomass in the upper ocean (10 - 300 m) was not distributed within the thermocline but in the shallower layer including the barrier layer and the mixing layer. Such results imply that abiotic or biotic factors, other than the thermohaline structure, drive the behaviour of scattering layer organisms. This led us to proposing to investigate in Chapter IV the fine-scale vertical relationships between acoustic biomass and a variety of environmental factors.

Objective 3: Investigate how environmental factors may be driving the vertical distribution of organisms in the southwestern tropical Atlantic. (Chapter IV)

Water column stratification is a key driver in the vertical positioning of SSLs. The vertical ocean stratification is projected to be stronger under climate change as response of increase of sea surface temperature (Le Borgne et al., 2011; Li et al., 2020; Sallée et al., 2021). In future scenarios, therefore, increased upper-ocean stratification, changes in wind forcing, and a changing Atlantic meridional overturning circulation will affect the transport of heat, salt and tracers, also causing decrease in oxygen concentrations in mesopelagic zones, and hence changes in the ecosystem (Foltz et al., 2019; Keeling and Gruber, 2010; Oschlies et al., 2018). A change from primary productivity to distribution of mesopelagic animals could affect pelagic food webs as well as biogeochemical cycles (Algar et al., 2009; Mojica et al., 2015; Netburn and Anthony Koslow, 2015). Therefore, this study contributes to the understanding of possible predictions of the vertical positions of SSLs in the SWTA. Indeed, in the epipelagic layer, the maximum stratification may be more "important" than the depth of the DCM, when these are not overlapping, as in the instance of the WBCS. We have also demonstrated that, in the SWTA the oxygen concentration is likely not a key driving factor where the water column is well oxygenated, as in the WBCS. While in SECS, deep SSLs show tendencies to be positioned at depths of low oxygen concentration. Finally,

our results suggest currents as a factor with high tendencies towards vertical structuring of SSLs in the WBCS.

Our study highlight that the vertical structuring of acoustic scatters depends on complex environmental interactions. Our results as well as the conceptual models can be especially useful in understanding the SWTA ecology. Despite the limitations presented here, these are the first fine-scale results of environmental relationships and acoustic ecology in the SWTA. We suggest for future research to consider larger scale analysis to reduce high frequency noise.

Overall, the work carried out in this PhD thesis is a contribution to the understanding the hydrodynamics in the SWTA and the consequences in terms of the vertical distribution of organisms. Under current climate warming, increased ocean stratification is expected as well as changes in wind forcing, and in the Atlantic meridional overturning circulation (Foltz et al., 2019; Li et al., 2020; Sallée et al., 2021). Understanding the ecological implications of these changes on marine ecosystems become an urgent issue. A change from primary productivity to distribution of mesopelagic animals could affect pelagic food webs as well as global biogeochemical cycles (Algar et al., 2009; Mojica et al., 2015; Netburn and Anthony Koslow, 2015). This study provides an image of the thermohaline structure and vertical biophysical interaction in the current period and can serve as a reference to fuel models and for future comparison in a warming ocean.

References

Algar, A.C., Kharouba, H.M., Young, E.R., Kerr, J.T., 2009. Predicting the future of species diversity: macroecological theory, climate change, and direct tests of alternative forecasting methods. Ecography (Cop.). 32, 22–33. https://doi.org/10.1111/j.1600-0587.2009.05832.x

Ariza, A., Lebourges-Dhaussy, A., Nerini, D., Pauthenet, E., Roudaut, G., Assunção, R.V. De, Bertrand, A., n.d. Acoustic seascape partitioning through Functional Data Analysis. Nat. Sci. Reports.

Campanella, F., van der Kooij, J., Fernand, L., 2021. An acoustic approach to estimate the Mixed Layer Depth. Work. Gr. Fish. Acoust. Sci. Technol.

Cheng, W., Chiang, J.C.H., Zhang, D., 2013. Atlantic meridional overturning circulation (AMOC) in CMIP5 Models: RCP and historical simulations. J. Clim. 26, 7187–7197. https://doi.org/10.1175/JCLI-D-12-00496.1

Dossa, A.N., Silva, A.C. da, Chaigneau, A., Eldin, G., Araújo, M., Bertrand, A., 2021. Near-surface western boundary circulation off Northeast Brazil. Prog. Oceanogr. 190, 102475. https://doi.org/10.1016/j.pocean.2020.102475

Eduardo, L.N., Bertrand, A., Mincarone, M.M., Martins, J.R., Freddou, T., Assunção, R.V. De, Lima, R., Menard, F., Le Loc'h, F., Lucena-Fredou, F., n.d. Distribution, vertical migration, and trophic ecology of lanternfishes (Myctophidae) in the western Tropical Atlantic. Prog. Oceanogr.

Farias, G.B., Molinero, J.-C., Carré, C., Bertrand, A., Bec, B., Melo, P., n.d. Uncoupled changes in phytoplankton biomass and size structure in the western tropical Atlantic. J. Mar. Syst.

Figueiredo, G.G.A.A. de, Schwamborn, R., Bertrand, A., Munaron, J.-M., Le Loc'h, F., 2020. Body size and stable isotope composition of zooplankton in the western tropical Atlantic. J. Mar. Syst. 212, 103449. https://doi.org/10.1016/j.jmarsys.2020.103449

Foltz, G.R., Brandt, P., Richter, I., Rodríguez-Fonseca, B., Hernandez, F., Dengler, M., Rodrigues, R.R., Schmidt, J.O., Yu, L., Lefevre, N., Da Cunha, L.C., McPhaden, M.J., Araújo, M., Karstensen, J., Hahn, J., Martín-Rey, M., Patricola, C.M., Poli, P., Zuidema, P., Hummels, R., Perez, R.C., Hatje, V., Lübbecke, J.F., Polo, I., Lumpkin, R., Bourlès, B., Asuquo, F.E., Lehodey, P., Conchon, A., Chang, P., Dandin, P., Schmid, C., Sutton, A., Giordani, H., Xue, Y., Illig, S., Losada, T., Grodsky, S.A., Gasparin, F., Lee, T., Mohino, E., Nobre, P., Wanninkhof, R., Keenlyside, N., Garcon, V., Sánchez-Gómez, E., Nnamchi, H.C., Drévillon, M., Storto, A., Remy, E., Lazar, A., Speich, S., Goes, M., Dorrington, T., Johns, W.E., Moum, J.N., Robinson, C., Perruche, C., de Souza, R.B., Gaye, A.T., López-Parages, J., Monerie, P.-A., Castellanos, P., Benson, N.U., Hounkonnou, M.N., Duhá, J.T., Laxenaire, R., Reul, N., 2019. The Tropical Atlantic Observing System. Front. Mar. Sci. 6. https://doi.org/10.3389/fmars.2019.00206

Li, G., Cheng, L., Zhu, J., Trenberth, K.E., Mann, M.E., Abraham, J.P., 2020. Increasing ocean stratification over the past half-century. Nat. Clim. Chang. 10, 1116–1123. https://doi.org/10.1038/s41558-020-00918-2

Mojica, K.D.A., van de Poll, W.H., Kehoe, M., Huisman, J., Timmermans, K.R., Buma, A.G.J., van der Woerd, H.J., Hahn-Woernle, L., Dijkstra, H.A., Brussaard, C.P.D., 2015. Phytoplankton

community structure in relation to vertical stratification along a north-south gradient in the Northeast Atlantic Ocean. Limnol. Oceanogr. 60, 1498–1521. https://doi.org/10.1002/lno.10113

Netburn, A.N., Anthony Koslow, J., 2015. Dissolved oxygen as a constraint on daytime deep scattering layer depth in the southern California current ecosystem. Deep Sea Res. Part I Oceanogr. Res. Pap. 104, 149–158. https://doi.org/10.1016/j.dsr.2015.06.006

Nogueira Neto, A. V., Giordani, H., Caniaux, G., Araújo, M., 2018. Seasonal and Interannual Mixed-Layer Heat Budget Variability in the Western Tropical Atlantic from Argo Floats (2007–2012). J. Geophys. Res. Ocean. 123, 5298–5322. https://doi.org/10.1029/2017JC013436

Sallée, J., Pellichero, V., Akhoudas, C., Pauthenet, E., Vignes, L., Schmidtko, S., Garabato, A.N., Sutherland, P., Kuusela, M., 2021. Summertime increases in upper-ocean stratification and mixed-layer depth. Nature 591, 592–598. https://doi.org/10.1038/s41586-021-03303-x

Silva, A.C. da, Chaigneau, A., Dossa, A.N., Eldin, G., Araújo, M., Bertrand, A., 2021. Surface circulation and vertical structure of upper ocean variability around Fernando de Noronha archipelago and Rocas atoll during spring 2015 and fall 2017. Front. Mar. Sci. https://doi.org/10.3389/fmars.2021.598101

Tosetto, E.G., Bertrand, A., Neumann-Leitão, S., Costa da Silva, A., Nogueira Júnior, M., 2021. Spatial patterns in planktonic cnidarian distribution in the western boundary current system of the tropical South Atlantic Ocean. J. Plankton Res. 43, 270–287. https://doi.org/10.1093/plankt/fbaa066

DOCTORAT SCIENCES BRETAGNE DE LA MER LOIRE ET DU LITTORAL

Université de Bretagne Occidentale

Titre : Stratification thermohaline dans l'Atlantique tropical sud-ouest : des processus physiques à l'écologie acoustique

Mots clés : Frontière occidentale, Analyse des données fonctionnelles, Écologie acoustique, structuration *bottom-up*

Résumé : La structure thermohaline de l'Atlantique tropical sud-ouest (SWTA) a un impact primordial sur le climat global et joue un rôle moteur dans la structuration verticale des habitats pélagiques. Afin de combler le manque d'information sur la structure thermohaline dans l'SWTA et d'apporter un éclairage sur les relations entre ces processus physiques et la distribution de l'énergie acoustique, nous avons profité des deux campagnes scientifiques, ABRAÇOS, réalisées au printemps 2015 et à l'automne 2017. Tout d'abord, nous caractérisons la structure thermohaline 3D de l'SWTA supérieure en appliquant une analyse fonctionnelle des données sur les profils de température et de salinité. Nos résultats révèlent un schéma spatial clair avec la présence de trois zones aux caractéristiques thermohalines significativement différentes. La zone 1, située le long de la pente continentale, correspond au système de courants de la limite ouest. La zone 2, située le long de la chaîne Fernando de Noronha, correspond au système du courant équatorial sud. Et la zone 3 se comporte comme une zone de transition entre ces zones. Deuxièmement, nous avons examiné la possibilité d'extraire la structure thermohaline supérieure à partir des données d'échosondeurs. Nos résultats montrent que, même si la structure thermohaline a un impact sur la distribution verticale des dispersions acoustiques, la structuration résultante ne permet pas une estimation robuste des limites thermohalines. Cependant, l'étude de la proportion de la biomasse acoustique au sein de chaque couche donne un aperçu de la structure de l'écosystème dans différentes thermohalines, ce qui nous a conduit à étudier les relations verticales à fine échelle entre la biomasse acoustique et d'autres facteurs environnementaux, comme troisième objectif. Nous montrons que la fluorescence, l'oxygène, le courant et la stratification sont des facteurs importants, mais que leur importance relative dépend de la zone, de la gamme de profondeur et du cycle diurne.

Title: Thermohaline stratification in the Southwestern Tropical Atlantic: from physical processes to acoustic ecology

Keywords: Boundary western, Functional Data Analysis, Acoustic ecology, structuring bottom-up

Abstract: The thermohaline structure of the southwest tropical Atlantic (SWTA) has prime impact on global climate and plays a driving role in the vertical structuring of pelagic habitats. To fill information gaps on the thermohaline structure in the SWTA and to bring insights into the relationships between these physical processes and the distribution of the acoustic energy, we took advantage of the two scientific surveys, ABRAÇOS, performed in austral spring 2015 and fall 2017. First, we characterise the 3D thermohaline structure of the upper SWTA by applying a Functional Data Analysis on temperature and salinity profiles. Our results reveal a clear spatial pattern with the presence of three areas with significantly different thermohaline characteristics. Area 1, located along the continental slope corresponds to the western boundary current system. Area 2, located along the Fernando de Noronha chain corresponds to the South Equatorial Current system and Area 3 behaves as a transition zone between these areas. Second, we examined the feasibility of extracting the upper thermohaline structure from echosounder data. Our results show that, even if the thermohaline structure impacts the vertical distribution of acoustic scatters, the resultant structuring does not allow for a robust estimation of the thermohaline limits. However, studying the proportion of acoustic biomass within each layer provides insights on ecosystem structure in different thermohaline, which led us to investigate the fine-scale vertical relationships between acoustic biomass and other environmental factors, as the third objective. We show that fluorescence, oxygen, current and stratification are important drivers, but that their relative importance depends on the area, the depth range and the diel cycle.